UNIVERSITY OF OTTAWA

Department of Mechanical Engineering

MODELING OF FLUID FLOW AND HEAT TRANSFER PROCESSES IN AN ENGINE

by

Achilles E. Carapanayotis, Dipl.Eng.(Greece), M.Eng.(Carl.)

A thesis submitted to the University of Ottawa in partial fulfillment of the requirements for the degree of

Doctor of Philosophy

in

Mechanical Engineering

ISBN 0-315-36474-2

UNIVERSITÉ D'OTTAWA
UNIVERSITY OF OTTAWA

ABSTRACT

This work presents the development of a thermodynamic simulation model for a two stroke turbo-charged diesel engine. The set of equations governing the fluid dynamics, combustion and thermodynamic state of the engine working medium is presented and the numerical procedure for solution is outlined. The combustion model that is used is a two equation zero dimensional model. The mass burning rate is calculated using a premixed and a mixing controlled reaction rate equation. The scavenging model is based on a scavenging efficiency-scavenging ratio equation. This equation is obtained by solving the momentum, energy and species conservation equations using finite difference approximations. The computed fuel burning rates are compared with fuel burning rates calculated from experimentally measured cylinder pressures. The experimentally obtained burning rates are calculated using the thermodynamic model with the pressure traces as input and the fuel burning rate as output. The indicated engine parameters (indicated horse power, indicated thermal efficiency, cylinder peak pressure etc.) obtained using the developed model are compared with experimentally measured values.

This work is dedicated to my wife Helen and my two children Maria and Anthoula for all their patience and love.

ACKNOWLEDGEMENT

The author wishes to express his gratitude to Dr. Martha Salcudean who initiated and supervised the present work. Her assistance was very valuable in completing the work and is very much appreciated.

Appreciation is also expressed to Dr. Bill Hallett who co-supervised the work since 1985.

The financial support was provided by the Department of National Defense of Canada through the Department of Supply and Services is gratefully acknowledged.

TABLE OF CONTENTS

LIST OF FIGURES

LIST OF TABLES

NOMENCLATURE

A	Area
A_p	Inlet port area
B	Engine bore
C	Concentration, heat capacity
C_d	Discharge coefficient
C_m	Piston mean velocity
d	Droplet diameter
d_o	Initial droplet diameter
D	Mass diffusivity
e	Specific internal energy
E	Internal energy
h	Heat transfer coefficient, specific enthalpy
H	Enthalpy, heat of formation
k	Thermal conductivity, isentropic coefficient
K	Turbulence kinetic energy
L	Latent heat
m_b	Fuel mass burned
M	Mass
M_e	Mass entering the cylinder
M_f	Fuel vapour mass fraction
M_i	Total fuel injected at a crank angle
M_l	Mass leaving the cylinder
M_o	Oxygen mass fraction
n	Number of moles
P	Pressure, Peclet number

P_{ab}	Air-box pressure
P_e	Pressure in the exhaust pipe
P_o	Oxygen partial pressure
q_{lhv}	Fuel lower heating value
Q	Heat transferred
Q_{comb}	Heat released due to combustion
r	Engine crank radius, radial coordinate
R	Equal to r for cylindrical coordinates and 1.0 for Cartesian coordinates
R_{mol}	Universal gas constant
R_{sc}	Scavenging ratio
S	Piston distance from TDC
t	Time
T	Temperature
u	Radial velocity
v	Axial velocity
V	Volume
V_{cl}	Clearance volume
w	Circumferential velocity
W	Work
y	Axial coordinate

GREEK SYMBOLS

α	Thermal diffusivity
δ	Equal to 1.0 for cylindriacl coordinates and 0.0 for Cartesian coordinates
ϵ	Energy dissipation rate

η	Number of moles,number of surfaces
η_{sc}	Scavenging efficiency
μ	Effective viscosity
μ_l	Fluid dynamic viscosity
ρ	Density
τ	Shear stress
ϕ	Fuel/air ratio

CHAPTER 1

INTRODUCTION

1.1 STATEMENT OF THE PROBLEM

In the past, internal combustion engines were improved and developed based only on previous experience and experimental studies. This is no longer the accepted practice. During the past ten years, high oil prices and the demand for engines with greater reliability and less pollution have led to the development of a large number of simulation models [1-5]. A simulation model helps the engine designer immensely because it: a) gives him a better understanding of the engine physical processes; b) can specify the most important parameters affecting the engine performance and emissions; c) can provide, at a relatively small cost, extensive parametric studies; and d) can identify the significant parameters for experimental studies. Although the development of such models requires large investments and time, they can be used on a number of different engines and the investment is much smaller compared to working on the actual engine in an experimental set-up.

The scope of this work is to develop an advanced simulation model for the General Motors GM6V53T six cylinder turbocharged, two-stroke, direct injection diesel engine. Simulation of an internal combustion (IC) engine is not an easy task. The physical model is extremely complex and even today many questions remain unanswered. For example, the heat transfer from the cylinder gases to the cylinder walls can differ by up to 200 per cent between data obtained using different models [6]. Another example is the scavenging process taking place in two stroke engines, where the cylinder gas composition cannot be accurately calculated and empirical models are therefore used.

Comparison of the simulation model with experimental data for verification is also very difficult. Global comparison of the indicated horse power (IHP), indicated thermal efficiency, peak pressure, peak pressure location, etc can lead to improper model evaluation. Even more detailed comparison during part of the thermodynamic cycle can lead to wrong conclusions if all the model assumptions do not describe accurately enough the experimental conditions. For example, fuel burning rates calculated from experimental pressures can vary significantly if the initial mass in the cylinder and the number of moles of the different existing species are not properly calculated (or estimated). Even if only a part of the cycle is examined, the study should be based on the proper overall model. Also, the simulation model has to be as close as possible to the actual engine physical processes in order to have a good predictive character.

1.2 LITERATURE REVIEW

1.2.1 Engine Modeling

The existing engine simulation models can be divided into two major categories: a) thermodynamic or zero-dimensional models; and b) multi-dimensional models. In the thermodynamic models, uniform pressure, temperature and mass composition within the cylinder are assumed. Equilibrium of the cylinder gases is assumed and the energy equation together with the state equation are used in the cycle calculations. In these types of models the engine geometry cannot be studied and is usually modeled empirically. Extensive experimental data are therefore needed for model refinement and verification. Thermodynamic models are used very often because of the low computer costs.

A second approach to engine modeling is multidimensional modeling. It is more fundamental than thermodynamic modeling and is also different in character. Multidimensional modeling of in-cylinder processes has received great attention during the last ten years and a significant number of technical papers have

been published [7-11]. However, due to the extreme complexity of the in-cylinder processes, multidimensional modeling has been, and is, presently directed towards the investigation of limited aspects of the processes during parts of the engine's operating cycle (e.g. flow pattern during compression or scavenging). All this work has to be considered as building blocks to a complete multidimensional model of the future.

In multidimensional models, the differential conservation equations which govern the flow, heat and mass transfer processes within the cylinder are solved numerically at a finite number of points. Their major advantages are: a) the information needed is limited to the boundaries of the cylinder only; and b) the velocity, pressure, temperature and species distributions can be calculated.

A large number of thermodynamic simulation models for diesel and spark ignition engines with four or two strokes have been published in the last twenty years [1-5,12,13]. The subject is of great importance because these models can predict performance trends for the fundamental design parameters and, using these predictions, time and investment can be saved by shortening the experimental testing.

During the cycle computations, the cylinder pressure and temperature are calculated using the energy and state equations. The internal energy of the cylinder gas mixture is needed during the thermodynamic cycle, and during scavenging the enthalpy of the cylinder gases and the fresh charge have to be calculated as a function of temperature. Values of thermodynamic properties as a function of temperature for a large number of species can be found in JANAF thermochemical tables [14]. In JANAF, the values are given in tabular form, making them rather difficult to use in the computer. In a number of references [15-18] coefficients from polynomial fitting of the heat capacity or internal energy are reported.

1.2.2 Heat Transfer

The heat transfer processes in internal combustion engines are complex and only empirical correlations based on experimental measurements are available. From the simulation point of view the heat transfer from the cylinder gas to the cylinder walls is more important than the heat transfer from the cylinder wall to the coolant. The heat transfer from the cylinder gas to the wall is due to convection and radiation. The radiation heat transfer is small compared to convection except in the case of high soot formation. According to Oguri and Inaba [19] under normal running conditions the heat transferred through radiation is about 15 per cent of the total heat transferred , but in a sooty engine it can go up to 30 per cent. It should be noted that the radiation is significant only during combustion and expansion where high temperatures occur. The convection heat transfer takes place under high gas velocities and is usually assumed to be through forced turbulent fluid flow.

Nusselt, performing experiments in a spherical bomb calorimeter, proposed an equation for the heat transfer coefficient consisting of a term for the heat transfer by convection and one for the radiation heat transfer. Later Annand [20], reviewing the existing correlations and performing a dimensional analysis, concluded that the major parameter affecting the convection heat transfer is the Reynolds number, and proposed a general equation for the heat transfer coefficient in which the convection term was based on the Reynolds number. Fitting this equation to experimental results for two and four stroke engines, he proposed values for the constants used in his model. Woschni [6], performing experiments in spherical combustion chambers, concluded in 1967 that the heat transfer in internal combustion engines is similar to the heat transfer in pipe flow under turbulent conditions. The equation that he proposed did not include a radiation heat loss term. The radiation heat was somehow included in the convection loss term. In

the proposed equation the velocity used in the computation of the Reynolds number is not constant but changes in the three main cycle periods: compression, combustion-expansion and scavenging. Woschni, performing experiments on turbocharged engines in 1979, concluded that the formula derived in 1967 agrees very well with the experimentally measured heat transfer rates [21].

1.2.3 Combustion

Combustion simulation is essential in order to obtain a good overall model. The nature of the process and the dominant factors are not yet clear. Combustion is strongly affected by many factors such as turbulence level in the cylinder, spray characteristics, evaporation rate, fuel-air mixing, engine geometry, scavenging efficiency, pressure and temperature in the cylinder. Combustion modeling can be categorized depending on the modeling used as:

a) Performance and efficiency

b) Engine emission

c) "Detonation"

Models dealing with performance and efficiency simulate the overall combustion effect and are usually empirical or semi-empirical and relatively simple. They are very useful because the engine performance can be predicted and parametric studies can be performed in an inexpensive way. Models concentrating on emission study the chemical kinetics and the formation of oxides of nitrogen, carbon monoxide, unburned hydrocarbons etc. These models are concerned with environment pollution but they are not used for performance prediction, because from the modeling point of view these species are not important. "Detonation" modeling is very complex for both spark ignition and diesel engines. These models study the irregular combustion and high pressure rise rates during the early part of combustion.

The combustion models from the analysis and study point of view can be classified as follows [22]:

a) Zero-dimensional or thermodynamic models

b) Quasi-dimensional or entrainment models

c) Multi-dimensional or detailed models

In the zero-dimensional models the overall combustion effect is modeled using empirical formulae for the apparent fuel burning rate (AFBR). In quasi-dimensional models the fuel burning rate is derived from physical sub-models of spray evaporation, fuel-air mixing and turbulent combustion. The multi-dimensional models are different in character since the conservation equations of mass, momentum, energy and species are solved numerically in the cylinder domain. The spray evaporation rate and the fuel-air mixing are calculated and the combustion reaction rate is usually explicitly supplied. Some of the proposed models of the three different categories will be discussed below.

Over the last twenty years a large number of zero-dimensional models have been proposed [23-27]. Lyn [28] correlated the apparent heat release to the fuel injection rate by assuming small time steps during injection where at each time step the fuel was prepared and burned according to an empirical mathematical formula. Later, Whitehouse and Way [24] proposed a similar model with the idea that the burning rate is proportional to the instantaneous total fuel area, assuming the fuel to be in uniform size droplets. This rate was then correlated to the fuel injection schedule. Borman in his early work [29] used experimental pressures during combustion to calculate the apparent heat release rate (AHRR) allowing for heat losses to the cylinder walls. This model gives very good information for the fuel burning rate but does not have a predictive character.

In 1968 Shipinski [30] calculated the AHRR from the fuel injection rate using Wiebe algebraic formula. Woschni and Anisits [31], using the same type of for-

mula, calculated the fuel burning rate without the use of the injection schedule. Later Watson et al. [27] used the same principle to calculate the fuel burning rate by using two Wiebe functions, one for the pre-mixed burning and one for the diffusion burning rate. The AHRR approach for modeling the combustion process determines the overall combustion efficiency and allows overall engine performance predictions but fails to give any information on the actual process and the significant factors affecting the combustion efficiency and pollution formation. Shipinski et al [25], assume that the fuel is beginning to evaporate by the time it is injected. The mass fraction burned is calculated from an empirical formula based on curve fitting of experimental results. Then, in order to have good agreement for different testing conditions, they performed parametric studies on the effect of pressure, temperature, overall fuel-air ratio and oxygen concentration to determine the constants used in the fuel burning equation.

In quasi-dimensional models the fuel burning rate (FBR) is derived from physical models simulating the fuel-air mixing and turbulent combustion [32-37]. Adler and Lyn [35] used the turbulent jet theory and derived a model for the air-fuel mixing process in diesel engines for steady conditions. Later, Chiu [36] proposed a model for calculating the FBR using transient spray mixing.

The multi-dimensional analysis was initially concentrated on velocity computations in IC engines during compression-expansion. The conservation equations were written in finite difference form and the velocities were computed for a discrete number of points. The difficulty in engine computation is that the computational domain is changing with time as the piston is moving.. Watkins [37] first introduced a mathematical transformation of the conservation equations that takes into account the grid expansion-contraction. Later, Flanagan et al.[38] and Chong [10] used the same transformation for similar studies. Gosman and his co-workers published a number of papers studying the fluid dynamics in IC engines[11,39-41].

In 1982 Gosman and Harvey [8] published their work dealing with the combustion process of a direct injection diesel engine. The model uses an empirical fuel burning rate based on Arrhenius kinetically controlled combustion. The reaction rate is a function of temperature, oxygen mass fraction and fuel vapor mass fraction. These quantities are calculated from the corresponding conservation equations. The model is qualitatively in agreement with experimental results.

1.2.4 Scavenging

The scavenging process takes place in two-stroke uniflow scavenged engines when the exhaust valves and inlet ports are open and the incoming fresh air replaces the combustion products. The development of two-stroke engines has concentrated for some time now on the improvement of the scavenging process. Improvement of the scavenging performance means decreasing the residual gases (ideally to zero) by replacing them with air. The scavenging process is best described by the scavenging efficiency, defined as the mass of air retained in the cylinder divided by the mass of air required to fill the cylinder volume at air-box pressure and temperature [42].

The amount of air retained in the cylinder during scavenging is very difficult to calculate because it depends on the cylinder geometry (inlet ports and exhaust valves), inlet port and exhaust valve timing, pressure and temperature in the cylinder, the exhaust manifold and the air-box. In early studies the following models have been proposed for the overall scavenging efficiency [43].

a) Pure mixing

b) Perfect scavenging

c) Short circuit

In the pure mixing model it is assumed that the incoming air mixes instantaneously with the cylinder gases and an equal amount of the cylinder mixture

leaves the cylinder. In the perfect scavenging model the incoming air is assumed to be replacing an equal amount of cylinder exhaust gas. In the short circuit model it is assumed that a part or all of the incoming fresh air goes directly to the exhaust valves without any contribution to the scavenging. In case of complete short circuit (all the air escapes) the scavenging efficiency is zero. Benson and Brandham [44] suggested a model which is a combination of the pure mixing and perfect scavenging models, called the mixing-displacement scavenging model. In this model the cylinder was assumed to be divided into two zones, a mixing zone close to the inlet ports and a displacement zone close to the exhaust valves. An arbitrary volume ratio of the two zones was assumed. Initially as the air is coming in, it is assumed that it is mixing with the existing gases in the mixing zone and the combustion gases are leaving the displacement zone. It is assumed that the two zones are not mixed and, therefore, the displacement zone is getting smaller and smaller. When the displacement zone is eliminated the scavenging continues as pure mixing. In 1977 Benson [45] published his work on scavenging for cross scavenged engines based on Deodeoglu's [46] experimental data. In this model he assumed that three zones existed in the cylinder: a) mixing region (air and residuals); b) air region; and c) gas region. He assumed that each zone has the same pressure but a different temperature. The scavenging period was divided into three phases. In each phase, a different zone arrangement was selected based on experimental observations. A number of similar models studying the scavenging process by dividing the cylinder into zones with different composition and the scavenging period in different phases have been published (see reference [47]). These types of models are not fully satisfactory for engine design and performance optimization because they are highly empirical and do not include the engine design parameters.

Because of the difficulty in modeling the scavenging process, many experiments

have been performed to study two-stroke engine performance from the scavenging point of view. These experiments are based on flow visualization or sampling [48-50]. The sampling approach predicts the overall scavenging efficiency but does not predict the intermediate scavenging steps and the exhaust gas composition within the cylinder.

Recently, a few studies have been reported based on multi-dimensional analysis [51-53]. Sher [51], using a code similar to the one used by Gosman and Watkins (TEACH), calculated the exhaust gas-air mixture in a loop-scavenged engine. He calculated the overall scavenging efficiency for the engine for certain flow conditions. Sung [52] studied the air motion in a uniflow-scavenged engine theoretically and experimentally. Experimentally, he measured the three velocity components across the cylinder radius at 2.5 cm from the TDC for two different flow rates, using doppler anemometry. Theoretically, he computed the velocity field by solving the vorticity function for four different exhaust openings. The predicted results were not in good agreement with the experimental results. Recently, Diwakar [53] studied the scavenging process in a two-stroke uniflow-scavenged engine using the "CONHAS SPRAY" code [54]. The study concentrated on the effect of the swirl angle on the scavenging efficiency. He concluded that the optimum efficiency occurs with a 22 degree swirl. These results were in disagreement with the Nishimoto and Kamimoto [55] experimental and theoretical work.

1.3 OBJECTIVES OF PRESENT WORK

The objective of the present work is to develop a thermodynamic simulation model for the General Motors GM6V53T turbo charged, two-stroke, direct injection, uniflow scavenged diesel engine with special attention to the scavenging process. Since the knowledge of the scavenging process in two-stroke engines is limited and the process can not be studied effectively using thermodynamic models alone, multi-dimensional modeling will be used to derive a scavenging efficiency

equation for use in the thermodynamic model. The multi-dimensional modeling gives information on the air concentration in the cylinder during scavenging. Studies are performed assuming two and three dimensional flow in the cylinder. The multi-dimensional model is turbulent and the conservation differential equations are approximated with finite differences and are solved numerically. The results of the multi-dimensional analysis are used in the thermodynamic model. The predictions of the thermodynamic model are compared with experimental data supplied by Flanagan and Menard [56-57].

The thermodynamic model (zero-dimensional) developed is divided into compression, combustion-expansion and blowdown-scavenging processes. These processes are discussed in chapters 2, 3 and 4 respectively. In chapter 5 the development of the two dimensional turbulent model for scavenging studies is presented. Chapter 6 gives computational details for the three-dimensional model used for scavenging studies and comparison between the two and three dimensional results. Chapter 7 presents the heat transfer model used in the thermodynamic program. A model developed for calculating the fuel mass burning rate during combustion using experimental data is presented in chapter 8. The comparison of the thermodynamic model with experimental data is given in chapter 9.

REFERENCES

1 Kumar, K., Gaur, R. R., Garg, R. D., and Gajenda Babu, M. K. "A Thermodynamic Simulation Model for a Four-Stroke Medium Speed Diesel Engine", SAE paper 840516, 1984

2 Yuen, W. W., and Servati, H. "A Mathematical Engine Model Including the Effect of Engine Emissions", SAE paper 840036, 1984.

3 Mansouri, S. H., Heywood, J. B., and Radhakrishnan, K. " Divided Chamber Diesel Engine Part I: A Cycle Simulation Which Predicts Performance and Emission", SAE paper 820273, 1982.

4 Streit, E. E., and Borman, G. L. " Mathematical Simulation of a Large Turbocharged Two-Stroke Diesel Engine", SAE 710176, 1971.

5 Flanagan, R. C., Carapanayotis, A., and Xia, Y. Q. "Thermodynamic Simulation of a Two Stroke Direct Diesel Engine", Proceedings, IASTED International Conference: Applied Simulation and Modeling, Montreal, Canada, June 1985.

6 Woschni, G. " A Universally Applicable Equation for the Instantaneous Heat Transfer Coefficient in the Internal Combustion Engines", SAE Paper 670931, 1967.

7 Bassoli, C., Biaggini, G., Bodritti, G., and Cornetti A." Two-Dimensional Combustion Chamber of Direct Injection Diesel", SAE paper 840228 1984

8 Gosman, A. D., and Harvey, P. S. "Computer Analysis of Fuel-Air Mixing and Combustion in an Axisymmetric D.I. Diesel", SAE paper 820036, 1982

9 Ramos, J. I., Humphrey, A. C., and Sirignano, W. A. "Numerical Predictions of Axisymmetric Laminar and Turbulent Flows in Motored Reciprocating Internal Combustion Engines", SAE 790356, 1979.

10 Chong, M. S., Milking, E. E., and Watson, H. C."The Prediction of Heat and Mass Transfer During Compression and Expansion in I.C. Engines ", SAE 670761, 1976.

11 Gosman, A. D., Melling, A., Whitelaw, J. H., and Watkins, P. " Axisymmetric Flow in a Motored Reciprocating Engine" , Proc. Instn. Mech. Engrs Vol. 192, 1978.

12 Gajendra Babu, M. K., and Murthy, B. S. " Simulation and Evaluation of a 4-Stroke Single Cylinder Spark, Ignition Engine", SAE paper 750687, 1975.

13 Lucas, G. G. and James, C. " A Computer Simulation of a Spark Ignition Engine", SAE paper, 730053, 1973.

14 DOW CHEMICAL COMPANY - JANAF Thermochemical Tables, 1962, Addendum 1966.

15 Way, R. J. B. "Methods for Determination of Composition and Thermodynamic properties of Combustion Products for Internal Combustion Engine Calculations", Proc. Instn. Mech. Engrs Vol. 190 60/70, 1977.

16 Zacharias, F. " Analytical Representation of the Thermodynamic Properties of Combustion Gases", SAE paper 670930, 1967.

17 Benson, R. S. "Advanced Engineering Thermodynamics", Pergamon Press, 1976.

18 McBride, B. J., Heimel, S., Ehlers, J. G., and Gordon, S. "Thermodynamic Properties to 6000 K for 210 Substances Involving the First 18 Elements", NASA Report SP-3001.

19 Oguri, T. and Inaba, S. " Radiation Heat Transfer in Diesel Engines", SAE paper SAE paper 720023, 1972.

20 Annand, W. K. D. " Heat Transfer in the Cylinder of Reciprocating Internal Combustion Engines", Proc. Instn. Mech. Engrs Vol. 177 No 36, 1963.

21 Woschni, G. "Prediction of Thermal Loading of Supercharged Diesel Engines", SAE 790821, 1979.

22 Bracco, F. V. " Introducing a New Generation of More Detailed and Informative Combustion Models", SAE Paper 741174, 1974.

23 Austen, A. E. W., and Lyn, W. T. " Relation Between Fuel Injection and Heat Release in a Direct Injection Engine and the Nature of the Combustion Processes", Proc. Instn. Mech. Engrs No 1, 1960-61.

24 Whitehouse, N. D., and Way, R. " Rate of Heat Release in Diesel Engines and its Correlation with Fuel Injection Data", Proc. Instn. Mech. Engrs Vol. 184 Pt3J, 1969-70 Paper 1.

25 Shipinski, J., Myers, P. S., and Uyehara, O. A. " A Spray-Droplet Model for Diesel Combustion", Proc. Instn. Mech. Engrs Vol. 184 Pt3J, 1969-70 paper 2.

26 Ghojel, J. I. "A Study of Combustion Chamber Arrangements and Heat Release in D.I. Diesel Engines", SAE Paper 821034, 1982.

27 Watson, N., Pilley, A. D., and Marzouk, A. "A Combustion Correlation for Diesel Engine Simulation", SAE Paper 800029, 1980.

28 Lyn, W. T. " Study of Burning rate and Nature of Combustion in a Diesel Engine", Intern. Symb. on Combustion, 1962.

29 Borman, G. L. "Mathematical Simulation of Internal Combustion Engine Processes and Performance Including Comparisons with Experiment", Ph.D. Thesis, University of Wisconsin, 1964.

30 Shipinski, J. H., Uyehara, O., and Myers, P. S. " Experimental Correlation Between Rate of Injection and Rate of Heat Release in a Diesel Engine", ASME Paper 68-DGP-11, 1968.

31 Woschni, G., and Anisits, F. "Experimental Investigation and Mathematical Presentation of Rate of Heat Release in Diesel Engines Dependent upon Engine

Operating Conditions", SAE Paper 740086, 1974.

32 Bracco, F. V. " Applications of Steady-State Spray Equations to Combustion Modeling", Journal of AIAA, Vol. 12, No 11.

33 Sorenson, S. C. " Modeling Turbulent Transient Combustion", SAE Paper 780639, 1978.

34 Kamimoto, T., Aoyagi, Y., Matsui, Y., and Matsuoka, S. "The Effect of Some Engine Variables on Measured Rates of Air Entrainment and Heat Release in a D.I. Diesel Engine", SAE Paper 800253, 1980.

35 Adler, B., and Lyn, W. T. " The Evaporation and Mixing of a Liquid Fuel Spray in a Diesel Air Swirl", Institution of Mechanical Engineers, 1970.

36 Chiu, W. S., Shahed, S. M., and Lyn, W. T. "A Transient Spray Mixing Model for Diesel Combustion", SAE Paper 760128, 1976.

37 Watkins, A. P. "Calculation of Flow and Heat Transfer in the Combustion Chamber of Reciprocating Engine", M.Sc. Thesis University of London, 1973.

38 Flanagan, R. C., Salcudean, S., Carapanayotis, A., and Xia, Y. Q. "A Study of Wide Boiling Range Fuel-Engine Interaction: Thermodynamic and Multi-Dimensional Modeling", Technical Report No UOME-EP-8404-1, 1984.

39 Gosman, A. D., Tsui, Y. Y., and Watkins, A. P. "Calculation of Three Dimensional Air Motion in Model Engines", SAE Paper 840229, 1984.

40 Gosman, A. D., and Johns, R. J. " Development of a Predictive Tool for In-Cylinder Gas Motion in Engines", SAE Paper 780315, 1978.

41 Gosman, A. D., Johns, R. J. and Watkins, A. P. " Development of Prediction Methods for In-Cylinder Processes in Reciprocating Engines", Proceedings of the Symposium on Combustion Modeling in Reciprocating Engines, Warren Michigan, November 1978.

42 Taylor, C. F. "The Internal Combustion Engine in Theory and Practice", The M.I.T. Press, Third Printing, 1979.

43 Schweitzer, P. H. " Scavenging of Two Stroke Cycle Diesel Engines", the MacMillan Publishing Company 1949.

44 Benson, R. S., and Brandham, P. T. A. "A Method for Obtaining a Quantitative Assessment of the Influence of Charging Efficiency on Two Stroke Engine Performance", Int. J. Mech. Sci. No 3, 1969.

45 Benson, R. S. "A New Gas Dynamics Model for the Gas Exchange Process in Two Stroke Loop and Cross Scavenged Engines", Int. J. Mech. Sci., Vol. 19 pp 693-711.

46 Deodeoglu, N. "Scavenging Model Solves Problems in Gas Burning Engine", SAE Paper 710579, 1971.

47 Baudequin, F., and Rochelle, P. " Some Scavenging Models for Two Stroke Engines", Proc. Inst. Mech. Engrs, Vol. 194, 1980.

48 Sanborn, D. S., Blair, G. P., Kenny, R. G., and Kingsbury, A. H. " Experimental Assessment of Scavenging Efficiency of Two Stroke Cycle Engines", SAE 800975, 1980.

49 Blair, G. P., and Kenny, R. G. " Further Developments in Scavenging Analysis for Two Cycle Engines", SAE Paper 800038, 1980.

50 Huber, E. W. " Measuring the Trapping Efficiency of Internal Combustion Engines Through Continues Exhaust Gas Analysis", SAE Paper 710144, 1971.

51 Sher, E. "An Improved Gas Dynamics Model Simulating the Scavenging Process in a two Stroke Cycle Engine", SAE Paper 800037 1980.

52 Sung, N. W., and Patterson, D. J. " Air Motion in a Two Stroke Engine Cylinder- The Effects of the Exhaust Geometry", SAE Paper 820751, 1982

53 Diwakar, R."Multidimensional Modeling of the Gas Exchange Processes in a Uniflow-Scavenged Two-Stroke Diesel Engine", presented at the Winter annual meeting of the ASME, November 17-22, 1985.

54 Cloutman, L. D., Dukowicz, J. K., Ramsaw, J. D. and Amsden, A. A. "CONCHAS-SPRAY: A Computer Code for Reactive Flows with Fuel Sprays", Los Alamos Report LA-9294-MS, 1982.

55 Nishimoto, K. and Kamimoto, T. " A Study of the Influence of the Inlet Angle and Reynolds Number on the Flow-Pattern of Uniflow Scavenging Air", SAE Paper 841056, 1984.

56 Flanagan, R. C., and Menard, L. "Effects of the Quality on the Performance of the High Speed Diesel Engine Part I: Brake and Indicated Characteristics", Proceedings of the Twenty-Second Automobile Technology Development Contractors" Coordination Meeting, 1984.

57 Menard, L., and Flanagan, R. C. "Effects of the Quality on the Performance of the High Speed Diesel Engine Part II: Combustion Parameter Characteristics", Proceedins of the Twenty-Second Automobile Techology Development Contractors Coordination Meeting, 1984.

CHAPTER 2

COMPRESSION PROCESS

2.1 INTRODUCTION

The engine thermodynamic cycle is divided into three processes, a) compression, b) combustion-expansion, and c) blowdown- scavenging. In this chapter the compression process is discussed. In chapters 3 and 4 the combustion-expansion and blowdown-scavenging processes respectively are presented. In every process all the individual models used are presented together with their governing equations. During the thermodynamic cycle the cylinder pressure and temperature are computed using the state and energy equations. The energy equation is approximated using finite differences for time derivatives and is solved simultaneously with the state equation using an iterative technique. The simulated engine is the General Motors GM6V53T six cylinder turbocharged two stroke diesel engine. The engine is uniflow scavenged with four overhead exhaust valves. The engine specifications and the engine cross section diagram [1] are shown in table 2.1 and in figure 2.1 respectively.

The compression process starts immediately after the inlet ports and exhaust valves have closed, as can be seen in figure 2.2. At that point the temperature and pressure in the cylinder are estimated. The pressure and temperature are assumed equal to the air-box pressure and temperature. The cylinder gas is assumed to be pure air and the mass is calculated from the state equation. The initial estimated values are compared with the final calculated values after the end of the thermodynamic cycle, and if the differences in the pressure and temperature values are greater than 1.35 kPa and 10.0 K respectively the final values are assigned as initial and the computations are repeated until convergence is reached. The cal-

culated cylinder mass and gas composition are also assigned as initial for the next iteration. The program usually converges within three iterations. The parameters used in the thermodynamic model are given in table 2.2.

2.2 ENERGY AND STATE EQUATIONS

The state and energy equations for the cylinder control volume are written as follows (no mass entering or leaving the cylinder, no heat released due to combustion)

Ideal Gas Equation

$$PV = MR_{mol}T \qquad (2-1)$$

Where:

P - is the cylinder pressure

V - is the cylinder volume

T - is the cylinder temperature

M - is the number of Kg-moles in the cylinder

R_{mol} - is the universal gas constant (8,131.4 $J/Kg-mol\ K$)

Energy Equation (First Law of Thermodynamics)

$$\frac{\partial E}{\partial t} = \frac{\partial Q}{\partial t} - \frac{\partial W}{\partial t} \qquad (2-2)$$

Where:

W - is the work done by the system

Q - is the heat transferred to the system

E - is the internal energy

A question arises concerning the behavior of the cylinder gas as ideal, particularly during combustion, where high pressures and temperatures are observed. The highest temperature and pressure during the cycle occur 5 to 7 degrees after the top dead center (TDC). Typical values for the GM6V53T engine are P_{max} = 12.2 MPa (120 atm) and T_{max} = 2400 K. Assuming the gas in the cylinder is air (this assumption is reasonable because about 75 percent of the cylinder gas is nitrogen and most of the oxygen has not yet been consumed), the critical pressure and temperature for the air are P_{cr} = 3.77 MPa (37.25 atm) and T_{cr} = 132.4 K respectively [2]. From the generalized compressibility chart (figure 2.3) [2] it can be seen that the compressibility factor Z is about 1.02 for $P/P_{cr} = 3.22$ and $T/T_{cr} = 18.12$. Therefore, equation (2-1) can be used safely for the entire simulation cycle.

The energy equation (eqn. (2-2)) is written in finite difference form for a time interval Δt between the time t and $t + \Delta t$ as follows:

$$E_2 - E_1 = \Delta Q - \Delta W \qquad (2-3)$$

Where:

E_2 - is the internal energy at time $= t + \Delta t$

E_1 - is the internal energy at time $= t$

ΔW - is the work done by the system during the time step Δt

ΔQ - is the heat transferred to the system during the time step Δt

Equations (2-1) and (2-3) are the basic equations for the pressure and temperature calculations during compression, the procedure will be discussed in section 2.5.

2.3 INTERNAL ENERGY CALCULATIONS

The method for computing the internal energy, enthalpy, and specific heat of a gas mixture is presented below. The mixture is assumed to consist of n species. Thermodynamic properties of a large number of chemical species can be found in reference [3-4] in a tabular form. In reference [5] polynomial fitting of the values of heat capacity as a function of temperature is presented for a limited number of species for a temperature range of 500.-3000 K. In reference [6] polynomial fitting of the heat capacity for more than 200 species is presented. The temperature range is 300-5000 K and two polynomials, one for the 300-1000 K range and one for the 1000-5000 K, are used. In this study the polynomials were obtained from reference [6]. During the cycle calculations the following species are used (the concentrations of these species are obtained from combustion calculations presented in chapter 3);

$$H,\ O,\ OH,\ CO,\ O_2,\ H_2,\ NO,\ H_2O,\ N_2,\ Ar,\ H,\ N,\ C_{13}H_{24}$$

The chemical formula for the fuel was found using results from the fuel stoichiometric analysis reported in reference [7] (the fuel properties are presented in table 2.3). The polynomial coefficients for the above mentioned species are given in tables 2.4 and 2.5 for the two different temperature ranges. The coefficients are presented as $A_{i,j,m}$ where i is the species , j the polynomial coefficient ($j = 1, 5$) and m is the temperature range, the values of m are $m = 1$ for the 300-1000 K range and $m = 2$ for the 1000-5000 K range. The specific heat capacities for species i are written as follows:

$$C_{p,i} = R_{mol} \sum_{j=1}^{5} A_{i,j,m} T^{j-1} \qquad (2-4)$$

$$C_{v,i} = R_{mol} \sum_{j=1}^{5} (A_{i,j,m} T^{j-1} - 1) \qquad (2-5)$$

The specific enthalpy for species i is written as:

$$h_i = \int_0^T C_{p,i} dT = R_{mol} \sum_{j=1}^{5} (1/j) A_{i,j,m} T^j \qquad (2-6)$$

Assuming zero enthalpy at zero degrees Kelvin the internal energy is written as:

$$e_i = R_{mol} \sum_{j=1}^{5} [(1/j) A_{i,j,m} T^j - T] \qquad (2-7)$$

The mixture specific enthalpy and internal energy are:

$$E = \sum_{i=1}^{n} M_i e_i \qquad (2-8)$$

$$H = \sum_{i=1}^{n} M_i h_i \qquad (2-9)$$

The mixture specific heat capacities are:

$$C_p = \frac{\sum_{i=1}^{n} M_i C_{p,i}}{M} \qquad (2-10)$$

$$C_v = \frac{\sum_{i=1}^{n} M_i C_{v,i}}{M} \qquad (2-11)$$

Where:

$M = \sum_{i=1}^{n} M_i$ and

M_i is the number of moles of species i.

The gas mixture internal energy U and enthalpy H are given as follows:

$$H = R_{mol} \sum_{i=1}^{n} M_i \sum_{j=1}^{5} (1/j) A_{i,j,m} T^j \qquad (2-12)$$

$$E = R_{mol} \sum_{i=1}^{n} M_i \sum_{j=1}^{5} [(1/j) A_{i,j,m} T^j - T] \qquad (2-13)$$

2.4 WORK CALCULATIONS

The work done by the system ΔW is calculated using the mean cylinder pressure during the time interval Δt which defined as:

$$P_m = 0.5(P_1 + P_2) \qquad (2-14)$$

Where:

P_1 - is the cylinder pressure at time $= t$

P_2 - is the cylinder pressure at time $= t + \Delta t$

The instantaneous cylinder volume V is calculated using the following formula [8]:

$$S = r[1.0 + R - (R^2 - sin(\theta))^{0.5} - cos(\theta)] \qquad (2-15)$$

$$V = V_{cl} + \pi B^2 S/4.0 \qquad (2-16)$$

Where:

B - is the engine bore

r - is the engine crank radius

θ - is the crank angle (degrees) measured from TDC

V_{cl} - is the cylinder clearance volume

R - is the ratio of connecting rod length to crank radius

S - is the piston distance from TDC

Thus the work done by the system during the step Δt is:

$$W = P_m(V_1 - V_2) \qquad (2-17)$$

Where:

V_1 - is the cylinder volume at time $= t$

V_2 - is the cylinder volume at time $= t + \Delta t$

2.5 SOLUTION PROCEDURE DURING COMPRESSION

As mentioned earlier the solution procedure is based on the state and energy equations (eqns (2-1) and (2-3)). It is assumed that the temperature, pressure, internal energy, heat capacity, etc. are known at time t and values of these parameters at time $t + \Delta t$ are being sought. It is not possible to solve equations (2-1) and (2-3) for temperature and pressure analytically and an iterative solution is used. The steps taken are as follows:

(A) The compression process is assumed to be isentropic and the temperature T_2 (at time $t + \Delta t$) is calculated as:

$$T_2 = T_1(\frac{V_1}{V_2})^{k-1} \qquad (2-18)$$

The value of $k-1$ (k is the specific heat ratio) can be estimated as $R_{mol}/C_v(T_1)$. The specific heat capacity $C_v(T_1)$ is known from the previous time step. The values of V_1 and V_2 are calculated using equations (2-15) and (2-16).

(B) The cylinder pressure at time $t + \Delta t$ is calculated from the state equation (eqn. (2-1)) as follows:

$$P_2 = MR_{mol}T_2/V_2 \qquad (2-19)$$

(C) The heat transfer to the cylinder walls ΔQ is calculated using equations presented in chapter 7 with mean values for the pressure and temperature.

(D) The internal energy of the cylinder gases E_2 is calculated at time $t + \Delta t$ using equations presented in section 2.3.

(E) The work ΔW during the time step Δt is calculated using equation (2-17).

(F) Check if the energy equation (eqn. (2-3)) is satisfied. It is assumed satisfied if:

$$\Delta T = \frac{E_1 - E_2 - \Delta W + \Delta Q}{MC_v(T_2)} < 0.01 \qquad (2-20)$$

If the energy equation is satisfied the pressure P_2 and temperature T_2 are correct and the computations for that time step are finished. To continue for the next time step the final conditions (T_2, P_2, V_2, etc) are set as initial (T_1, P_1, V_1, etc.) the time is advanced by the time step and the computations are repeated starting at (A).

(G) If the energy equation is not satisfied a new temperature (T_2) is estimated from:

$$(T_2)_n = (T_2)_{n-1} + \Delta T \qquad (2-21)$$

Where:

$(...)_n$ - is a new estimate

$(...)_{n-1}$ - is the previous estimate

The calculations are repeated starting at (B) until the correct temperature and pressure are found. In figure 2.4 the flow diagram for the cycle calculations is presented.

REFERENCES

1 Kates, E. J., and Luck, W. E. "Diesel and High Compression Gas Engines", An American Technical Society Publication, 1975 (Third Edition).

2 Reynolds, W. C., and Perkins, H. C. "Engineering Thermodynamics ", McGraw-Hill Book Company, 1977.

3 Way, R. J. B. "Methods for Determination of Composition and Thermodynamic properties of Combustion Products for Internal Combustion Engine Calculations", Proc. Instn. Mech. Engrs, Vol. 190 60/70, 1977.

4 Zacharias, F. "Analytical Representation of the Thermodynamic Properties of Combustion Gases", SAE paper 670930, 1967.

5 Benson, R. S. "Advanced Engineering Thermodynamics", Pergamon Press, 1976.

6 McBride, B. J., Heimel, S., Ehlers, J. G., and Gordon, S. "Thermodynamic Properties to 6000 K for 210 Substances Involving the First 18 Elements" NASA Report SP-3001.

7 Flanagan, R. C., and Menard, L. "A study of Wide Boiling Range Fuel-Engine Interaction: Engine Performance and Combustion Monitor Test", Technical Report No UOME-EP-8403-1, Department of National Defense, DREO, Ottawa, Canada, 1984.

8 Taylor, F. T. "The Internal Combustion Engine in Theory and Practice", The M. I. T. Press, Third printing, 1979.

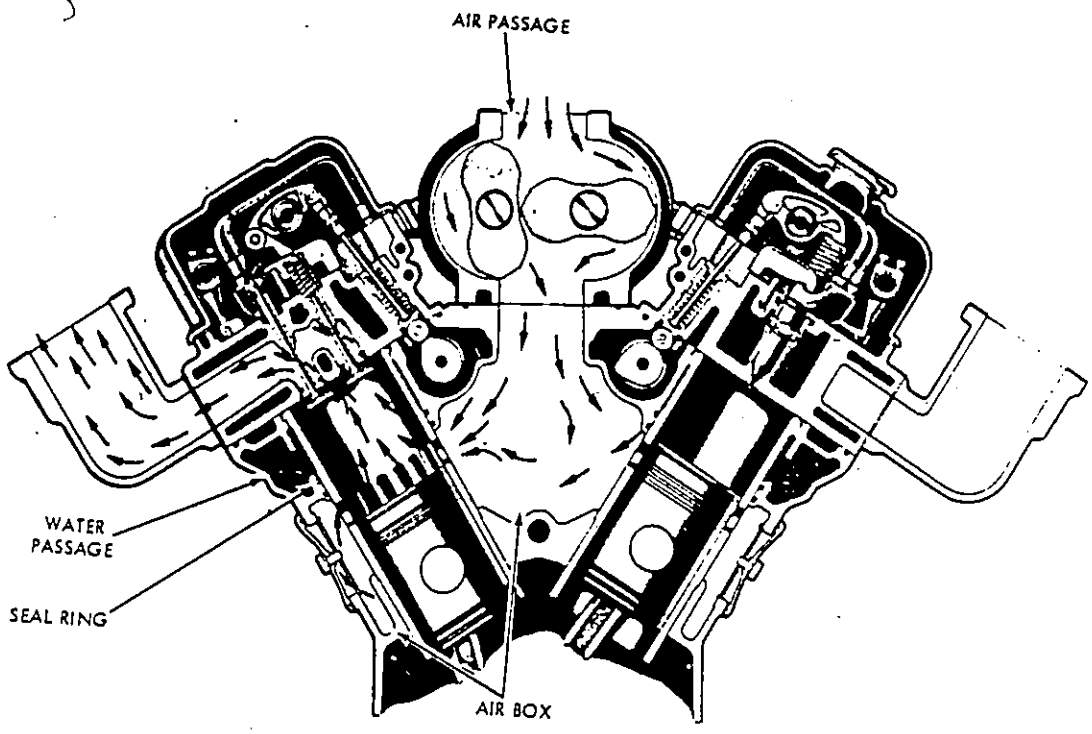

Figure 2.1 Section of the GM6V53T engine.

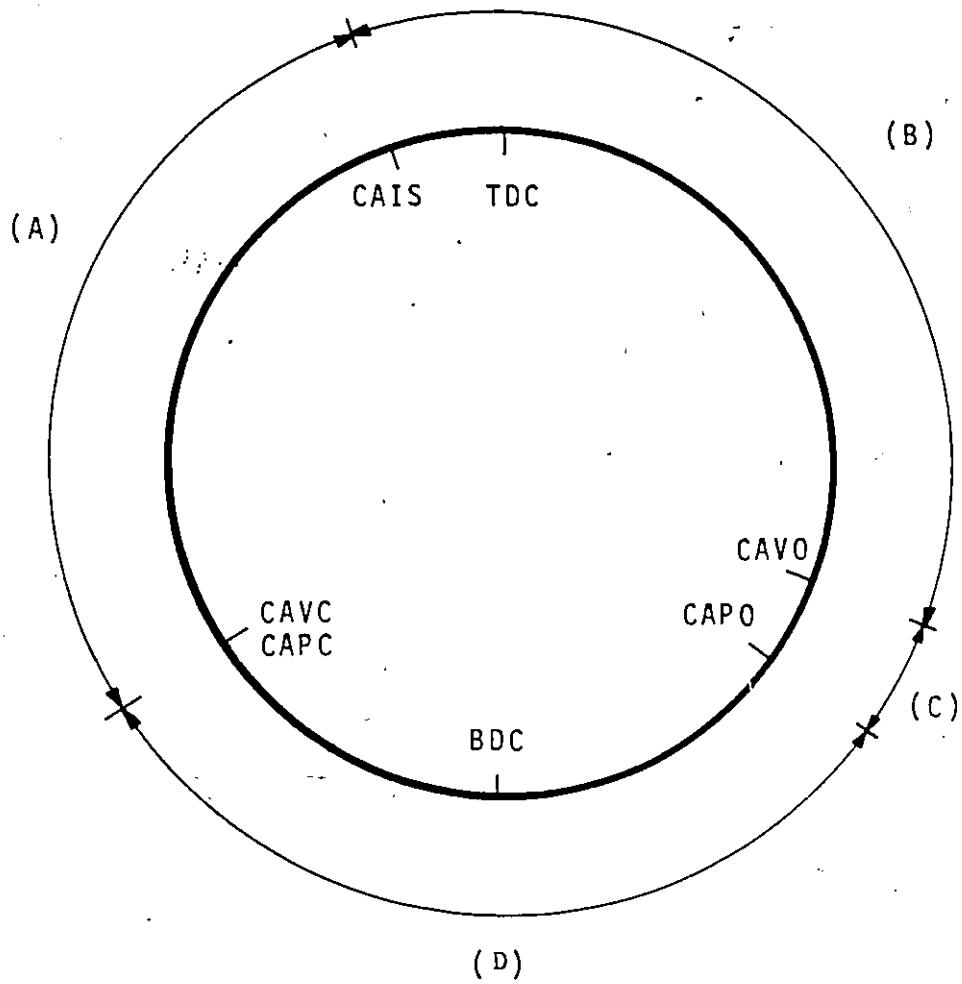

Where:

BDC - BOTTOM DEAD CENTER
TDC - TOP DEAD CENTER
CAVO - CRANK ANGLE VALVES OPENED (100 ATDC)
CAVC - CRANK ANGLE VALVES CLOSED (236 ATDC)
CAPO - CRANK ANGLE PORTS OPENED (125 ATDC)
CAPC - CRANK ANGLE PORTS CLOSED (236 ATDC)
CAIS - CRANK ANGLE INJECTION STARTS (VARIABLE)

A - COMPRESSION
B - COMBUSTION-EXPANSION
C - BLOW-DOWN
D - SCAVENGING

Figure 2.2 Diagram of the engine timing (two-stroke cycle).

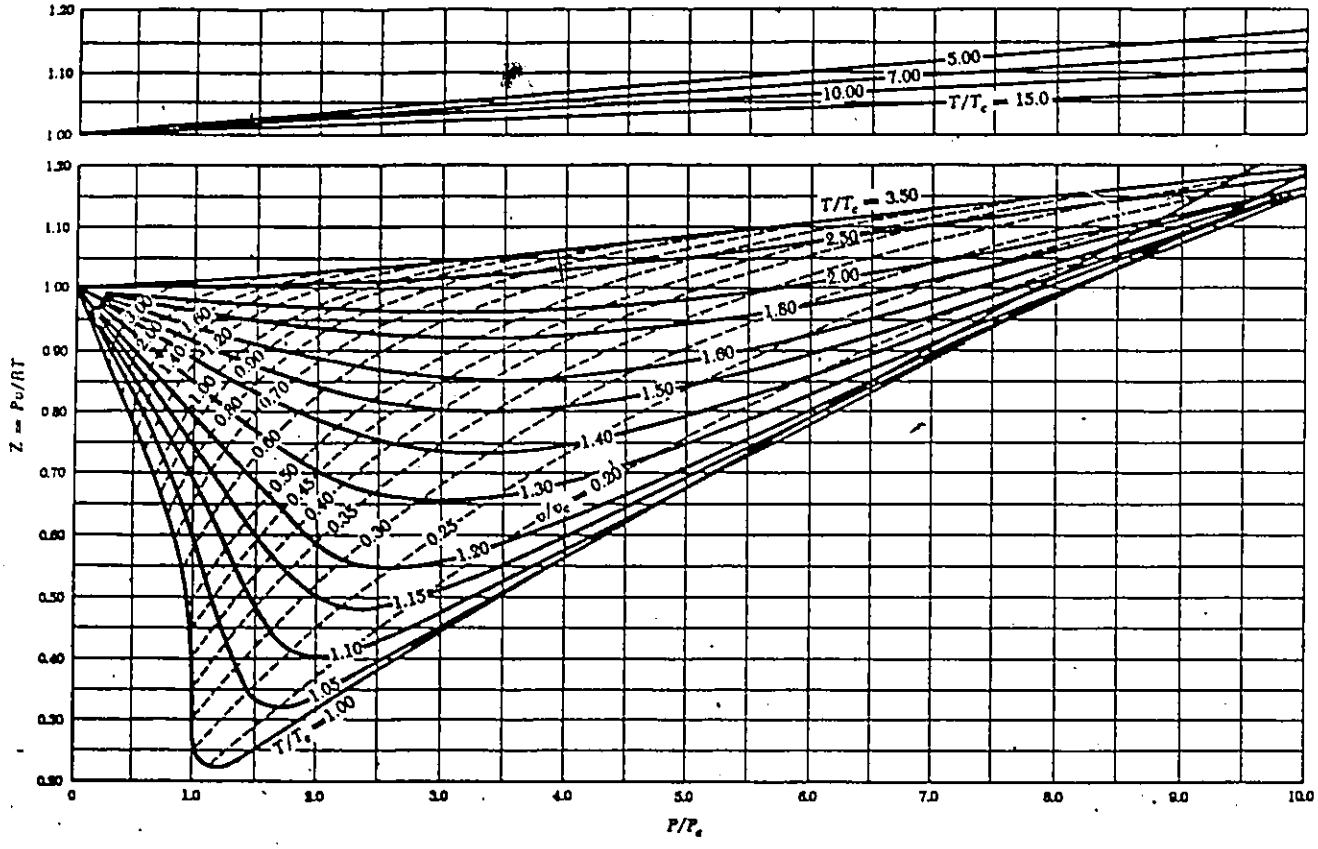

Figure 2.3 General compressibility chart (low pressure range).

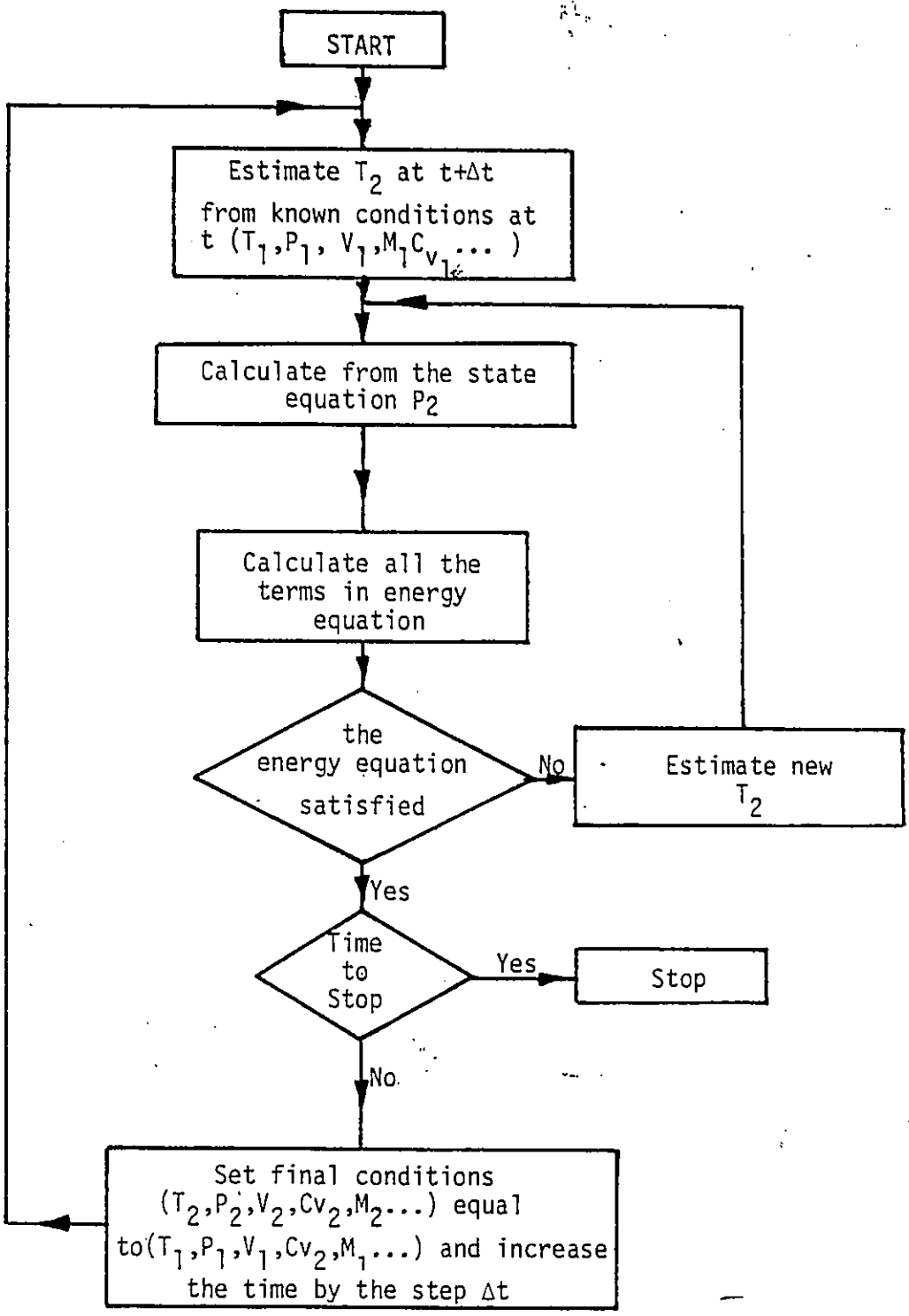

Figure 2.4 Basic flow diagram for the thermodynamic cycle calculations.

ENGINE DIMENSIONS

BORE	3.8750
STROKE	4.5000
ROD LENGTH	8.8000
PISTON TO HEAD CL.	0.0340
PORT TOP TO HEAD DIST	3.7630
NUMBER OF PORTS	18.0000
HEIGHT OF PORTS	0.8400
WIDTH OF PORTS	0.5000
NUMBER OF CYLINDERS	1.00

REFERENCE SPEED 2100.00 RPM

CAM LIFT DATA STARTING AT 80.70 DEGREES ATDC FOR EVERY 2.00 DEGREES

CAM INPUT DATA

0.0	0.000040	0.000160	0.000410	0.000950	0.001850	0.003290	0.005490	
0.008660	0.012970	0.018540	0.025440	0.033670	0.043190	0.053900	0.065670	
0.078310	0.091650	0.105490	0.119660	0.133990	0.148310	0.162510	0.176460	
0.190080	0.203290	0.216010	0.228190	0.239770	0.250750	0.261050	0.270650	
0.279540	0.287680	0.295080	0.301720	0.307600	0.312720	0.317060	0.320630	
0.323410	0.325400	0.326600	0.327000	0.326600	0.325400	0.323400	0.320600	
0.317000	0.312600	0.307400	0.301400	0.294600	0.287000	0.278610	0.269420	
0.259450	0.248710	0.237210	0.224980	0.212080	0.198550	0.184470	0.169960	
0.155140	0.140170	0.125240	0.110560	0.096360	0.082880	0.070350	0.058980	
0.048960	0.040380	0.033310	0.027690	0.023410	0.020250	0.017980	0.016310	
0.015000	0.013840	0.012720	0.011600	0.010480	0.009360	0.008240	0.007120	
0.006000	0.004900	0.003840	0.002840	0.001960	0.001240	0.000680	0.000280	
0.000040	0.0							

MASKING OF VALVES NOT CONSIDERED

CRANK ANGLE DEGREES FROM TDC	PISTON TRAVEL INCH FROM TDC	EXHAUST VALVE AREA SQUARE INCHES	INTAKE PORT AREA SQUARE INCHES
101.00	2.96100	0.001	0.0
105.00	3.10493	0.199	0.0
110.00	3.27731	0.530	0.0
115.00	3.44041	0.918	0.0
120.00	3.59344	1.326	0.0
125.00	3.73572	1.721	0.009
126.00	3.76283	1.796	0.103
127.00	3.78950	1.870	0.243
128.00	3.81570	1.942	0.410
129.00	3.84144	2.012	0.595
130.00	3.86672	2.081	0.792
131.00	3.89152	2.148	0.996
135.00	3.98600	2.397	1.830
140.00	4. [illegible]26	2.408	2.795
145.00	4.18823	2.408	3.650
150.00	4.27076	2.408	4.393
155.00	4.34072	2.408	5.022
160.00	4.39802	2.408	5.526
165.00	4.44262	2.408	5.893
170.00	4.47449	2.408	6.130
175.00	4.49362	2.408	6.259
180.00	4.50000	2.408	6.300
185.00	4.49362	2.408	6.259
190.00	4.47449	2.408	6.130
195.00	4.44262	2.408	5.893
200.00	4.39802	2.264	5.526
205.00	4.34072	1.910	5.022
210.00	4.27076	1.511	4.393
215.00	4.18823	1.091	3.650
220.00	4.09326	0.691	2.795
225.00	3.98601	0.358	1.830
229.00	3.89152	0.166	0.996
230.00	3.86672	0.130	0.792
231.00	3.84144	0.097	0.595
232.00	3.81570	0.069	0.410
233.00	3.78950	0.044	0.243
234.00	3.76284	0.024	0.103
235.00	3.73572	0.005	0.009
236.00	3.70815	0.0	0.0
237.00	3.68013	0.0	0.0

TABLE 2.1 Engine (GM6V53T) Geometrical Specifications.

TABLE 2.2: SIMULATION CYCLE INPUT PARAMETERS

A. ENGINE GEOMETRICAL DATA

1. Bore
2. Stroke
3. Connecting rod length
4. Compression ratio
5. Swept volume
6. Crank radius
7. Cam shaft profile
8. Valve opening area as a function of crank angle
9. Port geometry

B. OPERATING PARAMETERS

1. Air-box pressure
2. Exhaust manifold pressure
3. Air-box temperature
4. RPM
5. Injection schedule

TABLE 2-3

FUEL SPECIFICATIONS

PROPERTY	FUEL 1
Density @15°C, kg/L (D1298)	.8403
Distillation (D86)	
I.B.P., °C	173
10% recovered, °C	203
50% recovered, °C	257
90% recovered, °C	323
F.B.P., °C	351
Recovered % vol.	98.0
Carbon Residue, % mass (D524)	1.9
Cloud Point, °C (D2500)	-12
Pour Point, °C (D97)	-18
Kinematic Viscosity @40°C, mm2/S (D445)	2.41
Ash, % mass (D482)	0.000
Water and Sediment, % vol. (D1796)	0.000
Sulphur, % mass (D1552)	0.21
Nitrogen Content (chemiluminescent)ppm by wt	-
Flash Point, °C (D93)	57
Total Acid No. mg KOH/g (D974)	0.03
Corrosion, 3 hr. @100°C (D130)	1a
Cetane Number (D613)	46.7
Cetane Index, ASTM (D976)	48.0
CGSB	
Aniline Point, °C (D611)	64.4
Carbon (By Difference) % mass	86.6
Hydrogen Content, % mass (D3701)	13.4
C/H Ratio	6.6
Smoke Point, mm (D1322)	17.0
Heat of Combustion, MJ/kg (23.4M)	45.63
Hydrocarbon Type Analysis	
Saturates and Olefins, %	77.8
Poly-Aromatics and Polar Compounds, %	0.9
Total Aromatics %	21.3

Coef. / Spec	A(i,1,1)	A(i,2,1)	A(i,3,1)	A(i,4,1)	A(i,5,1)
H	2.5000000E 00	0.0	0.0	0.0	0.0
O	3.0218894E 00	-2.1737249E-03	3.7542203E-06	-2.9947200E-09	9.0777547E-13
N	2.5147937E 00	-1.1243791E-04	2.9647506E-07	-3.2464049E-10	1.2595465E-13
H_2	2.8460849E 00	4.1932116E-03	-9.6119332E-06	9.5122662E-09	-3.3093421E-12
OH	3.8234708E 00	-1.1187229E-03	1.2466819E-03	-2.1035896E-10	-5.2546551E-14
CO	3.7871332E 00	-2.1709526E-03	5.0757337E-06	-3.4737726E-09	7.7216841E-13
NO	4.1469476E 00	-4.1197237E-03	9.6922467E-06	-7.8633639E-09	2.2309512E-12
O_2	3.7189946E 00	-2.5167288E-03	8.5837353E-06	-8.2998716E-09	2.7082180E-12
H_2O	4.1565016E 00	-1.7244334E-03	5.6982316E-06	-4.5930044E-09	1.4233654E-12
CO_2	2.1701000E 00	1.0378115E-02	-1.0733938E-05	6.3459175E-09	-1.6280701E-12
N_2	3.6916148E 00	-1.3332552E-03	2.6503100E-06	-9.7688341E-10	-9.4772234E-14
Ar	2.5000000E 00	0.0	0.0	0.0	0.0
$C_{15}H_{24}$	1.120240 E 00	1.3905710E-02	2.6568370E-06	-1.1560270E-08	5.2386920E-12

Table 2.4: Polynomial coefficients for temperature range of 300-1000 K.

Coef. / Spec.	A(i,1,2)	A(i,2,2)	A(i,3,2)	A(i,4,2)	A(i,5,2)
H	2.5000000E 00	0.0	0.0	0.0	0.0
O	2.5372567E 00	-1.8422190E-05	-8.8017921E-09	5.9643621E-12	-5.5743608E-16
N	2.4422261E 00	1.2276187E-04	-8.4992719E-08	2.1400830E-11	-1.2511058E-15
H_2	3.0436897E 00	6.1187110E-04	-7.3993551E-09	-2.0331907E-11	2.4593791E-15
OH	2.8895544E 00	9.9835061E-04	-2.1879904E-07	1.9802785E-11	-3.842940E-16
CO	2.9511519E 00	1.5525567E-03	-6.1911411E-07	1.1350336E-10	-7.782732E-15
NO	3.1529360E 00	1.4059955E-03	-5.7078462E-07	1.0628209E-10	-7.3720783E-15
O_2	3.5976129E 00	7.8145603E-04	-2.2386670E-07	4.2490159E-11	-3.3460204E-15
H_2O	2.6707532E 00	3.0317115E-03	-8.5351570E-07	1.1790853E-10	-6.1973568E-15
CO_2	4.4129266E 00	3.1922896E-03	-1.2978230E-06	2.4147446E-10	-1.6742986E-14
N_2	2.8545761E 00	1.5976316E-03	-6.2566254E-07	1.1315849E-10	-7.6897070E-15
Ar	2.5000000E 00	0.0	0.0	0.0	0.0
$C_{13}H_{24}$	3.5023510E 00	1.1592100E-02	-4.4752300E-06	7.9452130E-10	-5.3235680E-14

Table 2.5: Polynomial coefficients for temperature range 1000-5000 K.

CHAPTER 3

COMBUSTION-EXPANSION PROCESS

3.1 INTRODUCTION

The combustion process is assumed to start at the time that the fuel starts to be injected in the cylinder. In reality, the process does not start before the end of the ignition delay; until then the compression continues with the addition of the fuel. The ignition delay as a part of the combustion process has been selected for study because the fuel injection and fuel evaporation continue during combustion. The combustion is assumed terminated when no more fuel or oxygen exists in the cylinder. After the end of combustion the expansion process starts until the exhaust valves open. The three processes and the models used will be discussed in the following sections.

3.2 IGNITION DELAY MODEL

Ignition delay is the period from the beginning of the fuel injection to the time when there is a measurable pressure rise due to combustion. The delay can be divided into physical and chemical delays. The physical delay is the time required for the fuel droplets to be partly vaporized and the fuel vapour to be mixed with the surrounding air. During that period preflame reactions are negligible and only physical processes are taking place. The chemical delay is the period from the end of the physical delay to the beginning of combustion. During the chemical delay, preflame chain reactions occur while physical processes continue. Many ignition delay models have been developed [1-4] and all of them are empirical, limited in application to one particular engine. Therefore, the empirical constants used in

such models must be adjusted to the particular engine using experimental data. In this study the Henein and Bolt [1] model is used.

The Henein and Bolt model [1] was derived from tests on a Lister-Blackstone engine and the effect of the following parameters on the ignition delay were studied: cylinder pressure, fuel/air ratio, fuel injection pressure, cooling water temperature and engine speed. In conclusion the following relation was proposed:

$$ID = \frac{a}{P^b} \qquad (3-1)$$

where:

P - is the cylinder pressure at the beginning of injection (atm)

a - is a constant or a function of the cylinder temperature

b - is a constant or a function of the engine speed

ID - is the ignition delay

3.3 FUEL INJECTION MODEL

The fuel injection schedule is an input to the simulation program. Typical schedules can be seen in table 3.1 for full rack, and speeds of 1600, 2100 and 2600 RPM. The simulation program uses both the crank angle and the corresponding total fuel injected as input. The injection model then converts these values to 0.1 degree increments with linear interpolation.

3.4 FUEL EVAPORATION MODEL

The droplet evaporation time and the rate of droplet disappearance are calculated using the following formulae [5,6]:

$$t_v = \frac{\rho_l d_o^2}{8\rho_g \alpha_g ln(B+1)} \qquad (3-2)$$

$$\frac{dd}{dt} = -\frac{4\rho_g \alpha_g ln(B+1)}{\rho_l d} \qquad (3-3)$$

$$B = \frac{C_g(T - T_g)}{L + C_l(T_b - T_f)} \qquad (3-4)$$

Where:

T - is temperature

L - is the fuel latent heat

C - is the heat capacity

ρ - is the density

α - is the thermal diffusivity

d - is the droplet diameter

d_o - is the initial droplet diameter

Subscripts:

g - gas

l - liquid

b - boiling point

f - fuel

The gas properties for the fuel vapour-air mixture surrounding the droplet are approximated by these of air. The gas temperature used for the computation of the properties is 1200 K, which is approximately the temperature of the cylinder gas during the ignition delay period. Therefore, the following values for the constants are used [7].

$\rho_g = 0.30 \ \frac{kg}{m^3}$

$C_g = 1.179 \ \frac{kJ}{kgC}$

$\alpha_g = 2.2510^{-4}\ \frac{m^2}{s}$

The temperature of the fuel (T_f) is 310 K. At this temperature the fuel properties are as follows [8]:

$\rho_l = 840\ \frac{kg}{m^3}$

$C_l = 1.88\ \frac{kj}{kgC}$

The fuel latent heat (L) is $25.75\frac{kj}{kgC}$ and the fuel boiling temperature (T_b) is 523 K. The equations for the evaporation time and the disappearance rate were derived by solving the energy and species concentration equations for a single droplet without combustion, assuming quasi-steady state, and no effect of change in boundary conditions because of fuel evaporation [6]. This model assumes that the evaporation rate of the fuel spray in the engine is proportional to that of a single droplet; the droplet diameter d_o then represents an effective average diameter for the spray, and becomes one of the model constants to be fitted to the experimental data. The amount of fuel vapor in the cylinder at any crank angle location after the start of injection is calculated as explained below.

Assume that the amount of fuel vapour in the cylinder at crank angle X is to be calculated. (X must be greater than the crank angle where injection starts ($CAIS$)). The fuel injected at each time step is assumed to be composed of equal size droplets with a specified diameter. It is also assumed that the cylinder temperature is known from the previous time step. The calculations are as follows:

(a) Calculate the evaporation time for the droplets first injected in the cylinder using equation (3-2).

(b) Check if the available time for evaporation (time corresponding to ($X - CAIS$) degrees) is greater than the droplet evaporation time. If the time is greater then all the injected fuel at that crank angle has been evaporated.

(c) If not, calculate the rate of disappearance from equation (3-3) and calcu-

late the evaporated fuel including vapour from partly-evaporated droplets from previous time steps.

(d) Accumulate all the evaporated fuel.

(e) Go to the next time step and calculate the evaporation time for the injected fuel at that time step.

(f) Check if the crank angle is greater than X. If it is, stop; if not, go back to step (B) and repeat the computations.

3.5 COMBUSTION MODEL

As discussed in section 3.2 during the ignition delay period part of the injected fuel is evaporated and mixed with the air forming a combustible mixture. In the early combustion the fuel burning rate is very high due to premixed conditions. During the period of premixed combustion the fuel burning rate is calculated using the following formula [6]:

$$PRR = aM_o^b M_f^c exp(-\frac{d}{T}) \qquad (3-5)$$

Where:

M_o - is the oxygen mass fraction

M_f - is the fuel vapour mass fraction

PRR - is the premixed reaction rate (kg/CA)

a, b, c, d - are constants

Equation (3-5) is assumed to be valid until the amount of fuel evaporated at the end of the ignition delay has been consumed. Therefore, when all the initial vapour has been consumed, the premixed reaction rate is zero and the combustion is assumed to be dominated by the fuel-oxygen mixing rate according to the following reaction rate equation derived by Whitehouse [9]:

$$MCR = aM_i^x M_{fu}^{x-1} P_o^b \qquad (3-6)$$

Where:

M_i - is the total fuel injected at that crank angle

P_o - is the oxygen partial pressure

MCR - is the mixing control reaction rate (kg/CA)

a, b, x - are constants

For the calculation of the mass burning rate both rates (equations (3-5) and (3-6)) are assumed to contribute to the early combustion, but, in the reality, the premixed combustion is dominant. Based on two stroke diesel measurements Whitehouse recommends the following values for the constants in equation (3-6):

$$a = 0.0170$$

$$x = 1.0$$

$$b = 0.4$$

3.6 COMBUSTION CALCULATIONS

During combustion the fuel burning rate is calculated using the combustion model discussed in section 3.3. The combustion is assumed to take place at the mean cylinder temperature and pressure. The following equation is used:

$$x_{13}[C_{13}H_{24} + \frac{37}{\phi}(O_2 + 3.7274N_2 + 0.0444Ar)] \Longrightarrow x_1H + x_2O + x_3N + x_4H_2 + x_5OH$$

$$+ x_6CO + x_7NO + x_8O_2 + x_9H_2O + x_{10}CO_2 + x_{11}N_2 + x_{12}Ar \qquad (3-7)$$

where x_1 to x_{12} are the mole fractions of the product and x_{13} the number of moles of fuel that will give one mole of products

The fuel-air equivalence ratio ϕ is calculated based on the instantaneous amount of fuel in the cylinder. During combustion chemical equilibrium is assumed and the mole fractions x_1 to x_{12} and x_{13} are calculated using reference [10]. The heat released during the time step is calculated from the heat of formation of the participating species in the reaction as follows:

$$Q_{comb} = \sum_{i=1}^{Pr} n_i H_{f,T_i} - \sum_{j=1}^{Rc} n_j H_{f,T_j} \qquad (3-8)$$

Where:

n_i - is the number of moles of the product species i

H_{f,T_i} - is the heat of formation of product species i

n_j - is the number of moles of the reactant species j

H_{f,T_j} - is the heat of formation of reactant species j

Pr - is the number of product species

Rc - is the number of reactance species

The heats of formation of the species used in the computations are given in table 3-2 [5,11]. The heat of formation of the fuel was calculated from the fuel lower heating value.

3.7 ENERGY EQUATION

The energy equation during ignition delay-combustion-expansion for the cylinder control volume is written as follows:

$$\frac{\partial E}{\partial t} = \frac{\partial Q}{\partial t} - \frac{\partial W}{\partial t} + \frac{\partial m_b}{\partial t} Q_{comb}$$

The heat absorbed by the fuel during ignition delay and combustion is negligible and is ignored (the heat of evaporation is approximately 0.5 per cent of the fuel lower heating value). The energy equation is written in finite difference form for a time interval Δt as follows:

$$E_2 - E_1 = \Delta Q - \Delta W + \Delta m_b Q_{comb} \qquad (3-9)$$

where Δm_b is the amount of fuel burned during the time step Δt.

During the ignition delay period the heat released due to combustion is zero. Therefore, the compression process continues up to the end of the delay period. After the end of the combustion period the expansion process continues up to the point where the exhaust valves open and the blowdown period starts. Usually in two stroke engines the expansion process is not observed because the available time for combustion is much shorter than in four stroke engines, and the combustion continues up to the beginning of the blowdown process.

3.8 SOLUTION PROCEDURE DURING IGNITION DELAY, COMBUSTION AND EXPANSION

The solution procedure is similar to the one used for compression (section 2.5) with different equations used. A short description will be presented next:

(A) The amount of fuel burned during the time step Δt is calculated using equations (3-5) and (3-6) (during the ignition delay the fuel burning rate is zero). In equations (3-5) and (3-6) the previous time step pressure, temperature, and gas composition are used.

(B) The temperature T_2 at the end of the time step Δt is calculated using the following simplified expression of the energy equation:

$$MC_v(T_1)(T_2 - T_1) = -P_1(V_1 - V_2) + q_{lhv}\Delta m_b \qquad (3-10)$$

where q_{lhv} - is the fuel lower heating value. The temperature T_2 is given by:

$$T_2 = T_1(1.0 + \frac{R_{mol}}{C_v(T_1)}(\frac{V_2}{V_1} - 1.0)) + \frac{q_{lhv}\Delta m_b}{MC_v(T_1)} \qquad (3-11)$$

(C) The cylinder pressure is calculated using the state equation (equation (2-1)).

(D) All the terms in the energy equation (eqn. (3-11)) are calculated to check if it is satisfied. It is assumed to be satisfied if:

$$\Delta T = \frac{E_1 - E_2 + Q - W + m_b Q_{comb}}{MC_v(T_2)} < 0.01 \qquad (3-12)$$

As in section 2.4, if the energy equation (eqn. 3-12) is satisfied, the estimated temperature and pressure are correct and the computations are advanced in time. If equation (3-12) is not satisfied a new temperature is estimated using equation (2-25) and the computations are repeated starting at step (C) until convergence is reached.

REFERENCES

1 Henein, N. A,. and Bolt, J. A."Ignition Delay in Diesel Engine", SAE Paper 670007, 1967.

2 Wong, C. C., and Steere, D. E. "The effects of Diesel Fuel Properties and Engine Operating Conditions on Ignition Delay", SAE Paper 821231, 1982.

3 Hardenberg, H. O., and Hase, F. W. " An Empirical Formula for Computing the Pressure Rise Delay of a Fuel from its Cetene Number and from the Relevant Parameters of Direct Compression Diesel Engines", SAE Paper 790493, 1979.

4 Wolfer, H. H. "Ignition Lag in the Diesel Engine", VDI Forschungsheft No 392, 1938.

5 Kanuri, A. M. "Introduction to Combustion Phenomena", Gordon and Breac Science Publishers, Second Printing, 1977.

6 Spalding, D. B. " Combustion and Mass Transfer", Pergamon Press, 1979.

7 Holman, J. P. " Heat Transfer", McGraw-Hill Book Company, New York, 1981.

8 Taylor, C. F. "The Internal Combustion Engine in Theory and Practice", The M.I.T. Press, 1979.

9 Whitehouse, N. D., and Way, R. " Rate of Heat Release in Diesel Engines and its Correlation with Fuel Injection Data", Proc. Instn. Mech Engrs Vol. 184 Pt3J, 1969-70, Paper 1.

10 Olikara, C., and Borman, G. " A Computer Program for Calculating Properties of Equilibrium Combustion Products With Some Applications to I.C. Engines", SAE Paper 750468, 1975.

11 DOW CHEMICAL COMPANY - JANAF Thermochemical Tables, 1962, Addendum 1966.

TABLE 3.1

INJECTION SCHEDULES FOR DIFFERENT RPM
(DATA FROM GENERAL MOTORS)

1600 RPM		2100 RPM		2600 RPM	
CRANK ANGLE DEGREES	INJECTED TOTAL mm^3	CRANK ANGLE DEGREES	INJECTED TOTAL mm^3	CRANK ANGLE DEGREES	INJECTED TOTAL mm^3
-18.170	0.0	-18.700	0.0	-18.410	0.0
-17.990	0.100	-18.000	0.300	-17.970	0.100
-16.990	1.100	-17.000	1.500	-16.970	0.900
-16.530	1.900	-16.700	1.900	-16.220	1.800
-15.990	2.800	-16.000	2.900	-15.970	2.100
-14.990	5.000	-15.000	4.700	-14.970	3.700
-13.990	7.500	-14.000	6.700	-13.970	5.500
-12.990	10.300	-13.000	9.000	-12.970	7.600
-11.990	13.300	-12.000	11.500	-11.970	9.800
-10.990	16.600	-11.000	14.100	-10.970	12.200
-9.990	20.100	-10.000	17.000	-9.970	14.800
-8.990	23.800	-9.000	20.100	-8.970	17.400
-7.990	27.600	-8.000	23.400	-7.970	20.300
-6.990	31.500	-7.000	26.900	-6.970	23.200
-5.990	35.500	-6.000	30.400	-5.970	26.200
-4.990	39.600	-5.000	34.100	-4.970	29.400
-3.990	43.900	-4.000	37.800	-3.970	32.600
-2.990	48.200	-3.000	41.500	-2.970	35.900
-1.990	52.600	-2.000	45.400	-1.970	39.400
-0.990	57.100	-1.000	49.300	-0.970	42.900
0.010	61.700	0.0	53.200	0.020	46.600
1.010	65.800	1.000	57.200	1.020	50.300
2.010	69.000	2.000	60.900	2.020	53.800
2.690	70.300	3.000	63.700	3.020	56.800
3.010	70.600	4.000	65.400	4.020	59.000
		5.000	65.600	5.090	60.400
				6.020	60.700

SPECIES	HEAT OF FORMATION j/kg-mol	SPECIES	HEAT OF FORMATION j/kg-mol
H	2.1501 E08	O_2	0.0
O	2.4579 E08	H_2O	-2.3853 E08
N	4.6645 E08	CO_2	-3.8815 E08
H_2	0.0	N_2	0.0
OH	3.8433 E07	Ar	0.0
CO	-1.0902 E08	$C_{13}H_{24}$	-2.1111 E08
NO	8.9143 E07		

Table 3.2: Heat of formation for the species used in the simulation program at 1 atm and 298.15 K.

CHAPTER 4

BLOWDOWN-SCAVENGING PROCESS

4.1 INTRODUCTION

The blowdown period runs from the time when the exhaust valves open (at 100 degrees ATDC) until the inlet ports open (at 125 degrees ATDC). During this period the cylinder pressure drops significantly to values close to the air-box pressure. The cylinder pressure near the end of the blowdown is usually higher than the air-box pressure; therefore, at the beginning of the scavenging process back flow through the inlet ports is observed. The scavenging process starts when the inlet ports open and continues until the exhaust valves and ports close (at 56 degrees ABDC). During scavenging both the exhaust valves and the inlet ports are open and the incoming air replaces the cylinder residual gases from the previous cycle. The process is very important because the available oxygen for combustion is strongly dependent on the scavenging efficiency, which is defined as the mass of air trapped in the cylinder divided by the mass of air required to fill the cylinder volume at air-box pressure and temperature. The scavenging efficiency is a function of the scavenging ratio, which is the mass of air supplied to the cylinder divided by the mass of air required to fill the cylinder volume at air-box pressure and temperature. From the modeling point of view the scavenging process is very difficult to study. The cylinder geometry with the inlet ports and exhaust valves is the most significant factor for the scavenging efficiency. Thermodynamic models, therefore, fail to provide information on the scavenging efficiency-scavenging ratio relationship. Such a relationship is obtained from multi-dimensional modeling discussed separately in chapters 5 and 6. Here, the models for computing the amount of air entering and the amount of gas leaving the cylinder will be presented

together with the method of computing the composition of the gas leaving the cylinder.

4.2 FLOW THROUGH THE EXHAUST VALVES AND INLET PORTS

The flow through the exhaust valves is unsteady, compressible and multidimensional. However, it has been shown by many investigators [1-5] in the engine modeling field that such a flow can be studied using the quasi-steady approach for isentropic compressible flow through a nozzle or an orifice.

The mass flow rate through the exhaust valves is calculated as follows:
A) For the gas flowing from the cylinder to the exhaust pipe ($P > P_e$, where P_e is the exhaust pipe pressure) two possibilities exist:

a) The flow is sonic at the valve throat:

$$\frac{P}{P_e} \geq \left(\frac{2}{k+1}\right)^{\frac{k}{k-1}} \qquad (4-1)$$

Then:

$$\frac{dM_l}{dt} = C_{d1} A_v P f_1 \qquad (4-3)$$

Where:

A_v - is the valve opening area

M_l - is the mass leaving the cylinder.

k - is the isentropic expansion coefficient

and

$$f_1 = \left[\frac{k}{RT}\left(\frac{2}{k+1}\right)^{\frac{k+1}{k-1}}\right]^{\frac{1}{2}} \qquad (4-2)$$

b) The flow is subsonic at the valve throat:

$$\frac{P}{P_e} < (\frac{2}{k+1})^{\frac{k}{k-1}} \qquad (4-4)$$

Then:

$$\frac{dM_l}{dt} = C_{d1} A_v P f_2 \qquad (4-5)$$

Where:

$$f_2 = [\frac{2k}{(k-1)RT}((\frac{P_e}{P})^{\frac{2}{k}} - (\frac{P_e}{P})^{\frac{k+1}{k}})]^{\frac{1}{2}} \qquad (4-6)$$

B) If the gas flows from the exhaust pipe to the cylinder ($P_e > P$) and:

a) The flow is sonic at the vaive throat, therefore:

$$\frac{P}{P_e} \leq (\frac{2}{k+1})^{\frac{k}{k-1}} \qquad (4-7)$$

Then:

$$\frac{dM_l}{dt} = -C_{d2} A_v P_e f_3 \qquad (4-8)$$

Where:

$$f_3 = [\frac{k}{RT_e}(\frac{2}{k+1})^{\frac{k+1}{k-1}}]^{\frac{1}{2}} \qquad (4-9)$$

b) The flow is subsonic at the valve throat, therefore:

$$\frac{P}{P_e} > (\frac{2}{k+1})^{\frac{k}{k-1}} \qquad (4-10)$$

Then:

$$\frac{dM_l}{dt} = -C_{d2} A_v P_e f_4 \qquad (4-11)$$

Where:

$$f_4 = [\frac{2k}{(k-1)RT_e}((\frac{P}{P_e})^{\frac{2}{k}} - (\frac{P}{P_e})^{\frac{k+1}{k}})]^{\frac{1}{2}} \qquad (4-12)$$

C_{d1} and C_{d2} are the discharge coefficients when gas flows out of and in to the cylinder respectively. Values for the coefficients are given in figure 4.1 [4].

It can be seen that the discharge coefficients are a function of the valve opening. In the simulation program a second order polynomial was fitted to the curves in figure 4.1. The coefficients are given next.

1) For out flow through the valves (fig. 4.1)

$$C_{d1} = 1.0 - 0.1583X - 0.2917X^2 \qquad (4-13)$$

Where:

$$X = \frac{V_{op}}{V_{max}} \qquad (4-14)$$

V_{op} is the valve opening which is input to the program using the cam shaft profile and V_{max} is the valve maximum lift (table 2.1).

B) For back flow through the valves (fig. 4.1)

$$C_{d2} = 0.60 + 1.6X - 1.6X^2 \qquad (4-15)$$

The value X is given in equation (4-14)

Using data obtained from General Motors (Table 2.1) the exhaust valve area is input as a function of the crank angle. For crank angle values between the ones given in table 2.1 linear interpolation is used

The mass flow rate through the inlet ports for subsonic flow is calçulated as follows:

A) If the gas flows from the air-box to the cylinder ($P_{ab} > P$, where P_{ab} is the air-box pressure):

$$\frac{dM_e}{dt} = C_d A_p P_{ab} f_5 \qquad (4-16)$$

Where:

A_p - is the port opening area

M_e - is the mass entering the cylinder.

and

$$f_5 = [\frac{2k}{(k-1)RT_{ab}}((\frac{P}{P_{ab}})^{\frac{2}{k}} - (\frac{P}{P_{ab}})^{\frac{k+1}{k}})]^{\frac{1}{2}} \qquad (4-17)$$

B) If the gas flows from the cylinder to the air-box ($P_{ab} < P$):

$$\frac{dM_e}{dt} = -C_d A_p P f_6 \qquad (4-18)$$

Where:

$$f_\theta = [\frac{2k}{(k-1)RT}((\frac{P_{ab}}{P})^{\frac{2}{k}} - (\frac{P_{ab}}{P})^{\frac{k+1}{k}})]^{\frac{1}{2}} \qquad (4-19)$$

As with the discharge coefficients for the exhaust valves, the value of C_d depends on the ports opening (see figure 4.1). In the simulation program, C_d is calculated as follows:

$$C_d = 0.4523 + 1.1947Y - 0.997Y^2 \qquad (4-20)$$

For: $Y \geq 0.7$

and

$$C_d = 0.8 \qquad for \quad Y < 0.7 \qquad (4-21)$$

Where

$$Y = \frac{A_p}{A_{max}}$$

A_p - is the port area

A_{max} - is the port maximum area

If S is the piston distance from the TDC, the port area A_p is calculated as a function of the crank angle as follows (S is calculated using equation (2-15))

(a) If $S_a < S < S_b$ (see figure 4.2) and

$$\theta = arcos(1.0 - \frac{S - S_a}{R_a}) \qquad (4-22)$$

Then:

$$A_p = 9.0R_a^2(\theta - sin(\theta)) \qquad (4-23)$$

(b) If $S_b < S < S_c$

Then:

$$A_p = 18[1.57R_a^2 + 2R_a(S - S_b)] \qquad (4-24)$$

(c) If $S_c < S < S_d$ and

$$\theta = arcos(\frac{S - S_c}{R_a}) \qquad (4-25)$$

Then:

$$A_p = 18[3.14R_a^2 + 2R_aR_s - R_a^2(\theta - sin(\theta))] \qquad (4-26)$$

4.3 BLOW-DOWN AND SCAVENGING PROCESSES

4.3.1 BLOW-DOWN

As mentioned earlier, the blow-down process runs from the time when the exhaust valves open until the inlet ports open. Assume that the cylinder species composition at the beginning of scavenging is X_i, $i = 1, 12$ (moles) with X_8 for oxygen and X_{11} for nitrogen. From section 4.2 the mass leaving the cylinder (ΔM_l) during the time step Δt can be calculated. Assuming the cylinder gas to be uniform the cylinder gas composition at the end of the time step Δt will be:

$$(X_i)_{new} = (X_i)_{old}(1 - \frac{\Delta M_l}{X_m}) \qquad (4-27)$$

Where:

$$X_m = \sum_{i=1}^{12} X_i M_{w,i} \qquad (4-28)$$

4.3.2 SCAVENGING

The scavenging process takes place when the inlet and exhaust ports are open and the incoming air replaces the residual gases from the previous cycle. The question about the scavenging process is how the air replaces the residual gases and therefore what the gas composition in the cylinder during scavenging is. At this stage the scavenging efficiency versus scavenging ratio equation is not known. Assuming that the scavenging efficiency is a function (F) of the scavenging ratio, or:

$$\eta_{sc} = F(R_{sc}) \qquad (4-29)$$

where: η_{sc} is the scavenging efficiency, defined as the mass of air trapped in the cylinder divided by the mass of air required to fill the cylinder volume at air-box pressure and temperature, and R_{sc} is the scavenging ratio, defined as the mass of air supplied to the cylinder divided by the mass of air required to fill the cylinder volume at air-box pressure and temperature.

The computations proceed in the following manner:

a) Normal scavenging (inflow from the ports, outflow from the exhaust valves):

Let us assume that the scavenging ratio at time t is known (can be calculated from the total amount of air supplied at time t). From equations (4-1) to (4-12) the amount of air entering the cylinder (ΔM_c) and the amount of gas leaving the

cylinder (ΔM_l) during the time stepΔt can be calculated. During scavenging the problem is to find what is the composition of the mass ΔM_l. If this composition is known the cylinder composition during scavenging can be calculated.

Suppose that air in the cylinder can still be identified after mixing with exhaust gases. During the step Δt the portion of the supplied air remaining in the cylinder will be:

$$\Delta M_{st} = \Delta M_c (\frac{d\eta_{sc}}{dR_{sc}})_{R_{sc}} \qquad (4-30)$$

Where:

ΔM_{st} - is the air staying (retained) in the cylinder

The amount of air escaping the cylinder will be:

$$\Delta M_{esc} = \Delta M_c - \Delta M_{st} \qquad (4-31)$$

Where:

ΔM_{esc} - is the air escaping the cylinder

Thus, the composition of the gas ΔM_l will be ΔM_{esc} of air and $(\Delta M_l - \Delta M_{esc})$ of residual gases. If $\Delta M_l < \Delta M_{esc}$ the air staying in the cylinder will be:

$$\Delta M_{st} = \Delta M_c - \Delta M_l \qquad (4-32)$$

andΔM_l will be pure air.

b) Early scavenging with back flow:

In early scavenging, back flow from the cylinder to the air-box can be observed. During that period the scavenging ratio is negative. The composition of the gas entering and leaving the cylinder is assumed to be the same as the cylinder composition. This continues until the scavenging ratio becomes positive.

c) Late scavenging with back flow from the cylinder to the air-box

This is observed when $\Delta M_e < 0$. The composition of the mass ΔM_e is assumed to be that of pure air. The composition of ΔM_l is assumed to be the same as in the previous time step.

d) Back flow through the valves:

If $\Delta M_l > 0$ the composition of ΔM_l of the previous time step is used.

It should be noted that cases c) and d) are very rare and the computations take place under the conditions of cases a) or b).

This computational technique has been developed because it can be used with any scavenging efficiency-scavenging ratio relationship. Such a formula can be derived from multidimensional models as will be seen later (chapters 5 and 6).

4.4 ENERGY EQUATION

The energy equation during scavenging is written as:

$$\frac{\partial E}{\partial t} = \frac{\partial Q}{\partial t} - \frac{\partial W}{\partial t} - h_l \frac{\partial M_l}{\partial t} + h_e \frac{\partial M_e}{\partial t} \qquad (4-33)$$

Equation (4-33) is written in finite difference form for a time interval Δt as follows:

$$E_2 - E_1 = \Delta Q - \Delta W - h_l \Delta M_l + h_e \Delta M_e \qquad (4-34)$$

Where:

h_l - is the enthalpy of the gas leaving the cylinder

h_e - is the enthalpy of the gas entering the cylinder

The enthalpies of the gases entering and leaving the cylinder are calculated using the formulae from section 2.3. The mass composition of the gases leaving and entering the cylinder and also the cylinder gas composition are calculated using the

scavenging model (section 4.3). The values of ΔM_e and ΔM_l have been calculated in section 4.2. Finally, the computations for the internal energy, work, and heat transfer are presented in section 2.3, section 2.4, and chapter 7 respectively.

4.5 SOLUTION PROCEDURE DURING BLOWDOWN AND SCAVENGING

During blowdown and scavenging the same iterative procedure described in section 2.5 is used. The temperature and pressure are estimated using the following formulae:

$$T_2 = T_1 (\frac{M_1}{M_2})(\frac{V_1}{V_2})^{\frac{R_{mol}}{C_v(T_1)}} \qquad (4-35)$$

$$P_2 = M_2 R_{mol} T_2 / V_2 \qquad (4-36)$$

and the energy equation is assumed to be satisfied if:

$$\Delta T = \frac{E_1 - E_2 + \Delta Q - \Delta W - h_l \Delta M_l + h_e \Delta M_e}{M C_v(T_2)} < 0.01 \qquad (4-37)$$

REFERENCES

1 Borman, G. L. "Mathematical Simulation of Internal Combustion Engine Processes and Performance Including Comparisons with Experiment", Ph.D. Thesis University of Wisconsin, 1964.

2 Taylor, C. F. "The Internal Combustion Engine in Theory and Practice", The M.I.T. Press, Third Printing, 1979.

3 Benson, R. S. "The Thermodynamics and Gas Dynamics of Internal Combustion Engines", Vol. 1, Clarenton Press, Oxford 1982.

4 Benson, R. S., and Galloway, K. "An Experimental and Analytical Investigation of the Gas Exchange Process in a Multi-Cylinder Pressure Charged Two Stroke Engine ", Instn. Mech. Engrs. Vol. 183, Pt 1, No 14, 1968-69.

5 Schweitzer, P. H. "Scavenging of Two Stroke Cycle Diesel Engines", The MacMillan Publishing Company, 1949.

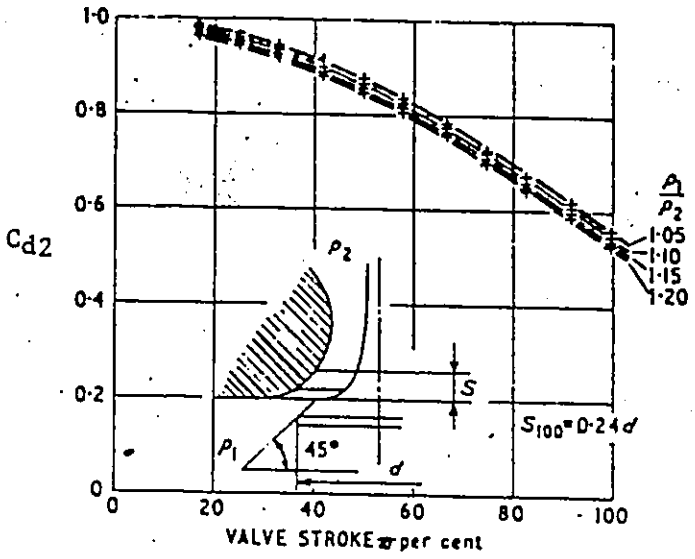

Flow from the exhaust pipe to the cylinder

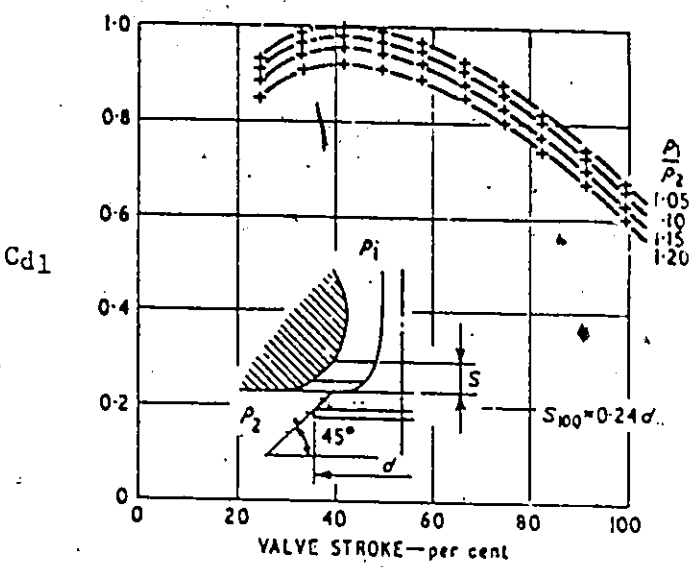

Flow from the cylinder to the exhaust pipe

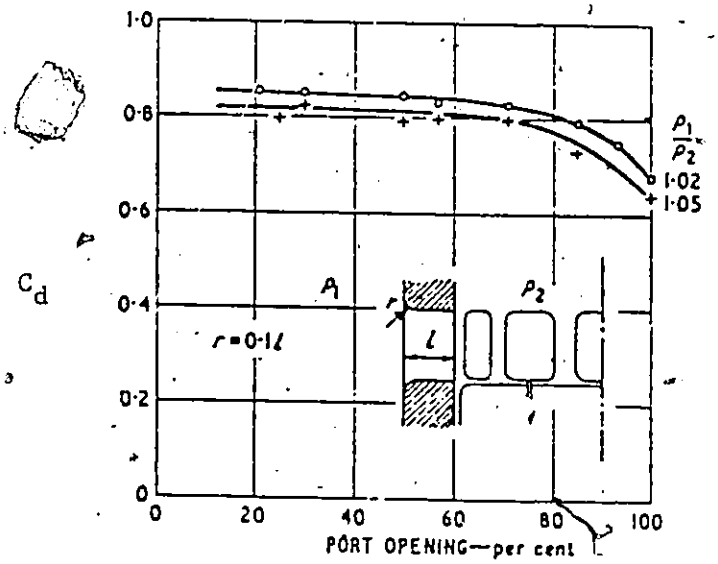

Figure 4.1 Discharge coefficients for the exhaust valves and inlet ports.

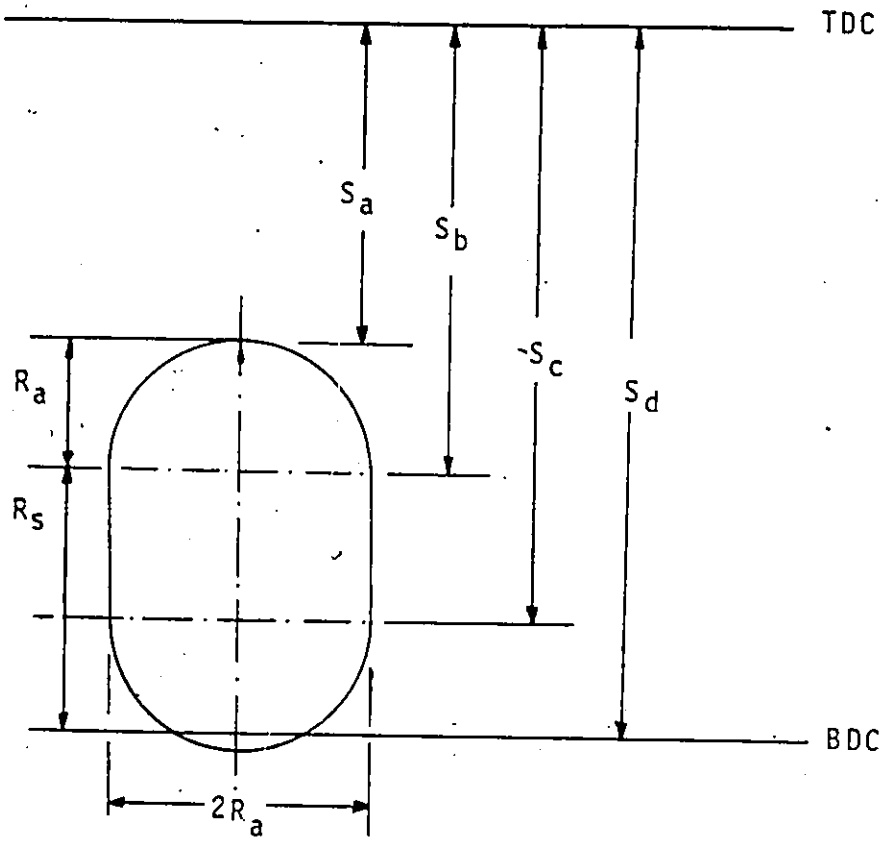

Where:

R_a - 6.35 mm	S_b - 101.1 mm
R_s - 8.64 mm	S_c - 109.7 mm
S_a - 94.72 mm	S_d - 114.3 mm

Figure 4.2 Engine port geometry.

CHAPTER 5

MULTIDIMENSIONAL ANALYSIS FOR SCAVENGING STUDIES TWO-DIMENSIONAL MODEL

5.1 INTRODUCTION

In the thermodynamic model presented and discussed in the previous sections, a number of simplifications were utilized to describe the physical phenomena in the engine. In thermodynamic models, the cylinder gas is assumed uniform and the pressure variation within the cylinder is ignored. The gas motion in the cylinder cannot be predicted and therefore cannot be modeled. Empirical formulae are used instead. In multi-dimensional models these types of assumptions are not needed and only information at the fluid boundaries is required. In multidimensional models, the differential conservation equations which govern the flow, heat and mass transfer processes within the cylinder are solved numerically at a finite number of points. Therefore, for problems which are geometry dependent, multi-dimensional models are used. However, in cases where the geometry does not strongly influence the processes taking places, thermodynamic models are used because they are less expensive to develop and use. In two-stroke engines the scavenging process strongly depends on the engine geometry, and therefore multi-dimensional models must be used.

In this work, a transient two-dimensional code with swirl has been developed for studying the scavenging process. The code is based on the Implicit Continuous-fluid Eulerian (ICE) numerical technique [1] for solving the continuity and momentum equations. The K - ϵ turbulence model is used for computing the effective viscosity. The energy, species and momentum equations are solved simultaneously. The model was tested against experimental data for channel-driven cavity

flow and the steady state TEACH code. The scavenging efficiency is calculated using results obtained from the solution of the species equation. The scavenging efficiency-scavenging ratio relationship is derived and later used in the thermodynamic model.

5.2 MATHEMATICAL FORMULATION

The mathematical formulation of the multidimensional model used for the computations of the scavenging efficiency is presented below. The fundamental differential equations which govern the properties of non-reacting flows are the conservation equations of mass, momentum, energy and species. These equations are written as follows for two-dimensional flows with swirl [2]:

MASS CONSERVATION

$$\frac{\partial \rho}{\partial t} + \frac{1}{R}\frac{\partial}{\partial r}(R\rho u) + \frac{\partial}{\partial y}(\rho v) = 0 \qquad (5-1)$$

MOMENTUM EQUATIONS

r - component

$$\frac{\partial}{\partial t}(\rho u) + \frac{1}{R}\frac{\partial}{\partial r}(\rho R u u) + \frac{\partial}{\partial y}(\rho v u) = -\frac{\partial P}{\partial r} + \frac{\partial}{\partial y}(\mu\frac{\partial u}{\partial y}) + \frac{2}{R}\frac{\partial}{\partial r}(\mu R\frac{\partial u}{\partial r}) + \frac{\partial}{\partial y}(\mu\frac{\partial v}{\partial r}) + \delta\frac{2\mu u}{r^2} - \delta\frac{\rho w w}{r} \qquad (5-2)$$

y - component

$$\frac{\partial}{\partial t}(\rho v) + \frac{1}{R}\frac{\partial}{\partial r}(\rho R u v) + \frac{\partial}{\partial y}(\rho v v) = -\frac{\partial P}{\partial y} + 2\frac{\partial}{\partial y}(\mu\frac{\partial v}{\partial y}) + \frac{1}{R}\frac{\partial}{\partial r}(\mu R\frac{\partial v}{\partial r}) + \frac{1}{R}\frac{\partial}{\partial r}(\mu R\frac{\partial u}{\partial r}) \qquad (5-3)$$

θ - component

$$\frac{\partial}{\partial t}(\rho w) + \frac{1}{R}\frac{\partial}{\partial r}(\rho R u w) + \frac{\partial}{\partial y}(\rho v w) = +\frac{1}{R}\frac{\partial}{\partial r}(\mu R \frac{\partial w}{\partial r}) + \frac{\partial}{\partial y}(\mu \frac{\partial w}{\partial y})$$
$$+\delta \frac{\rho w u}{r} + \frac{1}{R^2}\frac{\partial}{\partial r}(\rho \mu) \qquad (5-4)$$

ENERGY EQUATION

$$\frac{\partial}{\partial t}(\rho T) + \frac{1}{R}\frac{\partial}{\partial r}(\rho R u T) + \frac{\partial}{\partial y}(\rho v T) = \frac{1}{R}\frac{\partial}{\partial r}(R \frac{\mu}{Pr_t}\frac{\partial T}{\partial r}) + \frac{\partial}{\partial y}(\frac{\mu}{Pr_t}\frac{\partial T}{\partial y}) \qquad (5-5)$$

CONCENTRATION EQUATION

$$\frac{\partial}{\partial t}(\rho C) + \frac{1}{R}\frac{\partial}{\partial r}(\rho R u C) + \frac{\partial}{\partial y}(\rho v C) = \frac{1}{R}\frac{\partial}{\partial r}(R \frac{\mu}{Sc_t}\frac{\partial C}{\partial r}) + \frac{\partial}{\partial y}(\frac{\mu}{Sc_t}\frac{\partial C}{\partial y}) \qquad (5-6)$$

where:

u - is the fluid velocity in the radial direction

v - is the fluid velocity in the axial direction

w - is the fluid velocity in the circumferential direction

ρ - is the fluid density

P - is the fluid pressure

T - is the fluid temperature

C - is the fluid concentration (mass fraction)

Pr_t - is the Prandtl number

Sc_t - is the Schmidt number

R - is equal to r for cylindrical coordinates, and equal to 1.0 for Cartesian coordinates

δ - is equal to 1.0 for cylindrical coordinates, and equal to zero for Cartesian coordinates

For swirling flows, equation (5-4) must be solved for the velocity w. For non-swirling flows the velocity w is set equal to zero without solving equation (5-4).

Equations (5-1) to (5-6) are valid for both laminar and turbulent flows. In the case of laminar flows, the instantaneous values of the velocity, pressure, density etc coincide with the mean values and these equations are therefore relatively easily solved numerically and, in a simplified form, analytically. In the case of turbulent flows, the instantaneous values used in equations (5-1) to (5-6) are not necessarily the same as the mean fluid values.

In turbulent recirculating flows the small eddies play an important role in the flow pattern. The size of the small eddies is in the order of 10^{-3} of the flow characteristic length. Therefore, for numerical solution, an extremely fine grid would have to be used. The approach used in the past, and still used today, is that of averaging all turbulent fluctuating quantities over time and then modeling the effect of turbulence through an effective viscosity model. A number of turbulence models are used for different types of flows [3]. The K-ϵ model has been extensively used for recirculating flows in engine applications and has been shown to be successful [4]. This model uses the conservation equations of turbulence kinetic energy (K) and energy dissipation rate (ϵ) for modeling the effective viscosity [5]. After the averaging procedure the momentum equations remain unchanged, with the effective viscosity given by the following equation.

$$\mu = \mu_l + C_\mu \rho K^2/\epsilon \qquad (5-7)$$

where:

μ - is the effective viscosity

μ_l - is the fluid dynamic viscosity

K - is the turbulence kinetic energy

ϵ - is the energy dissipation rate

C_μ - is a constant

The turbulence kinetic energy and turbulence dissipation rate equations are written as follows:

TURBULENCE KINETIC ENERGY EQUATION

$$\frac{\partial}{\partial t}(\rho K) + \frac{1}{R}\frac{\partial}{\partial r}(\rho R u K) + \frac{\partial}{\partial y}(\rho v K) = \frac{1}{R}\frac{\partial}{\partial r}(\frac{\mu}{S_k} R \frac{\partial K}{\partial r}) + \frac{\partial}{\partial y}(\frac{\mu}{S_k}\frac{\partial K}{\partial y}) - \rho\epsilon C_d + G \qquad (5-8)$$

where G is the turbulence generation written as:

$$G = \mu[2((\frac{\partial v}{\partial y})^2 + (\frac{\partial u}{\partial r})^2 + \delta(\frac{u}{r})^2) + (\frac{\partial v}{\partial r} + \frac{\partial u}{\partial y})^2 + \delta(R\frac{\partial}{\partial r}(\frac{w}{r}))^2 + \delta(\frac{\partial w}{\partial y})^2] - \frac{2}{3}\nabla\cdot\vec{u}(\mu\nabla\cdot\vec{u} + \rho K) \qquad (5-9)$$

where:

$$\nabla\cdot\vec{u} = \frac{1}{R}\frac{\partial}{\partial r}(Ru) + \frac{\partial v}{\partial y}$$

ENERGY DISSIPATION RATE EQUATION

$$\frac{\partial}{\partial t}(\rho\epsilon) + \frac{1}{R}\frac{\partial}{\partial r}(\rho R u \epsilon) + \frac{\partial}{\partial y}(\rho v \epsilon) = \frac{1}{R}\frac{\partial}{\partial r}(\frac{\mu}{S_e} R \frac{\partial \epsilon}{\partial r}) + \frac{\partial}{\partial y}(\frac{\mu}{S_e}\frac{\partial \epsilon}{\partial y}) + \epsilon(C_1 G - C_2\rho\epsilon)/K \qquad (5-10)$$

where:

S_k, S_e, C_d, C_1 and C_2 - are constants

In table 5.1 the numerical values of the constants use in the K-ϵ model are given. These values are based on free turbulent flows, but they also can used for

wall flows [4]. The derivation of equations 5-8 and 5-10 is based on the following assumptions:

a) The Reynolds number of turbulence is assumed to be sufficient large that molecular transport can be neglected.

b) The turbulence is assumed to be isotropic.

c) The rate of diffusion of K and ϵ are proportional to the gradients of K and ϵ.

In laminar flow, μ is the fluid dynamic viscosity, while in turbulent flow μ is the effective viscosity obtained from equation (5-7).

5.3 FINITE DIFFERENCE EQUATIONS

A numerical method based on the Implicit Continuous-fluid Eulerian (ICE) technique is used for solving the momentum and continuity equations (eqns (5-1) to (5-3)). Equations (5-4) to (5-10) are solved explicitly in time. The governing differential equations are approximated by finite difference equations and are solved algebraically . The computational domain is divided into a finite grid and the algebraic equations are solved repeatedly at all grid points. This solution procedure is repeated in time.

Figure 5.1a shows the cell arrangement used in the computations. The velocities are defined at the faces of the cells and the scalar quantities (pressure, density, temperature, turbulence kinetic energy, energy dissipation and viscosity) at the cell center. In the computations non-uniform grid spacing is used to allow detailed computations in places where large gradients are expected.

In the derivation of the finite difference equations, the values of the velocities and scalar variables could be needed in locations where they are not defined (e.g. velocity at the corner of the cell, or, the temperature at the cell boundary). Figure 5.1b shows the numbering of the possible locations of the cell needed in the finite difference equations. Points 1, 2, 3 and 4 are the four corners of the cell. Points

5, 6, 7 and 8 are located in the middle of each cell side.

For example, the temperature at point 6 will be the weighted average of the temperatures of the adjacent cells (i,k) and (i+1,k) and is written as:

$$T_6 = (\Delta r_i T_{i+1,k} + \Delta r_{i+1} T_{i,k})/(\Delta r_i + \Delta r_{i+1}) \qquad (5-11)$$

The weighed average is used because of the unequal mesh used in the computations. The weighed average for representative quantities will be calculated below for corner 3 and face 6.

$$\begin{aligned}
u_6 &= u_{i,k} \\
v_6 &= (v_3 + v_2)/2.0 \\
w_6 &= (\Delta r_i w_{i+1,k} + \Delta r_{i+1} w_{i,k})/(\Delta r_i + \Delta r_{i+1}) \\
S_6 &= (\Delta r_i S_{i+1,k} + \Delta r_{i+1} S_{i,k})/(\Delta r_i + \Delta r_{i+1}) \qquad (5-12) \\
u_3 &= (\Delta y_k u_{i+1,k} + \Delta y_{k+1} u_{i,k})/(\Delta y_k + \Delta y_{k+1}) \\
v_3 &= (\Delta r_i v_{i+1,k} + \Delta r_{i+1} v_{i,k})/(\Delta r_i + \Delta r_{i+1})
\end{aligned}$$

where S is any scalar variable.

The values of the variables in the other corners and cell faces can be similarly obtained.

In the conservation equations, the convective and diffusive terms can be written in finite difference form using different numerical schemes. The simplest and most commonly used scheme for low cell Reynolds numbers is the central differencing scheme (CDS). The CDS is unstable at high cell Reynolds numbers, producing unrealistic results. To avoid these instabilities the upwind differencing scheme (UDS) was proposed by Courant, Isaacson and Rees [6]. Using the UDS the diffusive terms are written in finite difference form using the central differencing scheme. The convective terms are written in a form depending on the flow direction. The UDS is stable at high Reynolds numbers but produces false diffusion if it is used for Reynolds numbers less than 2.

In 1972 Spalding proposed a new differencing scheme derived from the exact solution of the one dimensional flow with convection-diffusion [7]. This scheme is called the hybrid differencing scheme (HDS) and is more realistic at both low and high Reynolds numbers. In the HDS the diffusion terms are set equal to zero for cell Peclet numbers greater than 2.0 and the convective terms are written in UDS. When the cell Peclet number is less than 2.0 the convective and diffusive terms are written using the CDS. In the model developed in this chapter the hybrid scheme is used.

The momentum equations are written in finite difference form as follows

5.3.1 MOMENTUM EQUATIONS

Momentum equation in radial direction

$$(\overline{\rho u})_{i,k} = [(\rho u)_{i,k} + \Delta t(DPX - CUX - CUY + DIFX1 + DIFX2 + DIFX3 + DIFX4)] \quad (5-13)$$

The quantity $(\overline{\rho u})_{i,k}$ is computed from known quantities at time t and is used to calculate the fluid velocity at time $t + \Delta t$ (see section 5.8), and

$$DPX = -\frac{\partial P}{\partial r} \quad (5-14)$$

$$CUX = \frac{1}{R}\frac{\partial}{\partial r}(\rho R u u) - \frac{1}{R}\frac{\partial}{\partial r}(\mu R \frac{\partial u}{\partial r}) \quad (5-15)$$

$$CUY = \frac{\partial}{\partial y}(\rho v u) - \frac{\partial}{\partial y}(\mu \frac{\partial u}{\partial y}) \quad (5-16)$$

$$DIFX1 = \frac{1}{R}\frac{\partial}{\partial r}(\mu R \frac{\partial u}{\partial r}) \quad (5-17)$$

$$DIFX2 = \frac{\partial}{\partial y}(\mu \frac{\partial v}{\partial r}) \quad (5-18)$$

$$DIFX3 = \delta \frac{2\mu u}{r^2} \quad (5-19)$$

$$DIFX4 = -\delta\frac{\rho w w}{r} \qquad (5-20)$$

These terms can be written in finite difference form as follows:

$$DPX = \frac{P_{i,k} - P_{i+1,k}}{0.5(\Delta r_i + \Delta r_{i+1})}$$

$$CUX = \frac{R_{i+1}COEFE - R_iCOEFW}{R_{i+\frac{1}{2}}(\Delta r_i + \Delta r_{i+1})}$$

where:

$COEFE = \rho_{i+1,k}U_R[u_{i,k} + u_{i+1,k} + SIGN(P_e)(u_{i,k} - u_{i+1,k})]$ for $|P_e| \geq 2$

or

$COEFE = 2\rho_{i+1,k}U_RU_R - 2\mu_{i+1,k}(u_{i+1,k} - u_{i,k})/\Delta r_{i+1}$ for $|P_e| < 2$

with

P_e = Peclet number $= \rho_{i+1,k}U_R\Delta r_{i+1}/\mu_{i+1,k}$

$U_R = 0.5(u_{i,k} + u_{i+1,k})$

$SIGN(P_e)$ is the algebraic sign of P_e

$COEFW = \rho_{i,k}U_C[u_{i,k} + u_{i-1,k} + SIGN(P_w)(u_{i-1,k} - u_{i,k})]$ for $|P_w| \geq 2$

or

$COEFW = 2\rho_{i,k}U_CU_C - 2\mu_{i,k}(u_{i,k} - u_{i-1,k})/\Delta r_i$ for $|P_w| \leq 2$

with

$P_w = \rho_{i,k}U_C\Delta r_i/\mu_{i,k}$

$U_C = 0.5(u_{i,k} + u_{i-1,k})$

$SIGN(P_w)$ is the algebraic sign of P_w

Similarly the term CUY is written as:

$$CUY = \frac{COEFN - COEFS}{2\Delta y_k}$$

where:

$$COEFN = \rho_3 v_3[u_{i,k} + u_{i,k+1} + SIGN(P_n)(u_{i,k} - u_{i,k+1})] \text{ for } |P_n| \geq 2$$

or

$$COEFN = 2\rho_3 v_3 u_3 - 2\mu_3(u_{i,k+1} - u_{i,k})/(0.5(\Delta y_{k+1} + \Delta y_k)) \text{ for } |P_n| \leq 2$$

with

$$P_n = 0.5\rho_3 v_3(\Delta y_k + \Delta y_{k+1})/\mu_3$$

$$COEFS = \rho_2 v_2[u_{i,k} + u_{i,k-1} + SIGN(P_s)(u_{i,k-1} - u_{i,k})] \text{ for } |P_s| \geq 2$$

or

$$COEFS = 2\rho_2 v_2 u_2 - 2\mu_2(u_{i,k} - u_{i,k-1})/(0.5(\Delta y_k + \Delta y_{k-1})) \text{ for } |P_s| \leq 2$$

with

$$P_s = 0.5\rho_2 v_2(\Delta y_k + \Delta y_{k-1})/\mu_2.$$

$$DIFX1 = \frac{r_{i+1}\mu_{i+1,k}(u_{i+1,k} - u_{i,k})/\Delta r_{i+1} - r_i\mu_{i,k}(u_{i,k} - u_{i-1,k})/\Delta r_i}{0.5r_{i+\frac{1}{2}}(\Delta r_i + \Delta r_{i+1})}$$

$$DIFX2 = \frac{\mu_3(v_{i+1,k} - v_{i,k}) - \mu_2(v_{i+1,k-1} - v_{i,k-1})}{0.5\Delta y_k(\Delta r_i + \Delta r_{i+1})}$$

$$DIFX3 = -\delta\frac{\mu_{i,k}(u_{i,k} + u_{i-1,k})}{r_i^2}$$

$$DIFX4 = \frac{\rho_{i,k}w_{i,k}^2}{r_i}$$

Similarly the momentum equations in the axial and circumferential directions

are written as:

Momentum equation in axial direction

$$(\overline{\rho v})_{i,k} = [(\rho v)_{i,k} + \Delta t(DPY - CVX - CVY + DIFY1 + DIFY2)] \quad (5-21)$$

where:

$$DPY = -\frac{\partial P}{\partial y} \quad (5-22)$$

$$CVX = \frac{1}{R}\frac{\partial}{\partial r}(\rho R u v) - \frac{1}{R}\frac{\partial}{\partial r}(\mu R \frac{\partial v}{\partial r}) \quad (5-23)$$

$$CVY = \frac{\partial}{\partial y}(\rho v v) - \frac{\partial}{\partial y}(\mu \frac{\partial v}{\partial y}) \quad (5-24)$$

$$DIFY1 = \frac{\partial}{\partial y}(\mu \frac{\partial v}{\partial r}) \quad (5-25)$$

$$DIFY2 = \frac{1}{R}\frac{\partial}{\partial r}(\mu R \frac{\partial u}{\partial r}) \quad (5-26)$$

Momentum equation in circumferential direction

$$w_{i,k}^{n+1} = [\rho_{i,k} w_{i,k} + \Delta t(-CWX - CWY + DIFW1 + DIFW2)]/\rho_{i,k}^{n+1} \quad (5-27)$$

where:

$$CWX = \frac{1}{R}\frac{\partial}{\partial r}(\rho R u w) - \frac{1}{R}\frac{\partial}{\partial r}(\mu R \frac{\partial w}{\partial r}) \quad (5-28)$$

$$CWY = \frac{\partial}{\partial y}(\rho v w) - \frac{\partial}{\partial y}(\mu \frac{\partial w}{\partial y}) \quad (5-29)$$

$$DIFW1 = -\delta \rho \frac{w u}{r} \quad (5-30)$$

$$DIFW2 = -\delta \frac{w}{R^2}\frac{\partial}{\partial r}(r\mu) \quad (5-31)$$

The convective and diffusive terms in equations (5-21) and (5-27) are written in finite difference form in a manner similar to that used for the corresponding terms in the momentum equation in the radial direction.

5.3.2 K-ϵ EQUATIONS

The turbulence kinetic energy (K) and the energy dissipation rate equations are written in finite difference form using the hybrid differencing scheme. As discussed in the introduction the K and ϵ are defined at the center of the cells, at the same location as the temperature, density, concentration and effective viscosity. Using the same notation as that for the momentum equations the turbulence kinetic energy equation is written as:

Turbulence Kinetic energy equation

$$K_{i,k}^{n+1} = [\rho_{i,k} K_{i,k} + \Delta t(-CKX - CKY + G - \rho_{i,k} DTR)]/\rho_{i,k}^{n+1} \qquad (5-32)$$

where:

$$CKX = \frac{1}{R}\frac{\partial}{\partial r}(\rho R u K) - \frac{1}{R}\frac{\partial}{\partial r}(\frac{\mu}{S_k} R \frac{\partial K}{\partial r}) \qquad (5-33)$$

$$CKY = \frac{\partial}{\partial y}(\rho v K) - \frac{\partial}{\partial y}(\frac{\mu}{S_k}\frac{\partial K}{\partial y}) \qquad (5-34)$$

$$DTR = \epsilon C_d \qquad (5-35)$$

The generation term G is defined in equation (5-9). The terms CKX, CKY and DTR are written in finite difference form as follows:

$$CKX = \frac{R_{i+\frac{1}{2}} COEFE - R_{i-\frac{1}{2}} COEFW}{2 R_i \Delta r_i}$$

where:

$$COEFE = \rho_6 u_{i,k}[K_{i,k} + K_{i+1,k} + SIGN(P_e)(K_{i,k} - K_{i+1,k})] \text{ for } |P_e| \geq 2$$

or

$$COEFE = 2\rho_6 u_{i,k} K_6 - 2\mu_6 (K_{i+1,k} - K_{i,k})/(0.5(\Delta r_i + \Delta r_{i+1})) \text{ for } |P_e| \leq 2$$

with

$$P_e = 0.5\rho_6 u_{i,k}(\Delta r_i + \Delta r_{i+1})/\mu_6$$

and

$$COEFW = \rho_8 u_{i-1,k}[K_{i,k} + K_{i-1,k} + SIGN(P_e)(K_{i-1,k} - K_{i,k})] \text{ for } |P_w| \geq 2$$

or

$$COEFW = 2\rho_8 u_{i-1,k} K_8 - 2\mu_8 (K_{i,k} - K_{i-1,k})/(0.5(\Delta r_i + \Delta r_{i-1})) \text{ for } |P_w| \leq 2$$

with

$$P_w = 0.5\rho_8 u_{i-1,k}(\Delta r_i + \Delta r_{i-1})/\mu_8$$

Similarly the term CKY is written as:

$$CKY = \frac{COEFN - COEFS}{2\Delta y_k}$$

where:

$$COEFN = \rho_7 v_{i,k}[K_{i,k} + K_{i,k+1} + SIGN(P_n)(K_{i,k} - K_{i,k+1})] \text{ for } |P_n| \geq 2$$

or

$$COEFN = 2\rho_7 v_{i,k} K_7 - 2\mu_7 (K_{i,k+1} - K_{i,k})/(0.5(\Delta y_{k+1} + \Delta y_k)) \text{ for } |P_n| \leq 2$$

with

$P_n = 0.5\rho_7 v_{i,k}(\Delta y_k + \Delta y_{k+1})/\mu_7$ and

$$COEFS = \rho_5 v_{i,k-1}[K_{i,k} + K_{i,k-1} + SIGN(P_s)(K_{i,k-1} - K_{i,k})] \text{ for } |P_s| \geq 2$$

or

$$COEFS = 2\rho_5 v_{i,k-1} K_5 - 2\mu_5 (K_{i,k} - K_{i,k-1})/(0.5(\Delta y_k + \Delta y_{k-1})) \text{ for } |P_s| \leq 2$$

with

$$P_s = 0.5\rho_5 v_{i,k-1}(\Delta y_k + \Delta y_{k-1})/\mu_5$$

and

$$\text{DTR} = C_d \epsilon_{i,k}$$

The generation term (eqn (5-9)) is written as:

$$G = \mu[2(DVDY^2 + DUDX^2 + CYLT^2) + (DVDX + DUDY)^2 + DWDX^2 + DWDY^2] - \frac{2}{3}DIV(\mu DIV + \rho K) \qquad (5-36)$$

where:

$$DVDY = \frac{v_{i,k} - v_{i,k-1}}{\Delta y_k}$$

$$DUDX = \frac{u_{i,k} - u_{i-1,k}}{\Delta r_i}$$

$$CYLT = \delta \frac{u_{i,k} + u_{i-1,k}}{2r_i}$$

$$DVDX = \frac{v_3 + v_2 - v_4 - v_1}{2\Delta r_i}$$

$$DUDY = \frac{u_3 + u_4 - u_2 - u_1}{2\Delta y_k}$$

$$DWDX = \delta \frac{r_{i+\frac{1}{2}}(w_{i+1,k}/r_{i+1} - w_{i,k}/r_i)}{0.5(\Delta r_{i+1} + \Delta r_i)}$$

$$DWDY = \delta \frac{w_{i,k+1} - w_{i,k-1}}{0.5(\Delta y_{k+1} + \Delta y_{k-1}) + \Delta y_k}$$

$$DIV = \frac{R_{i+\frac{1}{2}} u_{i,k} - R_{i-\frac{1}{2}} u_{i-1,k}}{R_i \Delta r_i} + \frac{v_{i,k} - v_{i,k-1}}{\Delta y_k}$$

The energy dissipation equation is written as follows:

Energy dissipation equation

$$\epsilon_{i,k}^{n+1} = [\rho_{i,k}\epsilon_{i,k} + \Delta t(-CEX - CEY + TERM)]/\rho_{i,k}^{n+1} \qquad (5-37)$$

where:

$$CEX = \frac{1}{R}\frac{\partial}{\partial r}(\rho R u \epsilon) - \frac{1}{R}\frac{\partial}{\partial r}(\frac{\mu}{S_e}R\frac{\partial \epsilon}{\partial r}) \qquad (5-38)$$

$$CKY = \frac{\partial}{\partial y}(\rho v \epsilon) - \frac{\partial}{\partial y}(\frac{\mu}{S_e}\frac{\partial \epsilon}{\partial y}) \qquad (5-39)$$

$$TERM = \epsilon(C_1 G - C_2 \rho \epsilon)/K \qquad (5-40)$$

The terms CEX and CEY are written in a similar finite difference form as the terms CKX and CKY by replacing the turbulence kinetic energy by the energy dissipation rate. The term TERM is written as:

$$TERM = \epsilon_{i,k}(C_1 G_{i,k} - C_2 \rho_{i,k}\epsilon_{i,k})/K_{i,k}$$

The effective viscosity is written as:

$$\mu = \mu_l + C_\mu \rho_{i,k} K_{i,k}^2/\epsilon_{i,k} \qquad (5-41)$$

5.3.3 ENERGY AND CONCENTRATION EQUATIONS

The energy and concentration equations are discretized in the same manner as the turbulence kinetic energy and the energy dissipation rate. Thus:

Energy equation

$$T_{i,k}^{n+1} = [\rho_{i,k}T_{i,k} + \Delta t(-CTX - CTY)]/\rho_{i,k}^{n+1} \qquad (5-42)$$

Concentration equation

$$C_{i,k}^{n+1} = [\rho_{i,k} C_{i,k} + \Delta t(-CCX - CCY)]/\rho_{i,k}^{n+1} \qquad (5-43)$$

The terms CCX and CTX are written in the same manner as the term CKX by replacing the turbulence kinetic energy by the concentration and the temperature respectively. Similarly, the terms CCY and CTY are written in the same manner as the term CKY.

5.4 INITIAL CONDITIONS

The equations presented are time dependent, therefore initial conditions must be specified in the computational domain for all variables. The fluid is assumed to be at rest at time zero (zero velocity). The turbulence kinetic energy and the energy dissipation rate are assumed to be very small (10^{-10}) and the effective viscosity to be equal to the molecular viscosity. The cylinder gas temperature is initially set equal to 700.0 K, which is an average value obtained from the thermodynamic model. The concentration of the cylinder residual gases is set equal to zero. The air supplied to the engine during scavenging is assumed to have a concentration of 1.0. Therefore, when the cylinder gases have been fully replaced by the air, the concentration will be equal to 1.0.

The assumption of zero initial velocity will affect only a short period at the beginning of the scavenging process. After that, the strong inflow will be dominant, eliminating the effect of the initial zero velocity.

5.5 BOUNDARY CONDITIONS

5.5.1 INTRODUCTION

In order to carry out the computations, boundary conditions associated with the conservation equations have been specified. In the cases that will be analyzed below, three types of boundary conditions are used:

a) Inflow-Outflow Condition

b) Rigid Wall Condition

c) Axis of Symmetry Condition

In the case of inflow-outflow boundaries, the fluid velocity components u, v and w together with the temperature and concentration must be specified. If the flow is turbulent, the turbulence kinetic energy and the dissipation rate must also be specified. At the wall, the fluid velocity must be equal to zero together with K and ϵ. In the case of adiabatic flow, the heat flux is set equal to zero, otherwise the temperature must be specified at the wall. In all cases zero mass flux should be imposed as a boundary condition for the concentration equation, except at the inlet, where the concentration must be specified. The flow under consideration is assumed to be axisymmetric, therefore the computational domain can be bounded on one side by an axis of symmetry.

At the axis of symmetry the velocity (u) perpendicular to the axis and the circumferential velocity (w) must be set equal to zero. Also the flux of all scalar quantities (K, ϵ, ρ, T, C and μ) together with the axial velocity (v) must be set equal to zero.

$$\frac{\partial K}{\partial r} = \frac{\partial \rho}{\partial r} = \frac{\partial T}{\partial r} = \frac{\partial C}{\partial r} = \frac{\partial \mu}{\partial r} = \frac{\partial v}{\partial r} = 0$$

The calculation domain and the grid used for the computations is shown in figure 5.2. The wall of the physical domain is coincident with the cell boundaries.

Therefore, the location where the velocity component perpendicular to the wall is defined is coincident with the wall boundary. In this case this velocity is set equal to zero. For the velocity components parallel to the wall (v and w for east and west boundaries or u and w for north and south boundaries) or for the scalar variables (T, K, ϵ, C etc) a fictitious cell is needed to impose the boundary conditions. The fictitious cells are outside the fluid domain and the conservation equations are not solved in these cells. For example, if non-slip condition is used at the east boundary (zero velocity), in order to impose zero axial velocity at the wall an equal and opposite in direction to the fluid velocity close to the wall is imposed in the fictitious cell. In case of free-slip condition at the boundary (axis of symmetry) velocity equal to and with the same direction to the fluid velocity close to the wall is imposed as boundary condition in the fictitious cell. In the computations 28 grid nodes in the axial direction and 22 in the radial direction are used.

5.5.2 MOMENTUM EQUATIONS

In the computations the wall is assumed as being no-slip and, therefore, a zero fluid velocity is imposed at the wall. For a better description of the boundary conditions the following notation is used (see figure 5.2).

$IMIN$- Smallest index in the radial direction

$KMIN$- Smallest index in the axial direction

$IMAX$- Biggest index in the radial direction

$KMAX$- Biggest index in the axial direction

$IM1 = IMIN + 1$

$KM1 = KMIN + 1$

$IM2 = IMAX - 1$

$KM2 = KMAX - 1$

The boundary conditions for the four fluid physical boundaries will be discussed below:

A) NORTH BOUNDARY

The north boundary consists of the exit opening simulating the four engine exhaust valves and a wall which is the engine cylinder head. The valves are simulated by an annulus opening because of the assumption that the flow is axisymmetric.

1. For the cells in front of the outlet the following conditions are used:

$u_{i,KMAX} = u_{i,KM2}$

$w_{i,KMAX} = w_{i,KM2}$

$v_{i,KM2} = UOUTLE$

$UOUTLE$ is the fluid outlet velocity obtained from the overall mass balance in the fluid domain.

2. For the cells adjacent to the cylinder head:

$u_{i,KMAX} = -u_{i,KM2}$

$v_{i,KM2} = 0$

$w_{i,KMAX} = -w_{i,KM2}$

B) WEST BOUNDARY

The west boundary is the axis of symmetry, therefore:

$u_{IMIN,k} = 0$

$v_{IMIN,k} = v_{IM1,k}$ for all k's

$w_{IMIN,k} = -w_{IM1,k}$

C) SOUTH BOUNDARY

The south boundary consists of the engine piston. The piston is not flat and has a bowl which is used as the cylinder combustion chamber. The piston bowl shape cannot be modeled; therefore, a cavity with the same volume is used (see figure 5.2). The following conditions are used:

$u_{i,KMIN} = -u_{i,KM1}$

$v_{i,KMIN} = 0$ for $1 \leq i \leq 17$

$$w_{i,KMIN} = -w_{i,KM1}$$

$$u_{i,5} = -u_{i,6}$$

$$v_{i,5} = 0 \text{ for } 18 \leq i \leq 14$$

$$w_{i,5} = -w_{i,6}$$

D) EAST BOUNDARY

The east boundary consists of the cylinder wall above the inlet ports, the inlet ports and the vertical portion of the piston.

1. For the cells in front of the inlet ports (see figure 5.3):

$$u_{IM2,k} = -UINLET$$

$$v_{IMAX,k} = UINLET tan(\theta)/cos(\phi)$$

$$w_{IMAX,k} = UINLET tan(\phi)$$

where $UINLET$ is the inlet velocity obtained from the engine flow rate (see section 5.11). When the inlet velocity is horizontal θ is equal to zero. For non-swirling flows ϕ is also equal to zero.

2. For the cells adjacent to the cylinder wall:

$$u_{IM2,k} = 0$$

$$v_{IMAX,k} = -v_{IM2,k}$$

$$w_{IMAX,k} = -w_{IM2,k}$$

3. For the cells adjacent to the vertical portion of the piston

$$u_{17,k} = 0$$

$$v_{18,k} = -v_{17,k} \text{ for } 2 \leq k \leq 5$$

$$w_{18,k} = -w_{17,k}$$

5.5.3 K-ϵ EQUATIONS

The value of the turbulence kinetic energy at the wall is equal to zero. At the inlet ports the value of K is assumed to be three percent of the inlet flow kinetic energy [8]. At the axis of symmetry and the outlet opening, zero turbulence kinetic energy flux is imposed. Therefore, the conditions used are as follows:

A) NORTH BOUNDARY

1. For the cells adjacent to the cylinder head:

$$K_{i,KMAX} = -K_{i,KM2}$$

2. For the cells adjacent to the outlet opening:

$$K_{i,KMAX} = K_{i,KM2}$$

B) WEST BOUNDARY (AXIS OF SYMMETRY)

$K_{IMIN,k} = K_{IM1,k}$ for all k's

C) EAST BOUNDARY

1) For the cells adjacent to the cylinder wall:

$$K_{IMAX,k} = -K_{IM2,k}$$

2) For the cells adjacent to the inlet ports:

$$K_{IMAX,k} = 0.03(UINLET)^2$$

3. For the cells adjacent to the vertical portion of the piston :

$K_{18,k} = -K_{17,k}$ for $2 \leq k \leq 5$

D) SOUTH BOUNDARY

$K_{i,KMIN} = -K_{i,KM1}$ for $2 \leq i \leq 17$

$K_{i,5} = -K_{i,6}$ for $18 \leq i \leq 23$

The dissipation equation is not solved in the cells adjacent to the walls (see section 5.7.2). Therefore, no boundary conditions are used for these cells. For the

cells adjacent to the outlet opening the following condition is used:

$\epsilon_{i,KMAX} = \epsilon_{i,KM2}$

For the axis of symmetry:

$\epsilon_{IMIN,k} = \epsilon_{IM1,k}$

At the inlet ports [7]:

$\epsilon_{IMAX,k} = C_{\mu}^{0.75} K_{IMAX,k}^{1.5} / (0.0075 r_{IM2})$

5.5.4 ENERGY AND CONCENTRATION EQUATIONS

The boundary conditions for the energy and concentration equations are imposed on the fictitious cells in a manner similar to the one used in the case of the turbulence kinetic energy equation. At the axis of symmetry zero heat flux is assumed, therefore:

$T_{IMIN,k} = T_{IM1,k}$ for all k's.

From the inputs to the thermodynamic model the following temperatures are used for the cylinder wall boundaries (see chapter 7):

Cylinder wall temperature = 393 K,

Piston Crown temperature = 493 K,

Cylinder head temperature = 473 K, and

Inlet air temperature = 320 K.

The temperatures at the boundary walls are imposed on the fictitious cells. For example, the boundary condition for the cylinder head is written as:

$T_{i,KMAX} = 473.0$ for all i's adjacent to the wall

For the concentration equation zero mass flux is imposed in all boundary cells except on the ones at the inlet opening where a concentration equal to 1.0 is used.

5.6 TREATMENT OF NEAR-WALL REGIONS

The near-wall regions need special treatment because of steep nonlinear variation of the variables and the fact that laminar and turbulent effects equally characterize the flow. Experiments by Gardner and Kestin [9] have shown that the near-wall region is characterized by uniform shear stress; therefore, the results of one-dimensional Couette flow can be used for modeling the near-wall region [3], yielding the universal logarithmic law of the wall:

$$U^+ = \frac{1}{k} ln(Ey^+) \qquad (5-44)$$

where:

$U^+ = \frac{U}{U_\tau}$

k, E are constants with values of 0.418 and 9.793 respectively [10].

$y^+ = \frac{\rho U_\tau y}{\mu_l}$

$U_\tau = \left(\frac{\tau_w}{\rho}\right)^{\frac{1}{2}}$

τ_w is the wall shear stress

y is the normal distance from the wall

It has been shown [10] that the near-wall region can be divided into three regions: a) the viscous or laminar sublayer ($0 < y^+ \leq 5$), b) the buffer layer ($5 < y^+ < 30$); and c) the inertial sublayer ($y^+ > 30$).

In the viscous sublayer the flow can be considered as laminar and the viscous forces are dominant. The buffer layer is a transition region between the laminar sublayer and the turbulent inertial layer. For convenience, and because the buffer layer is not easy to model, it is eliminated by assuming that the viscous layer extends up to the point $y^+ = 11.63$. The viscous sublayer is, therefore, assumed to be in the region of $0 < y^+ \leq 11.63$. In this region the shear stress is written as:

$$\tau = \mu_l \frac{\partial u}{\partial y} \qquad (5-45)$$

For $y^+ > 11.63$ the flow is assumed to be fully turbulent but with uniform shear stresses. In this region the shear stress is given by [3]:

$$\tau_w = u\rho k C_\mu^{\frac{1}{4}} K^{\frac{1}{2}} / ln(Ey^+) \qquad (5-46)$$

This equation was obtained from the universal velocity distribution and the assumption that the production of turbulence kinetic energy is equal to the dissipation rate.

The turbulence kinetic energy in regions close to the wall is obtained from equation (5-8) with appropriate modifications to the generation term (Section 5.7.2). The energy dissipation rate is obtained from the following equation assuming that the production and dissipation of K are equal [3]:

$$\epsilon = C_\mu^{\frac{3}{4}} \frac{K^{\frac{3}{4}}}{ky} \qquad (5-47)$$

In the momentum equations (5-2) to (5-4) the diffusion terms are modified by using the shear stress terms at the wall. These new equations are in turn used to obtain the velocities u, v and w at regions close to the wall.

The treatment of the energy equation close to the wall is similar to that of the momentum equations. By using the one-dimensional Couette flow analysis, a similar relationship to (5-44) can be obtained [11]:

$$T^+ = Pr_t(U^+ + F(\frac{Pr}{Pr_t})) \qquad (5-48)$$

where:

$T^+ = \frac{\rho U_\tau (T - T_w)}{F_T}$

F_T - is the heat flux at the wall

Pr_t - is the turbulent Prandtl number

and the proposed function $F(\frac{Pr}{Pr_t})$ has the following form [12]:

$$F(\frac{Pr}{Pr_t}) = 9.24[(\frac{Pr}{Pr_t})^{\frac{3}{4}} - 1][1.0 + 0.28exp(-0.007\frac{Pr}{Pr_t})] \qquad (5-49)$$

5.7 NUMERICAL IMPLEMENTATION OF THE NEAR-WALL CONDITIONS

In section 5.6 the treatment of the near-wall regions was discussed without details of the applications to the conservation equations. Below, each conservation equation will be discussed separately and the necessary modifications will be presented.

5.7.1 MOMENTUM EQUATIONS

A) Viscous Sublayer $(0 < y_+ \leq 11.63)$

If a cell adjacent to the wall has y^+ less than or equal to 11.63, this cell lies in the laminar sublayer and therefore the laminar viscosity dominates. Thus, the diffusion term, for example, $\mu\frac{\partial u}{\partial y}$ can be written as :

$$\mu\frac{\partial u}{\partial y} = \mu_l\frac{u}{\Delta y}$$

for a non-moving wall. Similar expressions can be written for the other diffusive terms.

B) Turbulent Region ($11.63 < y_+$)

Cells with y_+ greater than 11.63 lie in the turbulent region and the following treatment of the near wall region is considered.

Momentum equation in radial direction

The shear stress component τ_{yr} of the total shear stress τ_t at the north or south wall is written as :

$$\tau_{yr} = \mu(\frac{\partial u}{\partial y} + \frac{\partial v}{\partial r}) \qquad (5-50)$$

Close to the wall the term $\frac{\partial v}{\partial r}$ approaches zero. Thus :

$$\tau_{yr} = \mu\frac{\partial u}{\partial y} \qquad (5-51)$$

The total shear stress τ_t for the north and south wall is as follows using equation (5-46) :

$$\tau_t = -U_P \rho k C_\mu^{\frac{1}{4}} K^{\frac{1}{2}} / ln(Ey^+) \qquad (5-52)$$

where U_P is the velocity tangential to the wall at y and is equal to $(u^2 + w^2)^{\frac{1}{2}}$ for the south or north wall [13]. If Θ is the angle between u and U_P, then

$$\tau_{yr} = \tau_t cos(\Theta) \quad or$$
$$\tau_{yr} = -u\rho k C_\mu^{\frac{1}{4}} K^{\frac{1}{2}} / ln(Ey^+) \qquad (5-53)$$

which is the same expression as for non-swirling flows [14]. In equation 5-53 it

is assumed that the direction of the shear stress at the wall is the same as the direction of the velocity near the wall [15]. The term y^+ is written as follows:

$$y^+ = \frac{\rho y}{\mu_l}\sqrt{\frac{\tau_t}{\rho}} \qquad (5-54)$$

Now, assuming that the turbulent shear stress close to the wall is equal to the shear stress at the wall [5], the shear stress can be written as:

$$\tau_t = (C_d C_\mu)^{\frac{1}{2}} \rho k \qquad (5-55)$$

and, therefore,

$$y^+ = \rho y C_d^{\frac{1}{2}} C_\mu^{\frac{1}{4}} K^{\frac{1}{2}} / \mu_l \qquad (5-56)$$

where y is the distance of the tangential velocity (u) from the wall.

Summarizing, the shear stress at the north or south walls in the radial direction is :

$$\tau_{yr} = u \rho k C_\mu^{\frac{1}{4}} K^{\frac{1}{2}} / ln(E y^+) \qquad (5-57)$$

where:

$$y^+ = \rho y C_d^{\frac{1}{2}} C_\mu^{\frac{1}{4}} K^{\frac{1}{2}} / \mu_l \qquad (5-58)$$

A different approach of obtaining the shear stress at the wall uses the following iterative method :

a) Assume a value for y^+

b) Calculate the shear stress using equation (5-53)

c) Calculate y^+ using equation (5-54)

d) Compare the new value of y^+ with the assumed value. If the difference is within a specified tolerance, the values of the shear stress and y^+ are correct. If not, then use the calculated value of y^+ as the new assumed value and repeat.

Both approaches have been tested and both give the same results. In the program the non-iterative method is used.

Therefore, for cell (i,k), y^+ and the shear stress are written in numerical form as follows :

$$\tau_{yr}(i,k) = u_{i,k}\rho k C_\mu^{\frac{1}{4}} K_{i,k}^{\frac{1}{2}} / ln(E y_{i,k}^+) \qquad (5-59)$$

and

$$y_{i,k}^+ = \rho_{i,k} y C_d^{\frac{1}{2}} C_\mu^{\frac{1}{4}} K_{i,k}^{\frac{1}{2}} / \mu_l \qquad (5-60)$$

Close to the wall diffusion dominates over convection and the north coefficient can be written as :

$$COEFN = -2(\Delta r_{i+1}\tau_{ry}(i,k) + \Delta r_i \tau_{ry}(i+1,k))/(\Delta r_i + \Delta r_{i+1})$$

The same expression can be written for the south wall (coefficient $COEFS$).

Momentum equation in axial direction

The shear stress component τ_{ry} of the total shear stress τ_t at the east wall is written as :

$$\tau_{ry} = \mu(\frac{\partial v}{\partial r} + \frac{\partial u}{\partial y}) \qquad (5-61)$$

Close to the wall the term $\frac{\partial u}{\partial y}$ is small compared to $\frac{\partial v}{\partial r}$ and can be ignored. Thus, the shear stress is written as :

$$\tau_{yr} = \mu \frac{\partial v}{\partial r} \qquad (6-62)$$

The total shear stress τ_t for the east wall is written as :

$$\tau_t = V_P \rho k C_\mu^{\frac{1}{4}} K^{\frac{1}{2}} / ln(Ey^+) \qquad (5-63)$$

where V_P is the velocity tangential to the wall and is equal to $(v^2 + w^2)^{\frac{1}{2}}$ for the east wall . If Φ is the angle between v and V_P, then

$$\tau_{ry} = \tau_t cos(\Phi) \quad or$$
$$\tau_{ry} = v \rho k C_\mu^{\frac{1}{4}} K^{\frac{1}{2}} / ln(Ey^+) \qquad (5-64)$$

Using the shear stress equation the $COEFE$ can be written as:

$$COEFE = -2(\Delta y_{k+1} \tau_{yr}(i,k) + \Delta y_k \tau_{yr}(i,k+1))/(\Delta y_k + \Delta y_{k+1})$$

Momentum Equation in the circumferential direction

The shear stress component $\tau_{r\theta}$ of the total shear stress τ_t at the east wall is written as :

$$\tau_{r\theta} = \mu(\frac{\partial w}{\partial r} - \frac{w}{r}) \qquad (5-65)$$

The diffusive term $\mu \frac{\partial w}{\partial r}$, therefore, is written as :

$$\mu \frac{\partial w}{\partial r} = \tau_{r\theta} + \frac{\mu w}{r}$$

As in the previous analysis.

$$\tau_{r\theta} = -w\rho k C_{\mu}^{\frac{1}{4}} K^{\frac{1}{2}} // ln(Ey^{+}). \qquad (5-66)$$

Thus, the $COEFE$ is written as :

$$COEFE = 2(\tau_{r\theta} + \frac{\mu w}{r})$$

A similar expression is written for $COEFN$ and $COEFS$ using the shear stress component $\tau_{y\theta}$.

5.7.2 K - ϵ EQUATIONS

Turbulence Kinetic Energy Equation

In the turbulence kinetic energy equation the turbulence generation term (G) must be modified for the cells adjacent to the wall. The generation term can be written as :

$$G = \mu[2((\frac{\partial v}{\partial y})^2 + (\frac{\partial u}{\partial r})^2 + \delta(\frac{u}{r})^2) + (\tau_{ry}^2 + \tau_{r\theta}^2 + \tau_{y\theta}^2)] - \frac{2}{3}\nabla \cdot \vec{u}(\mu \nabla \cdot \vec{u} + \rho K) \quad (5-67)$$

For the east wall cells the total shear stress can be expressed as :

$$\tau_t^2 = \tau_{yr}^2 + \tau_{r\theta}^2$$

Also the stress $\tau_{y\theta}^2$ is approximated by $(\mu \frac{\partial w}{\partial y})^2$. Therefore, for the west wall:

$$G = 2\mu((\frac{\partial v}{\partial y})^2 + (\frac{\partial u}{\partial r})^2 + \delta(\frac{u}{r})^2) + \delta(\frac{\tau_t^2}{\mu} + \mu(\frac{\partial w}{\partial y})^2) - \frac{2}{3}\nabla \cdot \vec{u}(\mu \nabla \cdot \vec{u} + \rho K)$$

The value of τ_t^2 is obtained from equation (5-52). Similarly the generation term G for the north and south is written as:

$$G = 2\mu((\frac{\partial v}{\partial y})^2 + (\frac{\partial u}{\partial r})^2 + \delta(\frac{u}{r})^2) + \delta(\tau_t^2/\mu + \mu(\frac{\partial w}{\partial r} - \frac{w}{r})^2)$$
$$-\frac{2}{3}\nabla \cdot \vec{u}(\mu \nabla \cdot \vec{u} + \rho K)$$

Energy Dissipation Equation

The production and dissipation rate of K close to the wall are assumed equal, as mentioned earlier. Thus, close to the wall, the following equation is used instead of the conservation of ϵ equation :

$$\epsilon = C_\mu^{\frac{3}{4}} K^{\frac{3}{2}}/ky \qquad (5-68)$$

5.7.3 ENERGY AND CONCENTRATION EQUATIONS

In the present computations the walls are assumed as having constant but different temperatures. In order to calculate the heat flux at the wall, equations (5-48) and (5-49) are used.

Therefore, for the north wall, the coefficient $COEFN$ is modified as follows:

$$COEFN = -\rho(T - T_w)C_\mu^{\frac{1}{4}} K^{\frac{1}{4}}/[\frac{\mu}{Pr_t k} ln(Ey^+) + FUNC]$$

where:

$$FUNC = 9.24((\frac{Pr}{Pr_t})^{\frac{3}{4}} - 1)(1.0 + 0.28exp(-0.007\frac{Pr}{Pr_t}))$$

with y^+ as defined in equation (5-58)

Similar expressions are written for the east and south walls.

5.8 SOLUTION PROCEDURE

In section 5.3 the finite difference equations were derived in an explicit form, which means that the dependent variables are advanced in time based on the previous time step computations. The solution procedure is an iterative one and is based on the "guess and correct" method. The computations start by solving the momentum equations for the unknown mass fluxes ($\overline{\rho u}$ and $\overline{\rho v}$). In the momentum equation the values of the velocity, pressure, density and effective viscosity are from the time t. Then using the mass conservation equation, the barred values of density are calculated as follows [16]:

$$\overline{\rho}_{i,k} = \rho_{i,k} - (1-\theta)\Delta t[\frac{R_{i+\frac{1}{2}}(\rho u)_{i,k} - R_{i-\frac{1}{2}}(\rho u)_{i-1,k}}{R_i \Delta r_i} + \frac{(\rho v)_{i,k} - (\rho v)_{i,k-1}}{\Delta y_k}] \quad (5-69)$$

In equation (5-69) the right hand side terms are from time t and therefore known. Also, θ is a constant taking values of zero for a fully explicit calculation and one for a fully implicit one. A value of 0.5 is used in these computations. With the values of $\overline{\rho u}$ and $\overline{\rho v}$ computed from equations (5-13) and (5-21) the advanced values are calculated as follows:

$$(\rho u)_{i,k}^{n+1} = (\overline{\rho u})_{i,k} + \frac{\Delta t}{\Delta r}\Delta P_{i,k} \quad (5-70)$$

$$(\rho v)_{i,k}^{n+1} = (\overline{\rho v})_{i,k} + \frac{\Delta t}{\Delta y}\Delta P_{i,k} \quad (5-71)$$

$\Delta P_{i,k}$ is a pressure adjustment which will be calculated later. An iterative method is used for the solution of equations (5-70) and (5-71). Convergence is

reached when the continuity equation is satisfied. The continuity equation can be written as:

$$D_{i,k} = \rho_{i,k}^{n+1} - \overline{\rho}_{i,k} - \theta\Delta t[\frac{R_{i+\frac{1}{2}}(\rho u)_{i,k}^{n+1} - R_{i-\frac{1}{2}}(\rho u)_{i-1,k}^{n+1}}{R_i \Delta r_i} + \frac{(\rho v)_{i,k}^{n+1} - (\rho v)_{i,k-1}^{n+1}}{\Delta y_k}] \qquad (5-72)$$

Convergence is assumed to be reached if the absolute value of $D_{i,k}$ is smaller than a small quantity ϵ for all the computational cells. The iteration procedure starts using the mass fluxes obtained from the momentum equations and the barred value of density. Therefore, the continuity equation may not necessarily cause $D_{i,k} = 0$ at each cell. Whenever a negative value results, a net inflow to the cell is indicated. In order to eliminate this inflow the pressure in the cell must increase. Similarly, for a net outflow from the cell, the cell pressure must decrease to reduce the outflow. Assuming that ΔP is the necessary pressure adjustment to make the divergence vanish for the cell (i,k), the pressure and mass fluxes are corrected as follows:

$$P_{i,k} = P_{i,k} + \Delta P_{i,k}$$

$$\rho_{i,k} = \rho_{i,k} + \Delta P_{i,k}/c_{i,k}^2$$

$$(\rho u)_{i,k} = (\rho u)_{i,k} + \Delta t \Delta P_{i,k}/\Delta r_i$$

$$(\rho u)_{i-1,k} = (\rho u)_{i-1,k} - \Delta t \Delta P_{i,k}/\Delta r_i$$

$$(\rho v)_{i,k} = (\rho v)_{i,k} + \Delta t \Delta P_{i,k}/\Delta y_k$$

$$(\rho v)_{i,k-1} = (\rho v)_{i,k-1} - \Delta t \Delta P_{i,k}/\Delta y_k$$

At this point the value of $\Delta P_{i,k}$ is unknown. The new values of density and mass fluxes (at $t + \Delta t$) must satisfy the continuity equation (eqn. (5-72)). Therefore, by substituting these values into equation (5-72) the following equation for $\Delta P_{i,k}$ is obtained :

$$\Delta P_{i,k} = -\Omega D_{i,k}/\beta_{i,k} \qquad (5-73)$$

where:

$$\beta_{i,k} = \frac{1}{c_{i,k}^2} + 2\theta\Delta t^2\left(\frac{1}{\Delta r_i^2} + \frac{1}{\Delta y_k^2}\right)$$

$D_{i,k}$ is the divergence of the previous iteration. The variable Ω is a relaxation factor. It usually take values between 1.0 and 2.0 and is used to accelerate the convergence. In the computations the value of 1.7 was found as optimum and is used. If the convergence criterion for a cell (i,k) is satisfied, the pressure, density and momenta are not changed. After convergence has been reached for all cells the fluid velocities are obtained as follows:

$$u_{i,k} = \frac{(\rho u)_{i,k}}{\rho_6} \qquad (5-74)$$

$$v_{i,k} = \frac{(\rho v)_{i,k}}{\rho_7} \qquad (5-75)$$

After the velocity field has been obtained the turbulent kinetic energy and the energy dissipation rate are obtained by solving equations (5-32) and (5-37). The effective viscosity is calculated from equation (5-41). Then, the temperature and concentration equations are solved (eqns (5-42) and (5-43)). The density is updated using the ideal gas equation.

5.9 STABILITY AND ACCURACY

The solution procedure presented in the previous sections is not always stable. There are two stability requirements. The first one is analogous to the Courant condition [5]. This requires that the fluid does not cross the complete length of

the cell within a time step. Therefore, the stability requirement for the time step is:

$$\Delta t < min(\frac{\Delta r}{|u|}, \frac{\Delta y}{|v|}) \qquad (5-76)$$

The second requirement for stability is related to the fluid viscosity and is written as:

$$\Delta t < \frac{\frac{1}{2\nu}}{\frac{1}{(\Delta r)^2} + \frac{1}{(\Delta y)^2}} \qquad (5-77)$$

As can be seen, both requirements restrict the computational time step. This is one of the major disadvantages of the technique. For long real time computations, a large number of time steps must be used, increasing the computational cost.

It has been found that instability is avoided by using a time step which is at least two to three times smaller than the maximum time step given by equations (5-76) or (5-77).The requirement for accurate calculations impose a fine computational grid. By selecting a fine grid the time step must decrease, thus, increasing the computational cost. Therefore, trials must be made for selecting the best grid for a reasonable time step.

5.10 TESTING

In previous sections the model development and the solution procedure were presented. In this section, a number of tests for verification of the code will be presented before studying the scavenging process.

Two different tests will be performed. The first one is comparing the data obtained from the computer code against experimental data for cavity flow and the second against results computed using the steady state TEACH code.

The concept of cavity flow has been used for many years as a test-case for

comparison with numerical techniques for laminar and turbulent flows [17]. The cavity flow can be driven by a sliding wall or by a channel flow. The comparison here is based on the experimental data for channel driven cavity flow reported by Grand [18]. Grand measured the mean velocity and turbulence characteristics for Reynolds numbers of 5.10^4 to 4.10^5 and different Archimedes numbers (Ar=Grashof number/Re^2) for cavities with height to width ratio of 1.0 and 2.0 and span to width ratio of 1.0 (span is the dimension normal to the plane of flow). The comparison in this study is performed for a Reynolds number of 2.10^5, Archimedes number of 0.004 (with the top wall heated) and a height to width ratio of 1.0 ($H/W = 1.0$). In the computations a uniform grid is used with 37 grid points in the flow direction and 39 grid points in the direction perpendicular to the flow. The results obtained are presented in figures 5.4 to 5.9.

All the computations presented are for steady state conditions. For comparison purposes, the results of Ideriah [19] for the same conditions using the TEACH $K-\epsilon$ computational code are also presented. It can be seen that both codes yield similar results which are also in good agreement with the experimental measurements.

As a second test a more complex flow was selected. The physical model is shown in figure 5.10. All the computations are in cylindrical coordinates. Both laminar and turbulent flows with or without swirl velocity were considered. The comparison is based on tests performed by Salcudean and Lai using the TEMA code which was developed from the TEACH code [20]. The computations were for a low inlet velocity of $1.0m/s$ and a high convective flow with an inlet velocity of $20.0m/s$.

In the computations it is assumed that the air in the cylinder has a density of $1.0kg/m^3$, a dynamic viscosity of 2.10^{-5}, and Prandtl number of 0.7. Initially, zero velocity and values for a turbulence kinetic energy and energy dissipation rate are assumed. The viscosity is initially assumed to be equal to the laminar viscosity.

The following inlet conditions are used :

$$K_{in} = 0.01 V_{in}^2$$

$$\epsilon_{in} = K_{in}^{1.5}/(0.1R)$$

$$\mu = \mu_l + C_\mu \rho_{in} K_{in}^2/\epsilon_{in}$$

where:

V_{in} - is the radial inlet velocity

R - is the cylinder radius.

In the computations an unequal mesh is used having 20 grid points in the axial direction and 24 in the radial. Figures 5.11 and 5.12 show the comparison between the developed code and the TEACH steady-state code for laminar flow with no swirl for fluid inlet velocity of $1.0 m/s$ and $20.0 m/s$ respectively. It can be seen that they are in good agreement.

Figures 5.13 and 5.14 show the comparison with the TEACH steady-state code for turbulent flow with no swirl. It can be observed from the figures that the velocity field, the turbulent characteristics, and the effective viscosity are in good agreement.

Good agreement between the two codes is also evident for turbulent two-dimensional axisymmetric flow with swirl (see figures 5.15 and 5.16).

5.11 COMPUTATION OF THE SCAVENGING EFFICIENCY

The objective of the scavenging process is to replace the residual gases in the cylinder with air at air-box pressure and temperature. In order to improve the engine performance a) the scavenging efficiency must increase and b) the time that the process needs must decrease. Minimization of the scavenging time is very important because the available time for combustion can thus increase, leading to better performance. Also, by increasing the scavenging efficiency more oxygen

becomes available for combustion, which means that more fuel can be burned, thus increasing the engine output power.

The scavenging efficiency depends on the engine operating conditions (air-box pressure, exhaust manifold pressure, etc.) and on design geometry (cylinder geometry, piston shape, valve and ports timing, etc.). These parameters affect the process because they influence the generation of the fluid recirculation zones in the cylinder. The scavenging process, as will be seen later, is affected by the recirculation zones because they a) trap residual gases and b) increase the fluid speed towards the exhaust opening by reducing the available area.

The multi-dimensional model is used for evaluation of the scavenging process. The study of the process is performed with results obtained from the thermodynamic model because the inlet and outlet flow conditions are not known. Diwakar [21] assumes a constant pressure in the air-box and exhaust valves and calculates the inflow and outflow rates using the compressible orifice flow equations. In this study the flow rates are obtained from the thermodynamic model. The model, in its present stage of development, cannot model the piston motion which actually opens and closes the inlet ports. Instead the piston is assumed to be fixed at the Bottom Dead Center (BDC) and the available area of the ports is assumed to change with time. This was done by utilizing a fine mesh at the inlet ports and assuming that some cells behave as wall or port openings depending on the crank angle. Figure 5.17 shows how the inlet port opening area varies with time. This area was divided into eleven sections with different but constant area for eleven different crank angle inlet values. The total opening area is the same as that of the actual engine. The same procedure is used for the exhaust valves (see figure 5.18).

In the computations a variable mesh of 24 grid points in the radial direction and 28 grid points in the axial direction is used. Initially a zero velocity is assumed

in the cylinder. The cylinder residual gases are at a temperature of 700.0 K, the air-box at 320.0 K and the pressure is 115.1 kPa. A difficult task is the estimation of the inlet velocity orientation. Diwakar assumes the inlet velocity as being horizontal and inclined in the horizontal plane so as to impose the engine swirl. The engine sleeve has 18 inlet ports with a height of 2.13 cm and a width of 1.24 cm at a 22 degree incline to the radial direction. From computations for laminar flow, modeling the engine cylinder and the air-box (see figure 5.19), Flanagan et. al. [22] have shown that the flow enters the engine cylinder with a 20 degree incline to the horizontal. Also, it is expected that the inclination of the flow entering the cylinder to the radius will not be 22 degrees because of the relatively large width of the inlet ports. Therefore, the flow is assumed to enter the inlet ports with a 15 degree swirl angle to the radius and 20 degrees to the horizontal. These conditions will be considered as reference and comparisons will be performed later for horizontal inflow with a 22 degree swirl. The outflow velocity is assumed to be axial. Because the model is axisymmetric both the inlet ports and exhaust valves are modeled by assuming annular openings.

Figure 5.20 shows the flow development during the scavenging process at different crank angles. At a crank angle of 140 degrees there are two recirculation zones in the cylinder. The first one appears close to the cylinder wall (flow reattachment) and the second one in the piston bowl (which is not very strong). The maximum velocity in the cylinder is 44.13 m/s. In figure 5.21 the mass flux patterns (velocity $\times$ density) are shown for different crank angles. Comparison of the velocity and mass flux patterns shows that they are very similar in shape but with different magnitude at different locations because of the density variation within the field. As discussed in the solution procedure, the density varies with the temperature in the field, explaining the high mass flux close to the inlet ports. The temperature contours are shown in figure 5.22 for different crank angles. In the

computations a uniform constant-temperature is assumed at the cylinder walls. Every cylinder wall is assumed to be at a different temperature.

As the scavenging process progresses the two recirculation zones grow in size and at 165 degrees a weak recirculation zone appears close to the axis of symmetry due to swirl.It can be noted that at 165 degrees a change in the direction of the main flow occurs due to recirculation at the axis of symmetry. Until the end of the scavenging process these recirculation zones exist in the cylinder and are growing in size as the exhaust valves are closing.

The swirl velocity contours are shown in figure 5.23 for different crank angles. Initially, the swirl velocity is high due to a high inlet velocity during the scavenging process; the maximum swirl velocity in the cylinder appears at the lower part of the cylinder due to swirl introduced by the inclined inlet flow. The magnitude of the swirl velocity is of the same order of magnitude as the axial velocity.

The effect of the recirculation zones on the scavenging efficiency is not obvious from examining the velocity or the flux patterns. A better understanding can be gained from the concentration contours at different crank angles shown in figure 5.24. Initially the cylinder is assumed to have a zero air concentration, which indicates that only residual gases are present. The concentration of the air is assumed equal to one and is imposed at the inlet ports. As can be seen from figure 5.24, up to a 165.0 degree crank angle no air escapes the cylinder From about 175 degrees crank angle to the end of the process air starts escaping from the cylinder through the exhaust valves. At the upper section of the cylinder, close to the axis of symmetry where the recirculation zone due to swirl exists, low concentration contours are observed indicating a high concentration of residual gases. The volume occupied by this zone is rather small but, because of the high concentration of residual gases this area is expected to contribute to the reduction of the scavenging efficiency. Also, this zone reduces the available cylinder area

causing an increase in the velocity of the flow towards the exhaust opening. This results in air escaping faster from the cylinder. Close to the cylinder wall low concentration contours are also observed because of the recirculation zone. The concentration of residual gases in this area is smaller than that of the area close to the cylinder axis. However, because this area is close to the cylinder periphery it occupies a large percentage of the cylinder volume. Therefore, it is expected that the effect to the scavenging efficiency of this area will be similar to that of the area close to the cylinder axis.

Figure 5.25 shows the effective viscosity computed from the solution of the K and ϵ equations. In the figure the contour values are for the effective viscosity divided by the fluid dynamic viscosity. It can be seen that close to the end of the scavenging process the effective viscosity is about 600 times the fluid viscosity. The turbulence kinetic energy is given in figure 5.26.

As discussed earlier, the inlet flow conditions are not known and without experimental measurements can not be accurately predicted. For comparison the case of horizontal inflow with a 22 degree swirl angle was considered.

Figure 5.27 shows the fluid velocity development with the new inlet conditions. From 140 degrees the recirculation zone close to the cylinder axis is obvious. This recirculation appears because of high swirl velocity (47.83 m/s) as can be seen in figure 5.28. This velocity is almost two times larger than the swirl velocities observed in the reference case (see fig. 5.23). The effect of this recirculation zone is higher axial velocities until approximately 180 degrees. High axial velocities strongly affect the scavenging process as can be seen from the concentration contours in figure 5.29. In the reference case, because of smaller axial velocities, no air escapes the cylinder at 165 degrees crank angle (see fig. 5.24). For the case of the horizontal inflow with higher swirl some air escapes the cylinder at 165 degrees (see fig. 5.24), thus reducing the scavenging efficiency. After 180 degrees the flow

patterns in the two cases are quite similar. The reference case, though, produces a higher scavenging efficiency (3.4 percent higher).

In figure 5.30 the scavenging efficiency-scavenging ratio relation for the reference case is plotted, along with the perfect scavenging and pure mixing curves. It can be seen that the computed efficiency is approximately 86 percent. This results is in agreement with the Diwakar [21] computations for a similar engine.

REFERENCES

1 Harlow, F. H., and Amsdin, A. A. "A Numerical Fluid Dynamics Method for All Flow Speeds", Journal of Computational Physics 8, 197-213, 1971.

2 Bird, R. B., Steward, W. E., and Lightfoot, E. N."Transport Phenomena", New York 1960, J. Wiley.

3 Rodi, W. "Turbulence Models and Their Applications in Hydraulics - A State of the Art Review", Intern. Assos. for Hydr Research, Delft, 1980. Intrn. Assos. for Hydraulics Research, Delft, 1980.

4 Reynolds, W. C. "Modeling of Fluid Motions in Engines-An Introductory Overview", Proceedings of a Symposium Held at the General Motors Research Laboratories, Michigan U.S.A., Nov. 6, 1978.

5 Launder, B. E., and Spalding, D. B. "The Numerical Computation of Turbulent Flows", Comp. Meth. in Applied Mech. and Engineering 3 pp. 269-289, 1972.

6 Courant, R., Issacson, E., and Rees, M. "On the Solution of Non-linear Hyperbolic Differential Equations by Finite Differences", Comp. Pure Appl. Math., vol 5, p. 234, 1952.

7 Spalding, D. B. "A Novel Finite Difference Formulation for Differential Expressions Involving Both First and Second Derivatives", Intern. Journal for Numerical Methods in Engineering, vol. 4, 551-559, 1972.

8 Ramos, J. I., Humphrey, J. A. C., and Sirignano, W. A. "Numerical Predictions of Axisymmetric Laminar and Turbulent Flows in Motored, Reciprocating Internal Combustion Engines", SAE paper 790356, 1979.

9 Garner, G. O., and Kestin, J. "Calculation of the Spalding Function over a Range of Prandtl Numbers", Int. J. of Heat and Mass Transfer, vol. 6, 289-299, 1963.

10 Schlichting, H. "Boundary-Layer Theory", McGraw-Hill Book Company, Seventh Edition, 1979.

11 Spalding, B. "Contribution to the Theory of Heat Transfer Across a Turbulent Boundary Layer", Int. J. Heat and Mass Transfer, vol. 7, pp. 743-761, 1964.

12 Jayatillaka, C. L. V. "The influence of Prandtl Number and Surface Roughness on the, Resistance of the Laminar Sub-Layer to Momentum and Heat Transfer", Ph.D. Thesis, London University, 1967.

13 Lilly, D. G., and Rhode, D. L. "A Computer Code for Swirling Axisymmetric Recirculating Flows in Practical Isothermal Combustor Geometries", NASA Report 3442, 1982.

14 Gosman, A. D., and Pun, W. M. "Calculation of Recirculating Flows", Lecture Notes, Imperial College of Science and Technology, Mechanical Engineering Department, December, 1974.

15 Yowakim, F. M. "Experimental Investigation of Turbulent Swirling Flow in an Annulus", Ph.D. Thesis, Carleton University, 1985.

16 Butler, T. D., and O'Rourke, P. J. "A Numerical Method for Two Dimensional Reacting Flows", Proc. 16th Intern. Symp. Combustion, Massachusetts Institute of Technology, pp. 1503-1515, 1976.

17 Anderson, D. A., Tannehill, J. C., and Pletcher, R. C. "Computational Fluid Mechanics and Heat Transfer", McGraw-Hill Book Company, 1984.

18 Grand, D. "Contribution a L' etude des Courants de Recirculation", Ph.D. Thesis, L' Universite Scientifiaue et Medicale et inst. Nat. Polytechnique, Grenoble, 1975.

19 Ideriah, F. J. K "Turbulent Natural and Forced Convection in Plumes and Cavities", Ph.D. Thesis, University of London, 1977.

20 Salcudean, M., and Lai, K. Y. M. "Computer Simulation of Flow in Cylinders", Internal Report, University of Ottawa, Department of Mechanical Engineering, 1984.

21 Diwakar, R. "Multidimensional Modeling of the Gas Exchange Processes in

a Uniflow-Scavenged Two-Stroke Engine", Presented at the Winter Annual Meeting of ASME, Nov. 17-22, 1985.

22. Flanagan, R. C., Salcudean, M., Carapanayotis, A., and Xia, Y. "A Study of Wide Boiling Range Fuel-Engine Interaction: Thermodynamic and Multidimensional Modeling", Technical Report No. UOME-EP-8404-1, Department of National Defense, Ottawa Ontario, 1984.

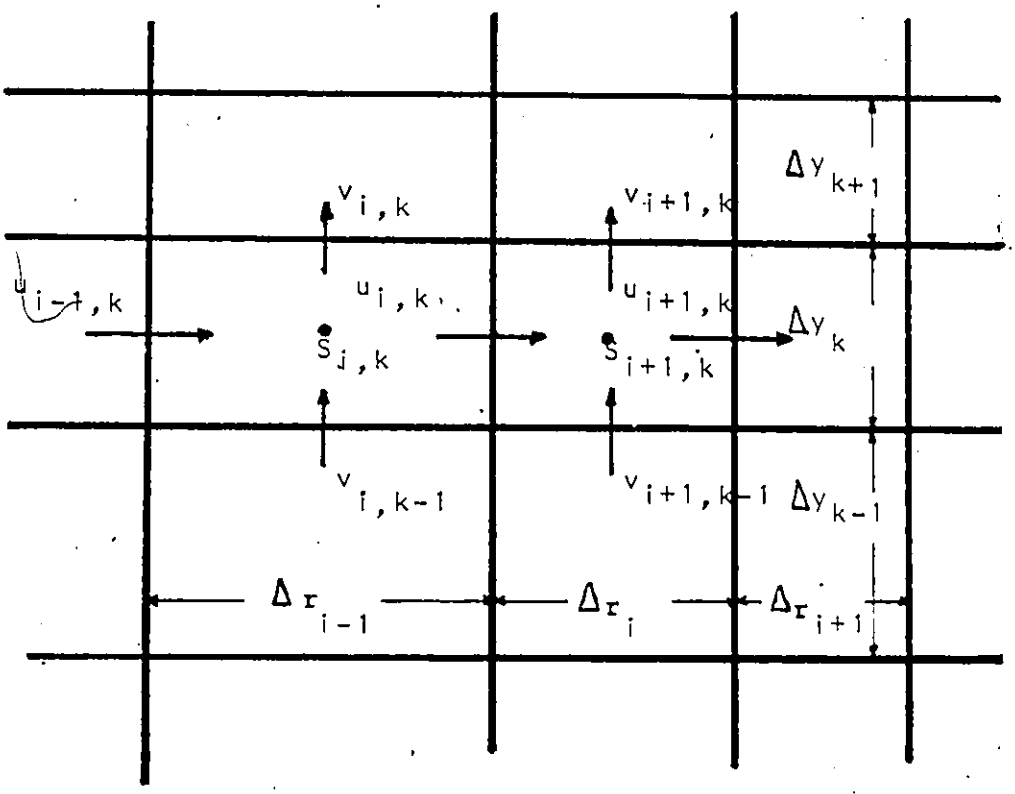

Figure 5.1a Cell arrangment used in the two-dimensional computations.

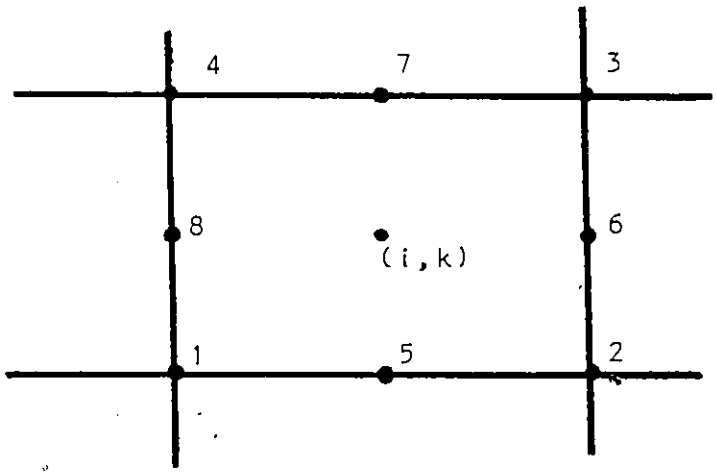

Figure 5.1b Numbering of the cell location used in the two-dimensional model

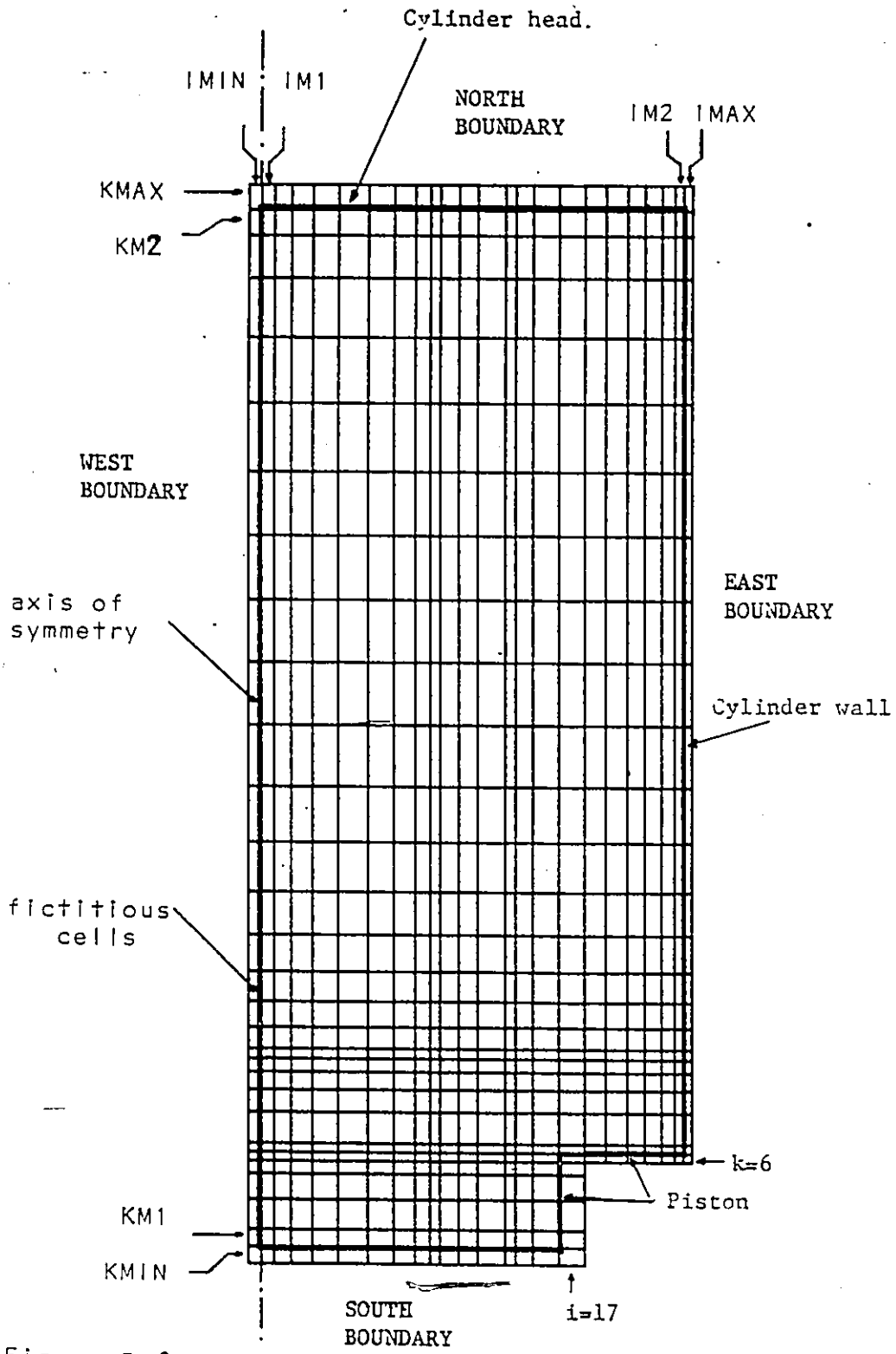

Figure 5.2 Grid used for the scavenging studies using the two-dimensional model.

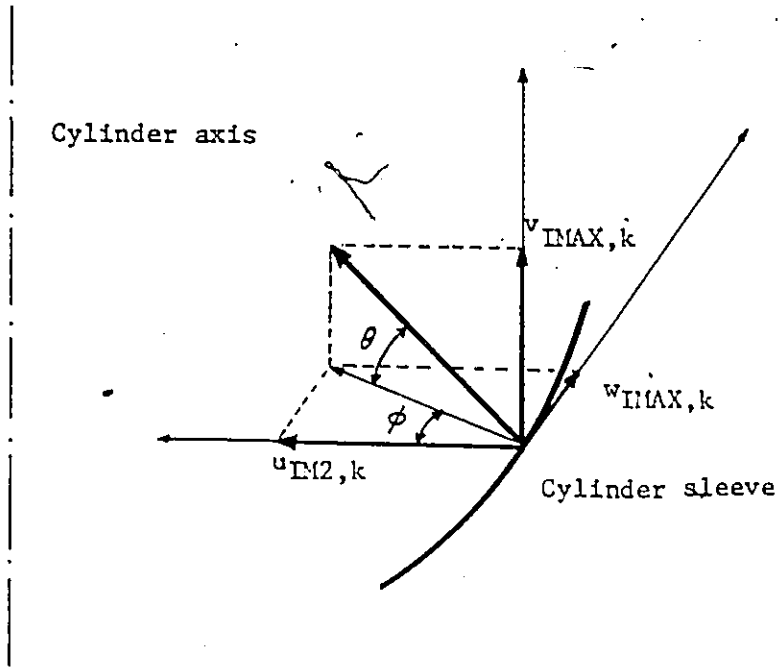

Figure 5.3 Inlet velocity geometry.

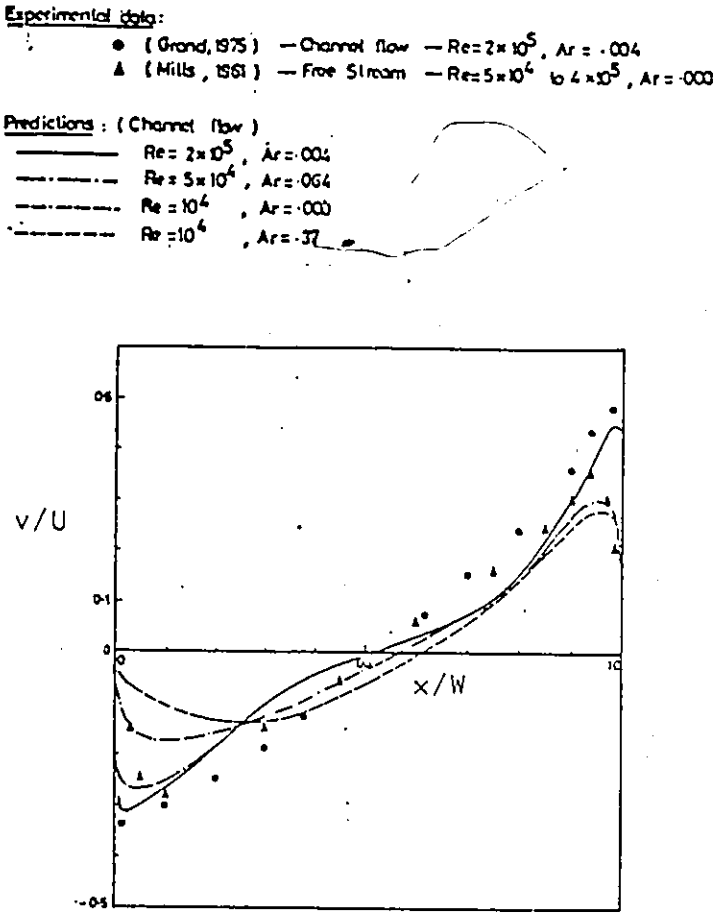

a) TEACH (from ref. [18]).

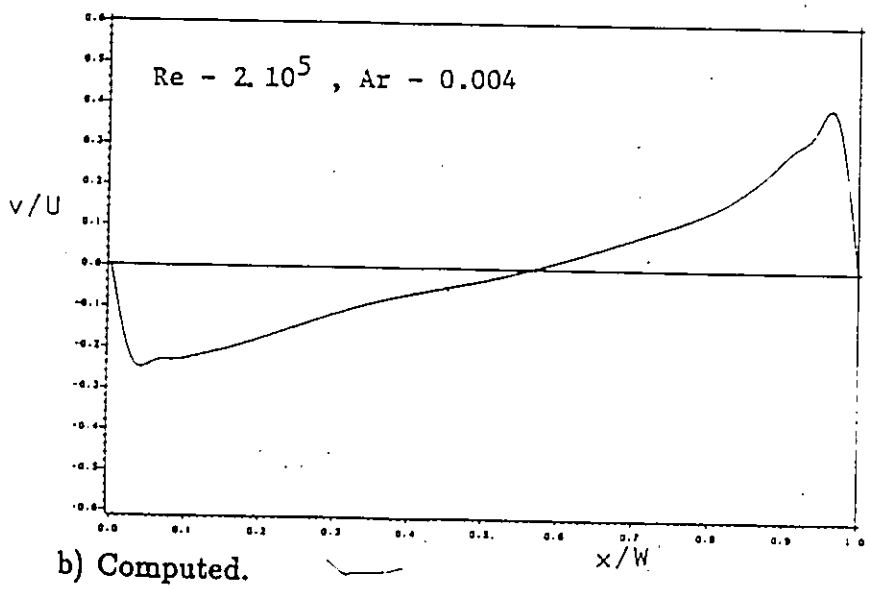

b) Computed.

Figure 5.4 Test case No. 1: Comparison between the developed 2-D code and the TEACH code for the vertical component of the mean velocity along the cavity's horizontal axis.

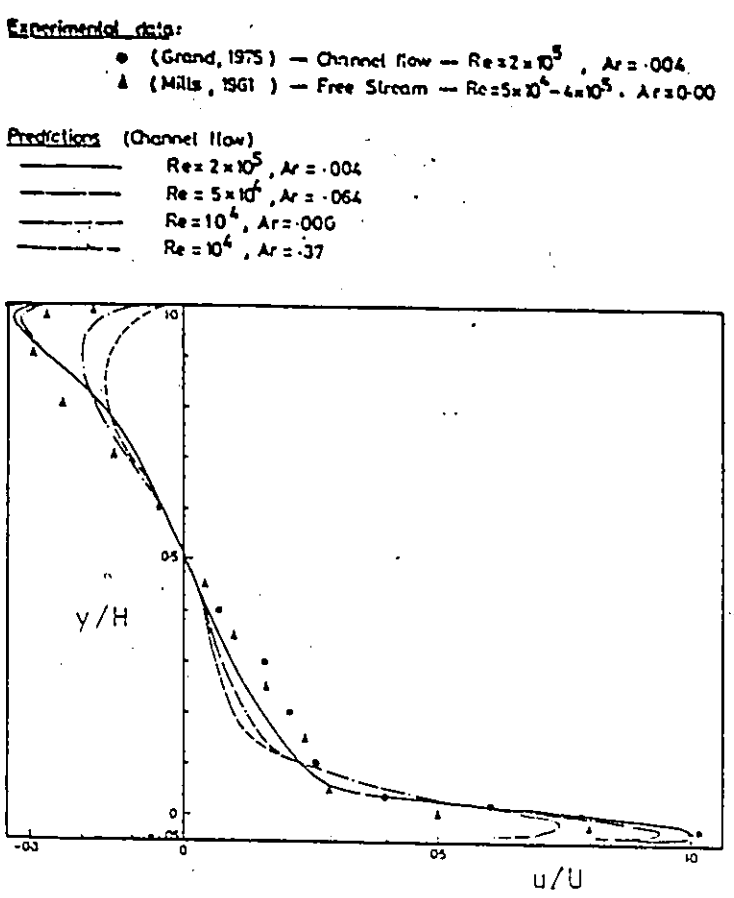

a) TEACH (from ref. [18]).

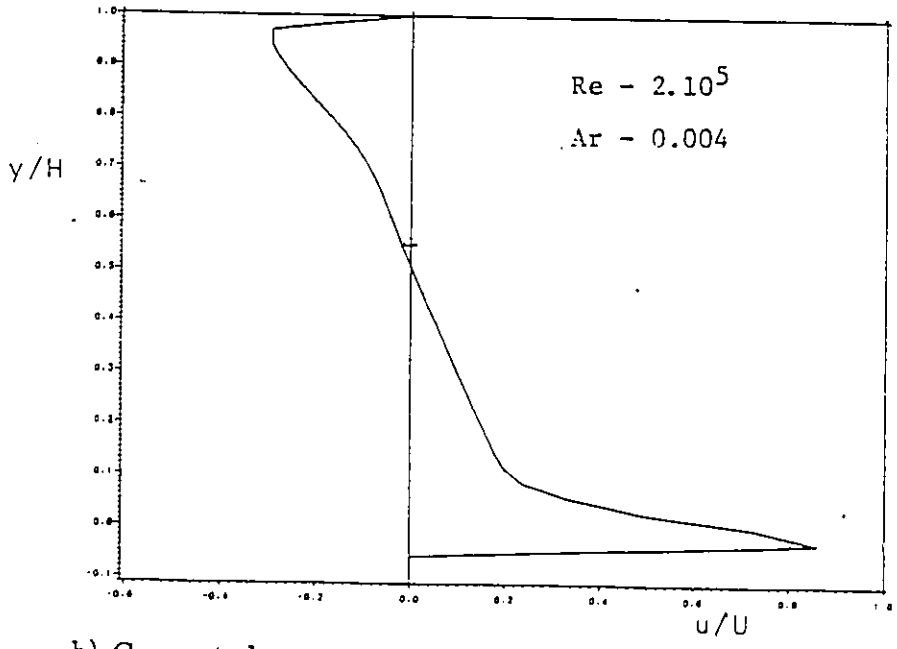

b) Computed.

Figure 5.5 Test case No. 1: Comparison between the developed 2-D code and the TEACH code for the horizontal component of the mean velocity along the cavity's vertical axis.

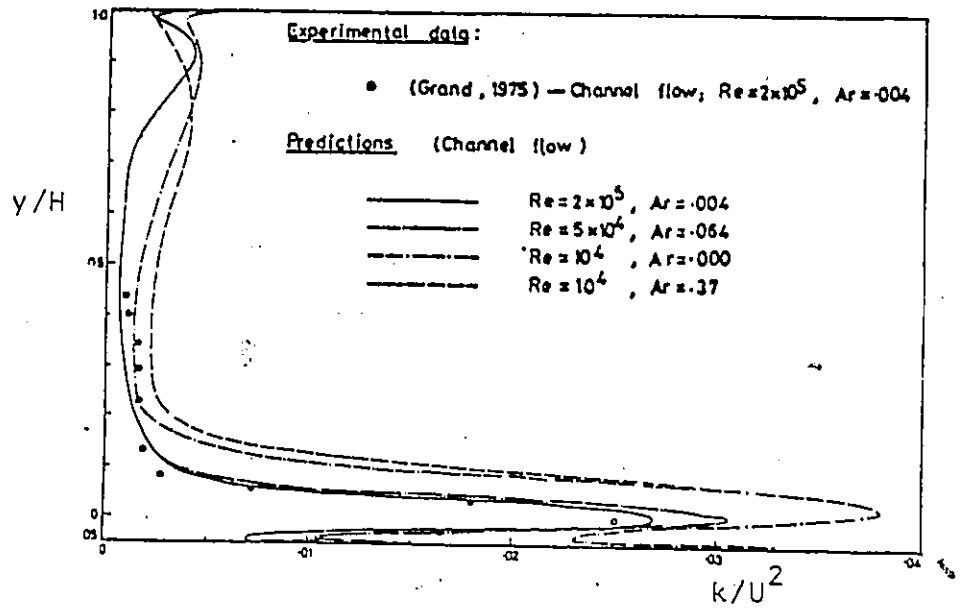

a) TEACH (from ref. [18]).

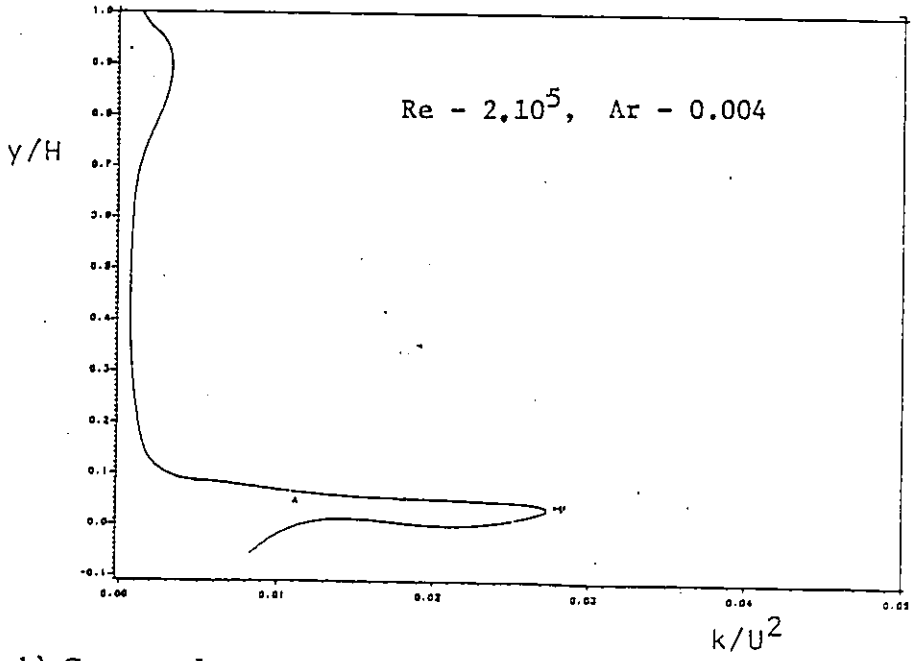

b) Computed.

Figure 5.6 Test case No. 1: Comparison between the developed 2-D code and the TEACH code for the turbulence kinetic energy along the cavity's vertical axis.

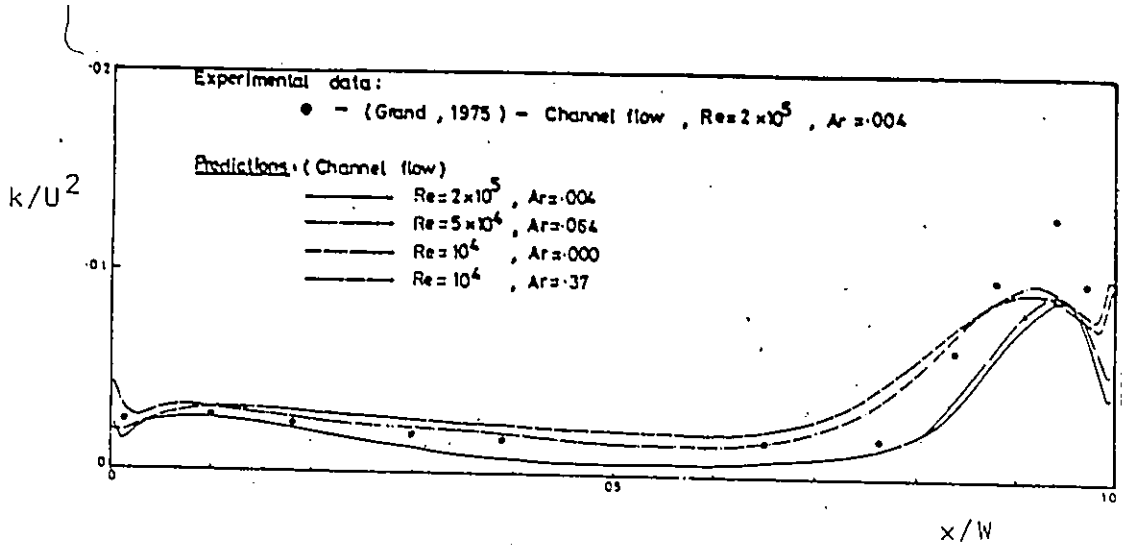

a) TEACH (from ref. [18]).

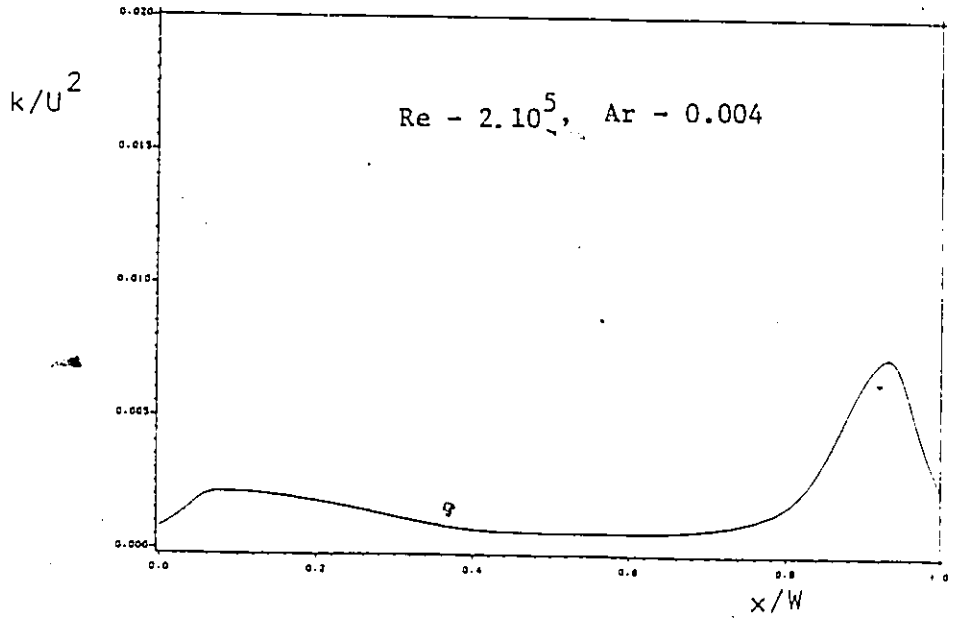

b) Computed.

Figure 5.7 Test case No. 1: Comparison between the developed 2-D code and the TEACH code for the turbulence kinetic energy along the cavity's horizontal axis.

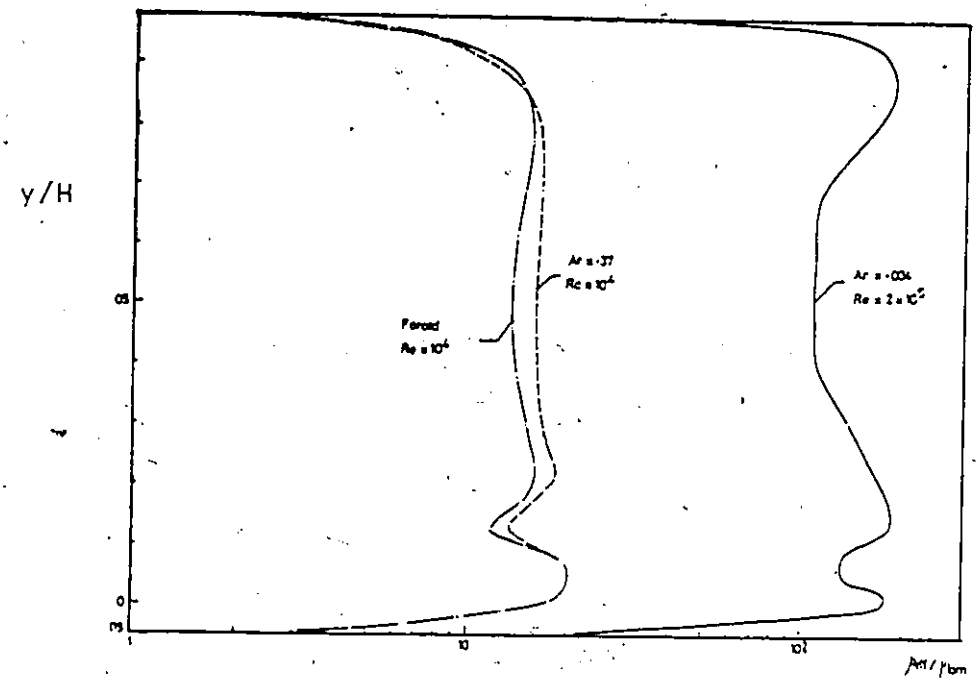

a) TEACH (from ref. [18]).

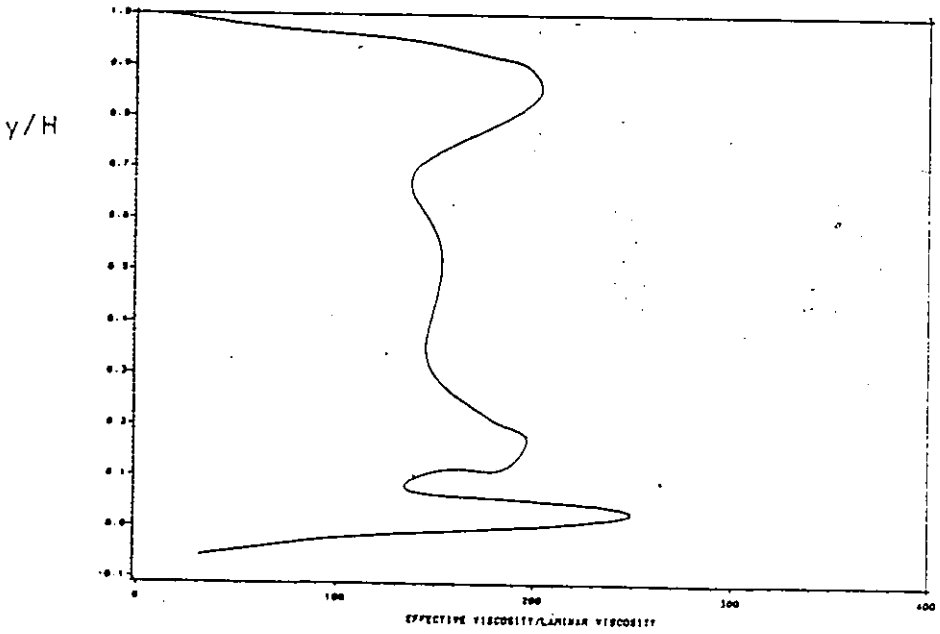

b) Computed.

Figure 5.8 Test case No. 1: Comparison between the developed 2-D code and the TEACH code for the effective viscosity along the cavity's vertical axis.

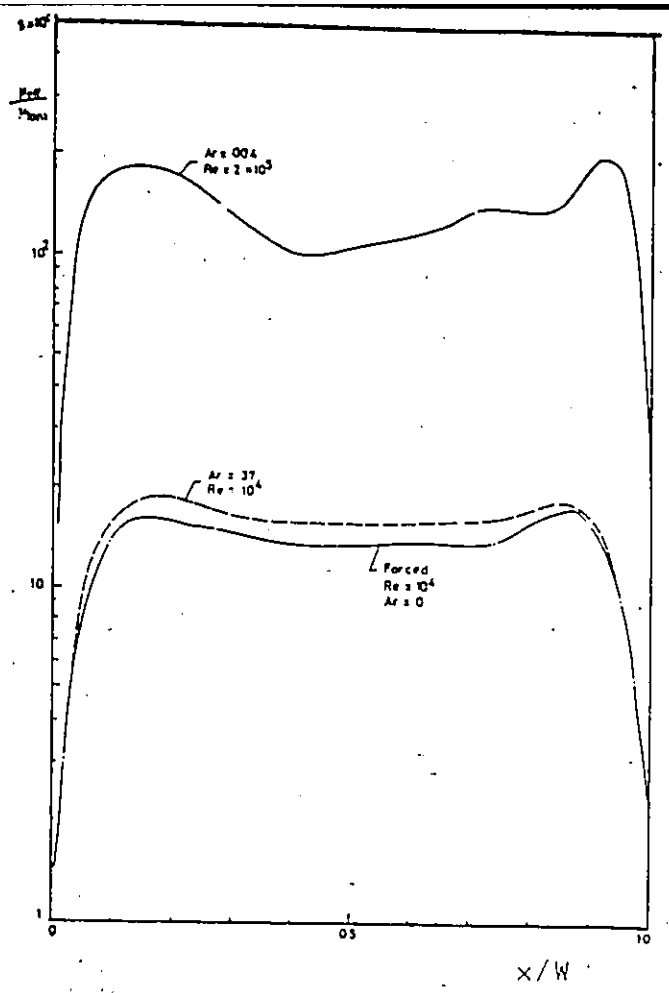

a) TEACH (from ref. [18]).

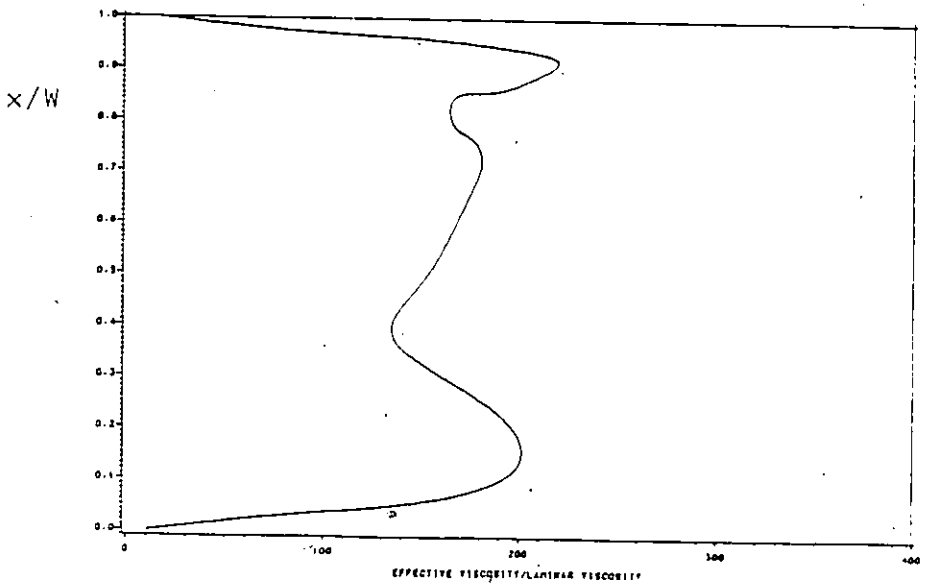

b) Computed.

Figure 5.9 Test case No. 1: Comparison between the developed 2-D code and the TEACH code for the effective viscosity along the cavity's horizontal axis.

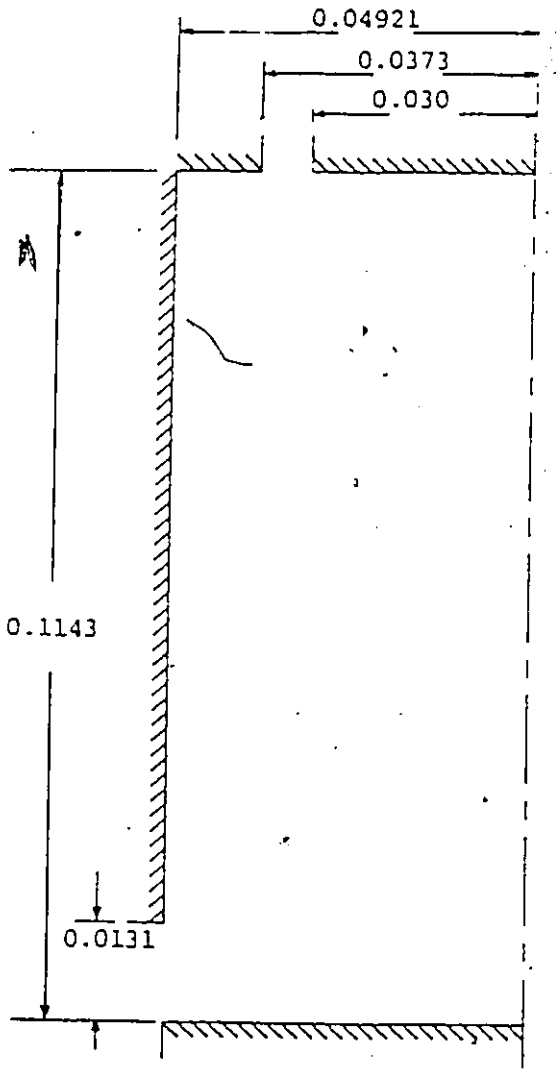

Figure 5.10 Computational domain for the test case No. 2.

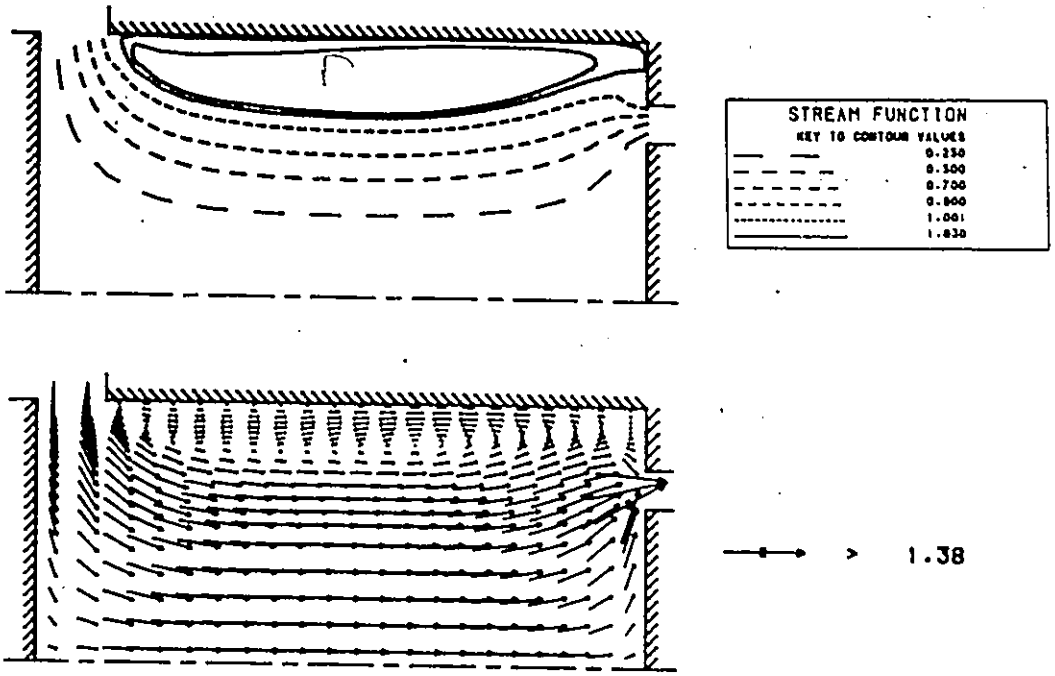

a) Computed.

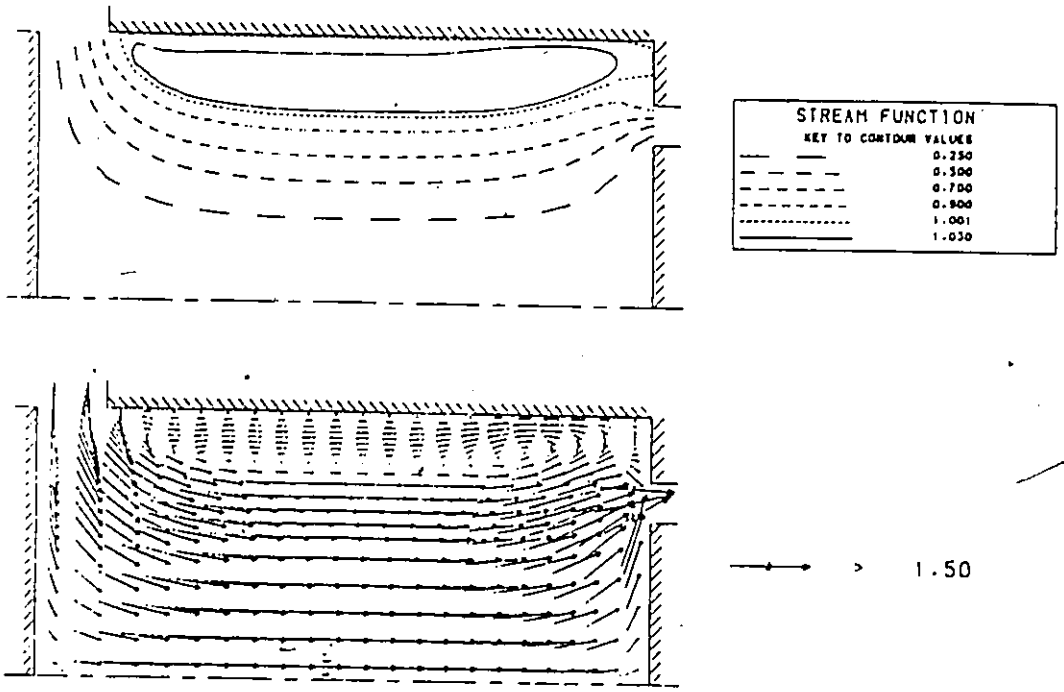

b) TEACH (from ref. [20]).

Figure 5.11 Test case No. 2: Comparison between the developed 2-D code and the TEACH code for laminar flow (inlet velocity 1.0 m/s with no swirl).

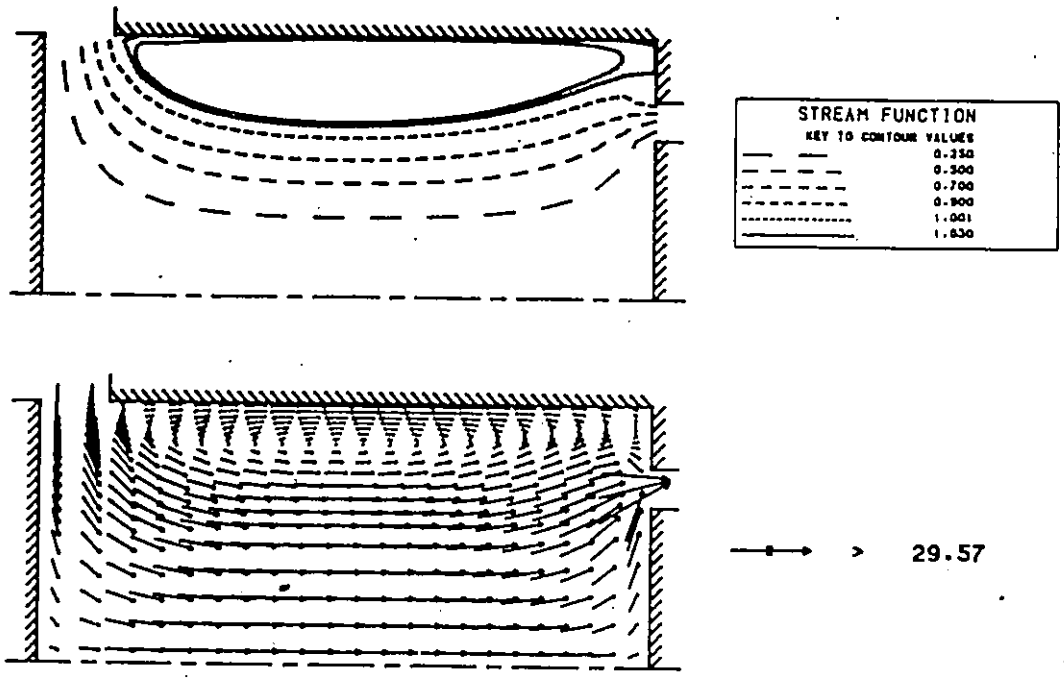

a) Computed.

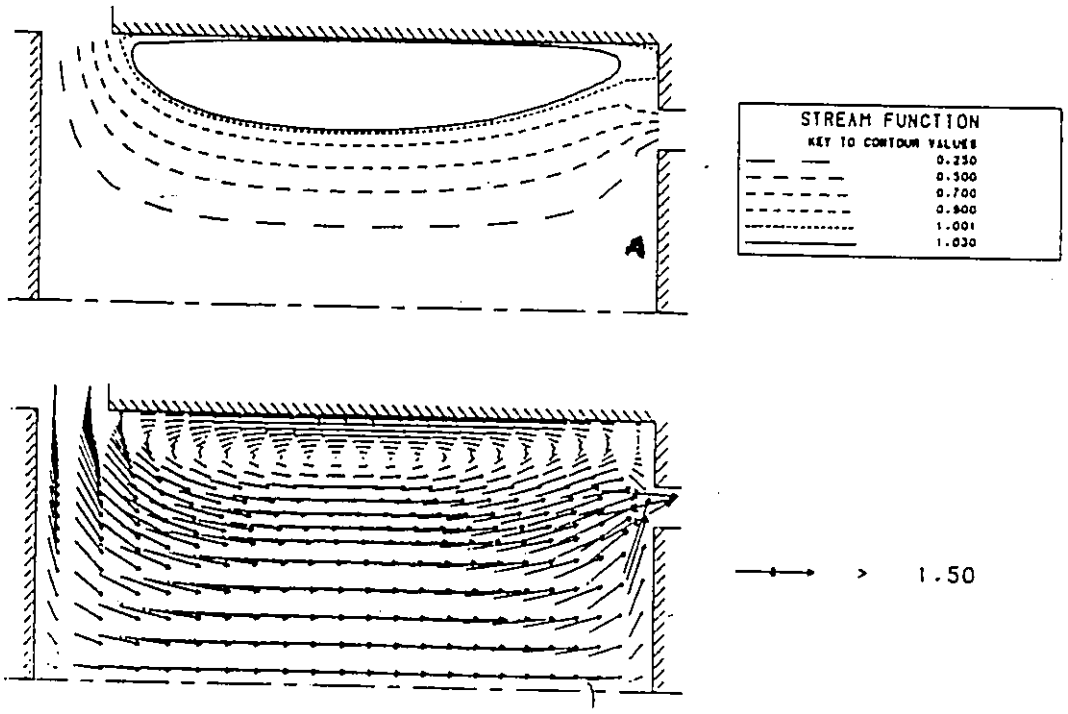

b) TEACH (from ref. [19]).

Figure 5.12 Test case No. 2: Comparison between the developed 2-D code and the TEACH code for laminar flow (inlet velocity 20.0 m/s with no swirl).

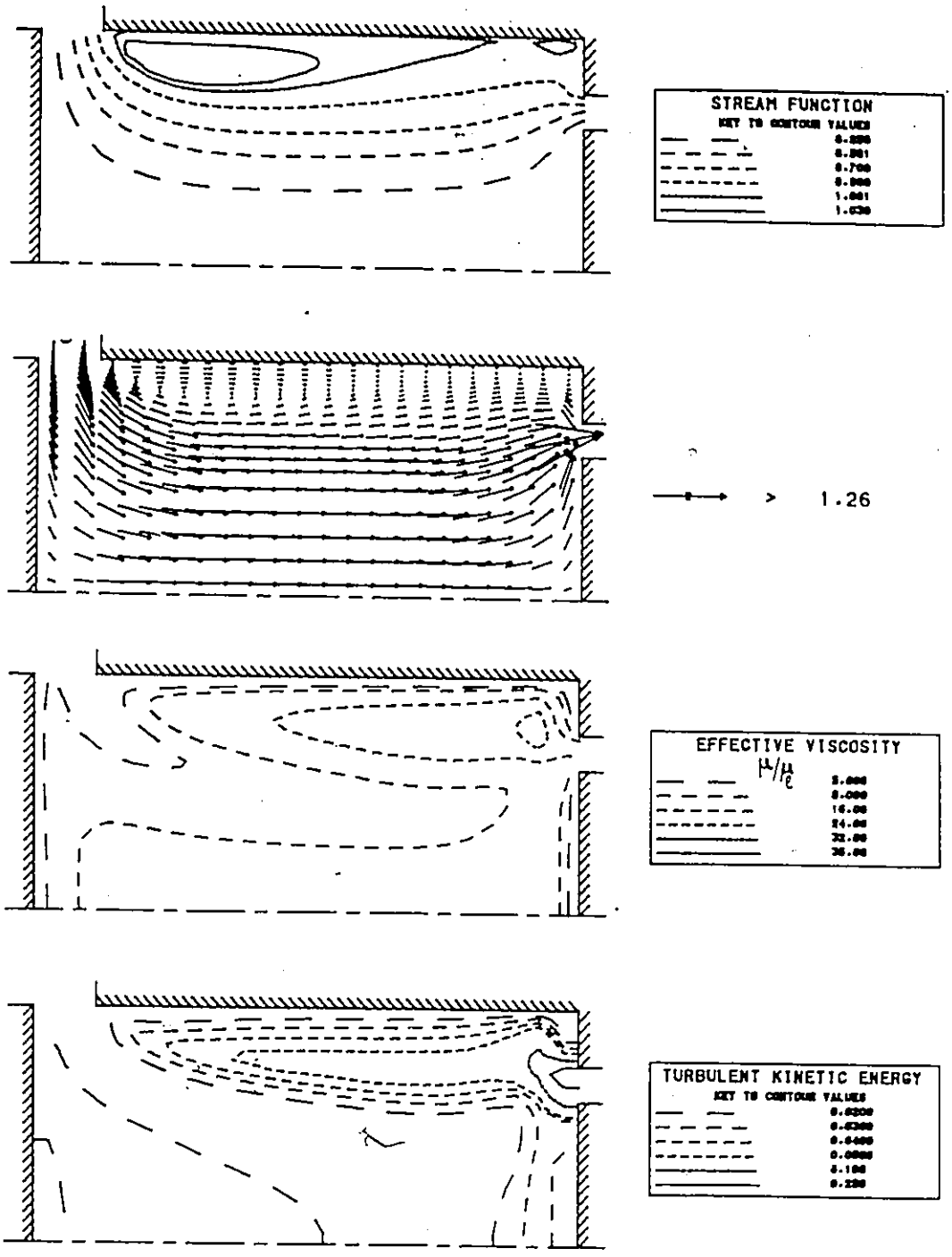

a) Computed.

Figure 5.13 Test case No. 2: Comparison between the developed 2-D code and the TEACH code for turbulent flow (inlet velocity 1.0 m/s with no swirl).

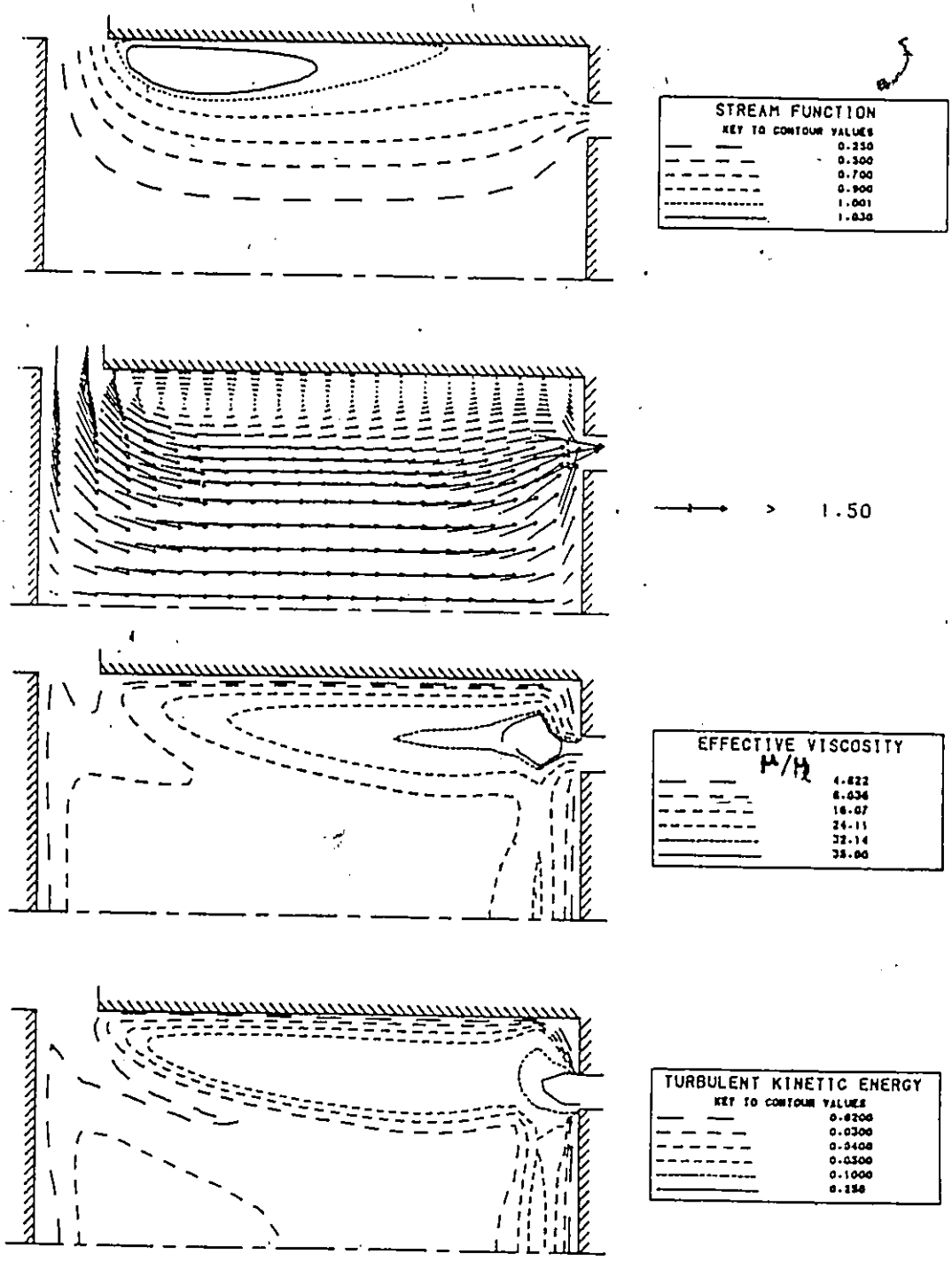

b) TEACH (from ref. [19]).

Figure 5.13 Continued.

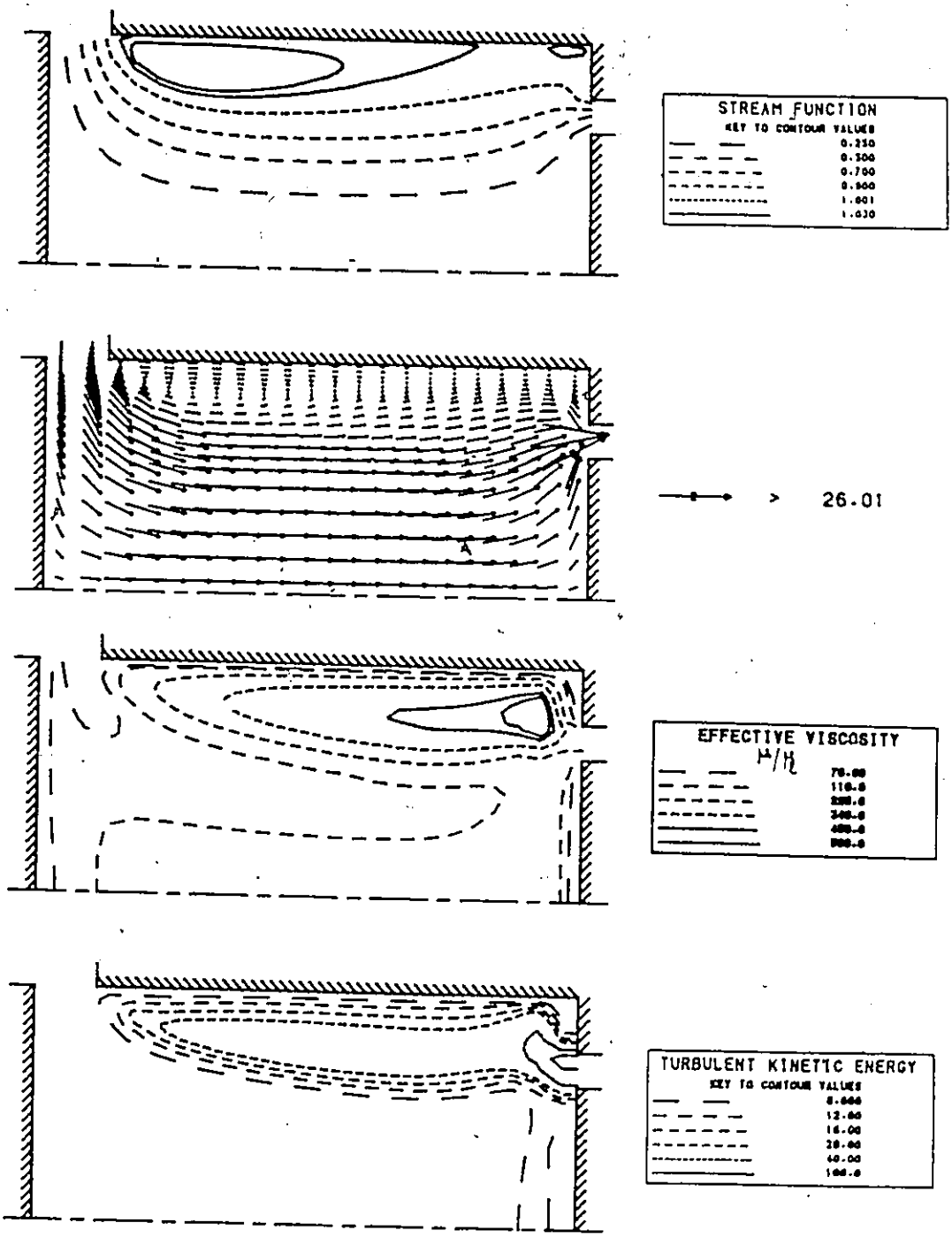

a) Computed.

Figure 5.14 Test case No. 2: Comparison between the developed 2-D code and the TEACH code for turbulent flow (inlet velocity 20.0 m/s with no swirl).

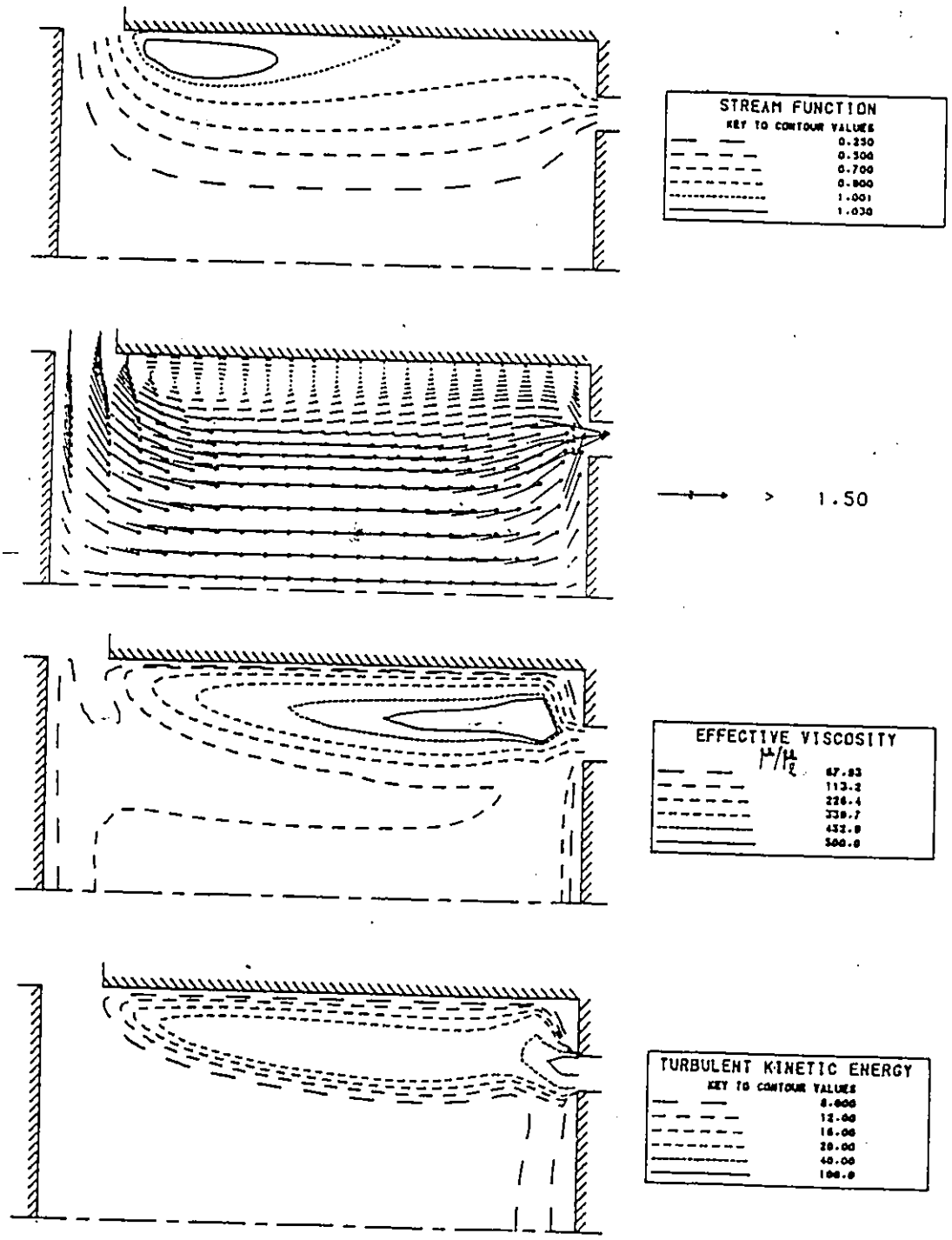

b) TEACH (from ref. [19]).

Figure 5.14 Continued.

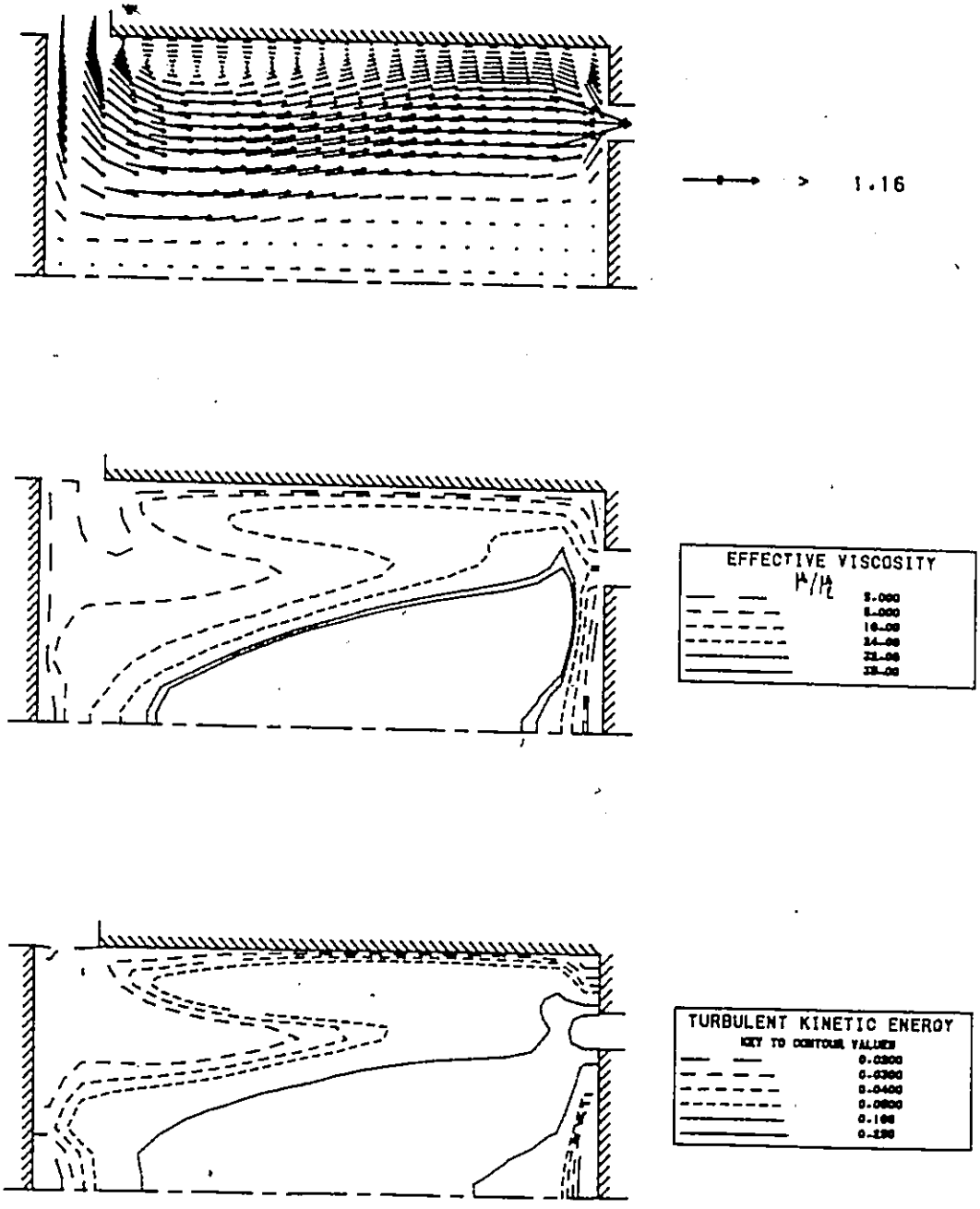

a) Computed.

Figure 5.15 Test case No. 2: Comparison between the developed 2-D code and the TEACH code for turbulent flow (inlet velocity 1.0 m/s with swirl).

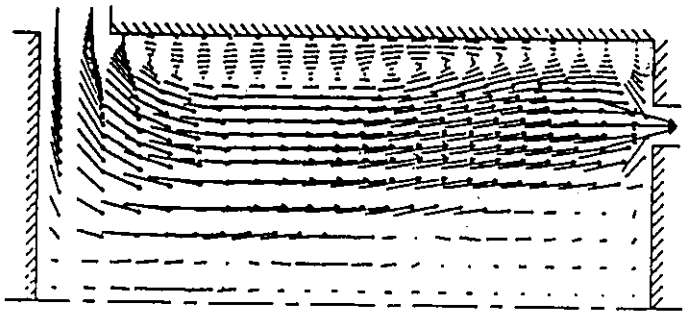

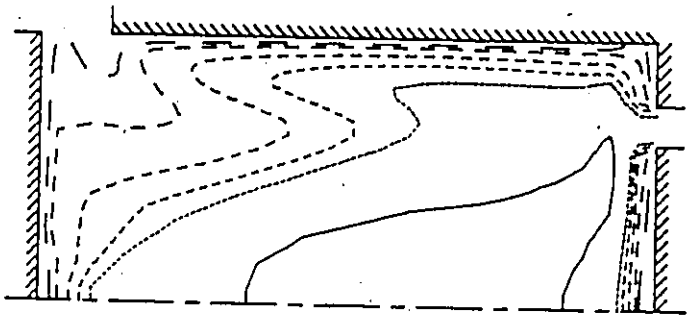

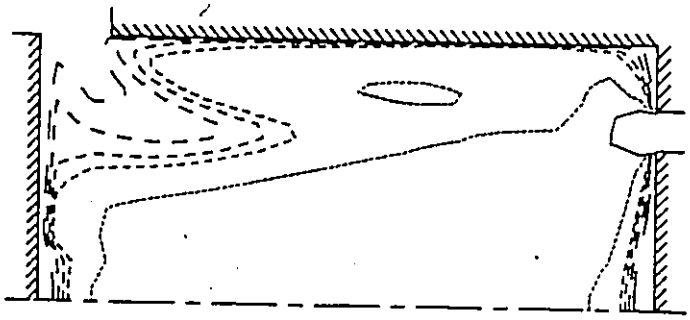

b) TEACH (from ref. [19]).

Figure 5.15 Continued.

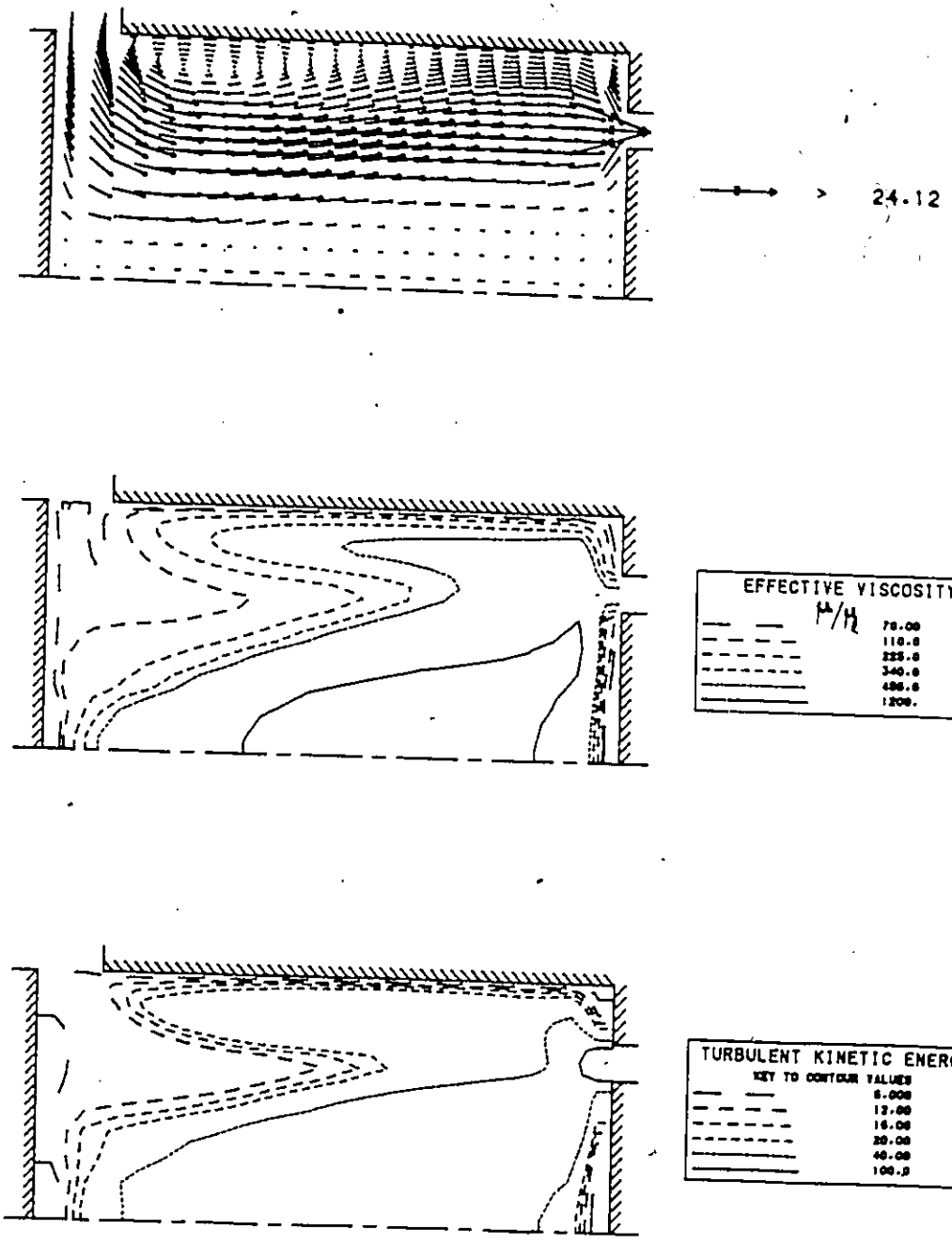

a) Computed.

Figure 5.16 Test case No. 2: Comparison between the developed 2-D code and the TEACH code for turbulent flow (inlet velocity 20.0 m/s with swirl).

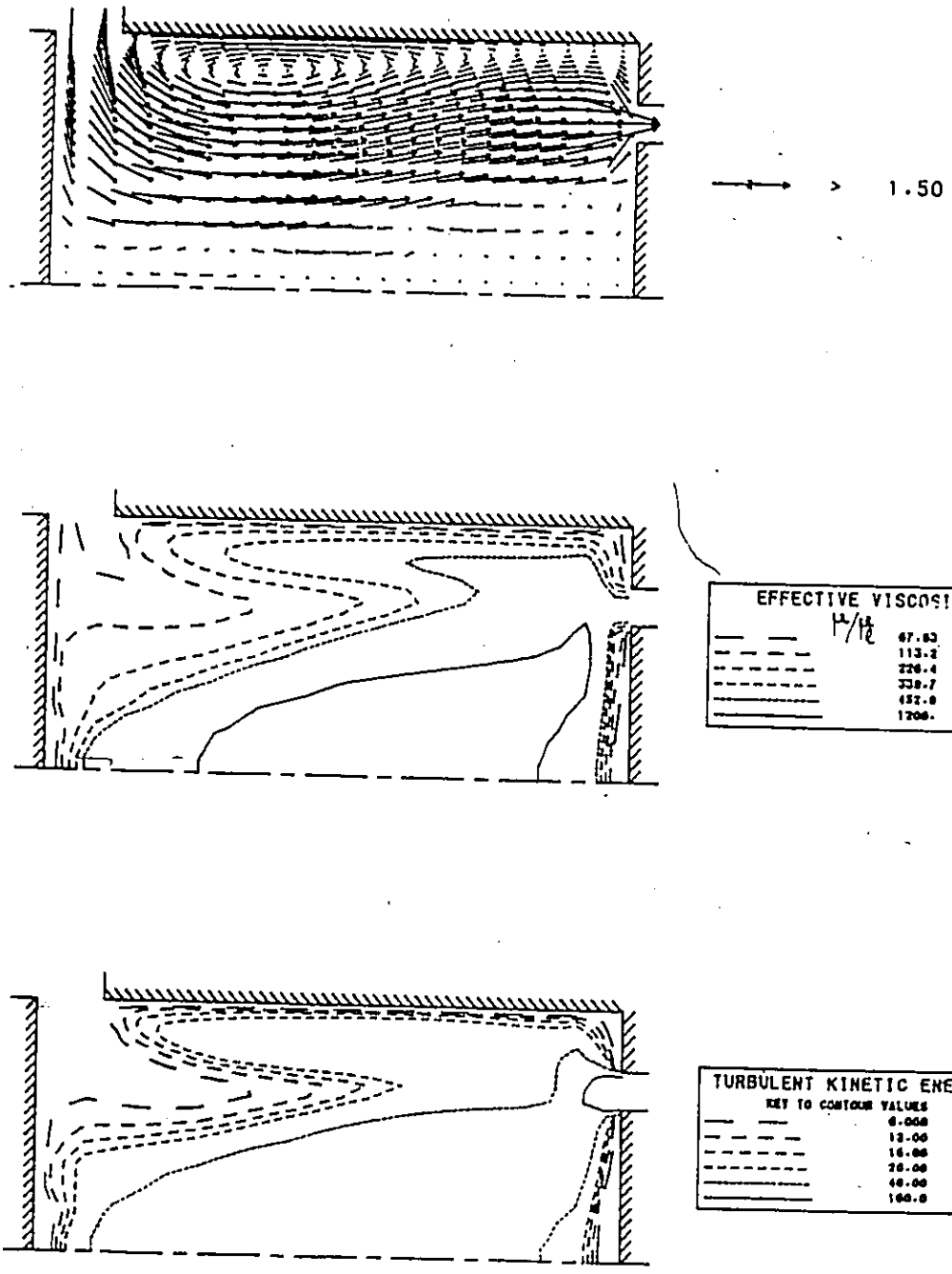

b) TEACH (from ref. [19]).

Figure 5.16 Continued.

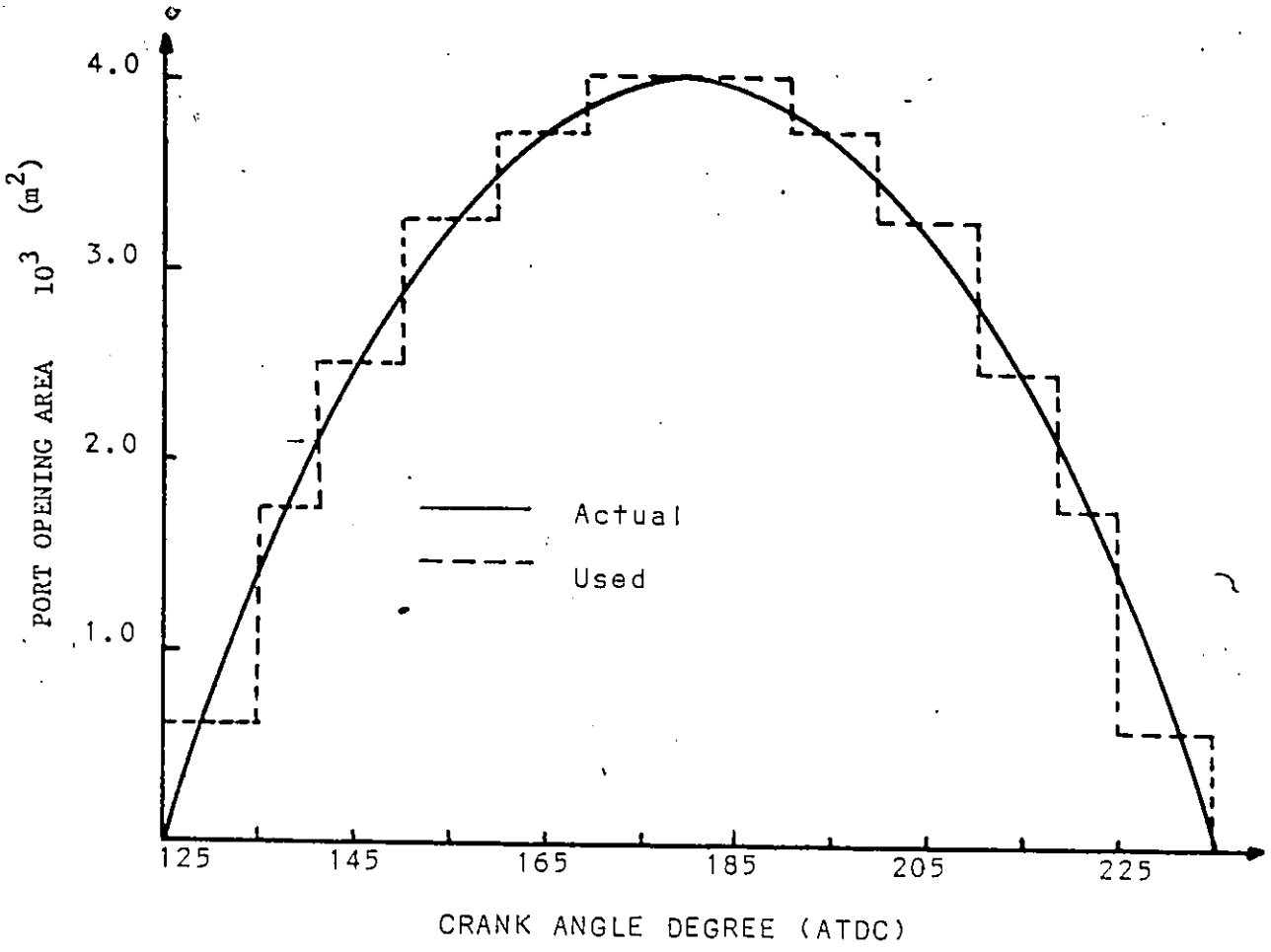

Figure 5.17 Port opening area as a function of crank angle location

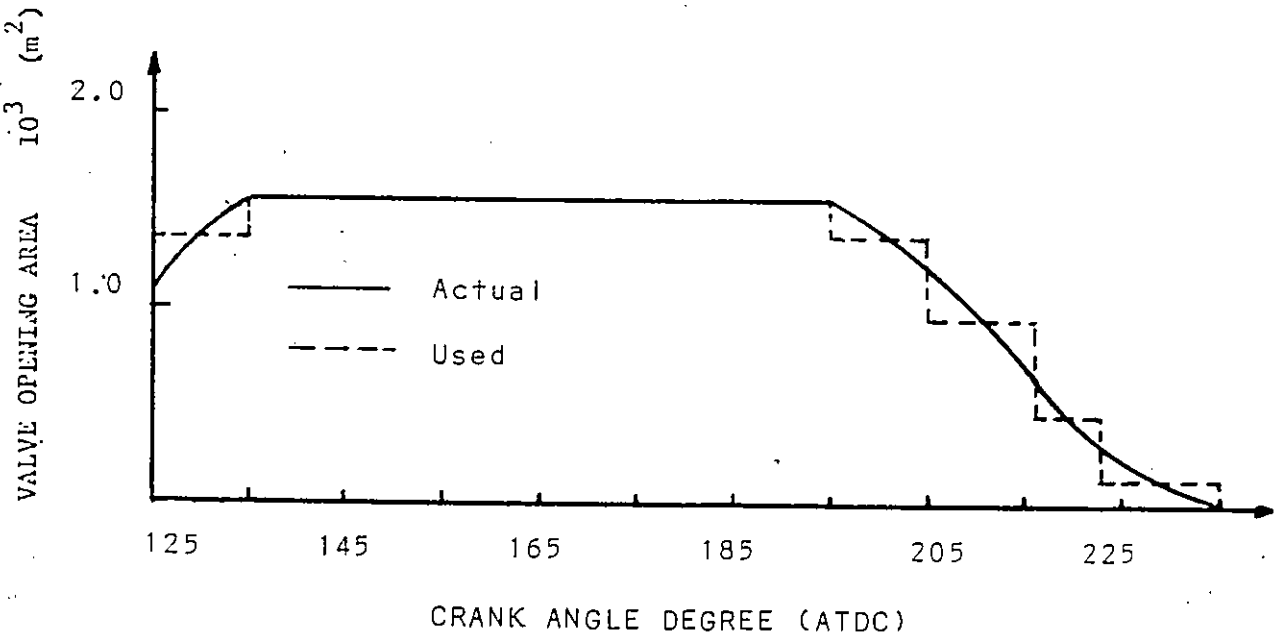

Figure 5.18 Valve opening area as a function of crank angle location.

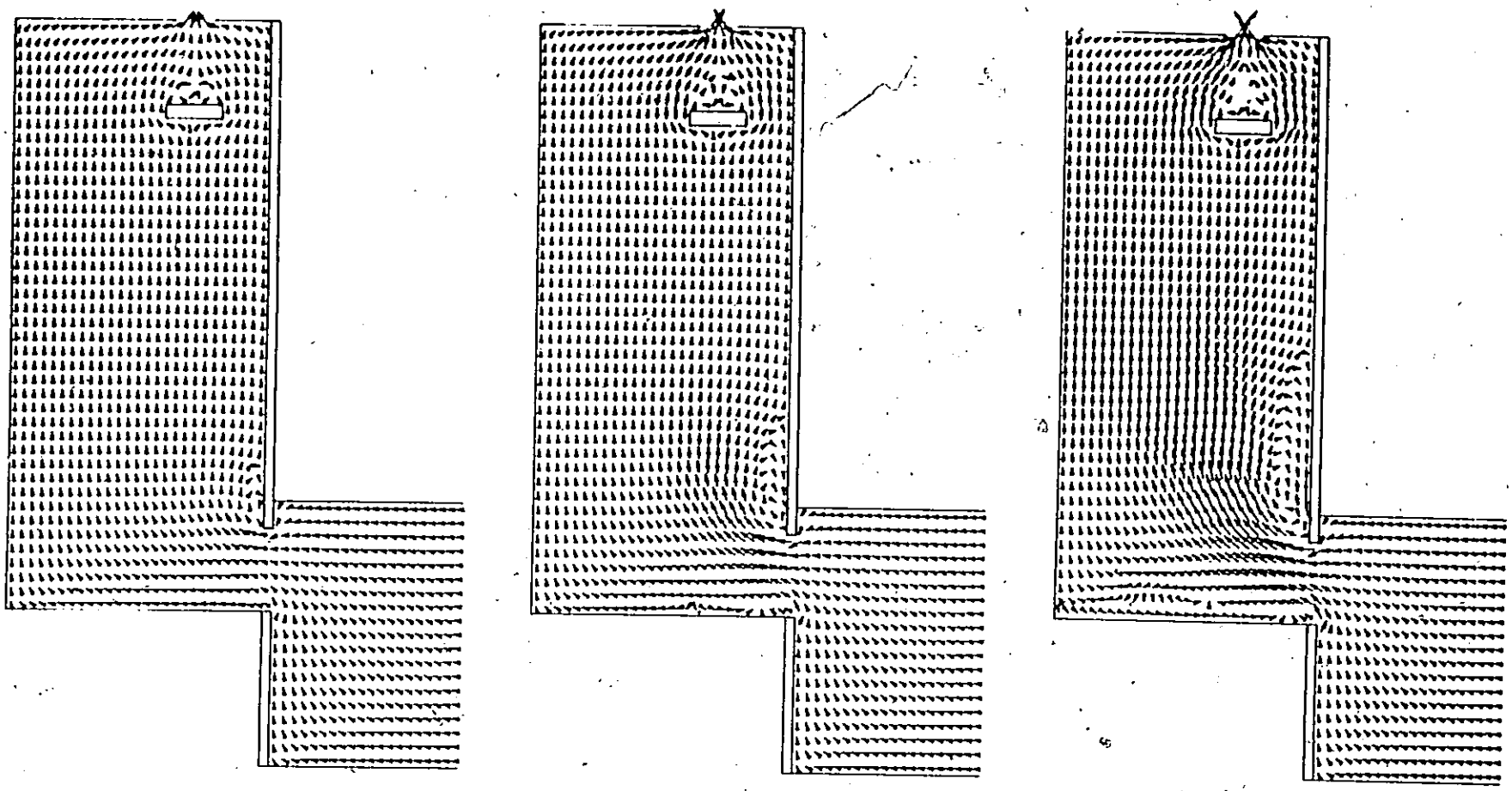

Figure 5.19 Flow development during scavenging (the cylinder and air-box are modeled).

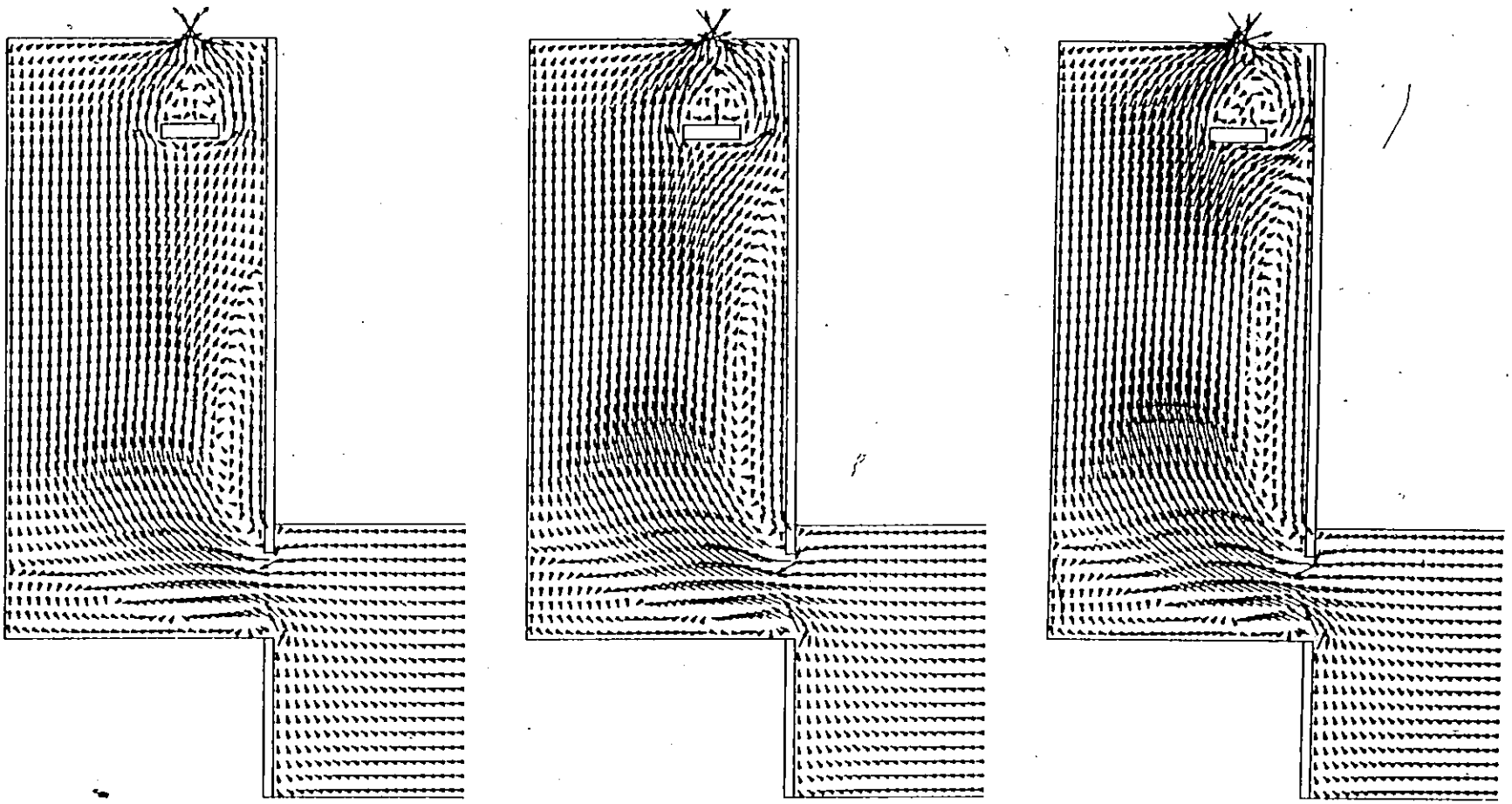

Figure 5.19 Continued.

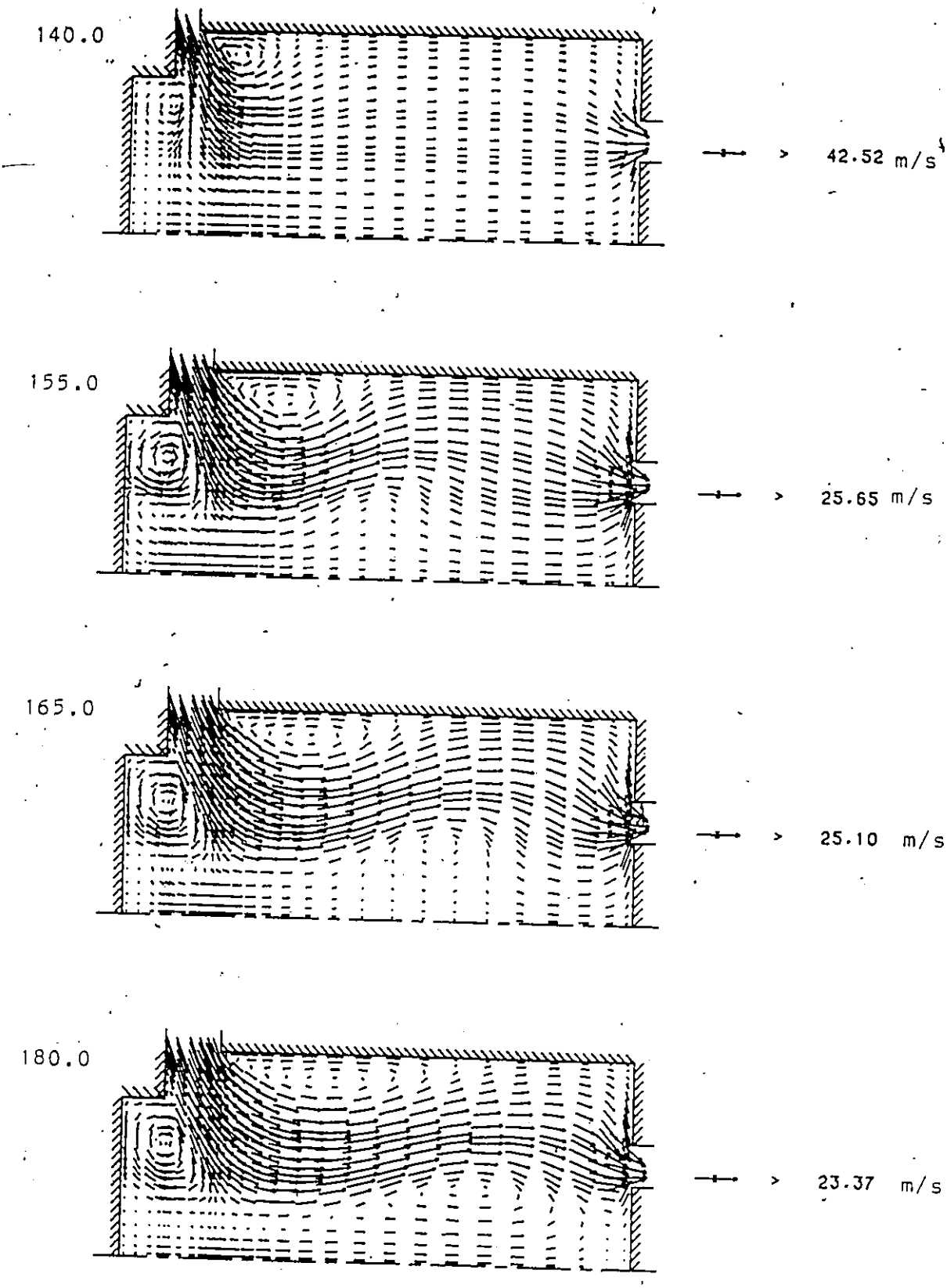

Figure 5.20 Velocity patterns during scavenging at different crank angles (inflow conditions: 20 degree incline to the horizontal with a 15 degree swirl).

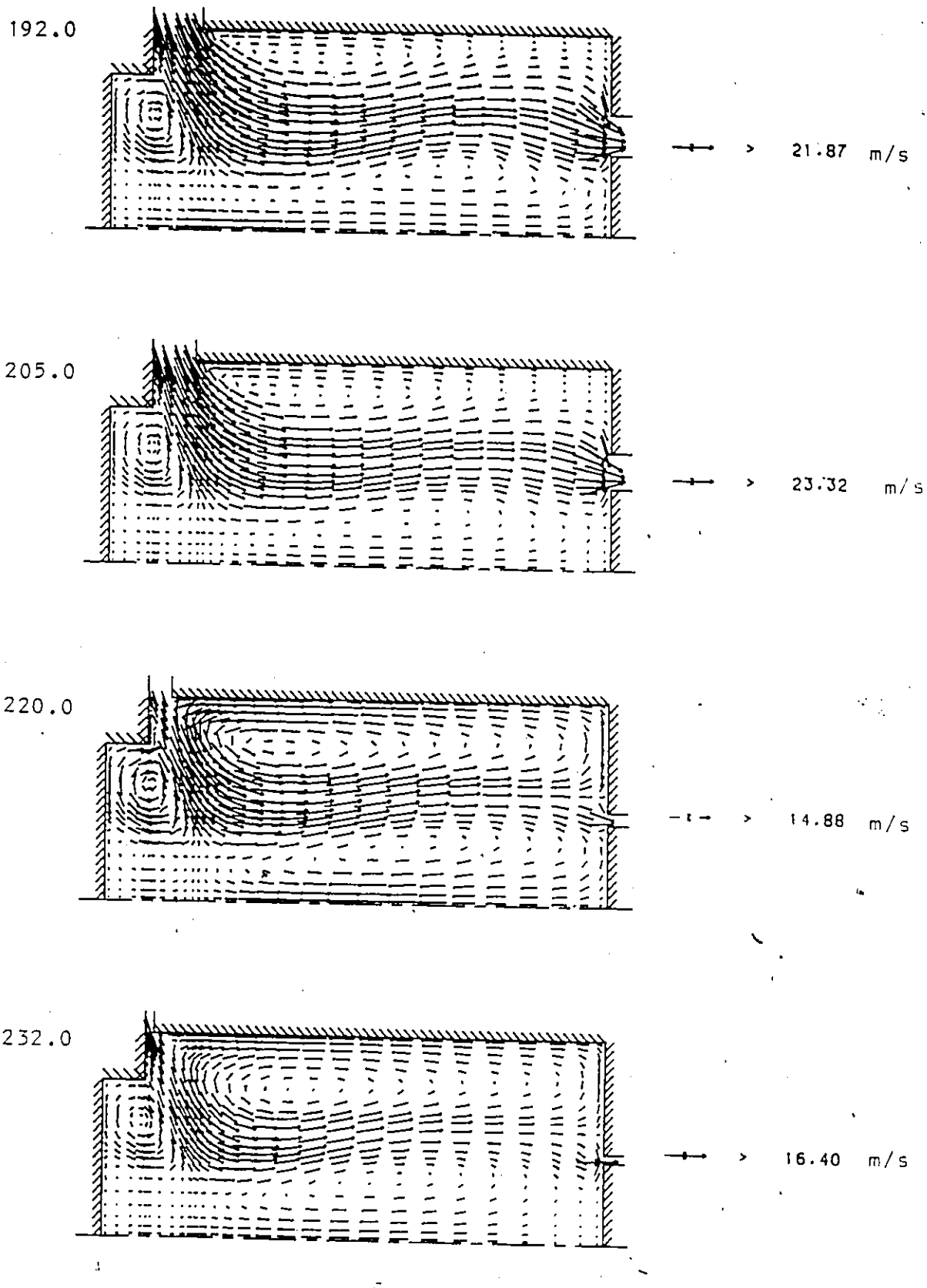

Figure 5.20 Continued.

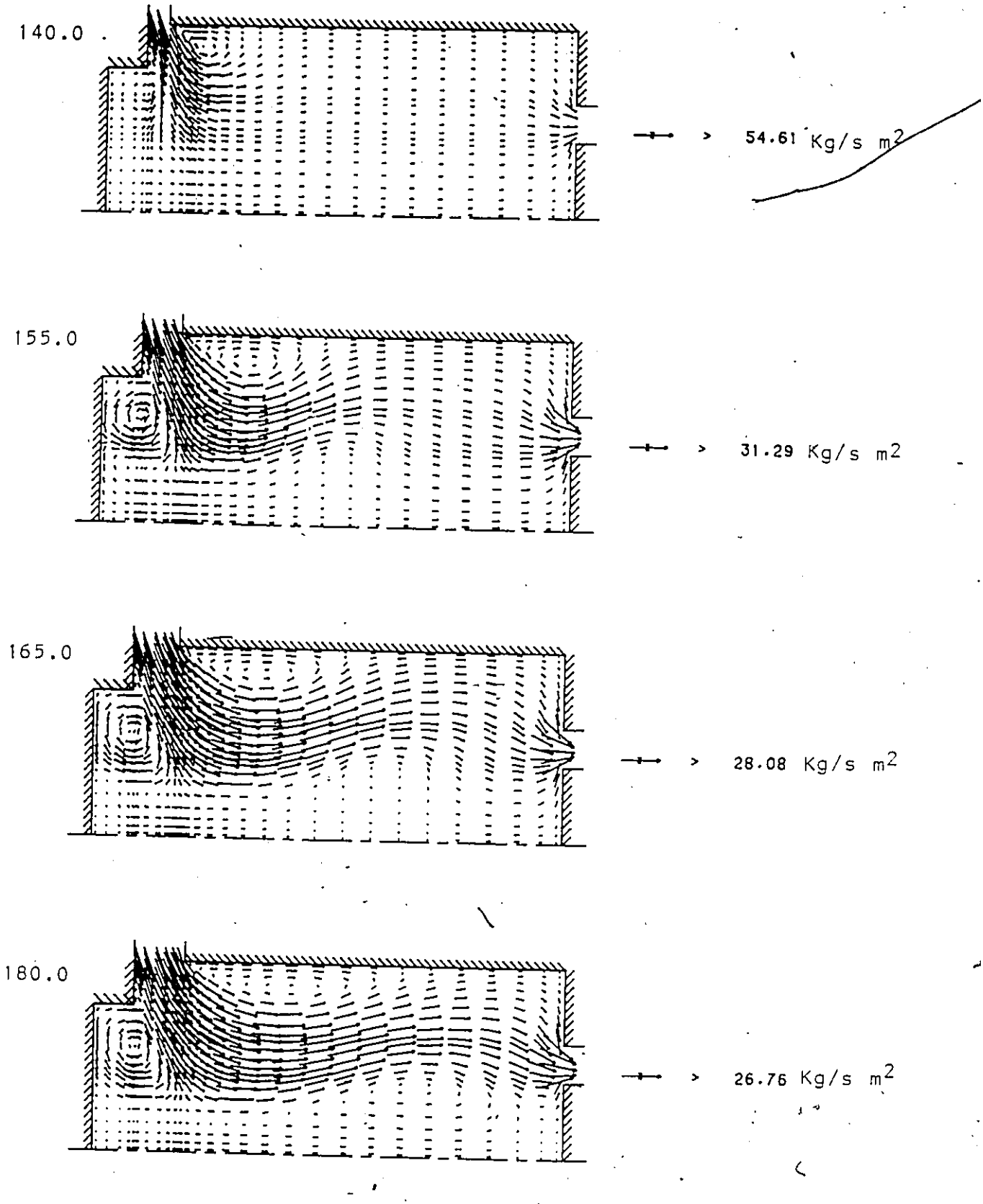

Figure 5.21 Mass flux patterns during scavenging at different crank angles (inflow conditions: 20 degree incline to the horizontal with a 15 degree swirl).

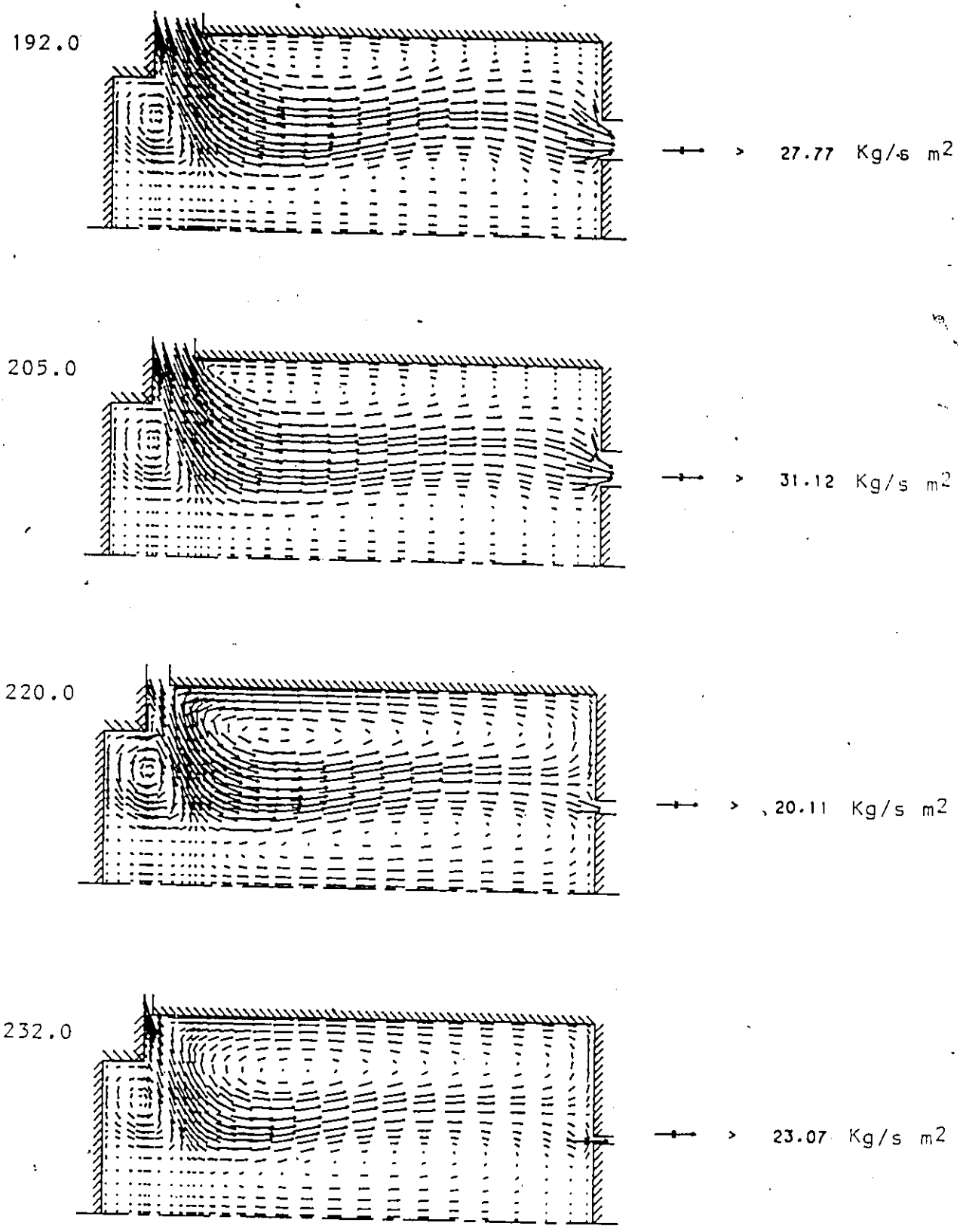

Figure 5.21 Continued.

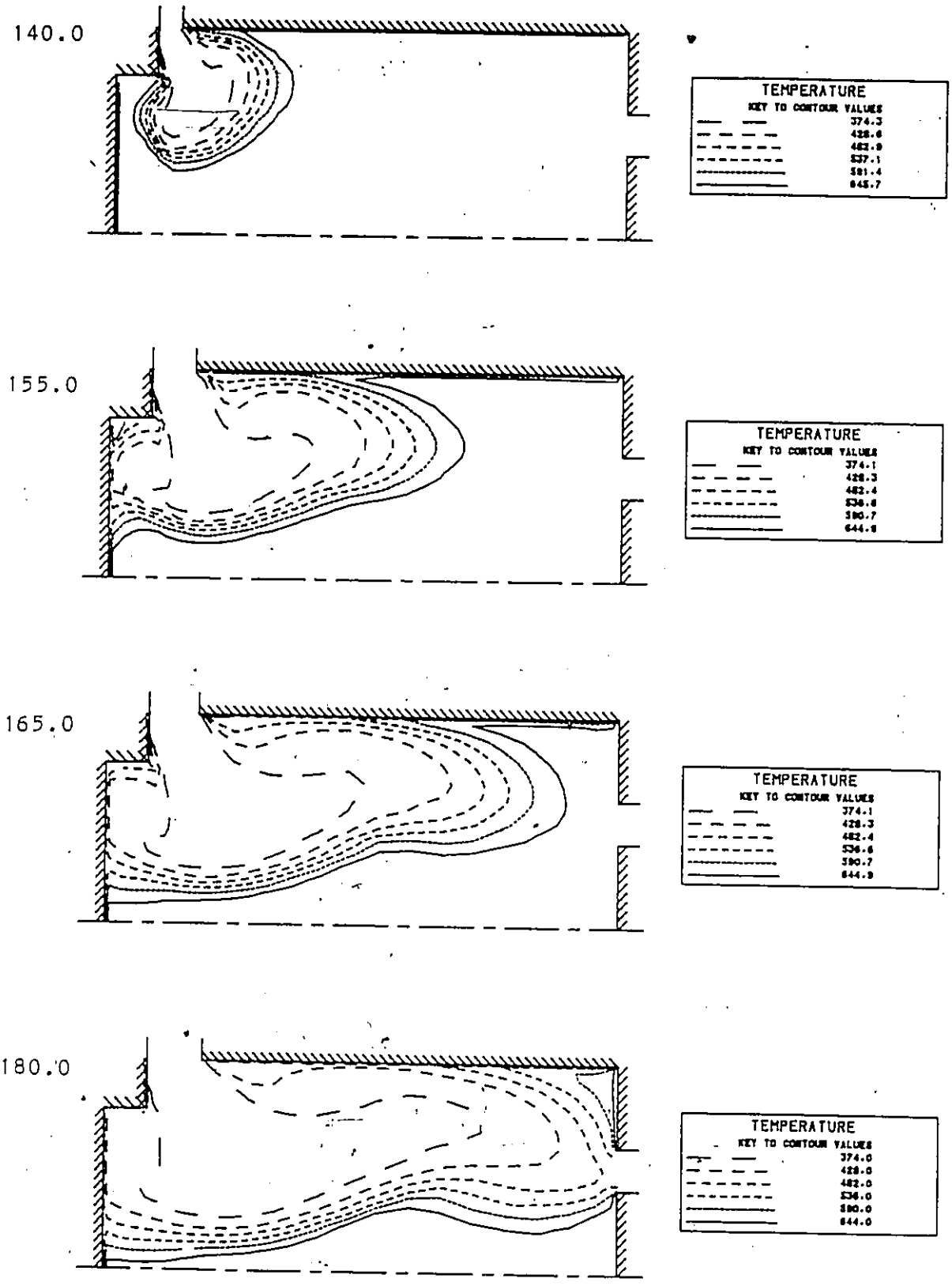

Figure 5.22 Temperature contours during scavenging at different crank angles (inflow conditions: 20 degree incline to the horizontal with a 15 degree swirl).

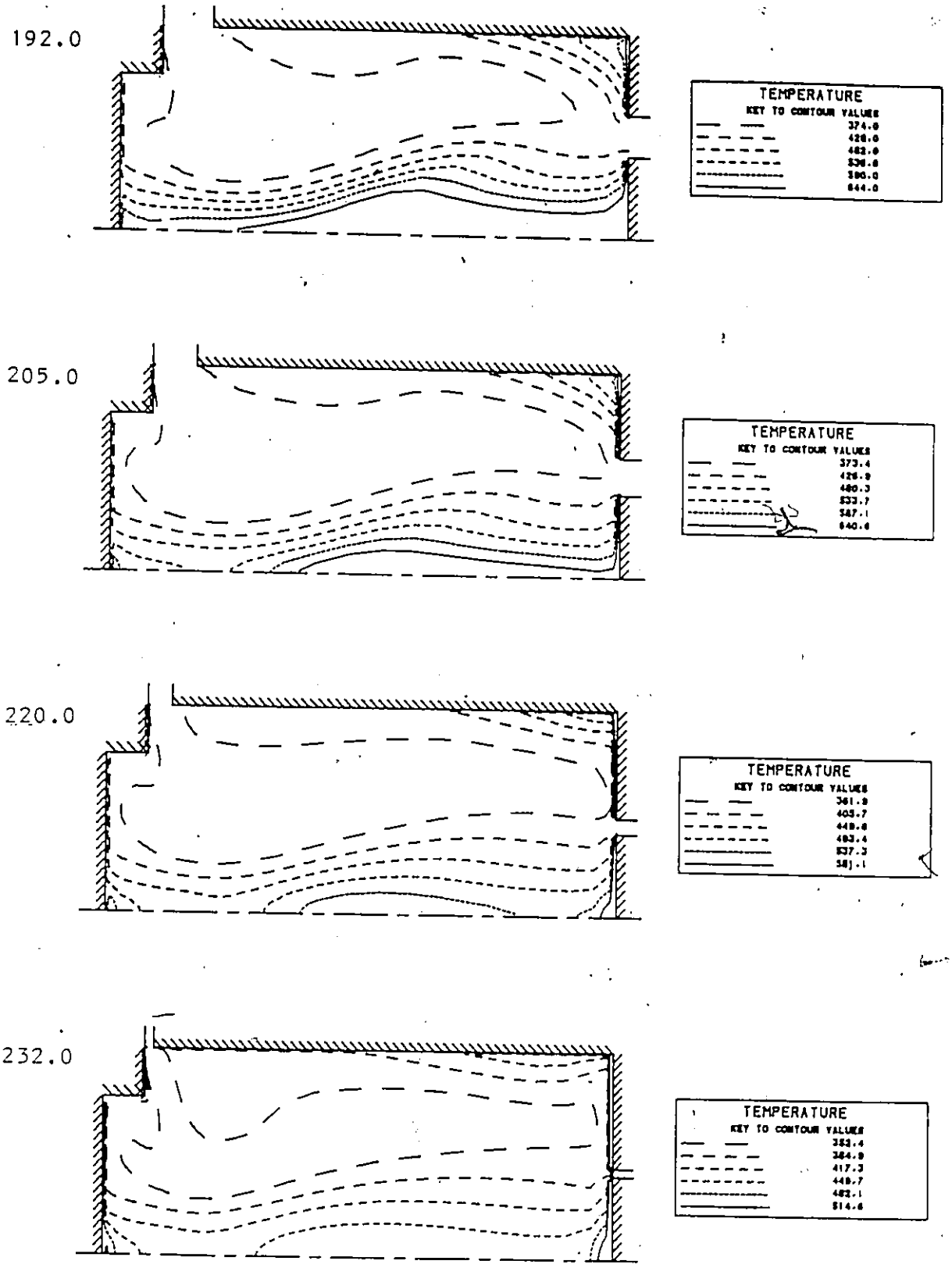

Figure 5.22 Continued.

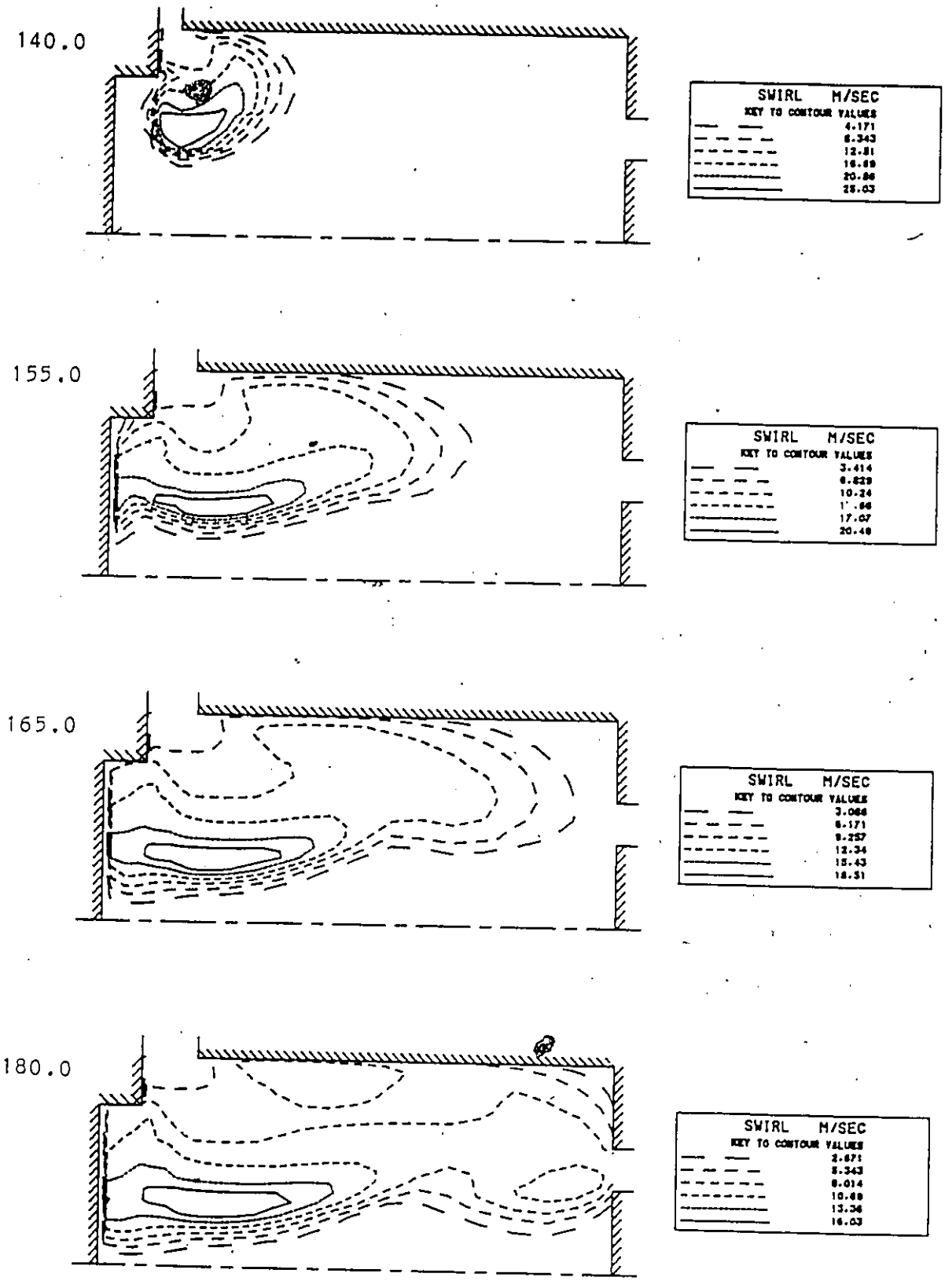

Figure 5.23 Swirl velocity contours during scavenging at different crank angles (inflow conditions: 20 degree incline to the horizontal with a 15 degree swirl).

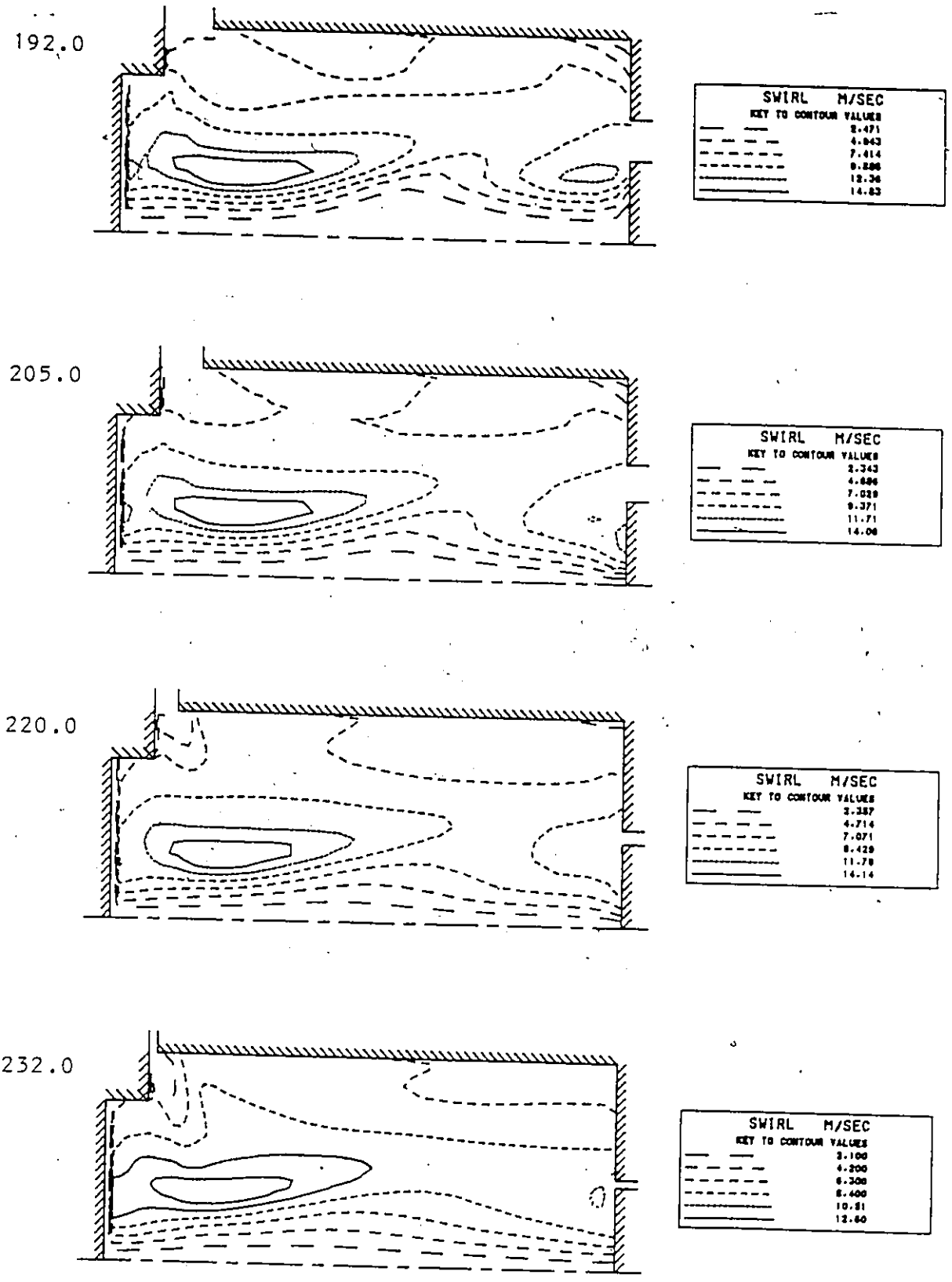

Figure 5.23 Continued.

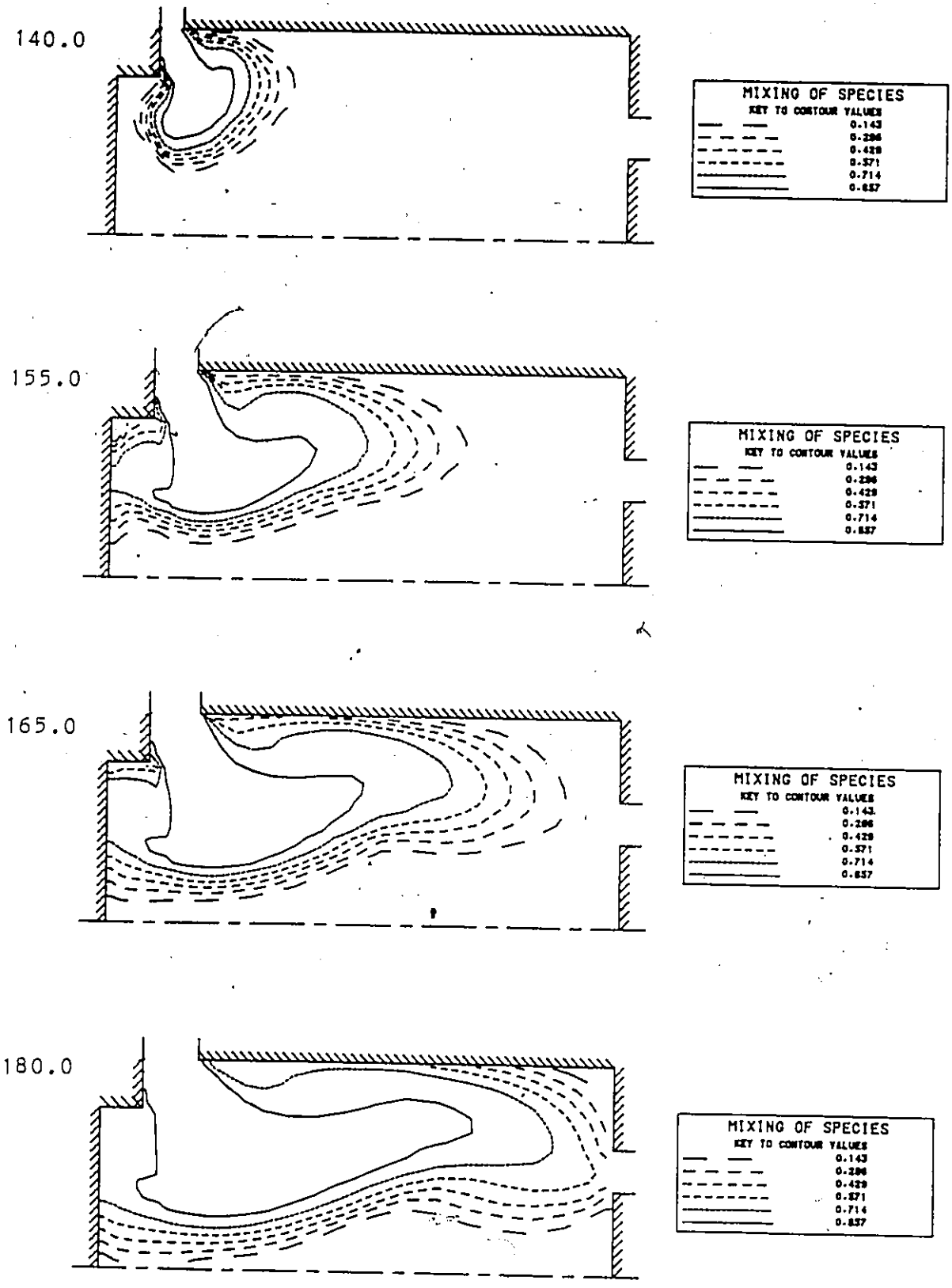

Figure 5.24 Concentration contours during scavenging at different crank angles (inflow conditions: 20 degree incline to the horizontal with a 15 degree swirl).

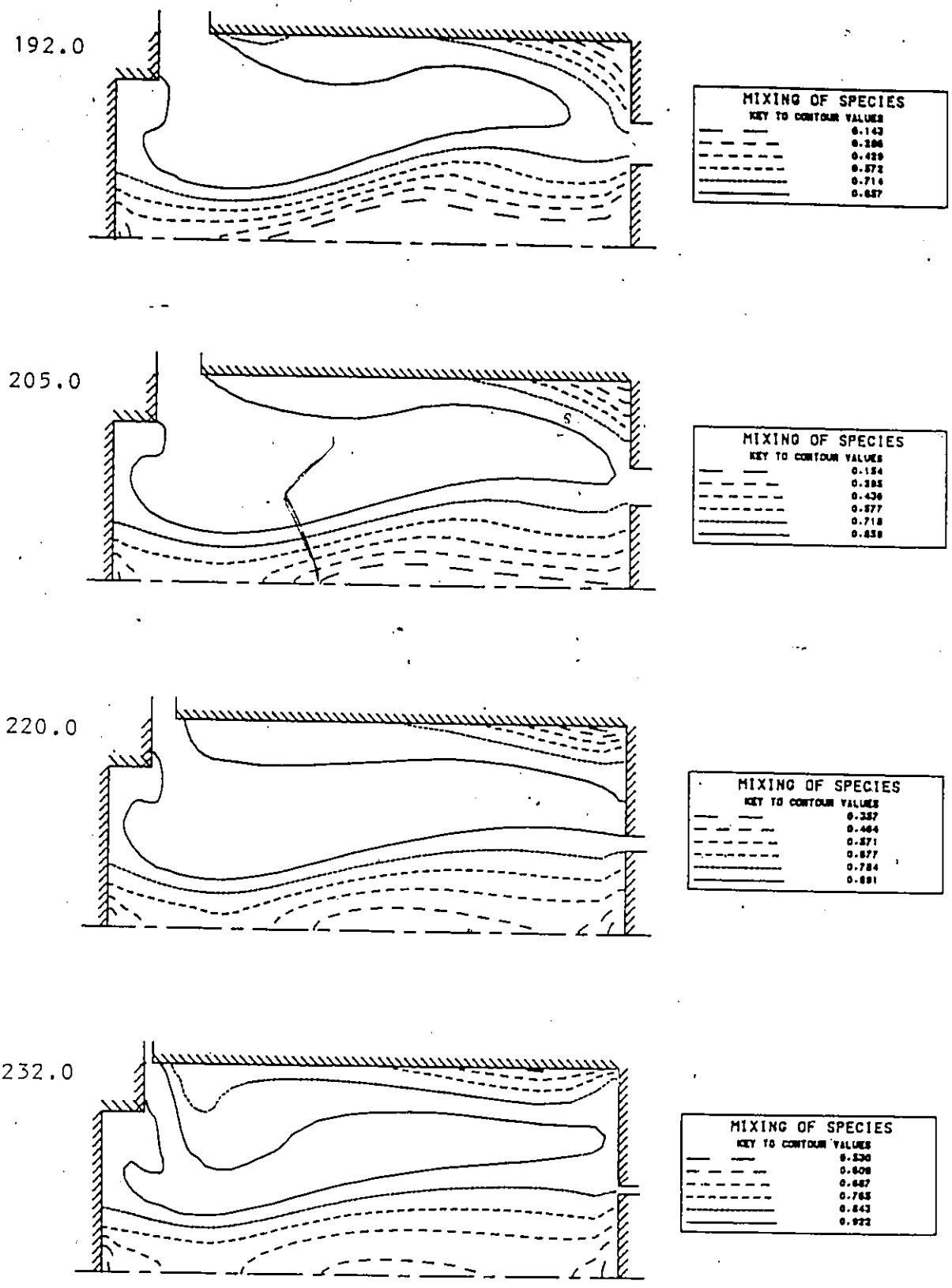

Figure 5.24 Continued.

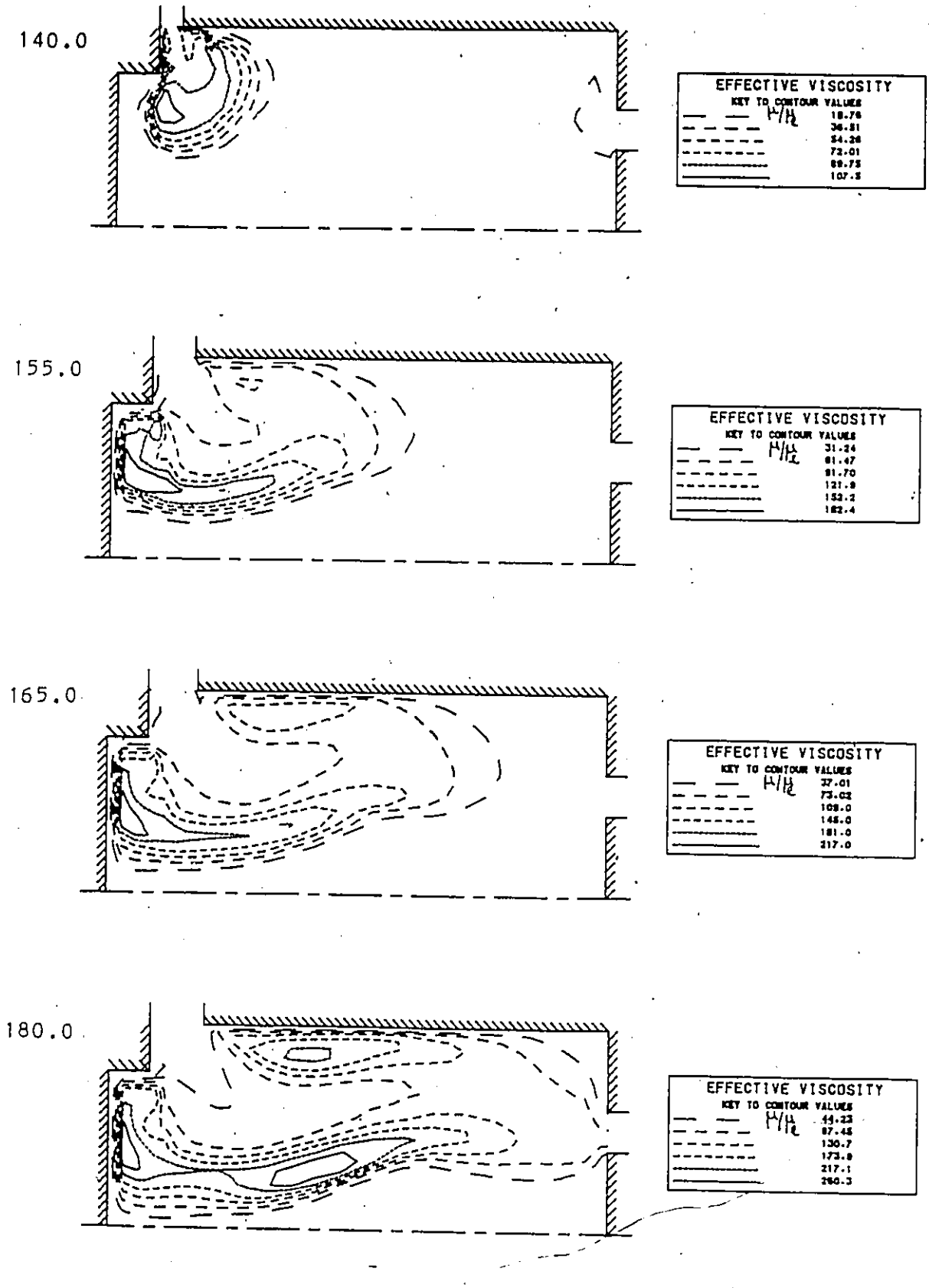

Figure 5.25 Effective viscosity contours during scavenging at different crank angles (inflow conditions: 20 degree incline to the horizontal with a 15 degree swirl).

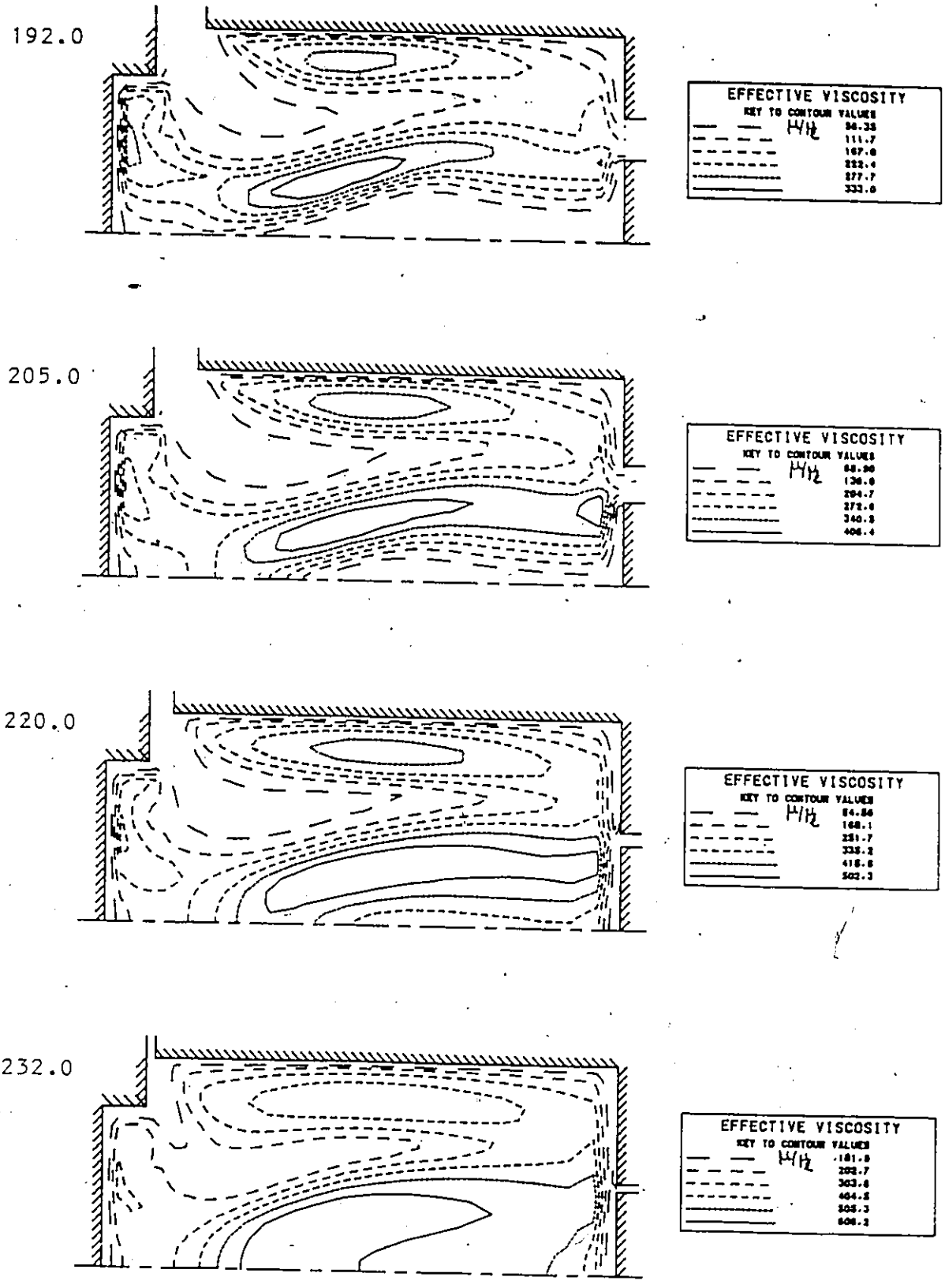

Figure 5.25 Continued.

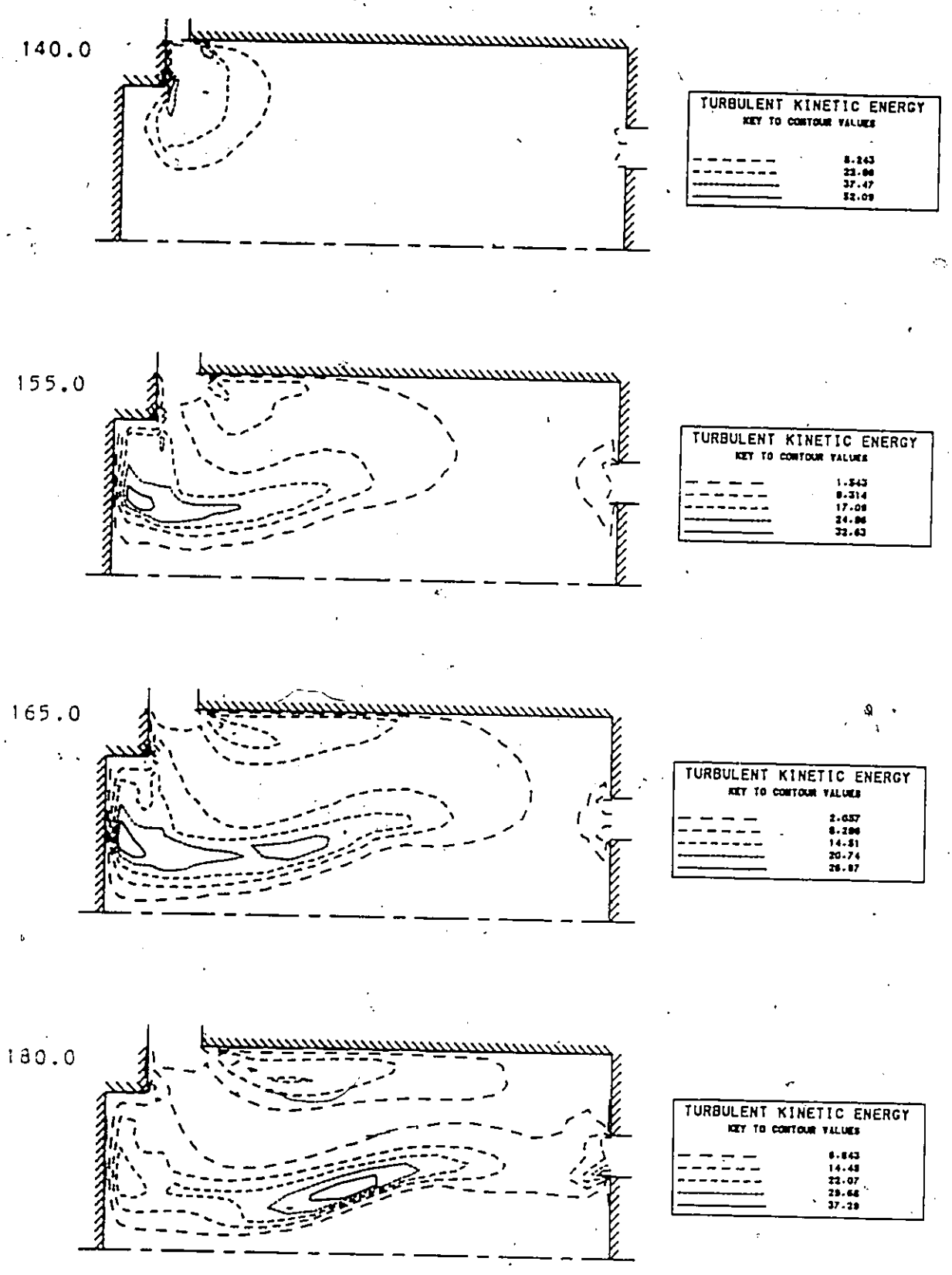

Figure 5.26 Turbulence kinetic energy contours during scavenging at different crank angles (inflow conditions: 20 degree incline to the horizontal with a 15 degree swirl).

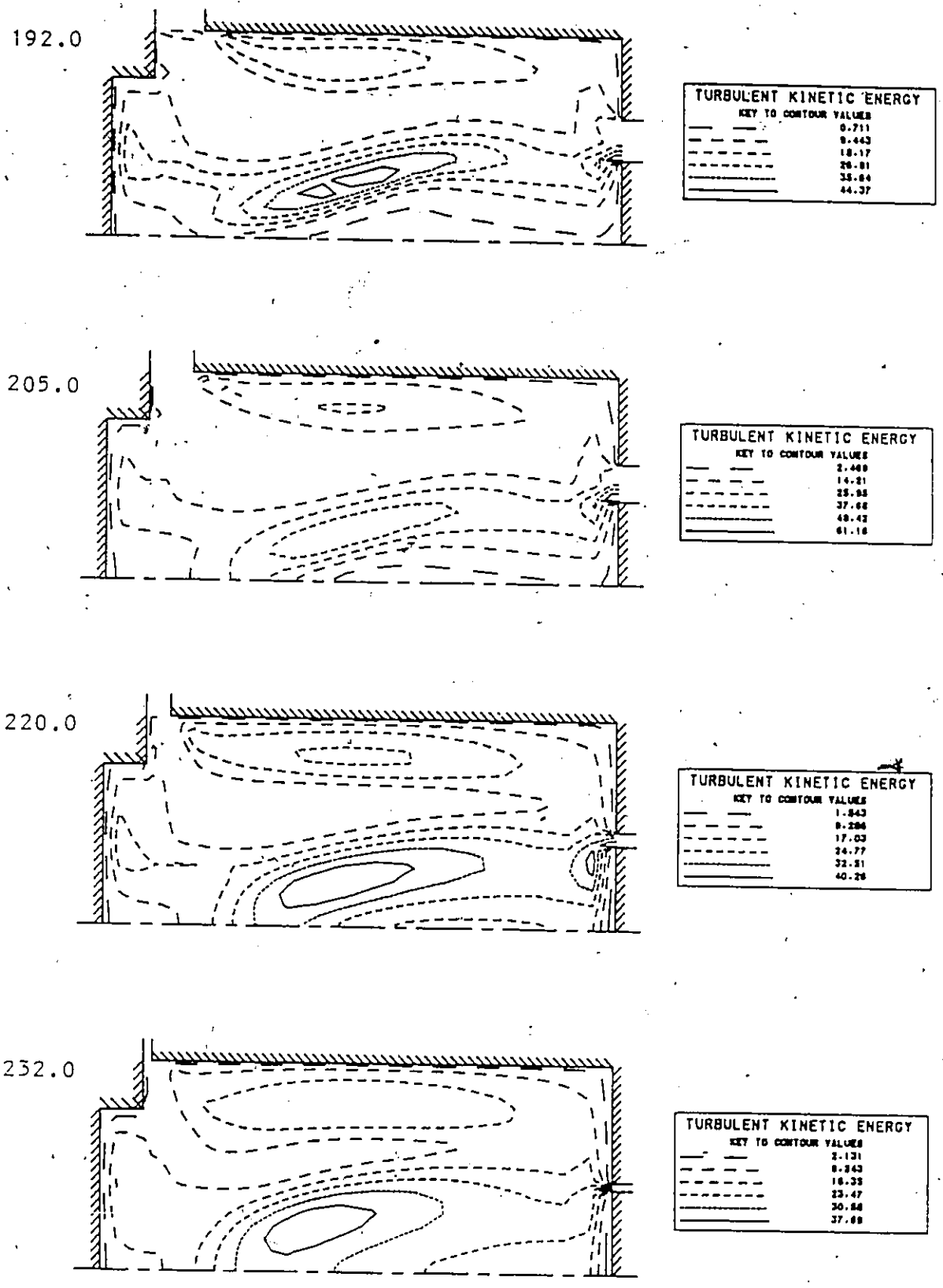

Figure 5.26 Continued.

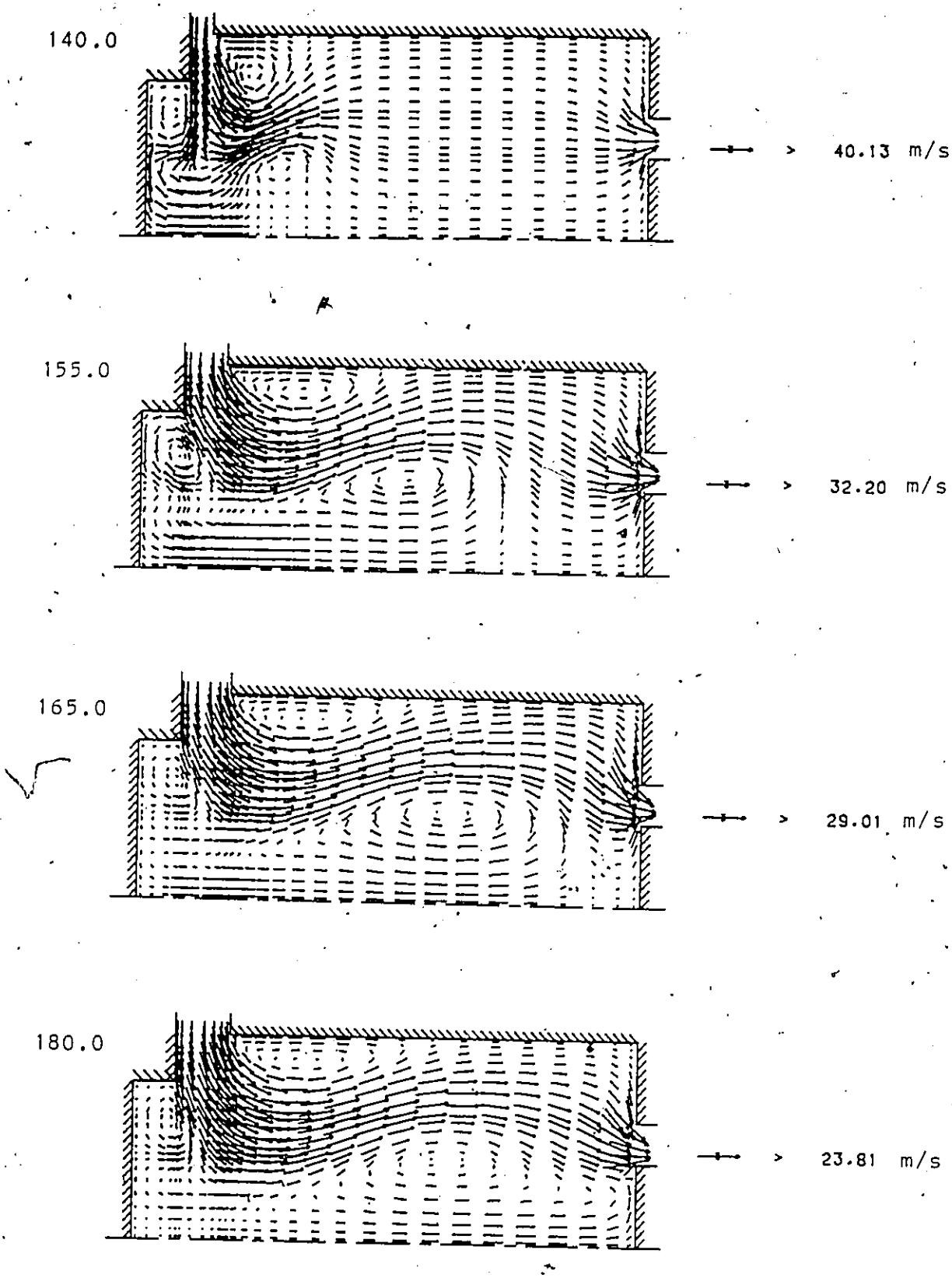

Figure 5.27 Velocity patterns during scavenging at different crank angles (inflow conditions: horizontal inflow with a 22 degree swirl).

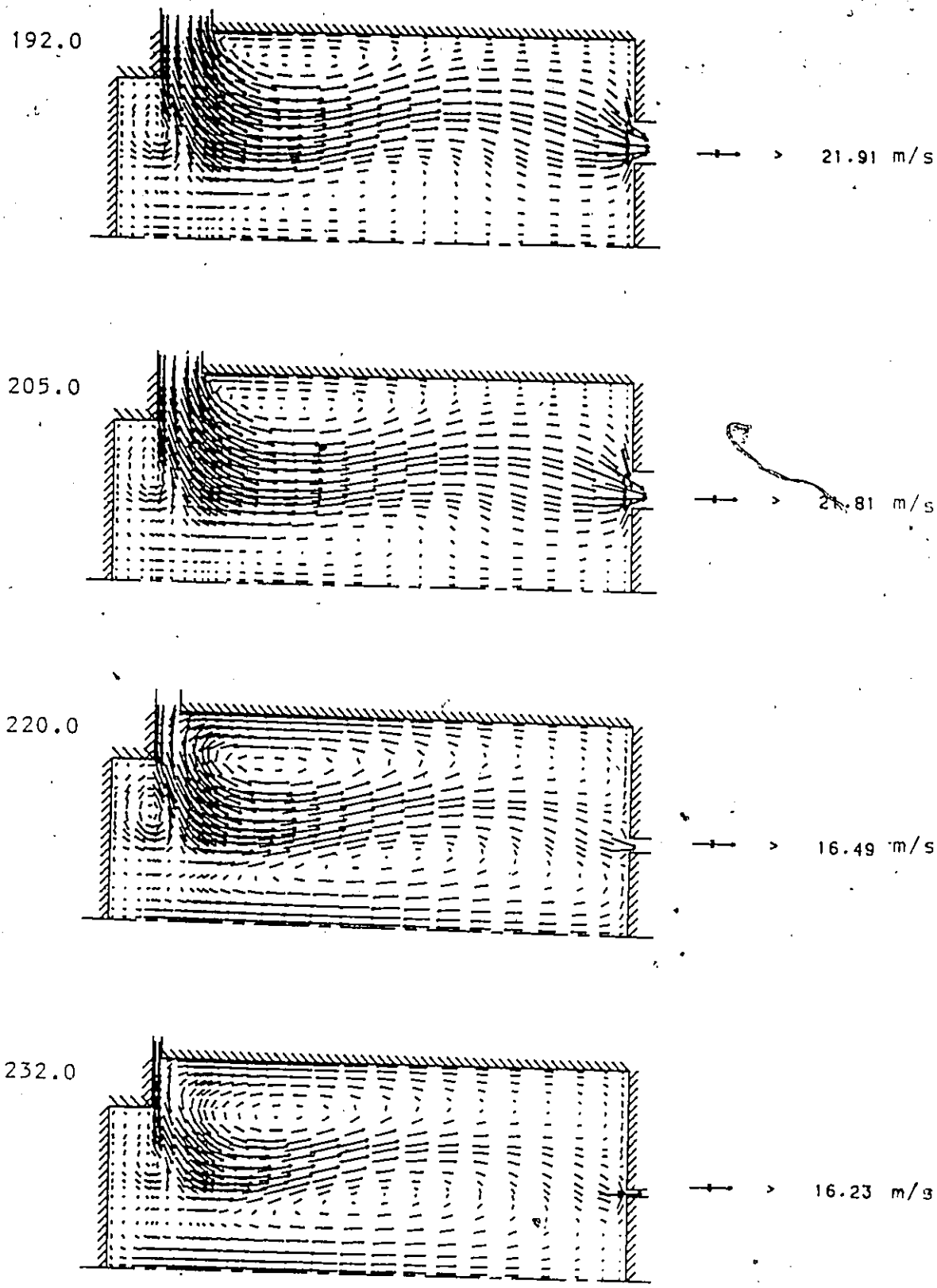

Figure 5.27 Continued.

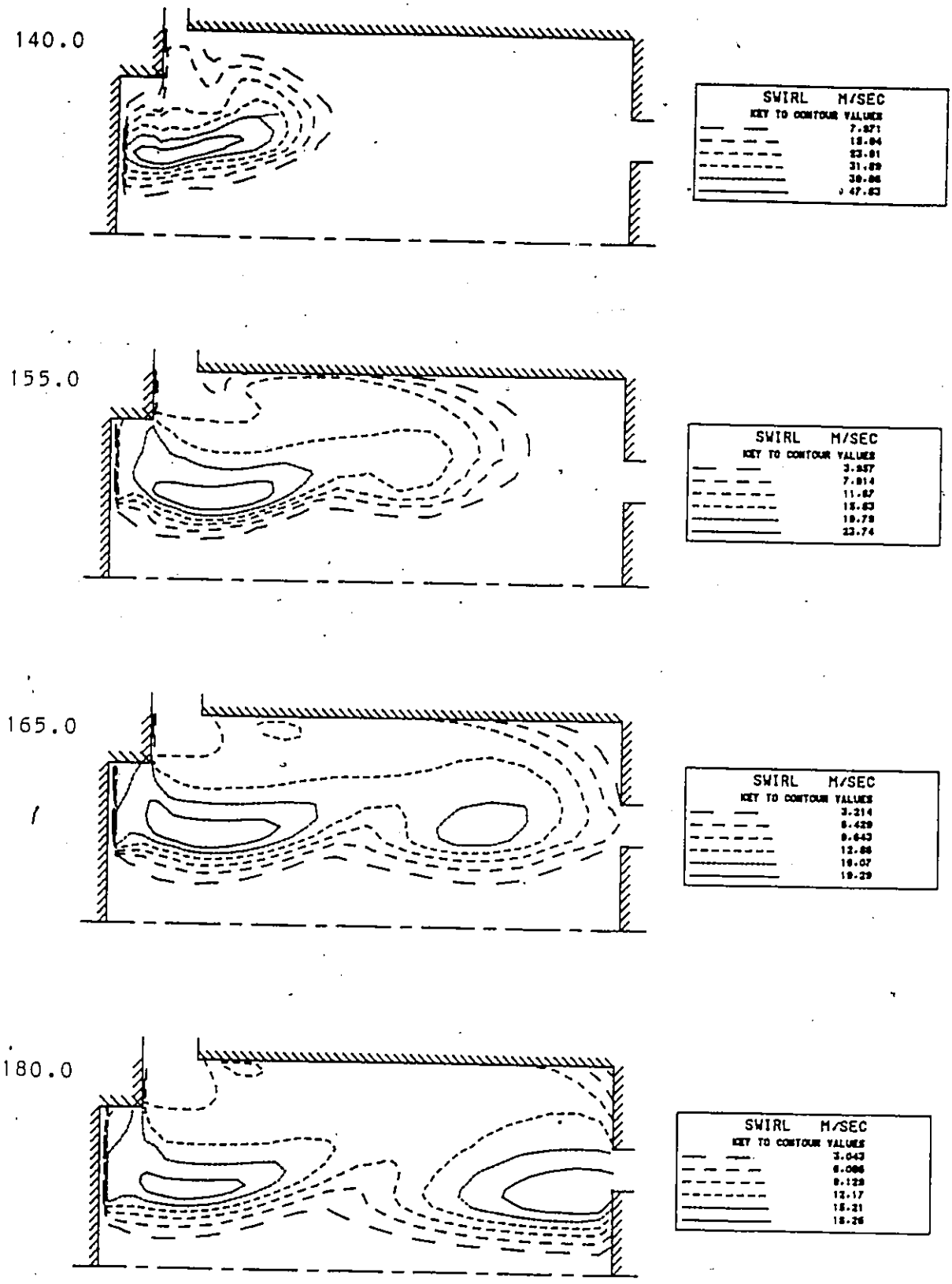

Figure 5.28 Swirl velocity contours during scavenging at different crank angles (inflow conditions: horizontal inflow with a 22 degree swirl).

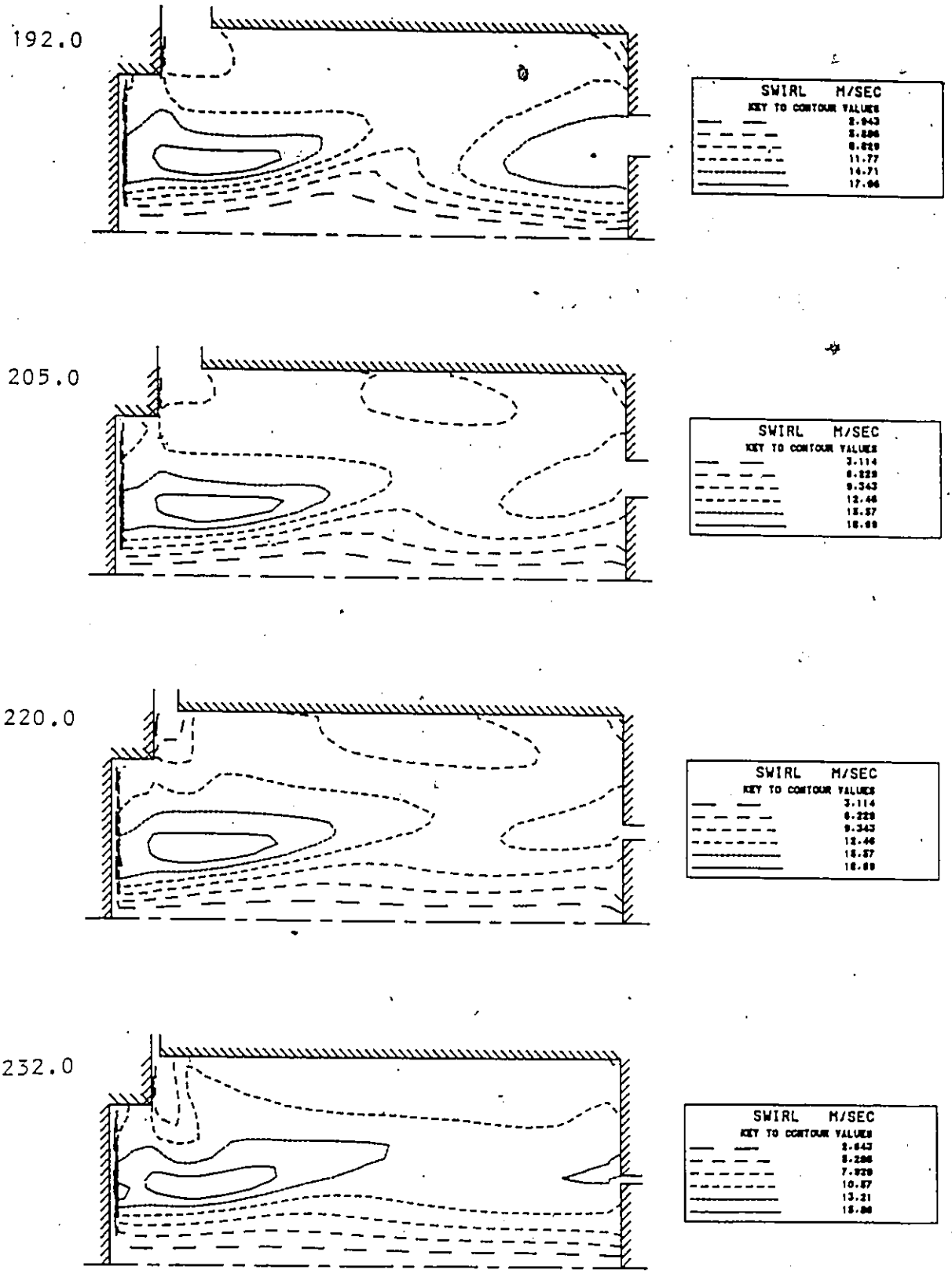

Figure 5.28 Continued.

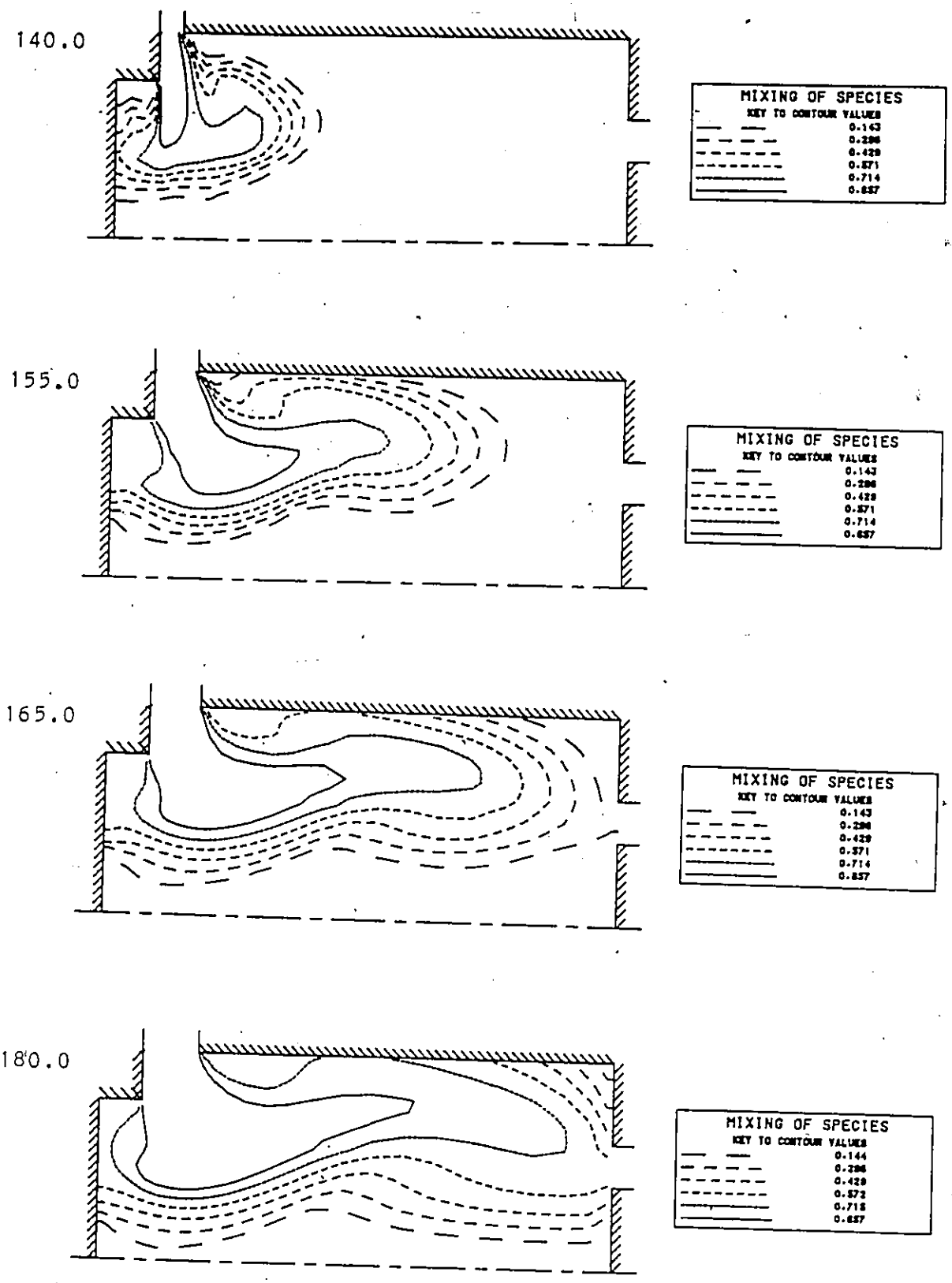

Figure 5.29 Concentration contours during scavenging at different crank angles (inflow conditions: horizontal inflow with a 22 degree swirl).

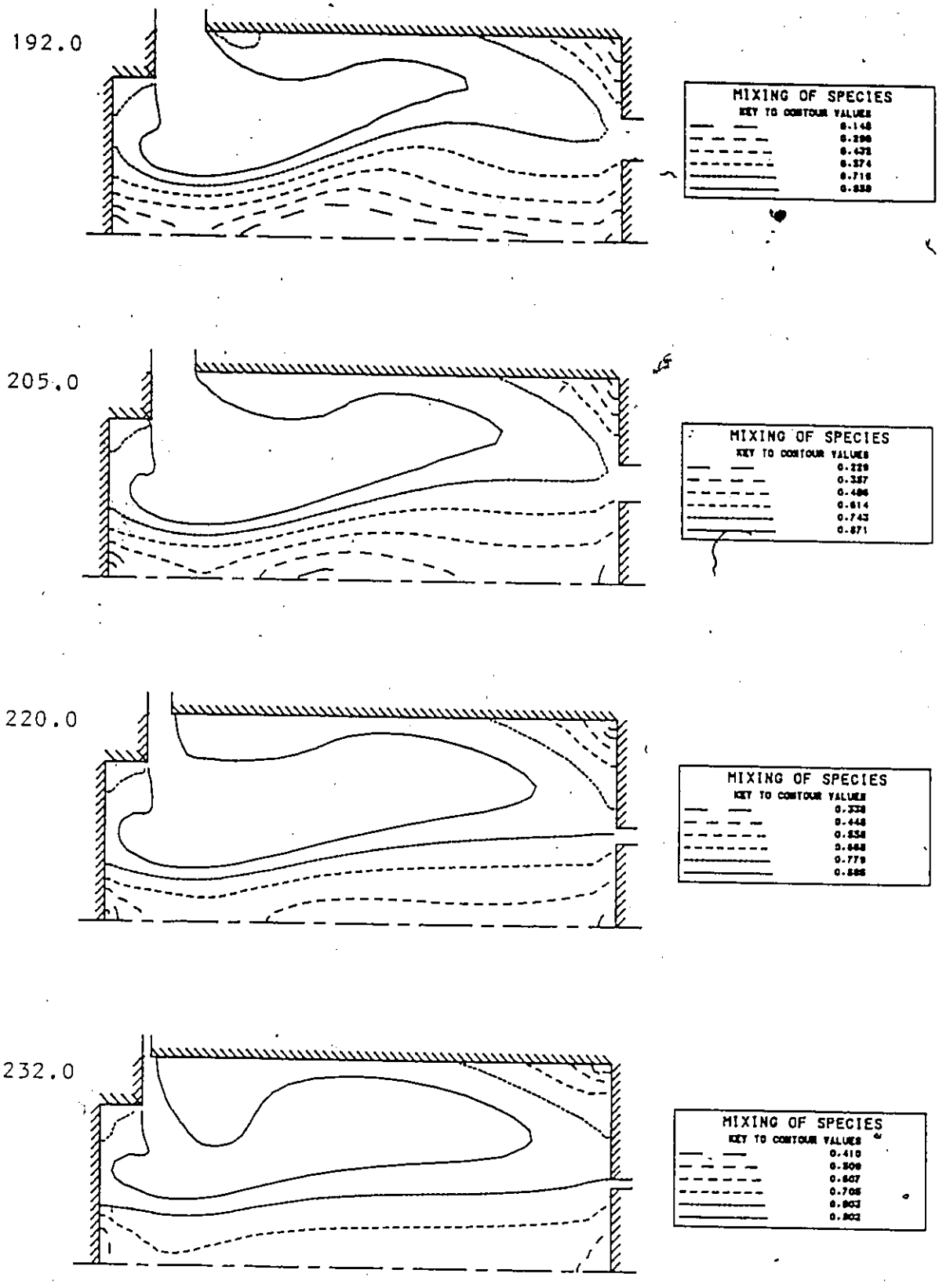

Figure 5.29 Continued.

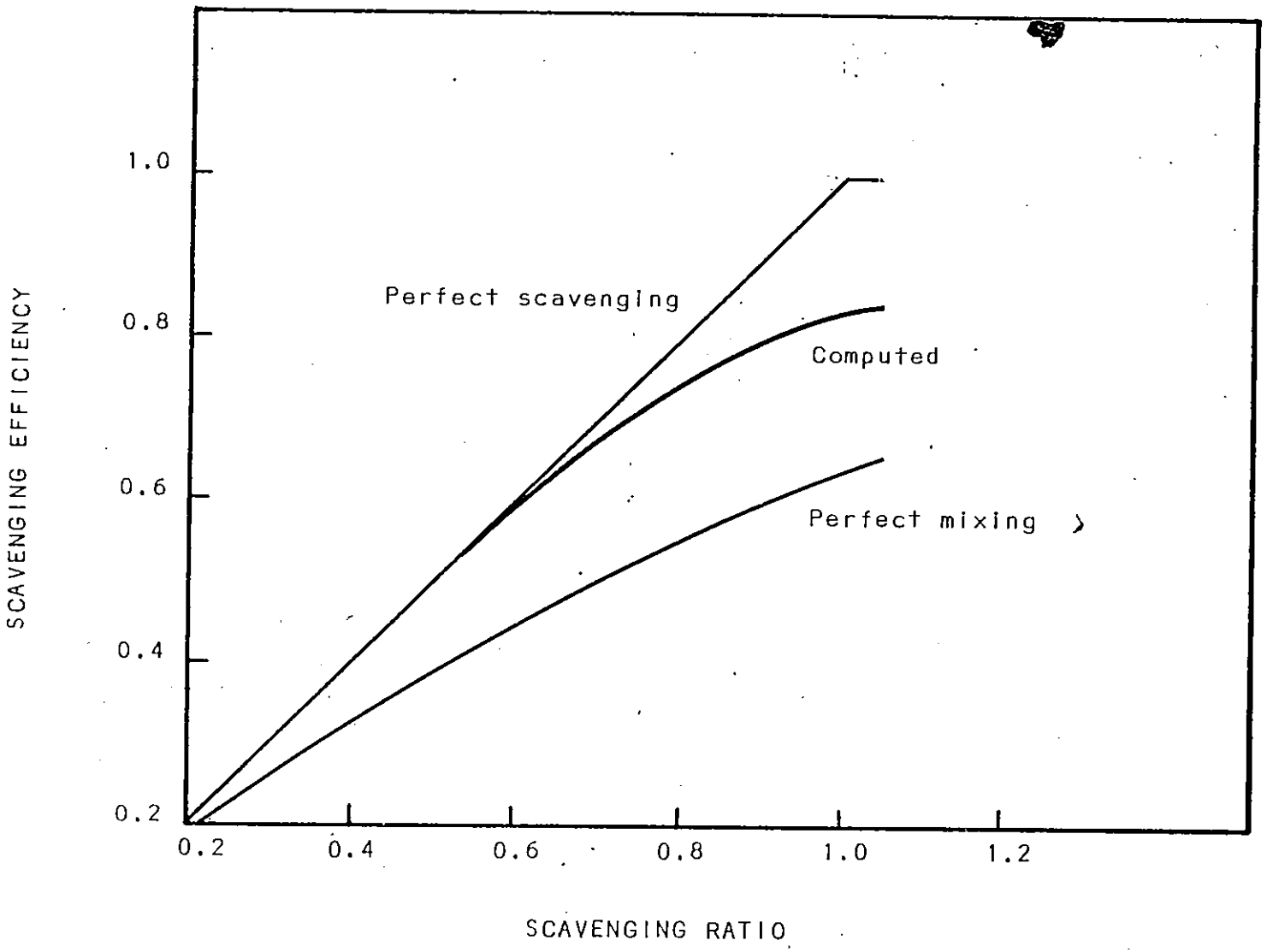

Figure 5.30 . Scavenging efficiency vs scavenging ratio

TABLE 5.1

THE VALUES OF THE CONSTANTS USED IN THE K-ε MODEL

C_1	C_2	S_k	S_e	C_μ	Pr_t	Sc_t	C_d
1.43	1.92	1.0	1.3	0.09	1.00	1.00	1.0

CHAPTER 6

MULTIDIMENSIONAL ANALYSIS FOR SCAVENGING STUDIES THREE-DIMENSIONAL MODEL

6.1 INTRODUCTION

The flow in internal combustion engines is generally three-dimensional due to the complex geometry introduced by the exhaust valves as well as the presence of swirl. Presently, three-dimensional flows are not only complex as far as mathematical formulation and numerical techniques are concerned but are also associated with high computing costs. However, considering the extremely fast development of computer facilities one can certainly expect that in the near future the real limitations will not be hardware related but rather given by the ability to develop suitable models and numerical techniques. This consideration, together with the desire to make engine simulation as realistic as possible, have prompted the three dimensional (3D) development presented in this chapter. The 3D model is based on the two dimensional (2D) model presented in chapter 5. Just as with the 2D model the continuity and momentum equations are solved using the Implicit Continuous-fluid Eulerian (ICE) technique. The effect of turbulence was studied using the K-ϵ model.

6.2 MATHEMATICAL FORMULATION

The differential equations solved for the three-dimensional case are the conservation equations of mass, momentum, energy and species. These equations are written as follows:

MASS CONSERVATION EQUATION

$$\frac{\partial \rho}{\partial t} + \frac{1}{R}\frac{\partial}{\partial r}(\rho R u) + \frac{\partial}{\partial y}(\rho v) + \frac{1}{R}\frac{\partial}{\partial \theta}(\rho w) = 0 \qquad (6-1)$$

MOMENTUM EQUATIONS

r - component

$$\frac{\partial}{\partial t}(\rho u) + \frac{1}{R}\frac{\partial}{\partial r}(\rho R u u) + \frac{\partial}{\partial y}(\rho v u) + \frac{1}{R}\frac{\partial}{\partial \theta}(\rho w u) =$$
$$-\frac{\partial P}{\partial r} + \frac{1}{R}\frac{\partial}{\partial \theta}(\mu \frac{1}{R}\frac{\partial u}{\partial \theta}) + \frac{\partial}{\partial y}(\mu \frac{\partial u}{\partial y}) + \frac{2}{R}\frac{\partial}{\partial r}(\mu R \frac{\partial u}{\partial r}) + \frac{\partial}{\partial y}(\mu \frac{\partial v}{\partial r})$$
$$+\frac{1}{R}\frac{\partial}{\partial \theta}(R\mu \frac{\partial}{\partial}\frac{w}{r}) + \delta \frac{2\mu}{r^2}\frac{\partial w}{\partial \theta} + \delta \frac{2\mu u}{r^2} - \delta \frac{\rho w w}{r} \qquad (6-2)$$

y - component

$$\frac{\partial}{\partial t}(\rho v) + \frac{1}{R}\frac{\partial}{\partial r}(\rho R u v) + \frac{\partial}{\partial y}(\rho v v) + \frac{1}{R}\frac{\partial}{\partial \theta}(\rho w v) =$$
$$-\frac{\partial P}{\partial y} + \frac{1}{R}\frac{\partial}{\partial \theta}(\mu \frac{1}{R}\frac{\partial v}{\partial \theta}) + 2\frac{\partial}{\partial y}(\mu \frac{\partial v}{\partial y}) + \frac{1}{R}\frac{\partial}{\partial r}(\mu R \frac{\partial v}{\partial r})$$
$$+\frac{1}{R}\frac{\partial}{\partial r}(\mu R \frac{\partial u}{\partial r}) + \frac{1}{R}\frac{\partial}{\partial \theta}(\mu \frac{\partial w}{\partial y}) \qquad (6-3)$$

θ - component

$$\frac{\partial}{\partial t}(\rho w) + \frac{1}{R}\frac{\partial}{\partial r}(\rho R u w) + \frac{\partial}{\partial y}(\rho v w) + \frac{1}{R}\frac{\partial}{\partial \theta}(\rho w w) =$$
$$-\frac{1}{R}\frac{\partial P}{\partial \theta} + \frac{1}{R}\frac{\partial}{\partial r}(\mu R \frac{\partial w}{\partial r}) + \frac{\partial}{\partial y}(\mu \frac{\partial w}{\partial y}) + \frac{2}{R}\frac{\partial}{\partial \theta}(\mu \frac{1}{R}\frac{\partial w}{\partial \theta}) - \delta \frac{\rho u w}{r} + \frac{\mu}{R}\frac{\partial w}{\partial r}$$
$$+\frac{1}{R^2}\frac{\partial}{\partial r}(\mu R \frac{\partial u}{\partial \theta}) - \frac{1}{R^2}\frac{\partial}{\partial r}(\mu R w) + \delta \frac{2}{r}\frac{\partial}{\partial \theta}(\mu \frac{u}{r}) + \frac{\partial}{\partial y}(\mu \frac{1}{R}\frac{\partial v}{\partial \theta}) \qquad (6-4)$$

ENERGY EQUATION

$$\frac{\partial}{\partial t}(\rho T) + \frac{1}{R}\frac{\partial}{\partial r}(\rho R u T) + \frac{\partial}{\partial y}(\rho v T) + \frac{1}{R}\frac{\partial}{\partial \theta}(\rho w T) = \frac{1}{R}\frac{\partial}{\partial r}(R \frac{\mu}{Pr_t}\frac{\partial T}{\partial r})$$

$$\frac{\partial}{\partial y}(\frac{\mu}{Pr_t}\frac{\partial T}{\partial y}) + \frac{1}{R}\frac{\partial}{\partial \theta}(\frac{\mu}{Pr_t}\frac{1}{R}\frac{\partial T}{\partial \theta}) \qquad (6-5)$$

CONCENTRATION EQUATION

$$\frac{\partial}{\partial t}(\rho C) + \frac{1}{R}\frac{\partial}{\partial r}(\rho RuC) + \frac{\partial}{\partial y}(\rho vC) + \frac{1}{R}\frac{\partial}{\partial \theta}(\rho wC) = \frac{1}{R}\frac{\partial}{\partial r}(R\frac{\mu}{Sc_t}\frac{\partial C}{\partial r})$$

$$\frac{\partial}{\partial y}(\frac{\mu}{Sc_t}\frac{\partial C}{\partial y}) + \frac{1}{R}\frac{\partial}{\partial \theta}(\frac{\mu}{Sc_t}\frac{1}{R}\frac{\partial C}{\partial \theta}) \qquad (6-6)$$

where:

u - is the fluid velocity in the radial direction

v - is the fluid velocity in the axial direction

w - is the fluid velocity in the circumferential direction

ρ - is the fluid density

P - is the fluid pressure

T - is the fluid temperature

C - is the fluid concentration (mass fraction)

Pr_t - is the Prandtl number

Sc_t - is the Schmidt number

The turbulence effects are modeled using the K-ϵ model. The conservation equation of the turbulent kinetic energy and turbulence dissipation rate are used for the computation of the effective viscosity. These equations are written as follows:

TURBULENCE KINETIC ENERGY EQUATION

$$\frac{\partial}{\partial t}(\rho K) + \frac{1}{R}\frac{\partial}{\partial r}(\rho RuK) + \frac{\partial}{\partial y}(\rho vK) + \frac{1}{R}\frac{\partial}{\partial \theta}(\rho wK) = \frac{1}{R}\frac{\partial}{\partial r}(\frac{\mu}{S_k}R\frac{\partial K}{\partial r})$$

$$\frac{1}{R}\frac{\partial}{\partial\theta}(\frac{\mu}{S_k}\frac{1}{R}\frac{\partial K}{\partial\theta})+\frac{\partial}{\partial y}(\frac{\mu}{S_k}\frac{\partial K}{\partial y})+\rho\epsilon C_d+G \qquad (6-7)$$

where G is the turbulence generation written as:

$$G=\mu[2((\frac{\partial v}{\partial y})^2+(\frac{\partial u}{\partial r})^2+(\frac{1}{R}(\frac{\partial w}{\partial\theta}+\delta\frac{u}{r})^2)+(\frac{\partial v}{\partial r}+\frac{\partial u}{\partial y})^2$$
$$+(\frac{1}{R}\frac{\partial u}{\partial\theta}+R\frac{\partial}{\partial r}(\frac{w}{R}))^2+(\frac{\partial w}{\partial y}+\frac{1}{R}\frac{\partial v}{\partial\theta})^2]-\frac{2}{3}\nabla\cdot\vec{u}(\mu\nabla\cdot\vec{u}+\rho K) \qquad (6-8)$$

where:

$$\nabla\cdot\vec{u}=\frac{1}{R}\frac{\partial}{\partial r}(Ru)+\frac{\partial v}{\partial y}+\frac{1}{R}\frac{\partial w}{\partial\theta}$$

ENERGY DISSIPATION RATE EQUATION

$$\frac{\partial}{\partial t}(\rho\epsilon)+\frac{1}{R}\frac{\partial}{\partial r}(\rho Ru\epsilon)+\frac{\partial}{\partial y}(\rho v\epsilon)+\frac{1}{R}\frac{\partial}{\partial\theta}(\rho w\epsilon)=\frac{1}{R}\frac{\partial}{\partial r}(\frac{\mu}{S_e}R\frac{\partial\epsilon}{\partial r})$$
$$\frac{1}{R}\frac{\partial}{\partial\theta}(\frac{\mu}{S_e}\frac{1}{R}\frac{\partial\epsilon}{\partial\theta})+\frac{\partial}{\partial y}(\frac{\mu}{S_e}\frac{\partial\epsilon}{\partial y})+\epsilon(C_1G-C_2\rho\epsilon)/K \qquad (6-9)$$

The effective viscosity is written as:

$$\mu=\mu_l+C_\mu\rho K^2/\epsilon \qquad (6-10)$$

where:

μ - is the effective viscosity

μ_l - is the fluid dynamic viscosity

K - is the turbulence kinetic energy

ϵ - is the energy dissipation rate

C_μ - is a constant

S_k, S_ϵ, C_d, C_1 and C_2 - are constants

In laminar flow, μ is the fluid dynamic viscosity. In turbulent flow μ is the effective viscosity obtained from equation (6-10).

6.3 FINITE DIFFERENCE EQUATIONS

The method used for solving the differential equations is the same as the one used in chapter 5 for axisymmetric flows. Figure 6.1 shows a cell in cylindrical coordinates used for the three-dimensional computations. The hybrid differencing scheme is used in the differential equations for writing the convective and diffusive terms in finite difference form. The velocities are defined at the center of the cell faces and the scalar quantities at the cell center. In the computations unequal grid spacing is used; therefore, a weighted-average procedure is used to compute quantities in locations different than those where they are defined.

For example, a scalar quantity S at the faces of a cell in the radial direction will be written as:

$$S_{i+\frac{1}{2},j,k} = (S_{i,j,k}\Delta r_{i+1} + S_{i+1,j,k}\Delta r_i)/(\Delta r_{i+1} + \Delta r_i)$$

$$S_{i-\frac{1}{2},j,k} = (S_{i,j,k}\Delta r_{i-1} + S_{i-1,j,k}\Delta r_i)/(\Delta r_{i-1} + \Delta r_i)$$

In case the value of S is needed at the cell corner $(i+\frac{1}{2}, j+\frac{1}{2})$ the following formula is used:

$$S_{i+\frac{1}{2},j+\frac{1}{2},k} = (S_{i,j+\frac{1}{2},k}\Delta r_{i+1} + S_{i+1,j+\frac{1}{2},k}\Delta r_i)/(\Delta r_{i+1} + \Delta r_i)$$

The same weighted average technique is used for the velocities. The finite difference form of the differential equations will be presented below.

6.3.1 MOMENTUM EQUATIONS

Momentum Equation in Radial Direction

$$(\overline{\rho u})_{i,j,k} = (\rho u)_{i,j,k} + \Delta t(DPX - CUX - CUY - CU\Theta + DIFX1$$

$$+DIFX2 + DIFX3 + DIFX4 + DIFX5 + DIFX6) \qquad (6-11)$$

The quantity $(\overline{\rho u})_{i,j,k}$ is computed from known quantities at time t and is used to calculate the fluid velocity at time $t + \Delta t$, and

$$DPX = -\frac{\partial P}{\partial r}$$

$$CUX = \frac{1}{R}\frac{\partial}{\partial r}(\rho R u u) - \frac{1}{R}\frac{\partial}{\partial r}(\mu R \frac{\partial u}{\partial r})$$

$$CU\Theta = \frac{1}{R}\frac{\partial}{\partial \theta}(\rho w u) + \frac{1}{R}\frac{\partial}{\partial \theta}(\mu \frac{1}{R}\frac{\partial u}{\partial \theta})$$

$$CUY = \frac{\partial}{\partial y}(\rho v u) - \frac{\partial}{\partial y}(\mu \frac{\partial u}{\partial y})$$

$$DIFX1 = \frac{1}{R}\frac{\partial}{\partial r}(\mu R \frac{\partial u}{\partial r})$$

$$DIFX2 = \frac{\partial}{\partial y}(\mu \frac{\partial v}{\partial r})$$

$$DIFX3 = \delta \frac{2\mu u}{r^2}$$

$$DIFX4 = \delta \frac{\rho w w}{r}$$

$$DIFX5 = \frac{1}{R}\frac{\partial}{\partial \theta}(R\mu \frac{\partial}{\partial} \frac{w}{r})$$

$$DIFX6 = -\delta \frac{2\mu}{r^2}\frac{\partial w}{\partial \theta}$$

These terms can be written in finite difference form as follows:

$$DPX = \frac{P_{i,j,k} - P_{i+1,j,k}}{0.5(\Delta r_i + \Delta r_{i+1})}$$

$$CUX = \frac{R_{i+1}COEFE - R_iCOEFW}{R_{i+\frac{1}{2}}(\Delta r_i + \Delta r_{i+1})}$$

where:

$COEFE = \rho_{i+1,j,k}U_R[u_{i,j,k} + u_{i+1,j,k} + SIGN(P_e)(u_{i,j,k} - u_{i+1,j,k})]$ for $|P_e| \geq 2$

or

$COEFE = 2\rho_{i+1,j,k}U_RU_R - 2\mu_{i+1,j,k}(u_{i+1,j,k} - u_{i,j,k})/\Delta r_{i+1}$ for $|P_e| \leq 2$

with

P_e = Peclet number $= \rho_{i+1,j,k}U_R\Delta r_{i+1}/\mu_{i+1,j,k}$

$U_R = 0.5(u_{i,j,k} + u_{i+1,j,k})$

$SIGN(P_e)$ is the algebraic sign of P_e

$COEFW = \rho_{i,j,k}U_C[u_{i,j,k} + u_{i-1,j,k} + SIGN(P_w)(u_{i-1,j,k} - u_{i,j,k})]$ for $|P_w| \geq 2$

or

$COEFW = 2\rho_{i,j,k}U_CU_C - 2\mu_{i,j,k}(u_{i,j,k} - u_{i-1,j,k})/\Delta r_i$ for $|P_w| \leq 2$

with

$P_w = \rho_{i,j,k}U_C\Delta r_i/\mu_{i,j,k}$

$U_C = 0.5(u_{i,j,k} + u_{i-1,j,k})$

$SIGN(P_w)$ is the algebraic sign of P_w

Similarly the term CUΘ is written as:

$$CU\Theta = \frac{COEFF - COEFB}{2R_i\Delta\theta_j}$$

where:

$COEFF = \rho_{i+\frac{1}{2},j+\frac{1}{2},k} w_{i+\frac{1}{2},j+\frac{1}{2},k} [u_{i,j,k} + u_{i,j+1,k} + SIGN(P_f)(u_{i,j,k} - u_{i,j+1,k})]$

for $|P_f| \geq 2$

or

$COEFF = 2\rho_{i+\frac{1}{2},j+\frac{1}{2},k} w_{i+\frac{1}{2},j+\frac{1}{2},k} - 2\mu_{i+\frac{1}{2},j+\frac{1}{2},k}(u_{i,j+1,k} - u_{i,j,k})/(0.5R_{i+\frac{1}{2}}(\Delta\theta_{j+1} + \Delta\theta_j))$

for $|P_f| \leq 2$

with

$P_f = 0.5R_i\rho_{i+\frac{1}{2},j+\frac{1}{2},k} w_{i+\frac{1}{2},j+\frac{1}{2},k}(\Delta\theta_j + \Delta\theta_{j+1})/\mu_{i+\frac{1}{2},j+\frac{1}{2},k}$

$COEFB = \rho_{i+\frac{1}{2},j-\frac{1}{2},k} w_{i+\frac{1}{2},j-\frac{1}{2},k} [u_{i,j,k} + u_{i,j-1,k} + SIGN(P_b)(u_{i,j-1,k} - u_{i,j,k})]$

for $|P_b| \geq 2$

or

$COEFB = 2\rho_{i+\frac{1}{2},j-\frac{1}{2},k} w_{i+\frac{1}{2},j-\frac{1}{2},k} - 2\mu_{i+\frac{1}{2},j-\frac{1}{2},k}(u_{i,j,k} - u_{i,j-1,k})/(0.5R_{i+\frac{1}{2}}(\Delta\theta_{j-1} + \Delta\theta_j))$

for $|P_b| \leq 2$

with

$P_b = 0.5R_i\rho_{i+\frac{1}{2},j-\frac{1}{2},k} w_{i+\frac{1}{2},j-\frac{1}{2},k}(\Delta\theta_j + \Delta\theta_{j-1})/\mu_{i+\frac{1}{2},j-\frac{1}{2},k}$

Similarly the term CUY is written as:

$$CUY = \frac{COEFN - COEFS}{2\Delta y_k}$$

where:

$COEFN = \rho_{i+\frac{1}{2},j,k+\frac{1}{2}} v_{i+\frac{1}{2},j,k+\frac{1}{2}} [u_{i,j,k} + u_{i,j,k+1} + SIGN(P_n)(u_{i,j,k} - u_{i,j,k+1})]$

for $|P_n| \geq 2$

or

$COEFN = 2\rho_{i+\frac{1}{2},j,k+\frac{1}{2}} v_{i+\frac{1}{2},j,k+\frac{1}{2}} - 2\mu_{i+\frac{1}{2},j,k+\frac{1}{2}} (u_{i,j,k+1} - u_{i,j,k})/(0.5(\Delta y_{k+1} + \Delta y_k))$

for $|P_n| \leq 2$

with

$$P_n = 0.5\rho_{i+\frac{1}{2},j,k+\frac{1}{2}} v_{i+\frac{1}{2},j,k+\frac{1}{2}} (\Delta y_k + \Delta y_{k+1})/\mu_{i+\frac{1}{2},j,k+\frac{1}{2}}$$

$COEFS = \rho_{i+\frac{1}{2},j,k-\frac{1}{2}} v_{i+\frac{1}{2},j,k-\frac{1}{2}} [u_{i,j,k} + u_{i,j,k-1} + SIGN(P_n)(u_{i,j,k-1} - u_{i,j,k})]$

for $|P_s| \geq 2$

or

$COEFS = 2\rho_{i+\frac{1}{2},j,k-\frac{1}{2}} v_{i+\frac{1}{2},j,k-\frac{1}{2}} - 2\mu_{i+\frac{1}{2},j,k-\frac{1}{2}} (u_{i,j,k} - u_{i,j,k-1})/(0.5(\Delta y_{k-1} + \Delta y_k))$

for $|P_s| \leq 2$

with

$$P_s = 0.5\rho_{i+\frac{1}{2},j,k-\frac{1}{2}} v_{i+\frac{1}{2},j,k-\frac{1}{2}} (\Delta y_k + \Delta y_{k-1})/\mu_{i+\frac{1}{2},j,k-\frac{1}{2}}$$

$$DIFX1 = \frac{R_{i+\frac{1}{2}} \mu_{i+1,j,k} (u_{i+1,j,k} - u_{i,j,k})/\Delta r_{i+1} - R_{i-\frac{1}{2}} \mu_{i,j,k} (u_{i,j,k} - u_{i-1,j,k})/\Delta_i}{0.5 R_i (\Delta r_i + \Delta r_{i+1})}$$

$$DIFX2 = \frac{\mu_{i+\frac{1}{2},j,k+\frac{1}{2}} (v_{i+1,j,k} - v_{i,j,k}) - \mu_{i+\frac{1}{2},j,k-\frac{1}{2}} (v_{i+1,j,k-1} - v_{i,j,k-1})}{0.5 \Delta y_k (\Delta r_i + \Delta r_{i+1})}$$

$$DIFX3 = -\delta \frac{2\mu_{i,j,k} u_{i-\frac{1}{2},j,k}}{r_i^2}$$

$$DIFX4 = \delta \frac{\rho_{i,j,k} w^2_{i,j-\frac{1}{2},k}}{r_i}$$

$$DIFX5 = \frac{\mu_{i+\frac{1}{2},j+\frac{1}{2},k}(w_{i+1,j,k}/r_{i+1} - w_{i,j,k}/r_i) - \mu_{i+\frac{1}{2},j-\frac{1}{2},k}(w_{i+1,j-1,k}/r_{i+1} - w_{i,j-1,k}/r_i)}{0.5(\Delta r_{i+1} + \Delta r_i)\Delta\theta_j}$$

$$DIFX6 = -\delta \frac{2\mu_{i,j,k}(w_{i,j,k} - w_{i,j-1,k})}{r_i^2 \theta_j}$$

Similarly the momentum equations in the axial and circumferential directions are written as:

Momentum Equation in Axial Direction

$$(\overline{\rho v})_{i,j,k} = (\rho v)_{i,j,k} + \Delta t(DPY - CVX - CVY - CV\Theta + DIFY1 + DIFY2 + DIFY3) \qquad (6-12)$$

where:

$$DPY = -\frac{\partial P}{\partial y}$$

$$CVX = \frac{1}{R}\frac{\partial}{\partial r}(\rho R u v) - \frac{1}{R}\frac{\partial}{\partial r}(\mu R \frac{\partial v}{\partial r})$$

$$CVY = \frac{\partial}{\partial y}(\rho v v) - \frac{\partial}{\partial y}(\mu \frac{\partial v}{\partial y})$$

$$CV\Theta = \frac{1}{R}\frac{\partial}{\partial \theta}(\rho w v) - \frac{1}{R}\frac{\partial}{\partial \theta}(\mu \frac{1}{R}\frac{\partial v}{\partial \theta})$$

$$DIFY1 = \frac{\partial}{\partial y}(\mu \frac{\partial v}{\partial r})$$

$$DIFY2 = \frac{1}{R}\frac{\partial}{\partial r}(\mu R \frac{\partial u}{\partial r})$$

$$DIFY3 = \frac{1}{R}\frac{\partial}{\partial \theta}(\mu \frac{\partial w}{\partial y})$$

Momentum Equation in Circumferential Direction

$$(\overline{\rho w})_{i,j,k} = (\rho w)_{i,j,k} + \Delta t(DP\Theta - CWX - CWY - CW\Theta + DIF\Theta 1 + DIF\Theta 2$$
$$+DIF\Theta 3 + DIF\Theta 4 + DIF\Theta 5 + DIF\Theta 6 + DIF\Theta 7) \qquad (6-13)$$

where:

$$DP\Theta = -\frac{1}{R}\frac{\partial P}{\partial \theta}$$
$$CWX = \frac{1}{R}\frac{\partial}{\partial r}(\rho R u w) - \frac{1}{R}\frac{\partial}{\partial r}(\mu R \frac{\partial w}{\partial r})$$
$$CWY = \frac{\partial}{\partial y}(\rho v w) - \frac{\partial}{\partial y}(\mu \frac{\partial w}{\partial y})$$
$$CW\Theta = \frac{1}{R}\frac{\partial}{\partial \theta}(\rho w w) - \frac{1}{R}\frac{\partial}{\partial \theta}(\mu \frac{1}{R}\frac{\partial w}{\partial \theta})$$
$$DIF\Theta 1 = -\delta \rho \frac{wu}{r}$$
$$DIF\Theta 2 = \frac{\mu}{R}\frac{\partial w}{\partial r}$$
$$DIF\Theta 3 = \frac{1}{R^2}\frac{\partial}{\partial r}(\mu R \frac{\partial u}{\partial \theta})$$
$$DIF\Theta 4 = -\frac{1}{R^2}\frac{\partial}{\partial r}(\mu R w)$$
$$DIF\Theta 5 = \frac{1}{R}\frac{\partial}{\partial \theta}(\mu \frac{1}{R}\frac{\partial w}{\partial \theta})$$
$$DIF\Theta 6 = \delta \frac{2}{r}\frac{\partial}{\partial \theta}(\mu \frac{u}{r})$$
$$DIF\Theta 7 = \frac{\partial}{\partial y}(\frac{\mu}{r}\frac{\partial v}{\partial \theta})$$

The convective and diffusive terms in equations (6-12) and (6-13) are written in finite difference form in a manner similar to that used for the corresponding terms in the momentum equation in the radial direction (equation (6-11)).

6.3.2 TURBULENCE MODEL EQUATIONS

The turbulence kinetic energy and the energy dissipation rate equations are written in finite difference form using the hybrid differencing scheme. Using the same notation to that for the momentum equations the turbulence kinetic energy equation is written as:

Turbulence Kinetic Energy Equation

$$K_{i,j,k}^{n+1} = [\rho_{i,j,k} K_{i,j,k} + \Delta t(-CKX - CKY - CK\Theta + G - \rho_{i,j,k} DTR)]/\rho_{i,j,k}^{n+1} \qquad (6-14)$$

where:

$$CKX = \frac{1}{R}\frac{\partial}{\partial r}(\rho R u K) - \frac{1}{R}\frac{\partial}{\partial r}(\frac{\mu}{S_k} R \frac{\partial K}{\partial r})$$
$$CKY = \frac{\partial}{\partial y}(\rho v K) - \frac{\partial}{\partial y}(\frac{\mu}{S_k}\frac{\partial K}{\partial y})$$
$$CK\Theta = \frac{1}{R}\frac{\partial}{\partial \theta}(\rho w K) - \frac{1}{R}\frac{\partial}{\partial \theta}(\frac{\mu}{S_k}\frac{1}{R}\frac{\partial K}{\partial \theta})$$
$$DTR = \epsilon C_d$$

The generation term G is defined in equation (6-8). The terms CKX, CKY, $CK\Theta$ and DTR are written in finite difference form as follows:

$$CKX = \frac{R_{i+\frac{1}{2}} COEFE - R_{i-\frac{1}{2}} COEFW}{2R_i \Delta r_i}$$

where:

$COEFE = \rho_{i+\frac{1}{2},j,k} u_{i,j,k}[K_{i,j,k} + K_{i+1,j,k} SIGN(P_e)(K_{i,j,k} - K_{i+1,j,k})]$ for $|P_e| \geq 2$

or

$$COEFE = 2\rho_{i+\frac{1}{2},j,k}u_{i,j,k}K_{i+\frac{1}{2},j,k} - 2\mu_{i+\frac{1}{2},j,k}(K_{i+1,j,k} - K_{i,j,k})/(0.5(\Delta r_i + \Delta r_{i+1}))$$

for $|P_e| \leq 2$

with

$$P_e = 0.5\rho_{i+\frac{1}{2},j,k}u_{i,j,k}(\Delta r_i + \Delta r_{i+1})/\mu_{i+\frac{1}{2},j,k}$$

and

$$COEFW = \rho_{i-\frac{1}{2},j,k}u_{i-1,j,k}[K_{i,j,k} + K_{i-1,j,k}SIGN(P_w)(K_{i-1,j,k} - K_{i,j,k})]$$

for $|P_w| \geq 2$

or

$$COEFW = 2\rho_{i-\frac{1}{2},j,k}u_{i-1,j,k}K_{i-\frac{1}{2},j,k} - 2\mu_{i-\frac{1}{2},j,k}(K_{i,j,k} - K_{i-1,j,k})/(0.5(\Delta r_i + \Delta r_{i-1}))$$

for $|P_w| \leq 2$

with

$$P_w = 0.5\rho_{1-\frac{1}{2},j,k}u_{i-1,j,k}(\Delta r_i + \Delta r_{i-1})/\mu_{i-\frac{1}{2},j,k}$$

Similarly, the term CKY is written as:

$$CKY = \frac{COEFN - COEFS}{2\Delta y_k}$$

where:

$$COEFN = \rho_{i,j,k+\frac{1}{2}}v_{i,j,k}[K_{i,j,k} + K_{i,j,k+1} + SIGN(P_n)(K_{i,j,k} - K_{i,j,k+1})]$$

for $|P_n| \geq 2$

or

$$COEFN = 2\rho_{i,j,k+\frac{1}{2}}v_{i,j,k}K_{i,j,k+\frac{1}{2}} - 2\mu_{i,j,k+\frac{1}{2}}(K_{i,j,k+1} - K_{i,j,k})/(0.5(\Delta y_{k+1} + \Delta y_k))$$

for $|P_n| \leq 2$

with

$$P_n = 0.5\rho_{i,j,k+\frac{1}{2}}v_{i,j,k}(\Delta y_k + \Delta y_{k+1})/\mu_{i,j,k+\frac{1}{2}}$$

and

$$COEFS = \rho_{i,j,k-\frac{1}{2}} v_{i,j,k-1}[K_{i,j,k} + K_{i,j,k-1} + SIGN(P_s)(K_{i,j,k-1} - K_{i,j,k})]$$

for $|P_s| \geq 2$

or

$$COEFS = 2\rho_{i,j,k-\frac{1}{2}} v_{i,j,k-1} K_{i,j,k-\frac{1}{2}} - 2\mu_{i,j,k-\frac{1}{2}}(K_{i,j,k} - K_{i,j,k-1})/(0.5(\Delta y_{k-1} + \Delta y_k))$$

for $|P_s| \leq 2$

with

$$P_s = 0.5\rho_{i,j,k-\frac{1}{2}} v_{i,j,k-1}(\Delta y_k + \Delta y_{k-1})/\mu_{i,j,k-\frac{1}{2}}$$

Similarly, the term $CK\Theta$ is written as:

$$CK\Theta = \frac{COEFF - COEFB}{2R_i \Delta\theta_j}$$

where:

$$COEFF = \rho_{i,j+\frac{1}{2},k} w_{i,j,k}[K_{i,j,k} + K_{i,j+1,k} SIGN(P_f)(K_{i,j,k} - K_{i,j+1,k})]$$

for $|P_f| \geq 2$

or

$$COEFF = 2\rho_{i,j+\frac{1}{2},k} w_{i,j,k} K_{i,j+\frac{1}{2},k} - 2\mu_{i,j+\frac{1}{2},k}(K_{i,j+1,k} - K_{i,j,k})/$$

$(0.5R_i(\Delta\theta_j + \Delta\theta_{j+1}))$ for $|P_f| \leq 2$

with

$$P_f = 0.5\rho_{i,j+\frac{1}{2},k} w_{i,j,k} R_i(\Delta\theta_j + \Delta\theta_{j+1})/\mu_{i,j+\frac{1}{2},k}$$

and

$$COEFB = \rho_{i,j-\frac{1}{2},k} w_{i,j-1,k}[K_{i,j,k} + K_{i,j-1,k} SIGN(P_b)(K_{i,j-1,k} - K_{i,j,k})]$$

for $|P_b| \geq 2$

or

$$COEFB = 2\rho_{i,j-\frac{1}{2},k} w_{i,j-1,k} K_{i,j-\frac{1}{2},k} - 2\mu_{i,j-\frac{1}{2},k}(K_{i,j,k} - K_{i,j-1,k})/$$
$(0.5R_i(\Delta\theta_j + \Delta\theta_{j-1}))$ for $|P_b| \leq 2$

with

$$P_b = 0.5\rho_{i,j-\frac{1}{2},k} w_{i,j-1,k} R_i(\Delta\theta_j + \Delta\theta_{j-1})/\mu_{i,j-\frac{1}{2},k}$$

and

$$\text{DTR} = C_d \epsilon_{i,j,k}$$

The generation term (eqn (6-8)) is written as:

$$\begin{aligned} G = \mu[&2(DVDY^2 + DUDX^2 + (CYLT + DWD\Theta)^2) \\ &+ (DVDX + DUDY)^2 + (DUD\Theta + DWDX)^2 \\ &+ (DWDY + DVD\Theta)^2] - \frac{2}{3} DIV(\mu DIV + \rho K) \end{aligned} \qquad (6-15)$$

where:

$$DVDY = \frac{v_{i,j,k} - v_{i,j,k-1}}{\Delta y_k}$$

$$DUDX = \frac{u_{i,j,k} - u_{i-1,j,k}}{\Delta r_i}$$

$$DWD\Theta = \frac{w_{i,j,k} - w_{i,j-1,k}}{R_i \Delta\theta_j}$$

$$CYLT = \delta \frac{u_{i+\frac{1}{2},j,k}}{2r_i}$$

$$DVDX = \frac{v_{i+\frac{1}{2},j,k-\frac{1}{2}} - v_{i-\frac{1}{2},j,k-\frac{1}{2}}}{\Delta r_i}$$

$$DUDY = \frac{u_{i-\frac{1}{2},j,k+\frac{1}{2}} - u_{i-\frac{1}{2},j,k-\frac{1}{2}}}{\Delta y_k}$$

$$DWDX = \frac{R_i(w_{i+\frac{1}{2},j-\frac{1}{2},k}/r_{i+\frac{1}{2}} - w_{i-\frac{1}{2},j-\frac{1}{2},k}/r_{i-\frac{1}{2}})}{\Delta r_i}$$

$$DUD\Theta = \frac{u_{i-\frac{1}{2},j+\frac{1}{2},k} - -u_{i-\frac{1}{2},j-\frac{1}{2},k}}{R_i \Delta\theta_j}$$

$$DVD\Theta = \frac{v_{i,j+\frac{1}{2},k-\frac{1}{2}} - v_{i,j-\frac{1}{2},k-\frac{1}{2}}}{R_i \Delta\theta_j}$$

$$DWDY = \frac{w_{i,j-\frac{1}{2},k+\frac{1}{2}} - w_{i,j-\frac{1}{2},k-\frac{1}{2}}}{\Delta y_k}$$

$$DIV = \frac{R_i u_{i,j,k} - R_{i-1} u_{i-1,j,k}}{R_i \Delta r_i} + \frac{v_{i,j,k} - v_{i,j,k-1}}{\Delta y_k} + \frac{w_{i,j,k} - w_{i,j-1,k}}{R_{i+\frac{1}{2}} \Delta\theta_j}$$

The energy dissipation equation is written as follows:

Energy Dissipation Equation

$$\epsilon^{n+1}_{i,j,k} = [\rho_{i,j,k}\epsilon_{i,j,k} + \Delta t(-CEX - CE\Theta - CEY + TERM)]/\rho^{n+1}_{i,j,k} \qquad (6-16)$$

where:

$$CEX = \frac{1}{R}\frac{\partial}{\partial r}(\rho R u \epsilon) - \frac{1}{R}\frac{\partial}{\partial r}(\frac{\mu}{S_e} R \frac{\partial \epsilon}{\partial r})$$

$$CEY = \frac{\partial}{\partial y}(\rho v \epsilon) - \frac{\partial}{\partial y}(\frac{\mu}{S_e}\frac{\partial \epsilon}{\partial y})$$

$$CE\Theta = \frac{1}{R}\frac{\partial}{\partial \theta}(w\epsilon) - \frac{1}{R}\frac{\partial}{\partial \theta}(\frac{\mu}{S_e}\frac{1}{R}\frac{\partial \epsilon}{\partial \theta})$$

$$TERM = \varepsilon(C_1 G - C_2 \rho \epsilon)/K$$

The terms CEX, CEY and $CE\Theta$ are written in a similar finite difference form as the terms CKX, CKY and $CK\Theta$ by replacing the turbulence kinetic energy with the energy dissipation rate. The term TERM is written as:

$$TERM = \epsilon_{i,j,k}(C_1 G_{i,j,k} - C_2 \rho_{i,j,k}\epsilon_{i,j,k})/K_{i,j,k}$$

The effective viscosity is written as:

$$\mu = \mu_l + C_\mu \rho_{i,j,k} K^2_{i,j,k}/\epsilon_{i,j,k} \qquad (6-17)$$

6.3.3 ENERGY AND CONCENTRATION EQUATIONS

The energy and concentration equations are discretized in the same manner as the turbulence kinetic energy and the energy dissipation rate. Thus:

Energy Equation

$$T_{i,j,k}^{n+1} = [\rho_{i,j,k} T_{i,j,k} + \Delta t(-CTX - CTY - CT\Theta)]/\rho_{i,j,k}^{n+1} \qquad (6-18)$$

Concentration Equation

$$C_{i,j,k}^{n+1} = [\rho_{i,j,k} C_{i,j,k} + \Delta t(-CCX - CCY - CC\Theta)]/\rho_{i,j,k}^{n+1} \qquad (6-19)$$

The terms CCX and CTX are written in the same manner as the term CKX by replacing the turbulence kinetic energy with the concentration and the temperature respectively. Similarly, the terms CCY and CTY are written in the same manner as the term CKY, and terms $CC\Theta$ and $CT\Theta$ in the same manner as the term $CK\Theta$.

6.4 SOLUTION PROCEDURE

The procedure used for the solution of the momentum and continuity equations is iterative and based on the ICE method [1] (same as in the two-dimensional code). The scalar quantities (temperature, concentration, turbulence kinetic energy and energy dissipation rate) are solved explicitly in time. The barred values of density are calculated as follows:

$$\overline{\rho}_{i,j,k} = \rho_{i,j,k} - (1-\theta)\Delta t[\frac{R_{i+\frac{1}{2}}(\rho u)_{i,j,k} - R_{i-\frac{1}{2}}(\rho u)_{i-1,j,k}}{R_i \Delta r_i}$$

$$+\frac{(\rho v)_{i,j,k} - (\rho v)_{i,j,k-1}}{\Delta y_k} + \frac{(\rho w)_{i,j,k} - (\rho w)_{i,j-1,k}}{R_i \Delta \theta_j}] \qquad (6-20)$$

The divergence equation is written as follows:

$$D_{i,j,k} = \rho^{n+1}_{i,j,k} - \overline{\rho}_{i,j,k} - \theta\Delta t[\frac{R_{i+\frac{1}{2}}(\rho u)^{n+1}_{i,j,k} - R_{i-\frac{1}{2}}(\rho u)^{n+1}_{i-1,j,k}}{R_i\Delta r_i}$$

$$+\frac{(\rho v)^{n+1}_{i,j,k} - (\rho v)^{n+1}_{i,j,k-1}}{\Delta y_k} + \frac{(\rho w)^{n+1}_{i,j,k} - (\rho w)^{n+1}_{i,j-1,k}}{R_i\Delta\theta_j}] \qquad (6-21)$$

The pressure, density and mass fluxes are corrected using the following formulae:

$$P_{i,j,k} = P_{i,j,k} + \Delta P_{i,j,k}$$

$$\rho_{i,j,k} = \rho_{i,j,k} + \Delta P_{i,j,k}/c^2_{i,j,k}$$

$$(\rho u)_{i,j,k} = (\rho u)_{i,j,k} + \Delta t\Delta P_{i,j,k}/\Delta r_i$$

$$(\rho u)_{i-1,j,k} = (\rho u)_{i-1,j,k} - \Delta t\Delta P_{i,j,k}/\Delta r_i$$

$$(\rho v)_{i,j,k} = (\rho v)_{i,j,k} + \Delta t\Delta P_{i,j,k}/\Delta y_k$$

$$(\rho v)_{i,j,k-1} = (\rho v)_{i,j,k-1} - \Delta t\Delta P_{i,j,k}/\Delta y_k$$

$$(\rho w)_{i,j,k} = (\rho w)_{i,j,k} + \Delta t\Delta P_{i,j,k}/R_i\Delta\theta_j$$

$$(\rho w)_{i,j-1,k} = (\rho w)_{i,j-1,k} - \Delta t\Delta P_{i,j,k}/R_i\Delta\theta_j$$

The value of $\Delta P_{i,k}$ is calculated from the following equation:

$$\Delta P_{i,j,k} = -\Omega D_{i,j,k}/\beta_{i,j,k} \qquad (6-22)$$

where:

$$\beta_{i,j,k} = \frac{1}{c^2_{i,j,k}} + 2\theta\Delta t^2(\frac{1}{\Delta r_i^2} + \frac{1}{\Delta y_k^2} + \frac{1}{(R_i\Delta\theta_j)^2}) \qquad (6-23)$$

As with the two-dimensional code the values of θ and Ω are 0.5 and 1.7 respectively. After convergence has been reached for all cells the fluid velocities are obtained as follows:

$$u_{i,j,k} = \frac{(\rho u)_{i,j,k}}{\rho_{i+\frac{1}{2},j,k}} \qquad (6-24)$$

$$v_{i,j,k} = \frac{(\rho v)_{i,j,k}}{\rho_{i,j,k+\frac{1}{2}}} \qquad (6-25)$$

$$w_{i,j,k} = \frac{(\rho w)_{i,j,k}}{\rho_{i,j+\frac{1}{2},k}} \qquad (6-26)$$

After the velocity field has been obtained the turbulent kinetic energy and the energy dissipation rate are obtained at time $t + \Delta t$ by solving equations (6-14) and (6-16). The effective viscosity is calculated from equation (6-10). Then, the temperature and concentration equations are solved (eqns (6-18) and (6-19)). The density is updated using the ideal gas equation.

6.5 DESCRIPTION OF THE PHYSICAL PROBLEM AND BOUNDARY CONDITIONS

The General Motors GM6V53T engine has four overhead exhaust valves and 18 inlet ports. The inlet ports are inclined at 22 degrees to the radius and are located in the cylinder sleeve close to the BDC. Figure 6.2 shows the top view of the cylinder head with the four exhaust openings. In the computations, because of symmetry, only one quarter of the cylinder domain is studied. In figure 6.3 the grid used in the computations for the plane perpendicular to the cylinder axis is shown. The symmetry is imposed as follows.[2](see figure 6.4):

SCALAR (P,T,C,K,ϵ and ρ)

$S_{i,JMAX,k} = S_{i,JM1,k}$ for $IMAX > i > IMIN$ and $KMAX < k < KMIN$

$S_{i,JMIN,k} = S_{i,JM2,k}$ for $IMAX > i > IMIN$ and $KMAX < k < KMIN$

VELOCITIES

$w_{i,JMAX,k} = w_{i,JM1,k}$ for $IMAX > i > IMIN$ and $KMAX < k < KMIN$

$w_{i,JMIN,k} = w_{i,JM2,k}$ for $IMAX > i > IMIN$ and $KMAX < k < KMIN$

$v_{i,JMAX,k} = v_{i,JM1,k}$ for $IMAX > i > IMIN$ and $KMAX < k < KMIN$

$v_{i,JMIN,k} = v_{i,JM2,k}$ for $IMAX > i > IMIN$ and $KMAX < k < KMIN$

$u_{i,JMAX,k} = u_{i,JM1,k}$ for $IMAX > i > IMIN$ and $KMAX < k < KMIN$

$u_{i,JMIN,k} = u_{i,JM2,k}$ for $IMAX > i > IMIN$ and $KMAX < k < KMIN$

where:

$IMIN$- Smallest index in the radial direction

$KMIN$- Smallest index in the axial direction

$JMIN$- Smallest index in the circumferential direction

$IMAX$- Biggest index in the radial direction

$KMAX$- Biggest index in the axial direction

$JMAX$- Biggest index in the circumferential direction

$IM1 = IMIN + 1$

$KM1 = KMIN + 1$

$JM1 = JMIN + 1$

$IM2 = IMAX - 1$

$KM2 = KMAX - 1$

$JM2 = JMAX - 1$

The boundary conditions used in the three-dimensional model are very similar to the ones used in the two-dimensional model discussed in sections 5.5 to 5.7. At the cylinder axis the radial and circumferential velocities are set equal to zero. Free-slip condition is assumed in the axial direction. The conditions are imposed using the first cell adjacent to the cylinder axis as a fictitious cell. At all solid boundaries non-slip conditions are used for the velocities. Also, wall conditions are used for all solid boundaries in the K-ϵ model. The initial conditions and

the temperatures in the cylinder surfaces are the same as those used in the two-dimensional model. The valve surface is assumed to be at a temperature of 700 K. The initial and boundary conditions for the solution of the concentration equations are the same with those used in the two-dimensional model. In the computations twelve nodal points in the radial direction, eleven nodal points in the circumferential and 28 nodal points in the axial direction are used. The model discussed in the previous sections uses cylindrical coordinates; therefore, the shape of the actual valve cannot be used in the computations. Instead, the valve shape shown in figure 6.3 is used. Figure 6.5 shows the grid in the plane containing the cylinder axis. In the computation the inlet area changes with time in the same manner as in the two-dimensional model. The outlet area is between the valve peripheral and the cylinder head. This area changes with time by moving the valve location upwards or downwards. This motion is performed in finite steps using the grid nodal points. This explains the fine grid used close to the cylinder head.

6.6 SCAVENGING STUDIES USING THE THREE-DIMENSIONAL CODE

The results presented in this section are an extension to the studies performed using the two-dimensional code presented in chapter 5.The three dimensional model gives the ability to study the effect of the circumferential variation of the flow and also a more realistic representation of the exhaust valve. The inflow can be considered to be axisymmetric, therefore the inflow conditions used are the same with the ones used in the two-dimensional reference case discussed in section 5.11 (the flow is assumed to enter the cylinder with a 15 degree swirl angle and to be inclined at 20 degrees to the horizontal). The grid used in the computations has 12 grid points in the radial, 28 in the axial and 11 in the circumferential direction. The total number of grid points used in the fluid domain is 2340. Surrounding

the fluid domain 1356 fictitious cells are used. The total number of grid points used in the axial and radial directions is 260 compared to 616 points used in the two-dimensional computations. The main restriction for using this grid was the computational time. The three-dimensional model with the grid discussed above uses six times more CPU time than the two-dimensional model. The computational time increases enormously if a fine grid is used close to the axis of symmetry. This is because by using a fine grid in the radial direction the distances between the cell faces in the circumferential direction become very small. Also with high swirl velocities close to the cylinder axis, a very small time step is required for stability.

For every run of the code the results were stored on a tape at approximately 15 degree intervals. The data stored are the three velocity components, the turbulence kinetic energy, the effective viscosity, temperature and concentration. Some of these results are presented and discussed below. Results during scavenging are presented at 161, 178, 205 and 230 degree crank angles. At every crank angle the results are given at four levels (A, B, C and D) across the cylinder axis as shown in figure 6.5 and four sections (A, B, C and D) shown in figure 6.3

Figure 6.6 shows the axial-radial velocity patterns in the four sections at 161 degrees crank angle. At this crank angle there are two recirculation zones in the cylinder. The first one is in the piston bowl and the second close to the cylinder wall (flow reattachment). In all four sections the flow is very similar at the lower half of the cylinder. In the upper half the flow is different, being affected by the exhaust geometry. The flow patterns shown in figure 6.6 are different than those shown in figure 5.20 computed using the two-dimensional code at 165 degrees crank angle. In the two dimensional code a recirculation zone close to the cylinder axis is present. The reason for this recirculation zone is that higher swirl velocities are observed in the two-dimensional computations. The swirl velocity

contours in the 3D computations are presented in figure 6.7 at 161 degrees for the four cylinder sections. The swirl velocity in the cylinder is affected by the imposed swirl velocity at the inlet ports and by the exhaust valve geometry. High swirl velocities are observed at the lower part of the cylinder close to the cylinder axis of symmetry. These values are smaller than those observed in the two-dimensional computations (see figure 5.23). At the upper part of the cylinder high positive values for the circumferential velocities are observed at section B and high negative values at section D. Figure 6.8 shows very clearly how the circumferential and radial velocities are affected by the cylinder geometry and inlet and outlet conditions in the four levels. In level A (which is close to the inlet port elevation) high radial velocities exist close to the cylinder wall because of the inlet conditions. High swirl velocities close to the cylinder axis are observed. At this level there is no velocity variation in the circumferential direction indicating no effect of the exhaust valve (axisymmetric flow). The flow behaves in a similar manner at level B with small velocities close to the cylinder wall. The effect of the valve starts to be seen at level C and is very obvious at level D. At this level the flow is dominated by the outlet conditions at the valve. The decrease of the swirl velocities is produced by the negative circumferential velocities observed close to the exhaust valve. The smaller swirl velocities produce no recirculation at the cylinder axis.

Figures 6.9 and 6.10 show the mass flux (velocity x density) at the four sections and four levels of the cylinder at 161 degrees crank angle. Comparison between the velocity and the mass flux patterns show the density variation in the field. The density is computed in the same way as in the two dimensional code from the ideal gas equation using the computed temperature field. The temperature contours are shown in figure 6.11 at four different levels at 161 degree crank angle. The temperature contours are very similar at the lower part of the cylinder in the four cylinder levels, at the upper part are different because of the presence

of the exhaust valve. The concentration contours are given in figure 6.12 for the four cylinder sections at 161 degrees crank angle. It can be seen that there is no concentration variation in the four sections. There are, however, small differences between the two and three dimensional results. Because the same inlet conditions are used in both computations (two and three dimensional), the same amount of fresh air enters the cylinder. In the three dimensional computations it appears that the bottom part of the cylinder has been cleared from the residual gases more efficiently. This can be seen from the high concentration contours close to the cylinder wall and from the fact that in the two-dimensional computations the fresh air concentration contours have been advanced closer to the exhaust valve. The effective viscosity and turbulent kinetic energy contours are shown in figures 6.13 and 6.14 respectively. The shape of the contours is very similar in the two and three dimensional computations. The values in the three-dimensional computations are smaller than those in the two-dimensional computations, probably due to the smaller swirl velocities in the field.

The axial-radial velocity patterns at different sections in the cylinder at 178 degrees crank angle are shown in figure 6.15. It can be seen that a small recirculation zone appears at the cylinder axis of symmetry, accelerating the main flow towards the exhaust valve. The recirculation zones in the piston bowl and at the cylinder wall have been increased in size compared to the zones observed at 161 crank angle degree. The swirl velocity contours are shown in figure 6.16. The contours at the lower part of the cylinder are very similar to those observed at 161 degrees. At the upper part of the cylinder the swirl velocity has been increased as can be seen in figure 6.17 at level C with a maximum value of 7.22 m/s compared to a maximum value of 1.58 m/s observed at 161 degrees (figure 6.8). The swirl velocity values predicted by the 3D model remain smaller than the values obtained by the 2D model. The fresh air concentration contours are shown in figure 6.18 at

the four cylinder sections at 178 degrees crank angle. It can be seen that there is no variation between the four sections in the lower part of the cylinder. In the upper part of the cylinder the contours at section C differ from those of sections A,B and D. Comparison of these results with those shown in figure 5.24 at 180 degrees show that the cylinder residual gases close to the axis of symmetry in the 3D computations have been replaced by fresh air more efficiently. The effective viscosity and turbulence kinetic energy are shown in figures 6.19 and 6.20. at 178 degrees crank angle. The contour patterns are very similar to those computed using the two-dimensional code (figures 5.25 and 5.26) but the values are approximately 25 percent lower.

The axial-radial velocity patterns at 205 degrees for the four cylinder sections are shown in figure 6.21. The recirculation zone close to the cylinder wall has been significantly increased in size compared with the one at 178 degrees. This recirculation is very similar in size to the one computed using the 2D code at 205 degrees (figure 5.20). The recirculation zone close to the cylinder axis has been increased compared to the one observed at 178 degrees but is much smaller than the zone predicted by the 2D code. The swirl velocity contours at 205 degrees are shown in figure 6.22. At the lower part of the cylinder the swirl velocities are very similar to those computed by the 2D code. The only difference is the location of the maximum swirl velocity, which in the 3D computations is closer to the cylinder axis of symmetry. In the upper part of the cylinder the swirl velocity is highly affected by the exhaust opening. In figure 6.23 the radial-circumferential velocity patterns are shown at 205 degrees crank angle. The velocities at levels A, B and C are higher than those at 178 degrees. At level D the velocities are much lower because the exhaust valve has started to close, and therefore level D is now below the valve. Figure 6.24 shows the concentration contours at the four cylinder sections at 205 degrees. Comparison between the concentration contours computed using

the two and three dimensional models shows: a) the air concentration close to the cylinder axis in the 3D computations is higher than the air concentration computed by the 2D model, and b) the concentration close to the cylinder wall in the 3D computations is lower than the air concentration predicted by the 2D model. As discussed earlier, the amount of fresh air supplied to the cylinder is the same in both computations (two and three dimensional). Therefore, in the computations in which a minimum amount of air escapes will have the highest scavenging efficiency (highest amount of fresh air trapped in the cylinder). Examining the results obtained using the 2D code shows that no gases containing more than 85.9 percent air (0.859 contour) have escaped from the cylinder. The situation is similar in the three-dimensional computations. This means that the scavenging efficiency should be similar. However, the difference in the concentration patterns is important. The conclusion from the two-dimensional computations is that both recirculation zones (close to the cylinder axis and close to the cylinder wall) are important in the scavenging efficiency. From the three-dimensional computations, however, it has been shown that only the recirculation zone close to the cylinder wall affects the efficiency. The effective viscosity and turbulence kinetic energy at 205 degrees are shown in figures 6.25 and 6.26 respectively. Comparison between the two and three dimensional results show that the values and shape of the contours are very similar in the field except in the upper part of the cylinder.

The axial-radial velocity patterns at the end of the scavenging process (232 degrees) are shown in figure 6.27. There are three recirculation zones in the cylinder. The first one is in the piston bowl, the second close to the cylinder axis and the third close to the cylinder wall. The first two recirculation zones are small compared to the third, which predominates. In the flow predicted by the 2D model the recirculation close to the cylinder axis is equal in size to the one close to the cylinder wall. The swirl velocity contours are shown in figure 6.28. It can

be seen that in the four cylinder sections the contours are very similar because the exhaust valve is almost closed and therefore has no effect in the flow. The location of the maximum swirl velocity predicted by the 3D model is closer to the cylinder axis than the location predicted by the 2D model. In figure 6.29 the radial-circumferential velocity patterns are shown for the four levels. The velocities at level D are almost the same as those at level C because the valve is almost closed, and hence the velocities at level D are not affected. The concentration contours are shown in figure 6.30. The same conclusion can be drawn from the concentration contours at 232 degrees as at 205 degrees. In the 2D computations the recirculation zone close to the cylinder axis is as important as the one close to the cylinder wall. From the 3D model, it can be concluded that only the recirculation zone close to the cylinder wall affects the scavenging efficiency. The effective viscosity and the turbulence kinetic energy contours are shown in figures 6.31 and 6.32 respectively. The values and the shape of the contours are very similar as those predicted using the 2D model.

In figure 6.33 the scavenging efficiency-scavenging ratio relation derived from the 3D computations is plotted, along with one derived from the 2D computations. It can be seen that the computed efficiencies are almost the same during scavenging. In the thermodynamic model the following equations are used, approximating the scavenging efficiency plotted in figure 6.33.

$$\eta_{sc} = R_{sc} \quad for \quad R_{sc} < 0.45 \quad ^{\circ}and \tag{6-27}$$

$$\eta_{sc} = 1.134 - 1.362e^{-1.5R_{sc}} \quad for \quad 0.45 < R_{sc} < 1.10 \tag{6-28}$$

REFERENCES

1 Harlow, F. H., and Amsdin, A. A. "A Numerical Fluid Dynamics Method for All Flow Speeds" Journal of Computational Physics, 8, 197-213 (1971).

2 Serag-Eldin, M. A., and Spalding, D. B. "A Computational Procedure for Three-Dimensional Recirculating Flows Inside Can Combustors" Numerical Methods in Heat Transfer, John Wiley and Sons, 1981.

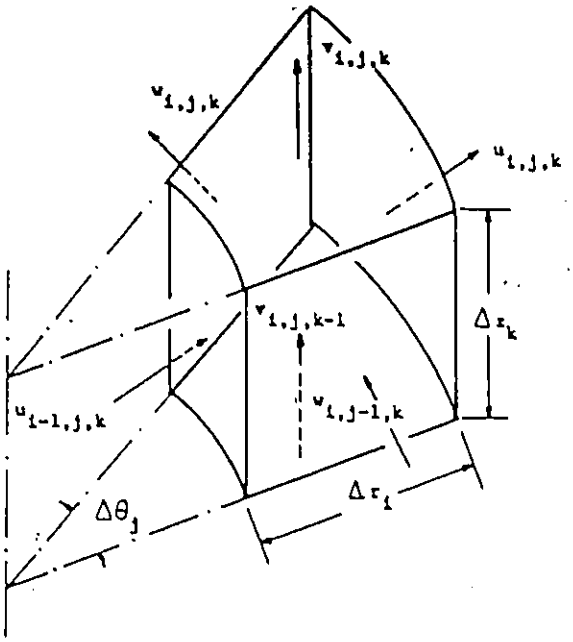

Figure 6.1 Typical cell used in the three-dimensional computations.

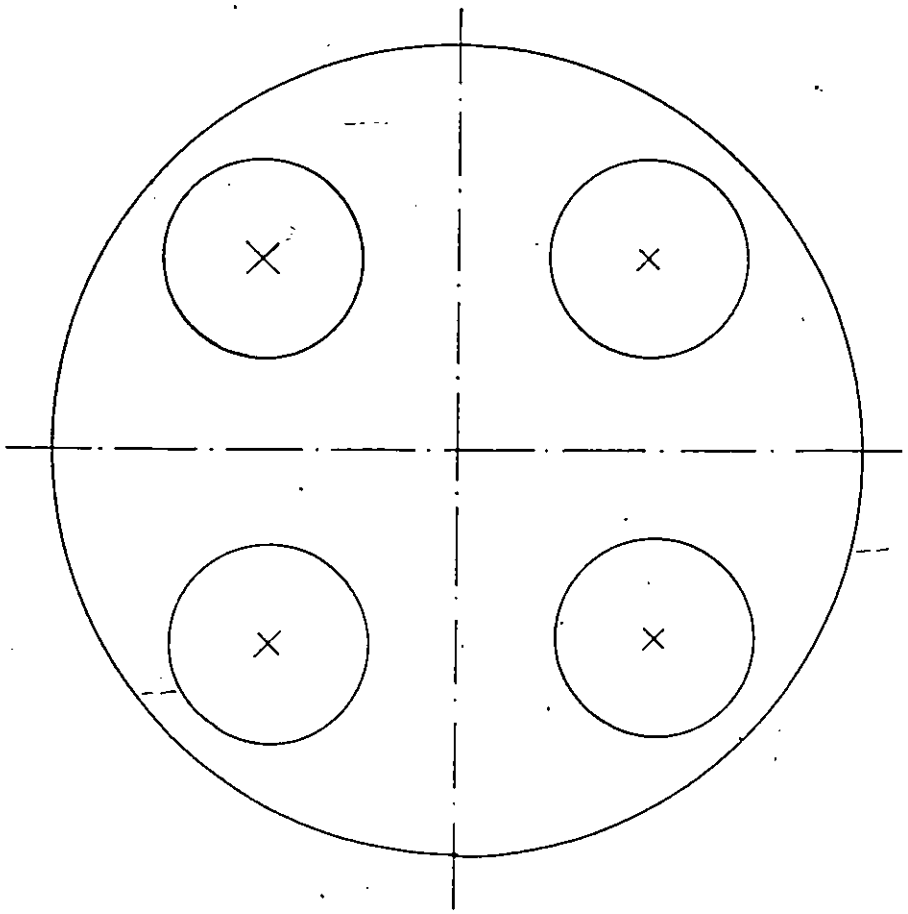

Figure 6.2 Cylinder head geometry with the four exhaust valves shown.

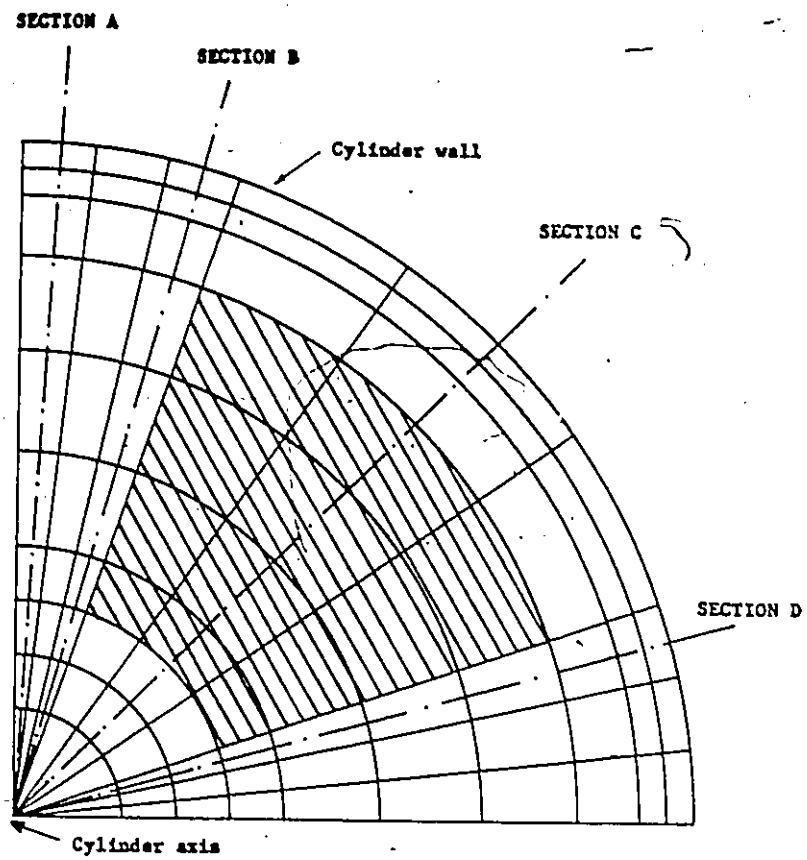

Figure 6.3 Computational grid used in the 3D computations for the plane perpendicular to the cylinder axis.

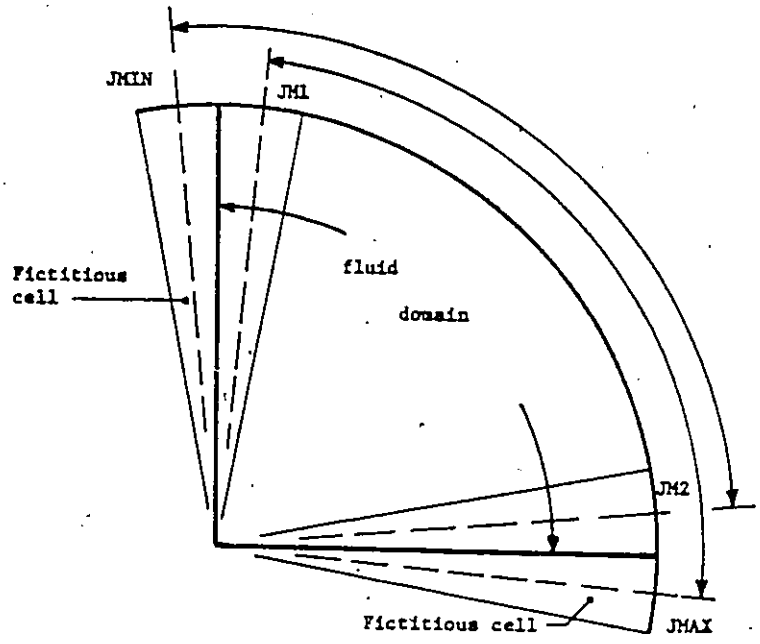

Figure 6.4 Symmetry boundary conditions.

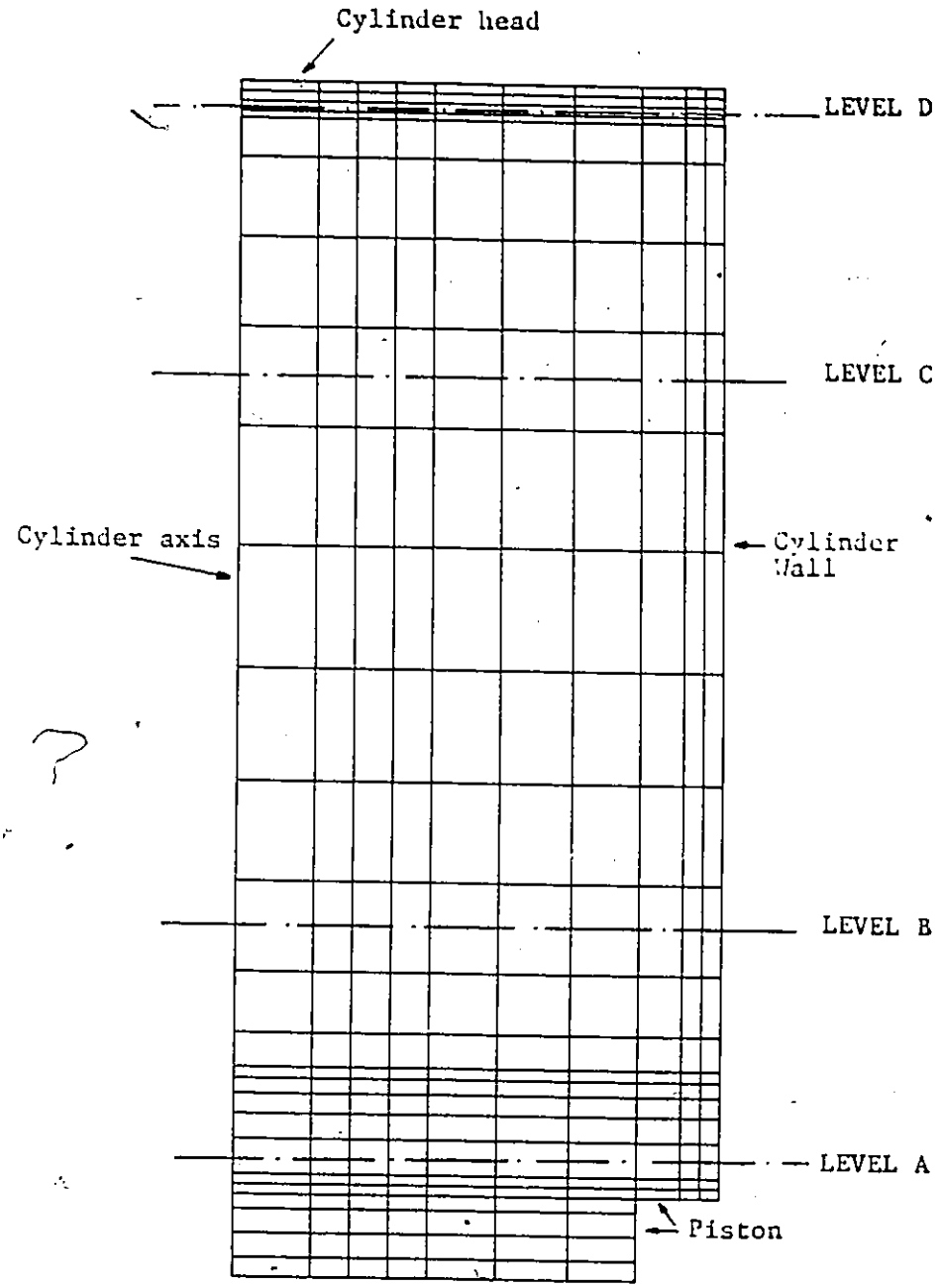

Figure 6.5 Computational grid used in the 3D computations for the plane containing the cylinder axis.

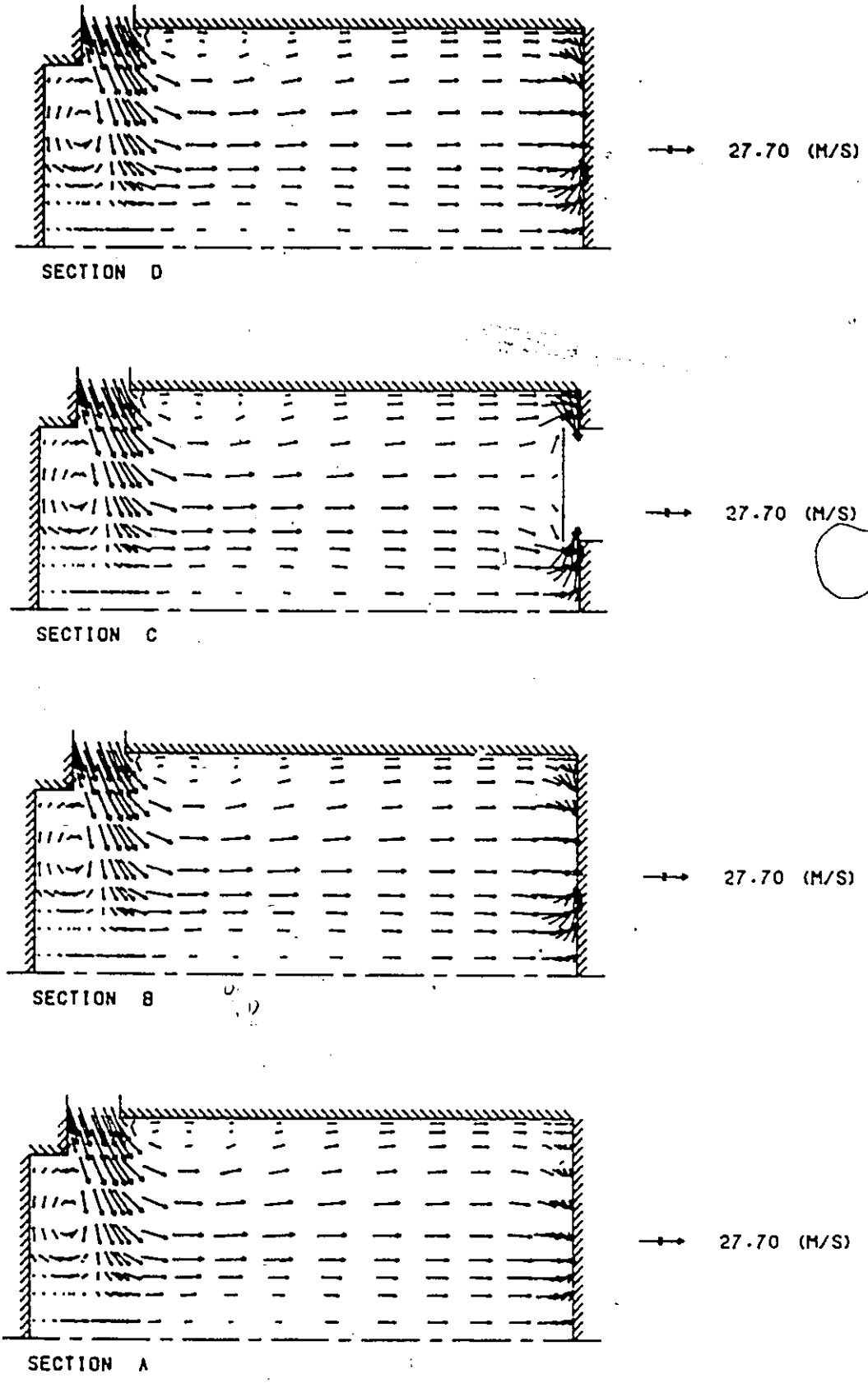

Figure 6.6 Velocity patterns computed using the 3D code at different cylinder sections at 161 crank angle degrees.

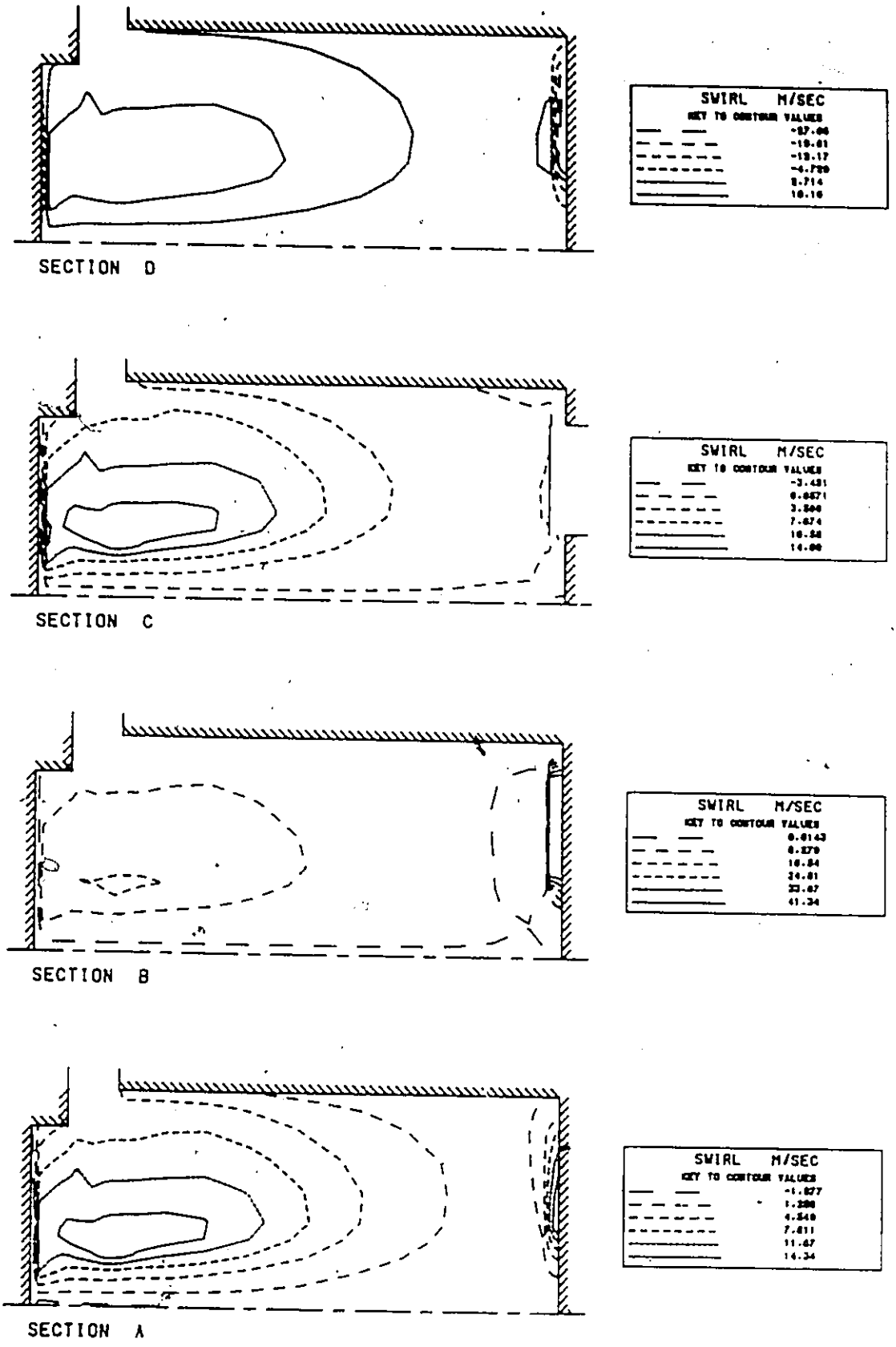

Figure 6.7 Swirl velocity contours computed using the 3D code at different cylinder sections at 161 crank angle degrees.

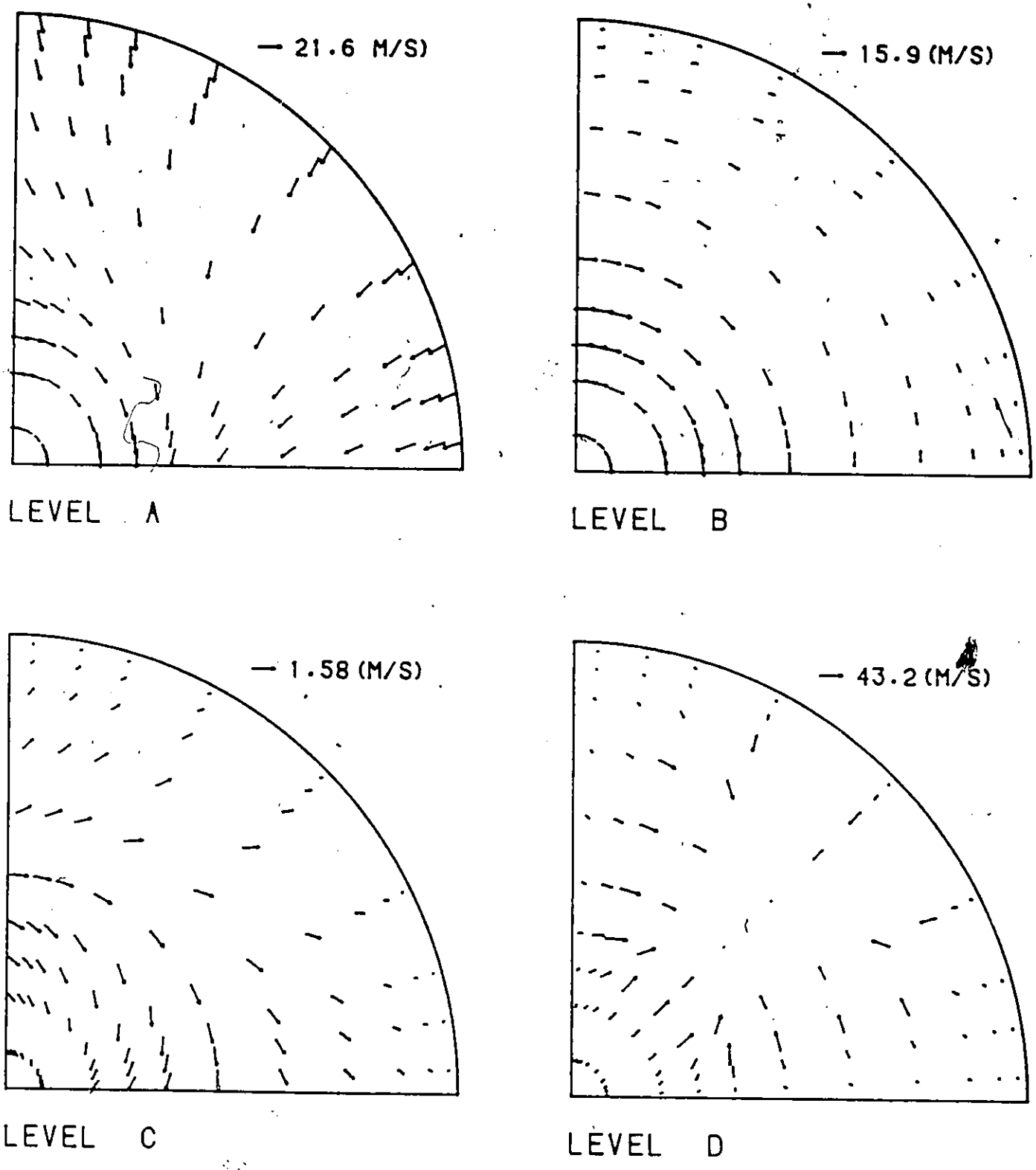

Figure 6.8 Velocity patterns computed using the 3D code at different cylinder levels at 161 crank angle degrees.

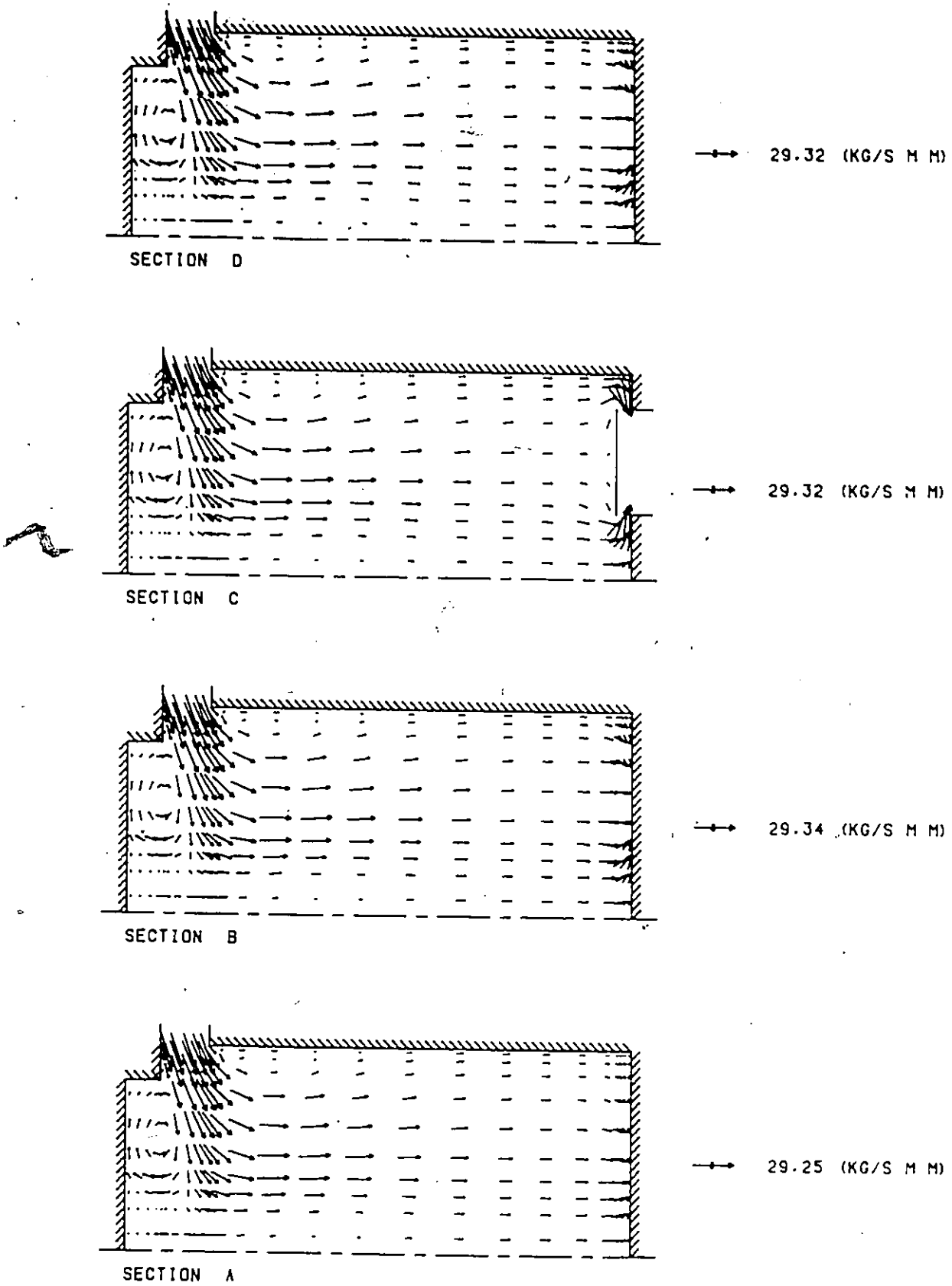

Figure 6.9 Mass flux patterns computed using the 3D code at different cylinder sections at 161 crank angle degrees.

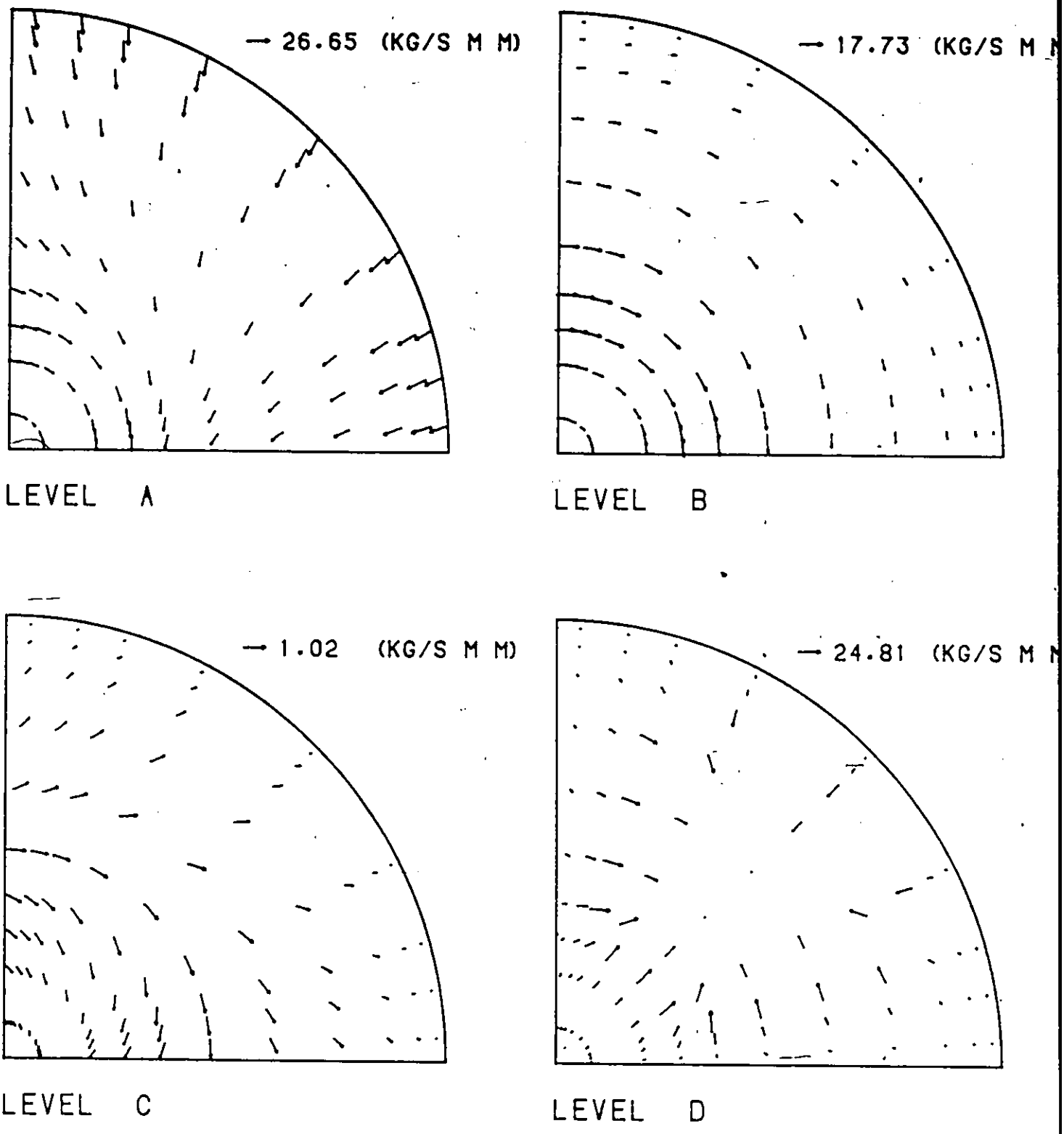

Figure 6.10 Mass flux patterns computed using the 3D code at different cylinder levels at 161 crank angle degrees.

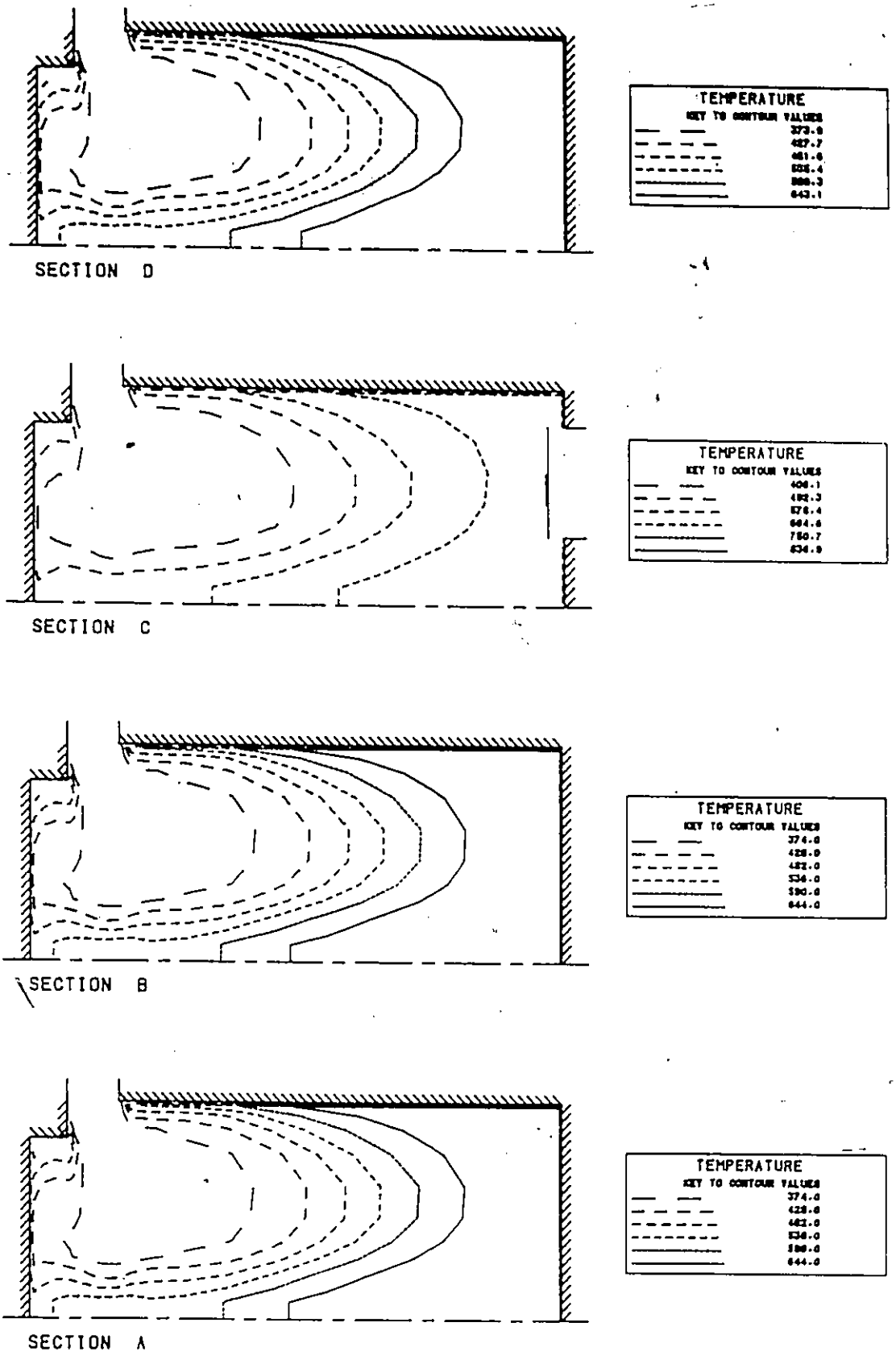

Figure 6.11 Temperature contours computed using the 3D code at different cylinder levels at 161 crank angle degrees.

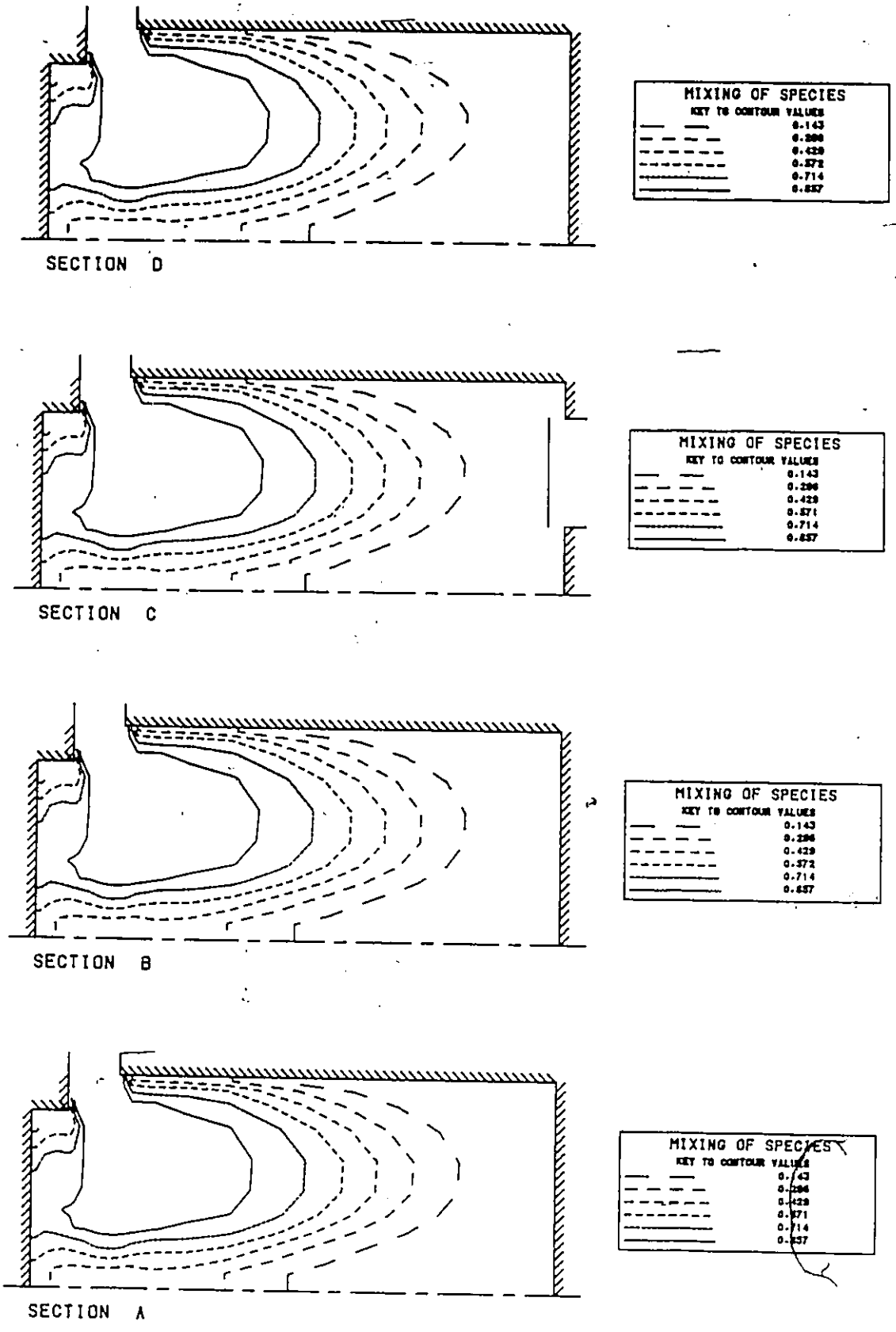

Figure 6.12 Concentration contours computed using the 3D code at different cylinder levels at 161 crank angle degrees.

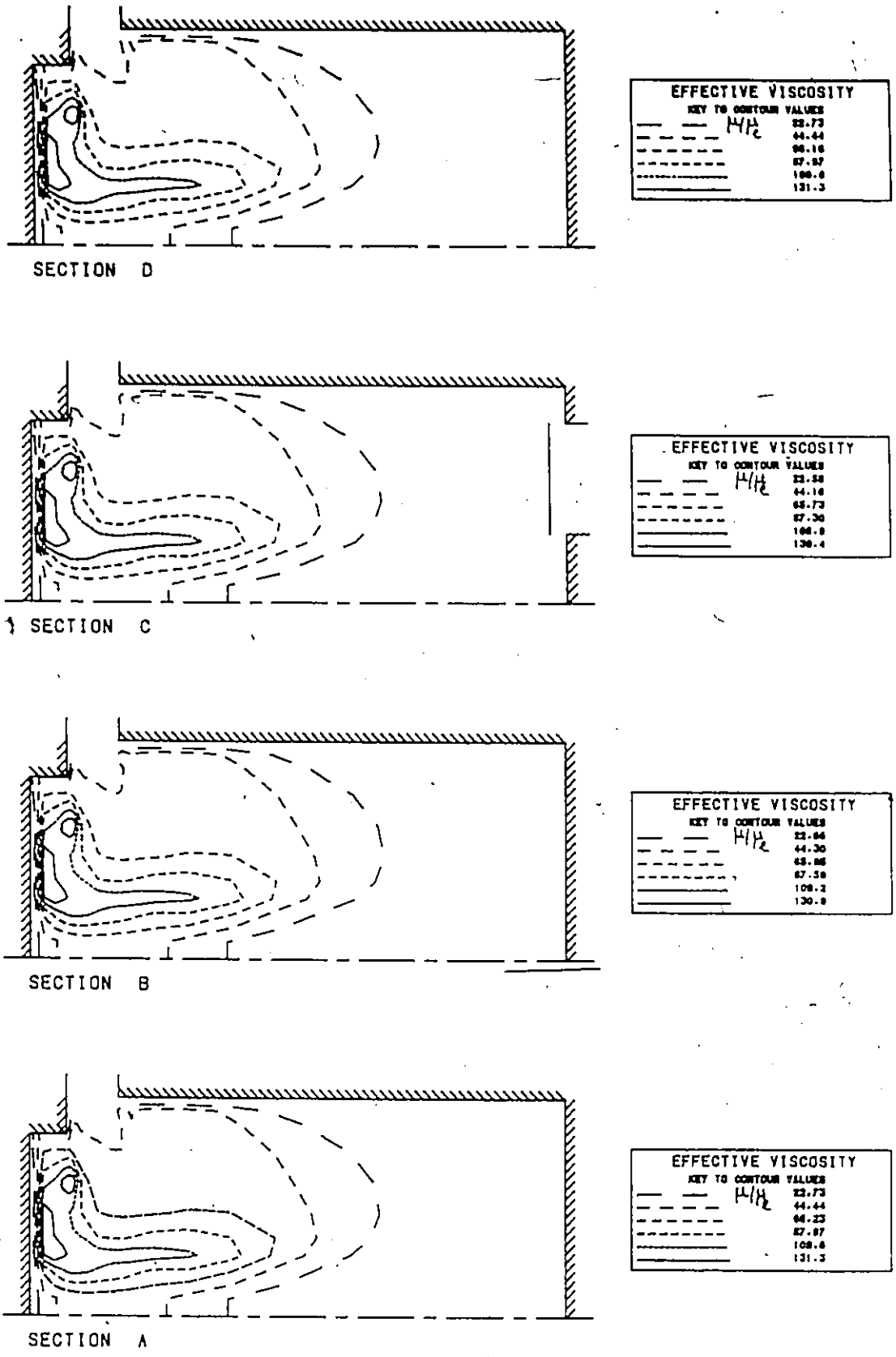

Figure 6.13 Effective viscosity contours computed using the 3D code at different cylinder levels at 161 crank angle degrees.

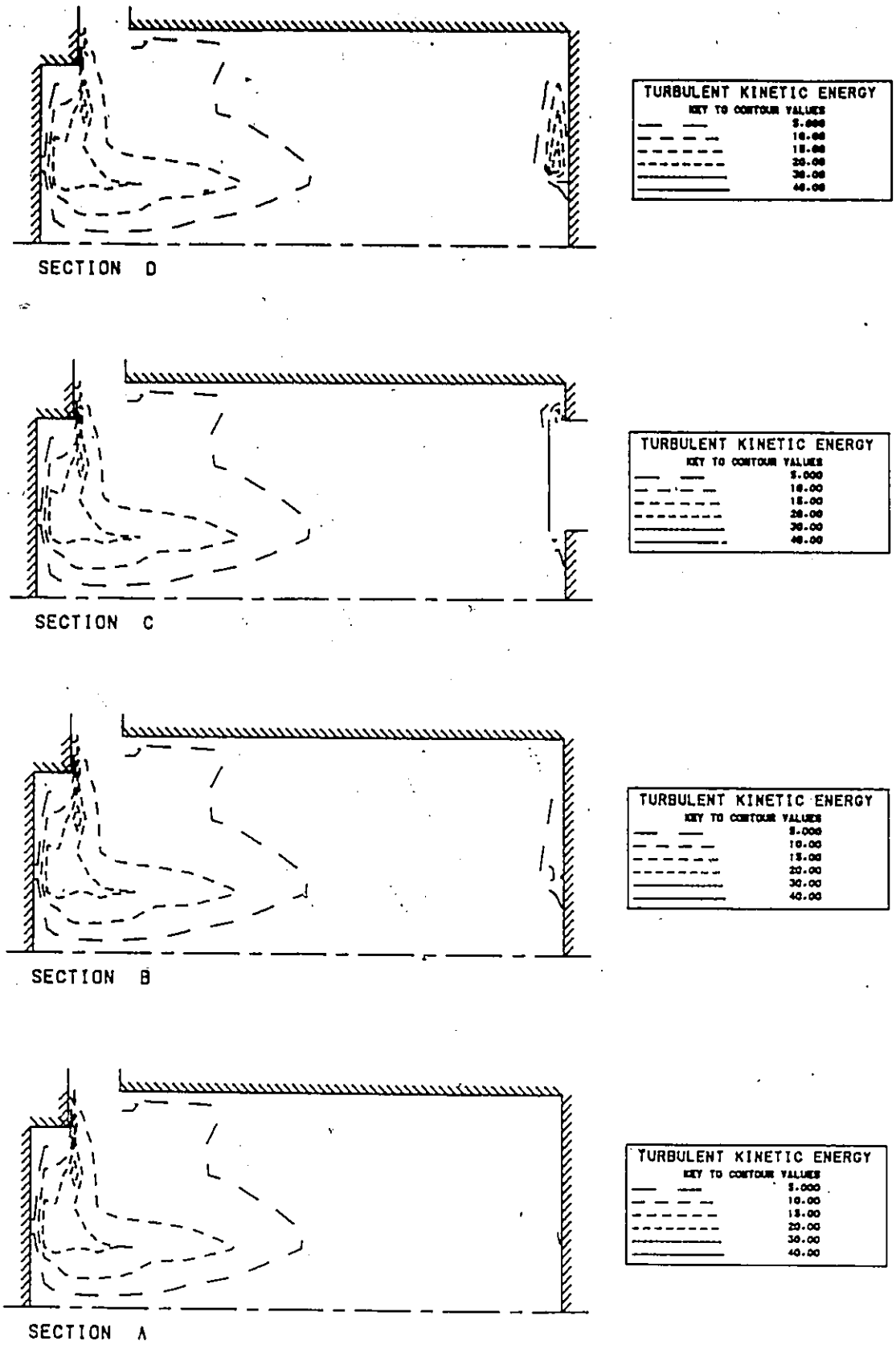

Figure 6.14 Turbulence kinetic energy contours computed using the 3D code at different cylinder levels at 161 crank angle degrees.

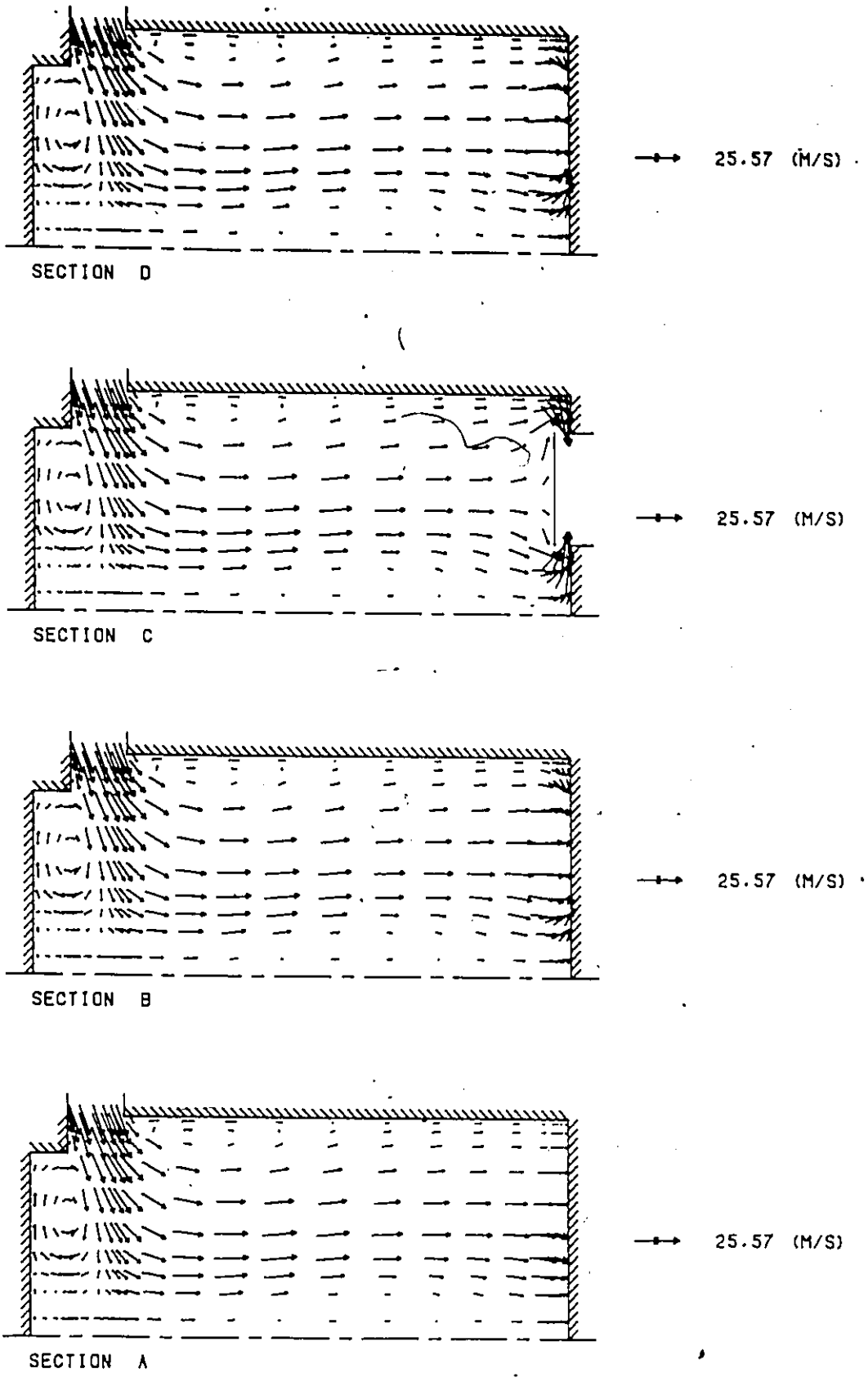

Figure 6.15 Velocity patterns computed using the 3D code at different cylinder sections at 178 crank angle degrees.

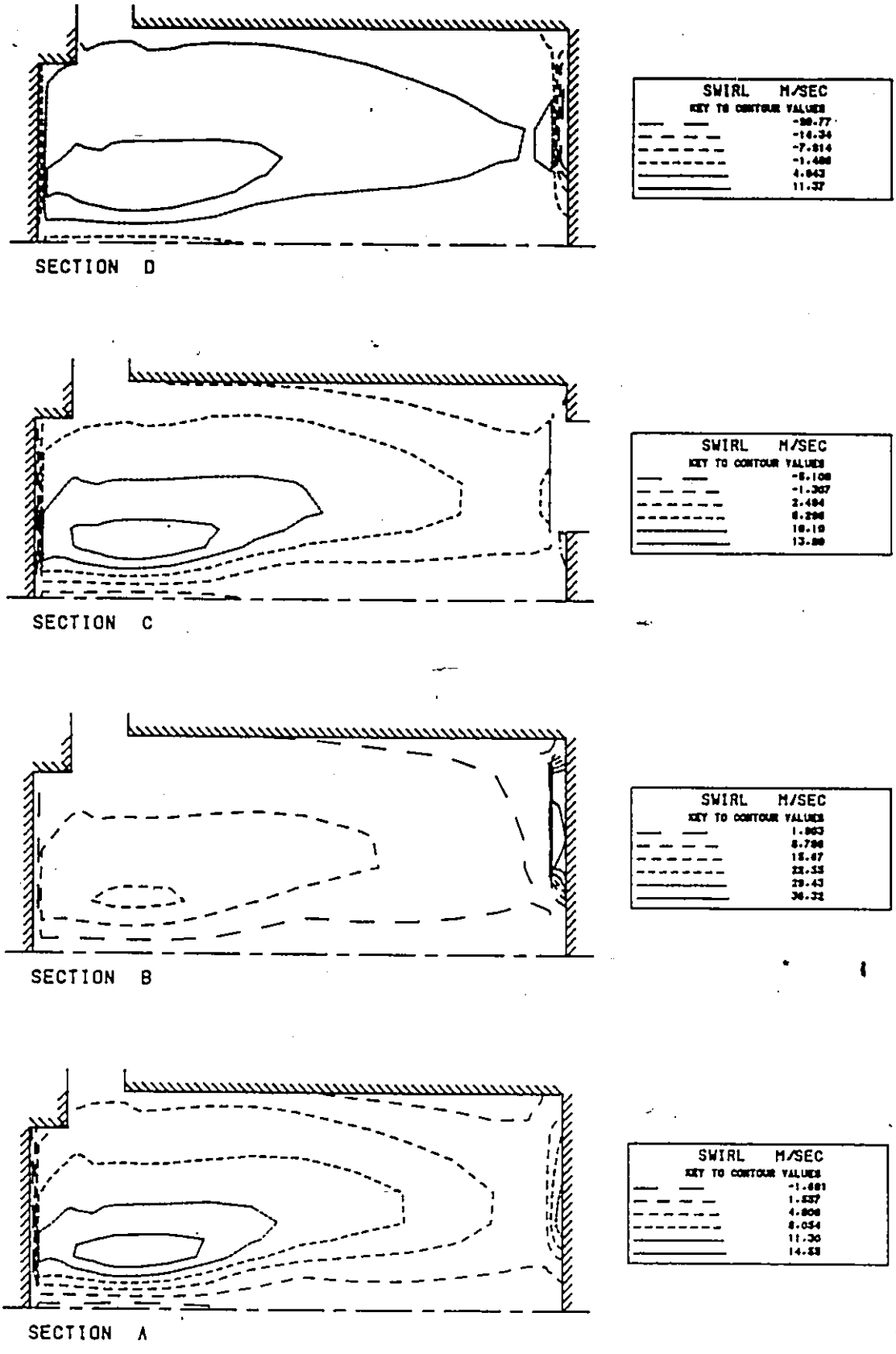

Figure 6.16 Swirl velocity contours computed using the 3D code at different cylinder sections at 178 crank angle degrees.

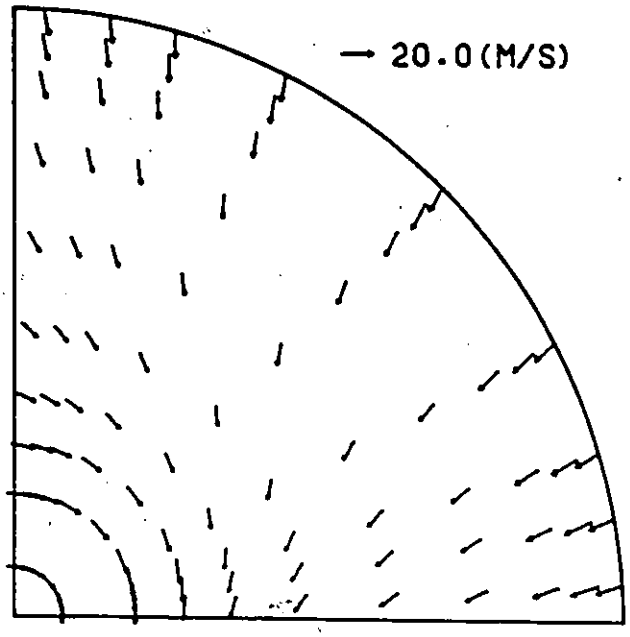

LEVEL A

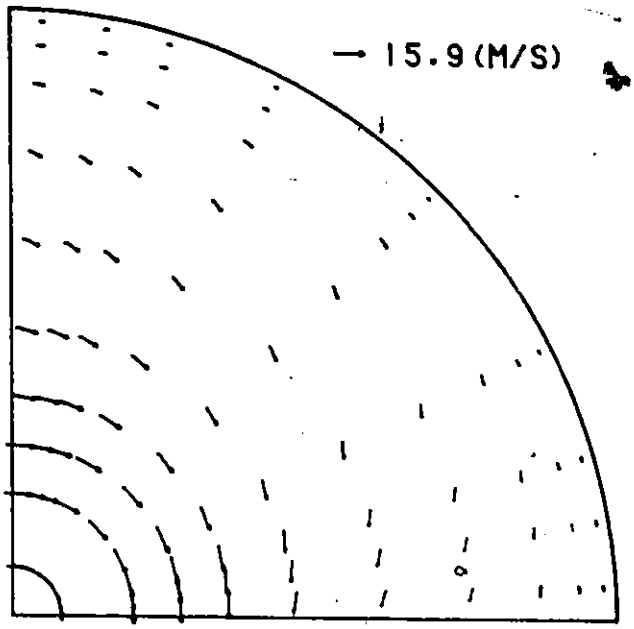

LEVEL B

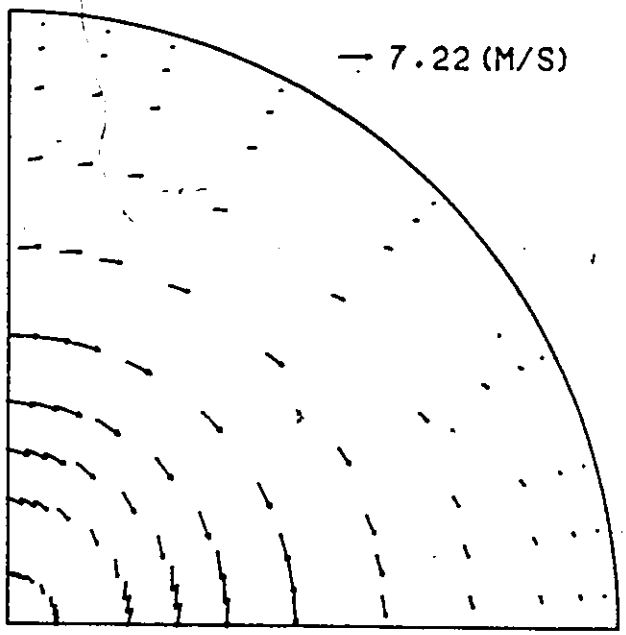

LEVEL C

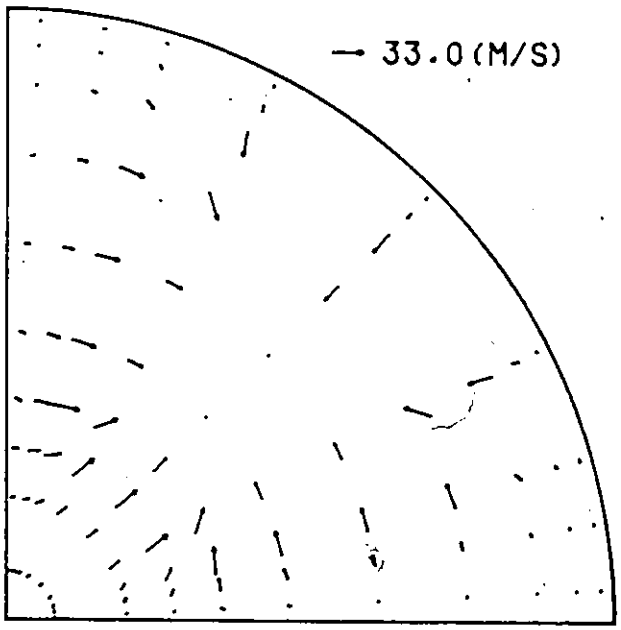

LEVEL D

Figure 6.17 Velocity patterns computed using the 3D code at different cylinder levels at 178 crank angle degrees.

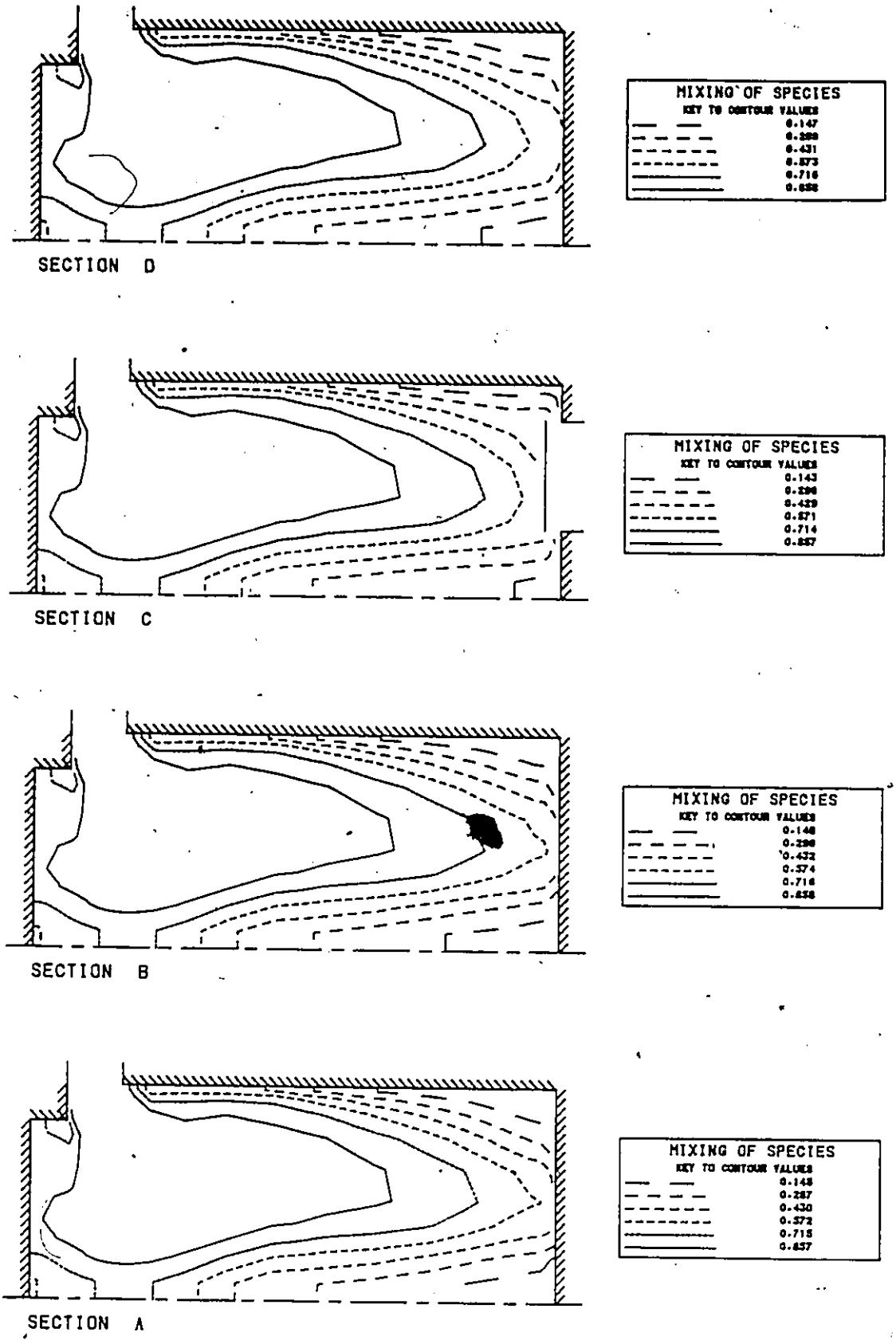

Figure 6.18 Concentration contours computed using the 3D code at different cylinder levels at 178 crank angle degrees.

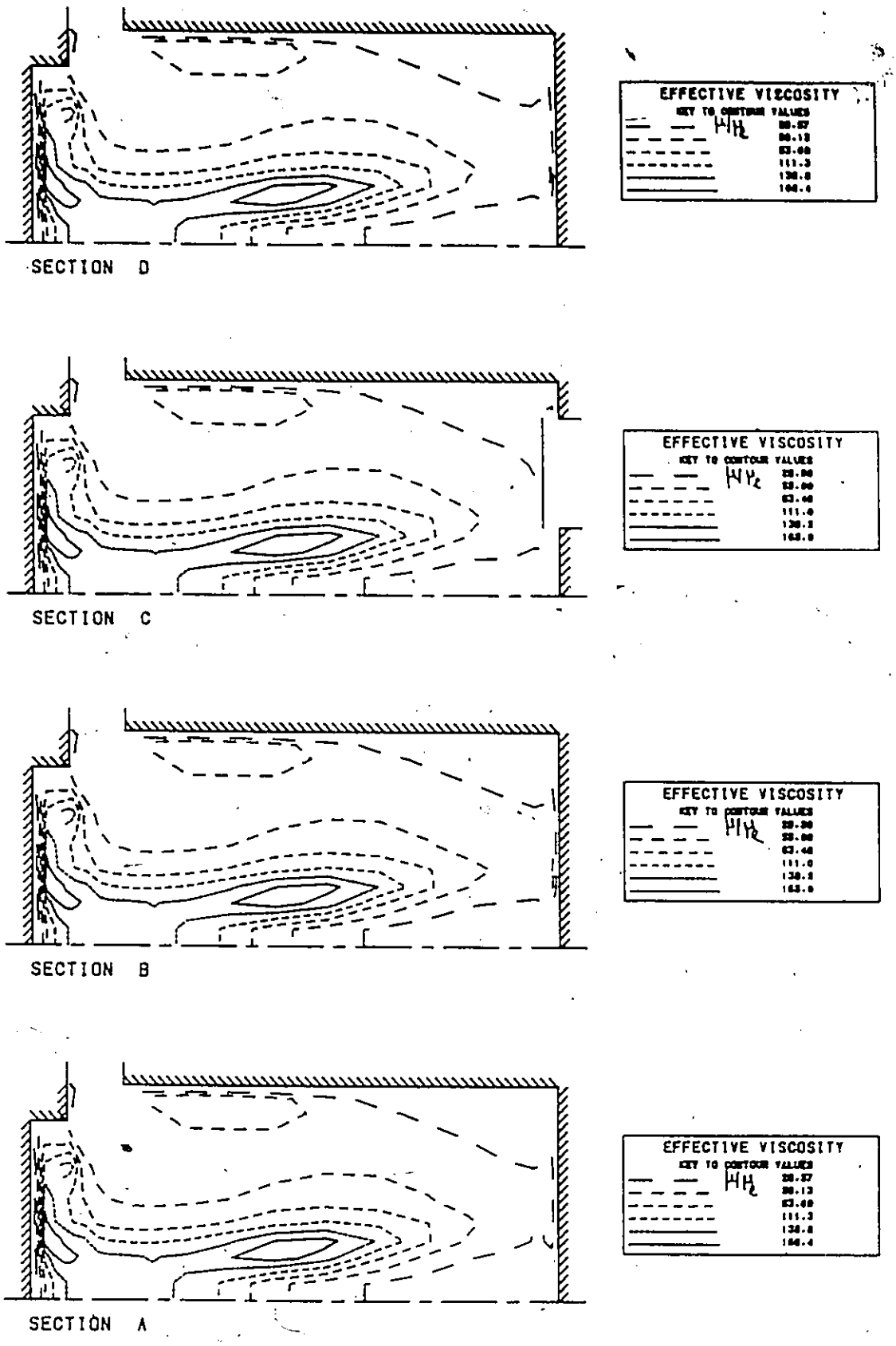

Figure 6.19 Effective viscosity contours computed using the 3D code at different cylinder levels at 178 crank angle degrees.

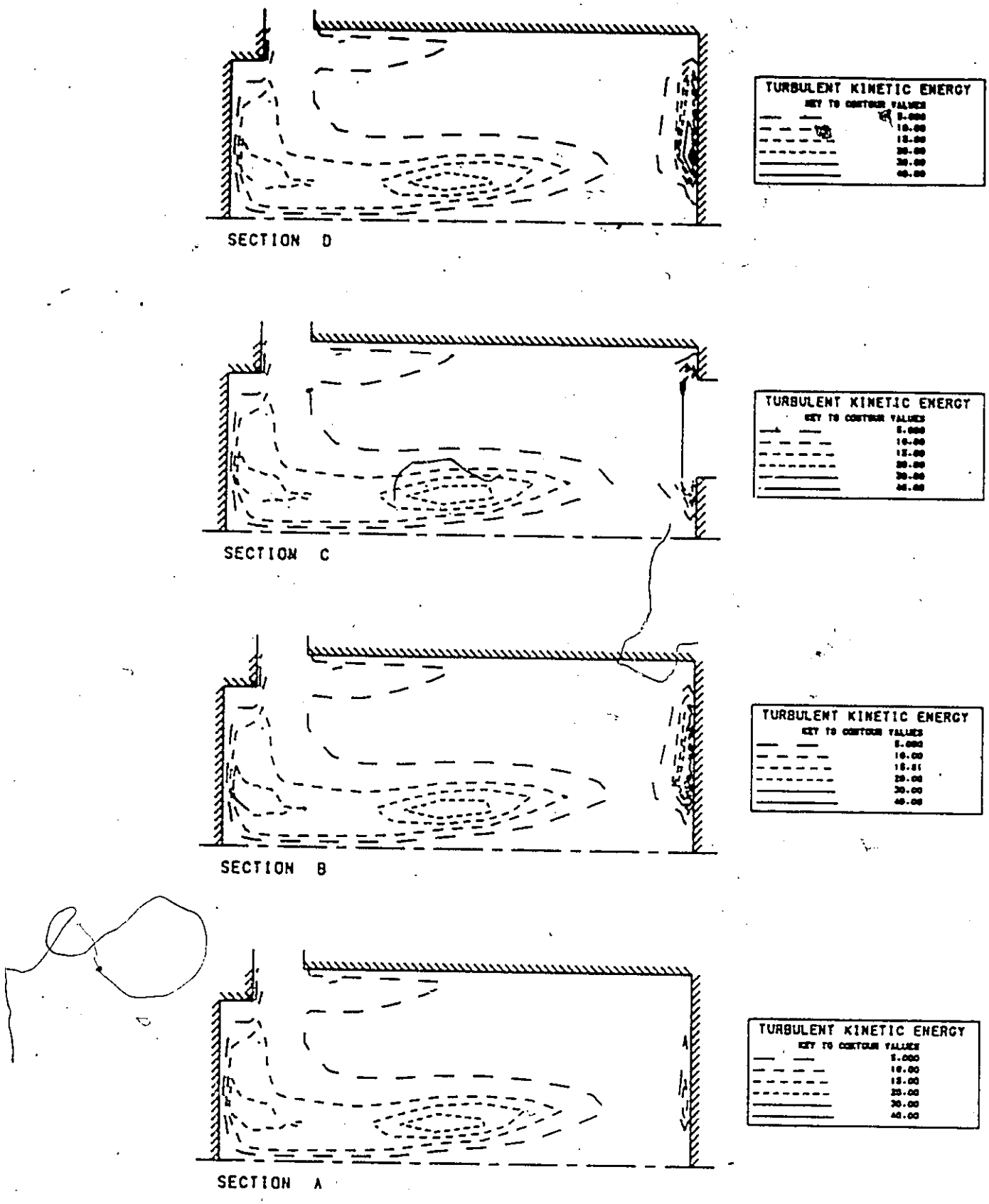

Figure 6.20 Turbulence kinetic energy contours computed using the 3D code at different cylinder levels at 178 crank angle degrees.

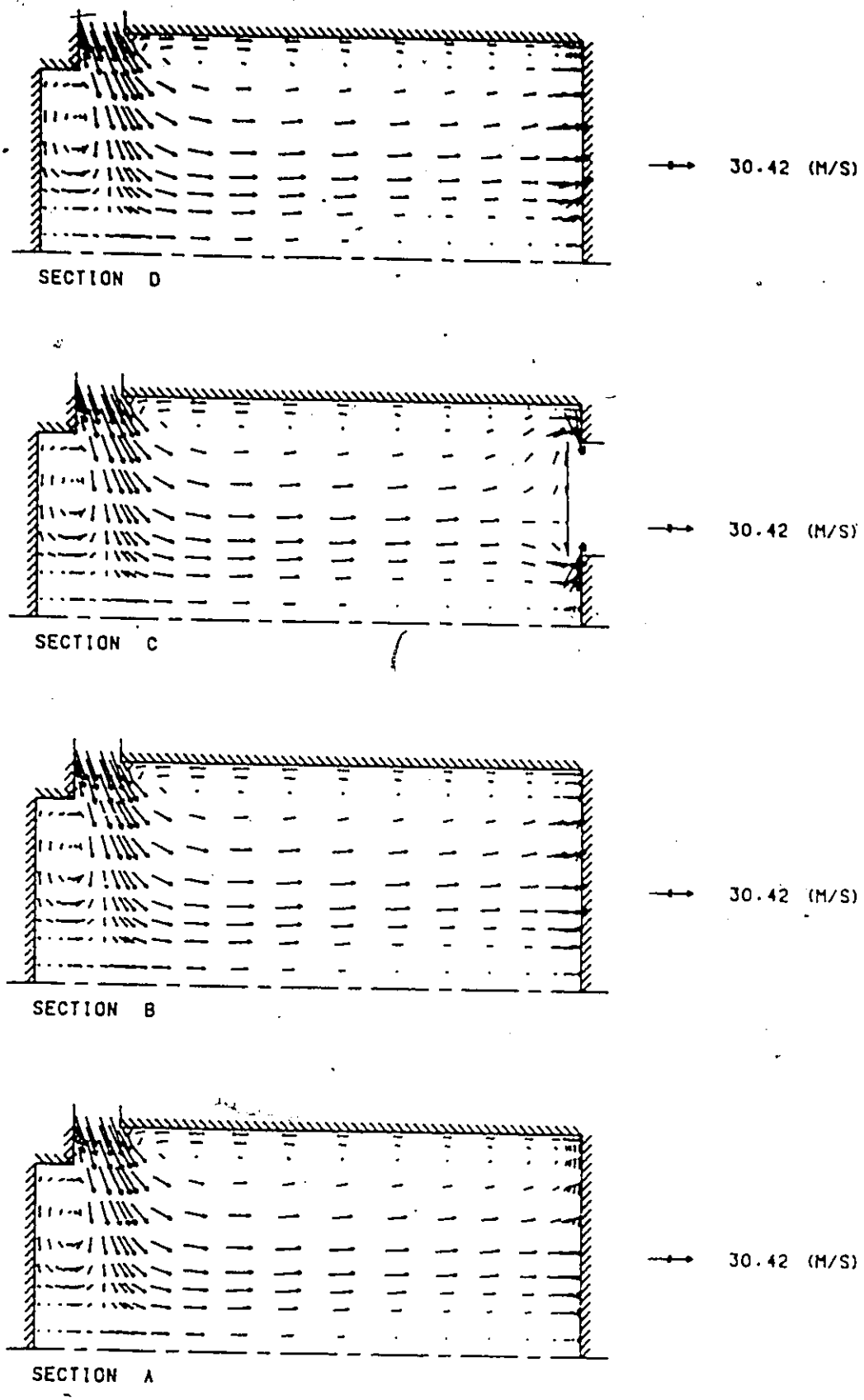

Figure 6.21 Velocity patterns computed using the 3D code at different cylinder sections at 205 crank angle degrees.

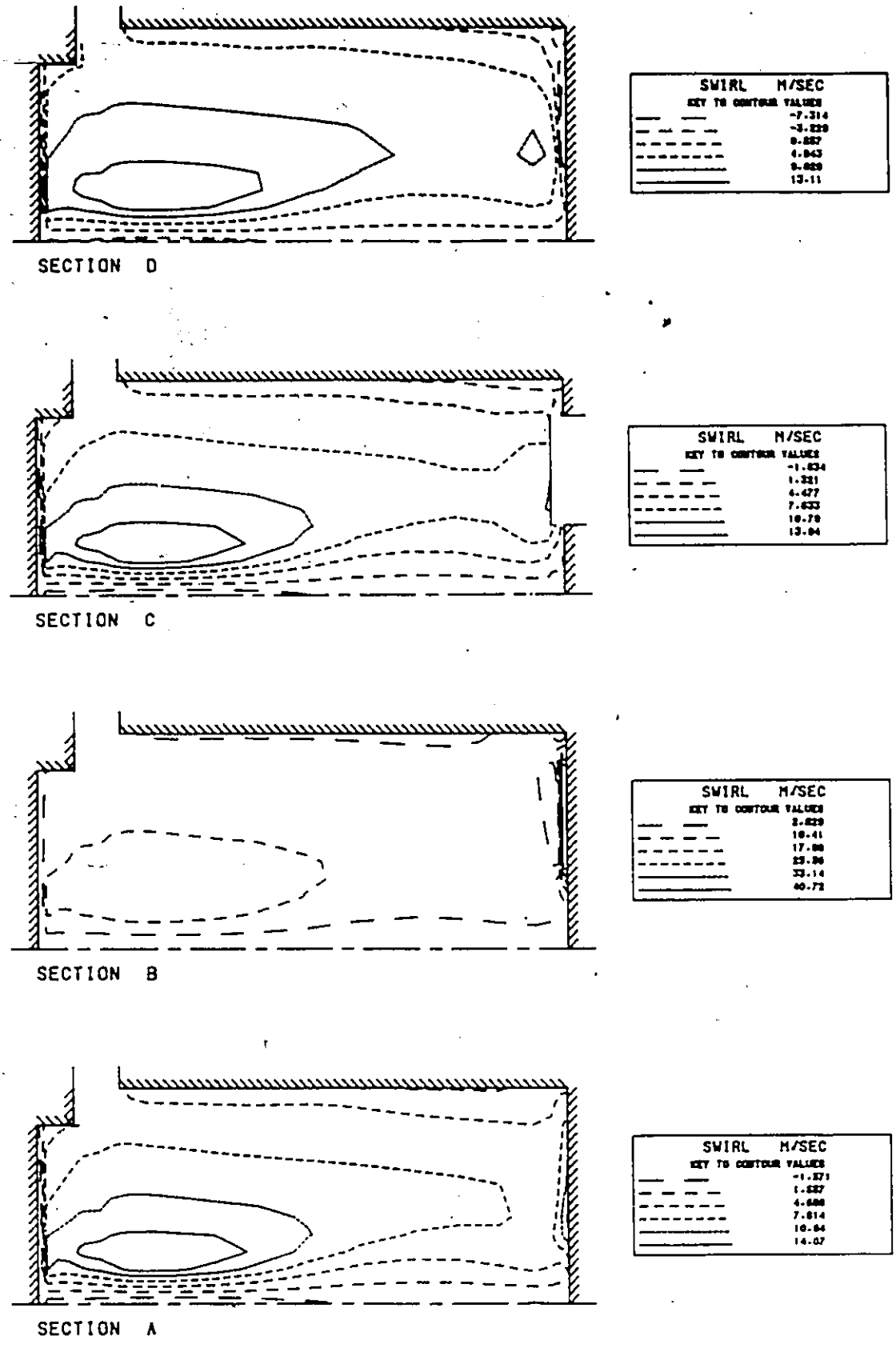

Figure 6.22 Swirl velocity contours computed using the 3D code at different cylinder sections at 205 crank angle degrees.

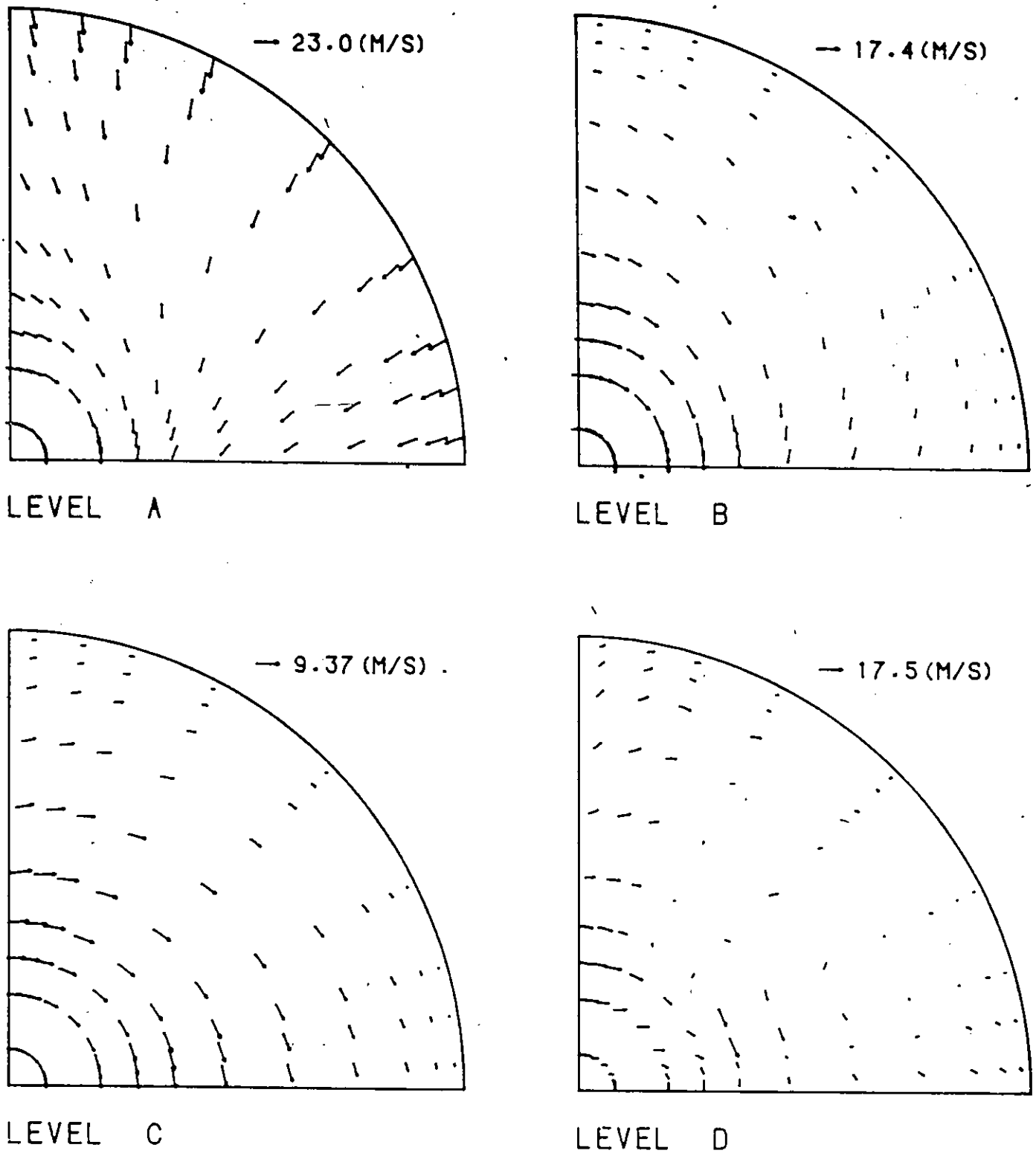

Figure 6.23 Velocity patterns computed using the 3D code at different cylinder levels at 205 crank angle degrees.

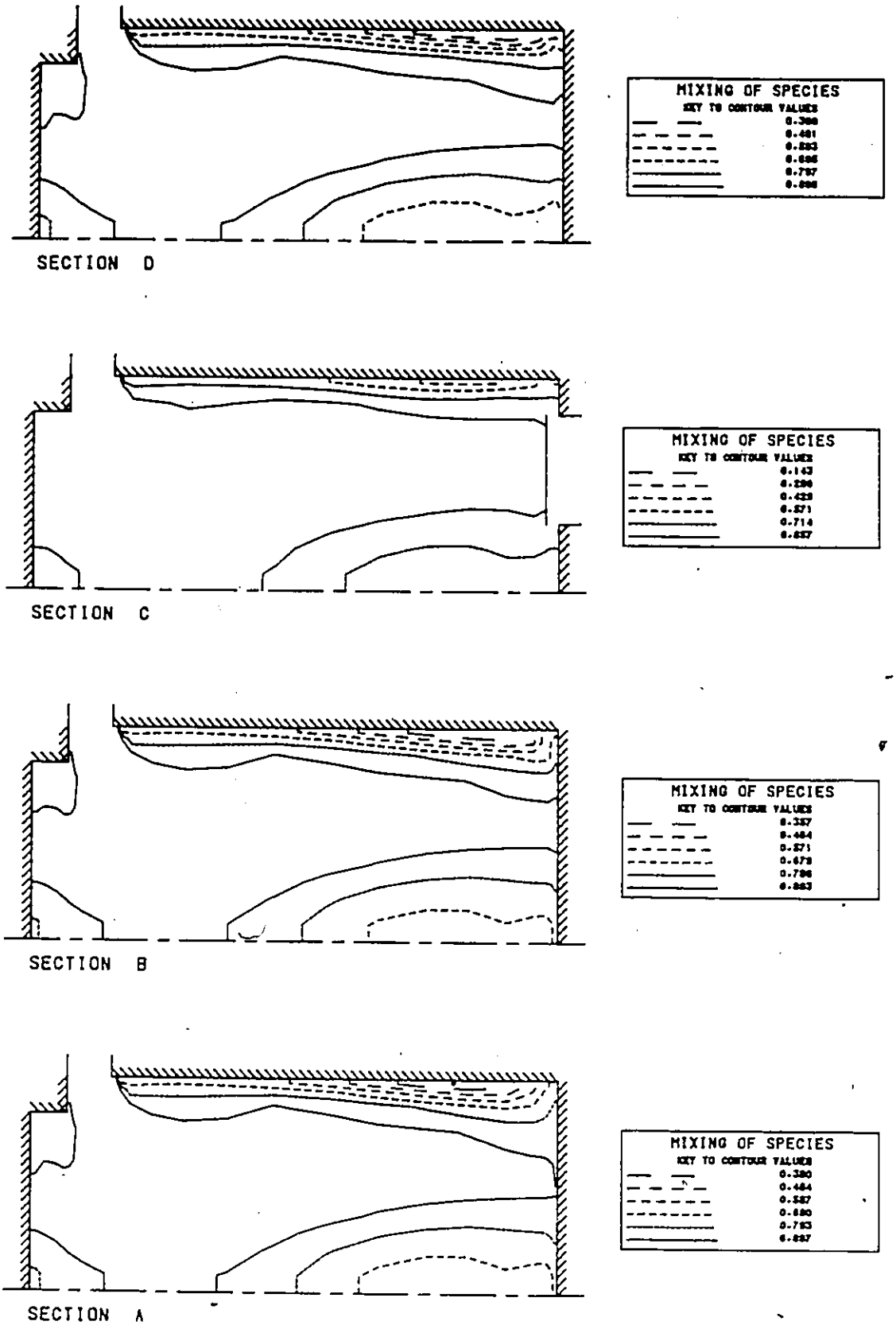

Figure 6.24 Concentration contours computed using the 3D code at different cylinder levels at 205 crank angle degrees.

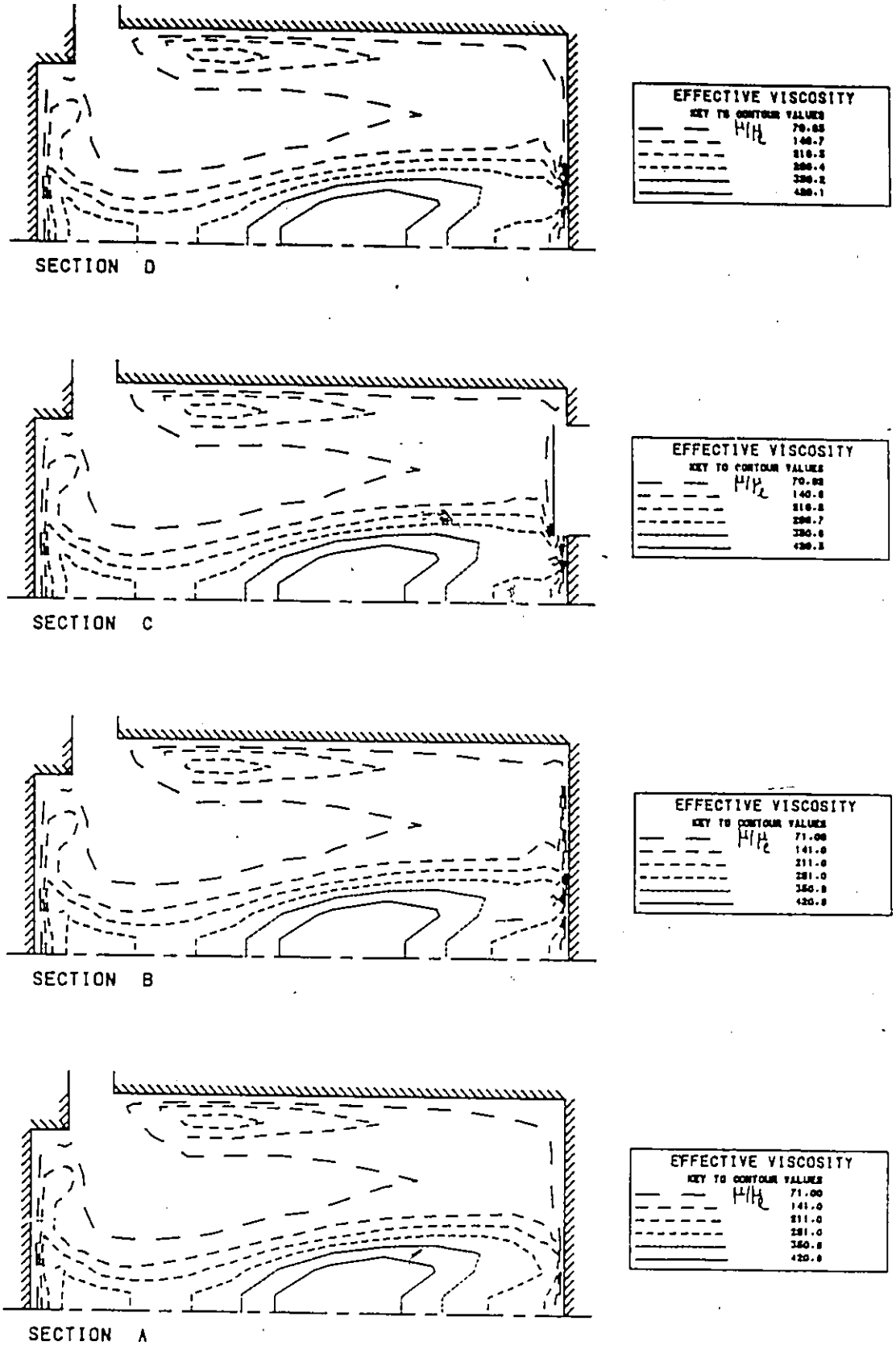

Figure 6.25 Effective viscosity contours computed using the 3D code at different cylinder levels at 205 crank angle degrees.

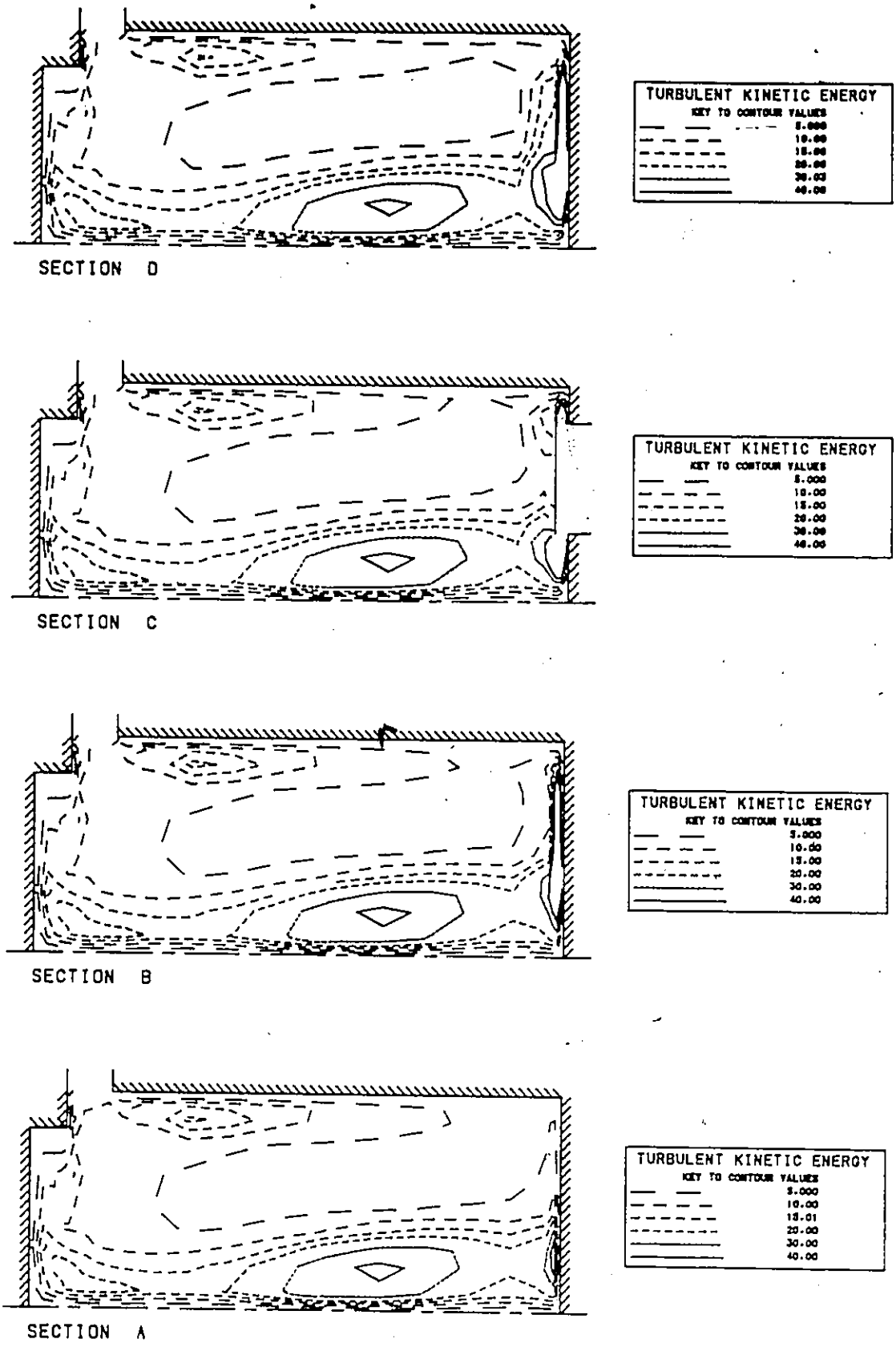

Figure 6.26 Turbulence kinetic energy contours computed using the 3D code at different cylinder levels at 205 crank angle degrees.

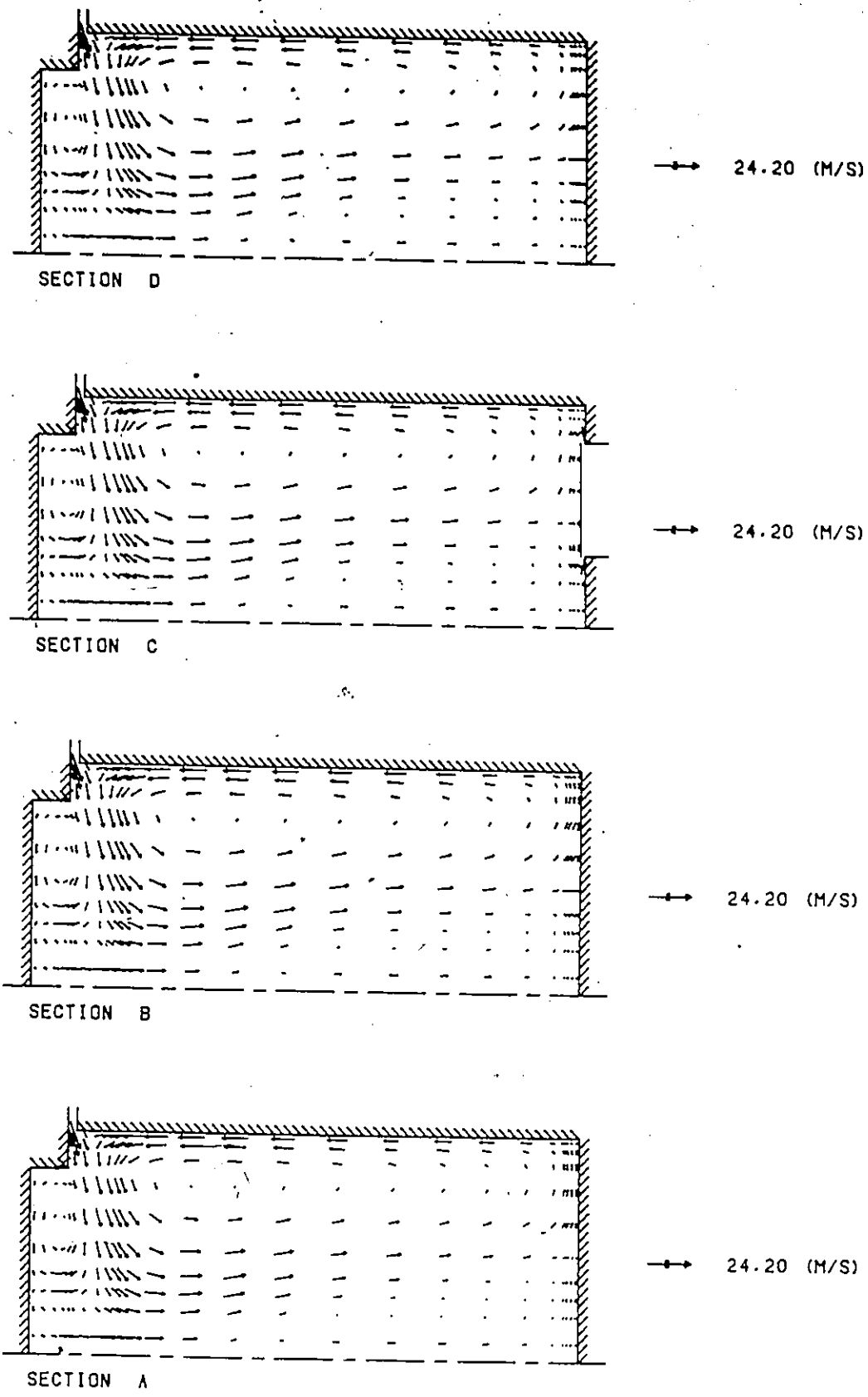

Figure 6.27 Velocity patterns computed using the 3D code at different cylinder sections at 232 crank angle degrees.

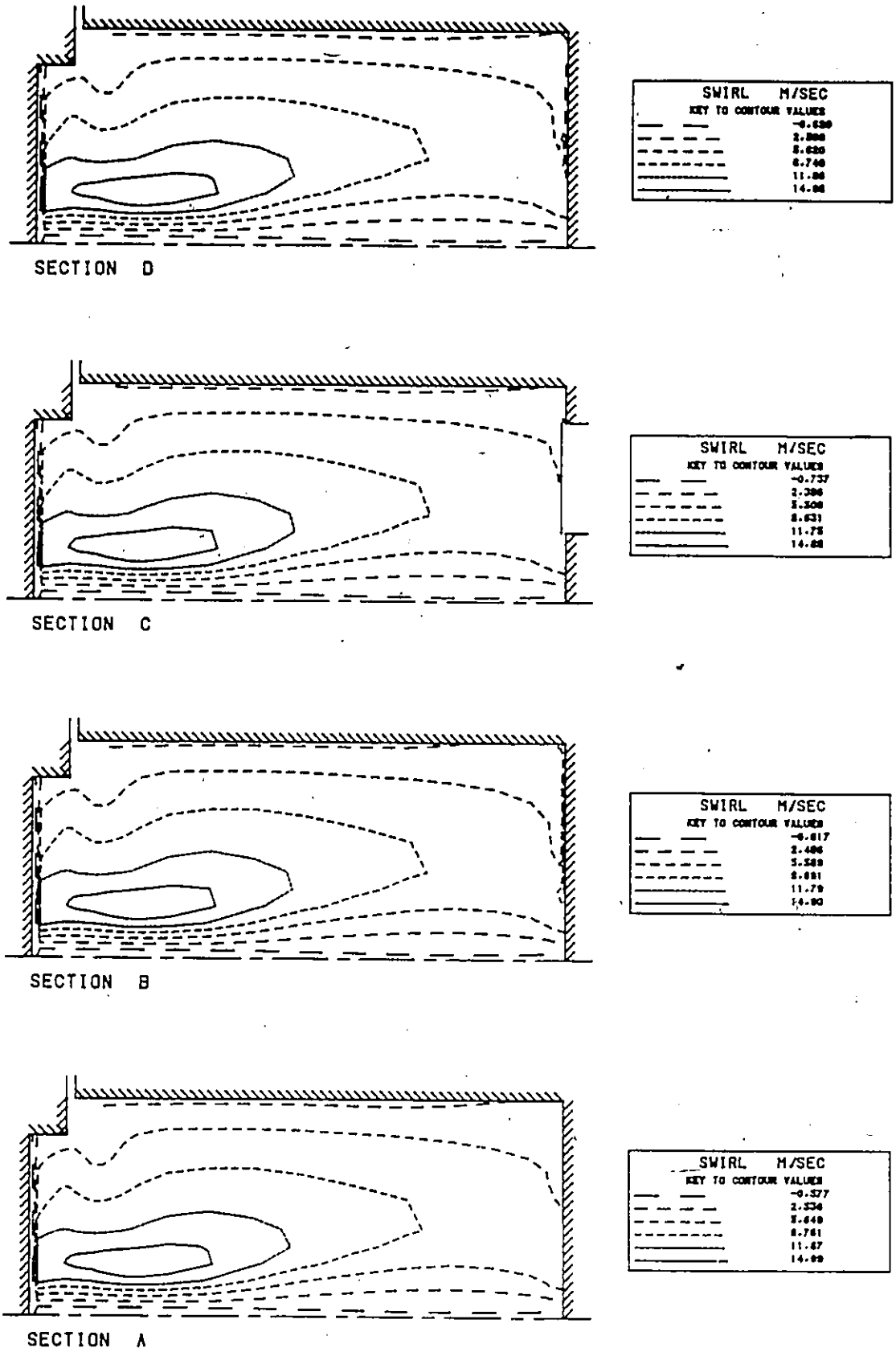

Figure 6.28 Swirl velocity contours computed using the 3D code at different cylinder sections at 232 crank angle degrees.

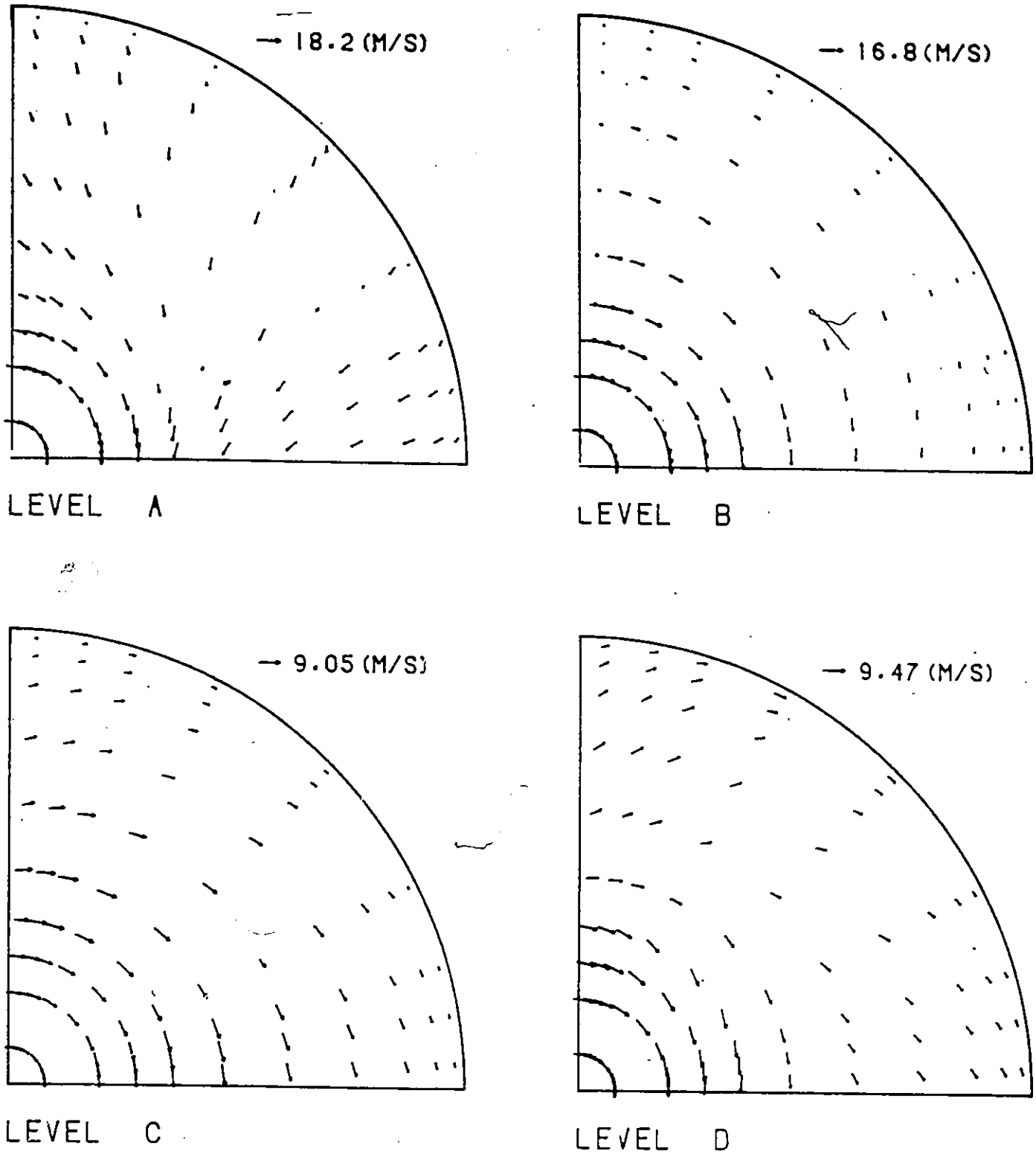

Figure 6.29 Velocity patterns computed using the 3D code at different cylinder levels at 232 crank angle degrees.

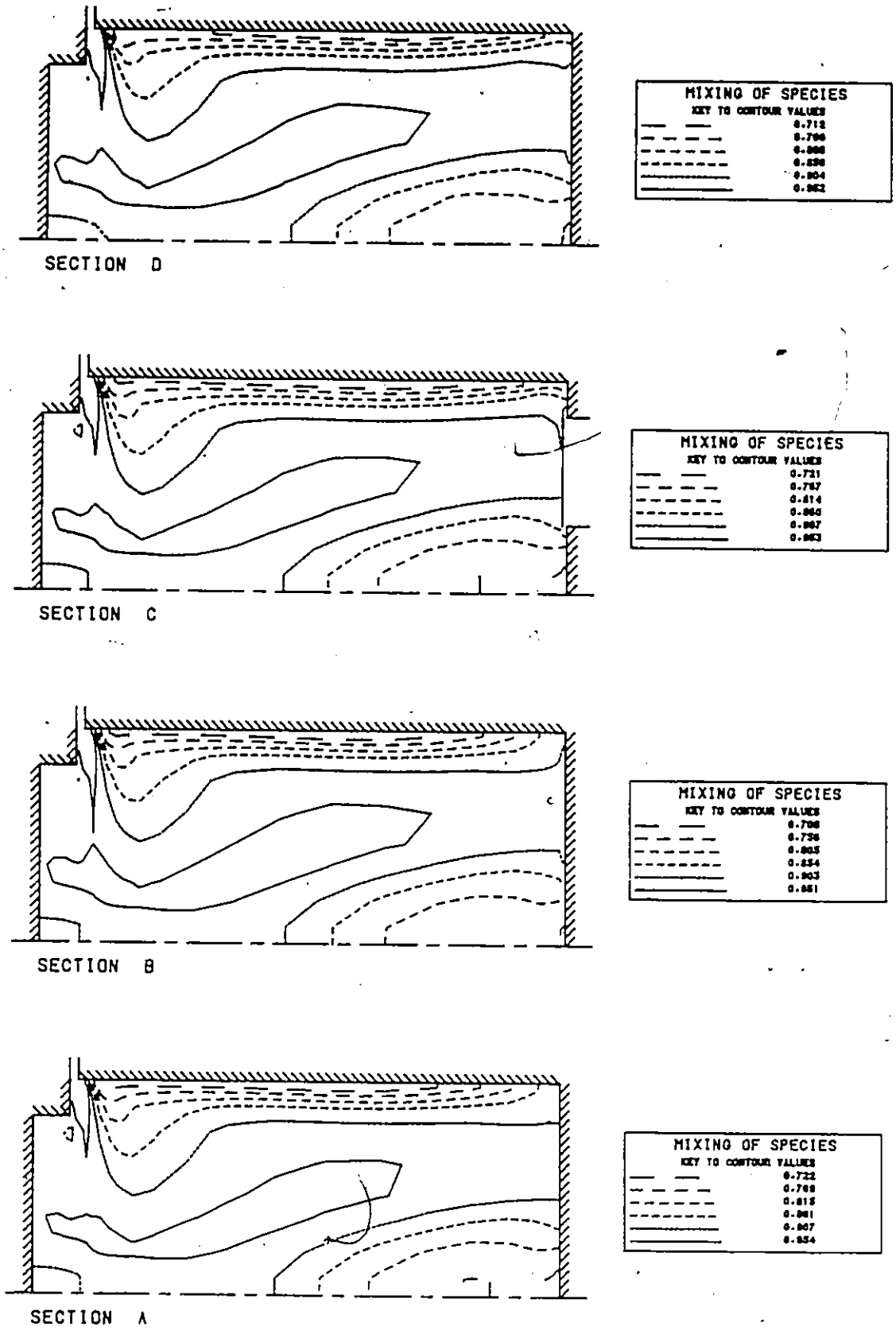

Figure 6.30 Concentration contours computed using the 3D code at different cylinder levels at 232 crank angle degrees.

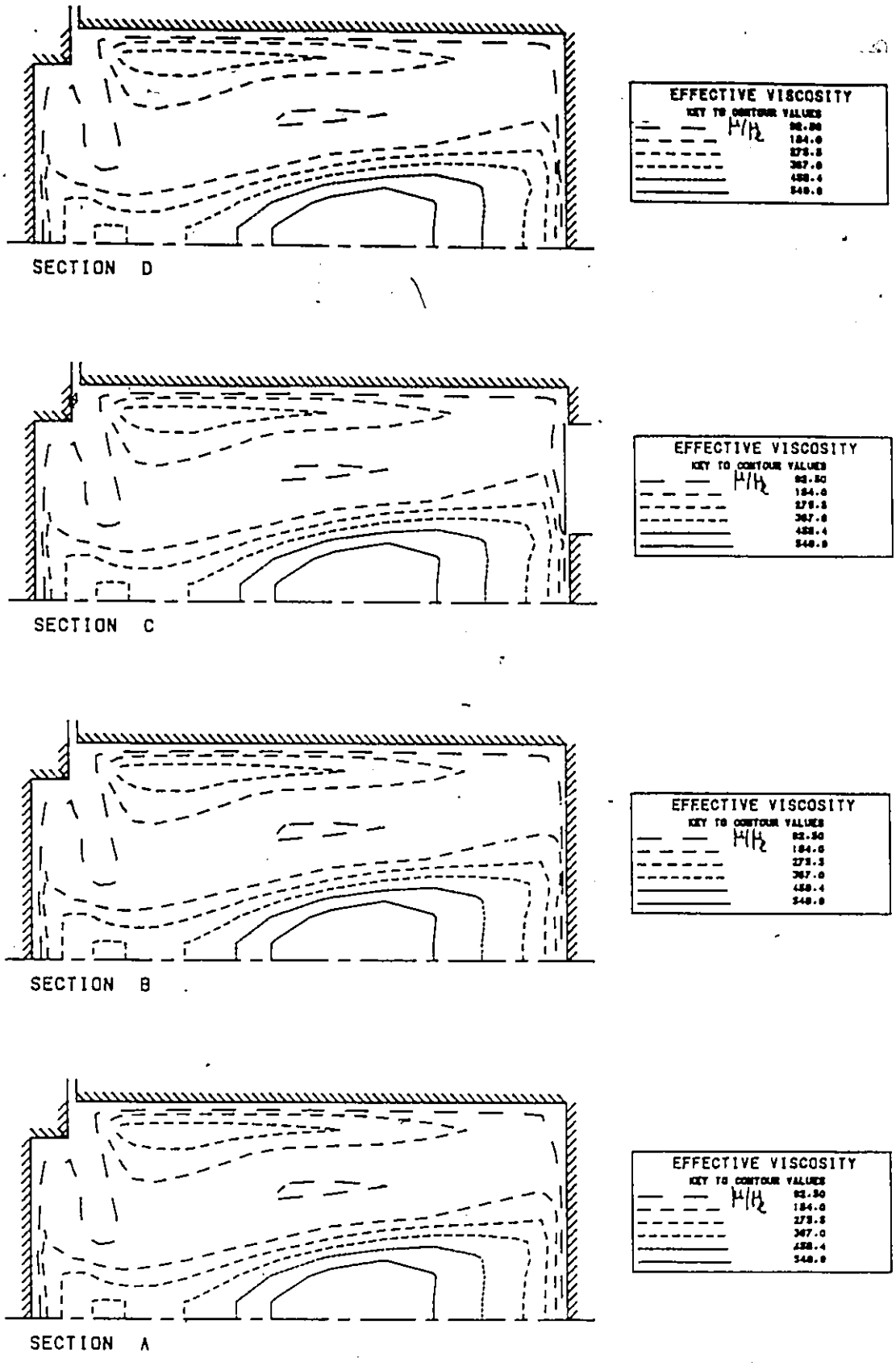

Figure 6.31 Effective viscosity contours computed using the 3D code at different cylinder levels at 232 crank angle degrees.

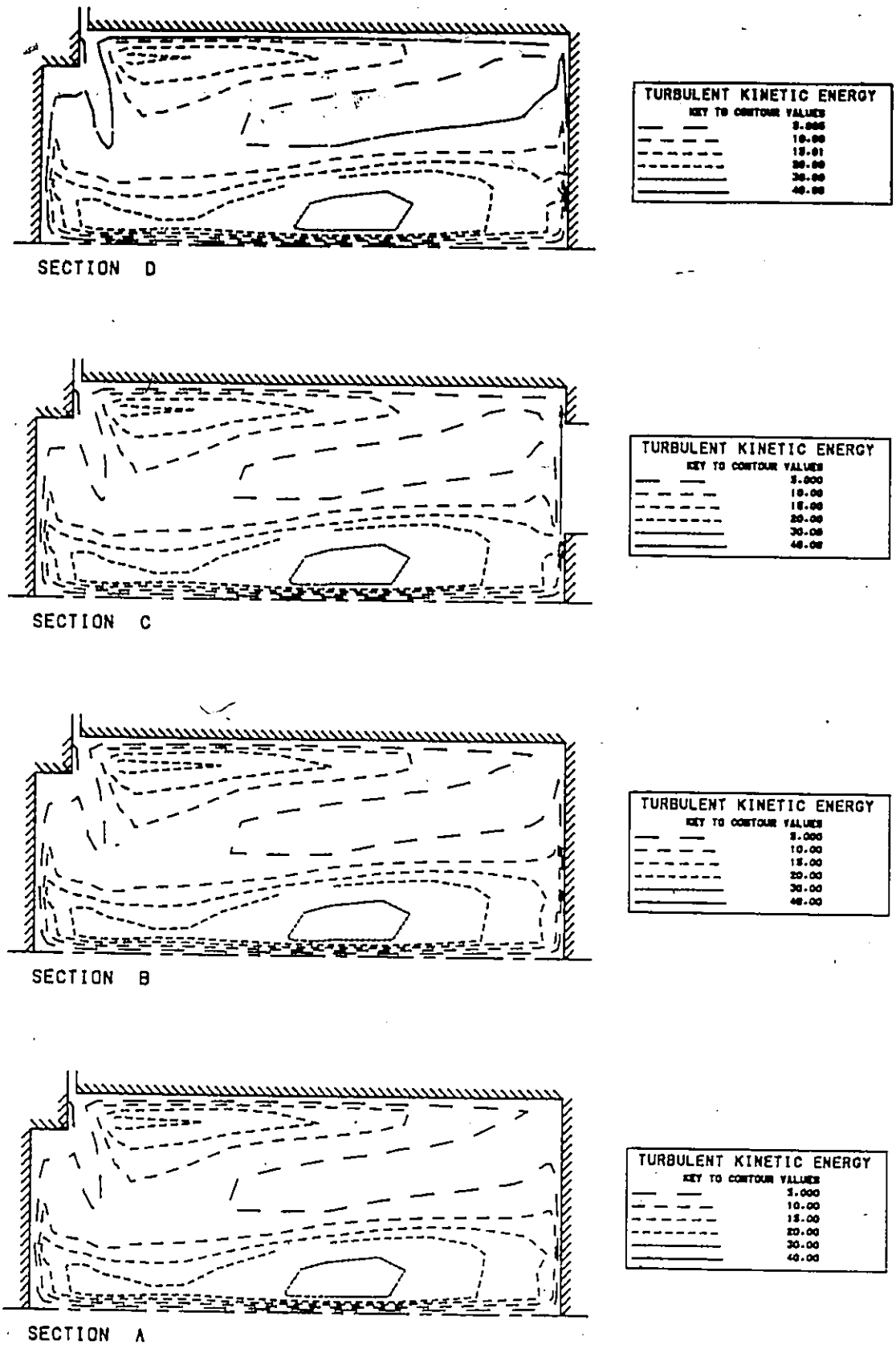

Figure 6.32 Turbulence kinetic energy contours computed using the 3D code at different cylinder levels at 232 crank angle degrees.

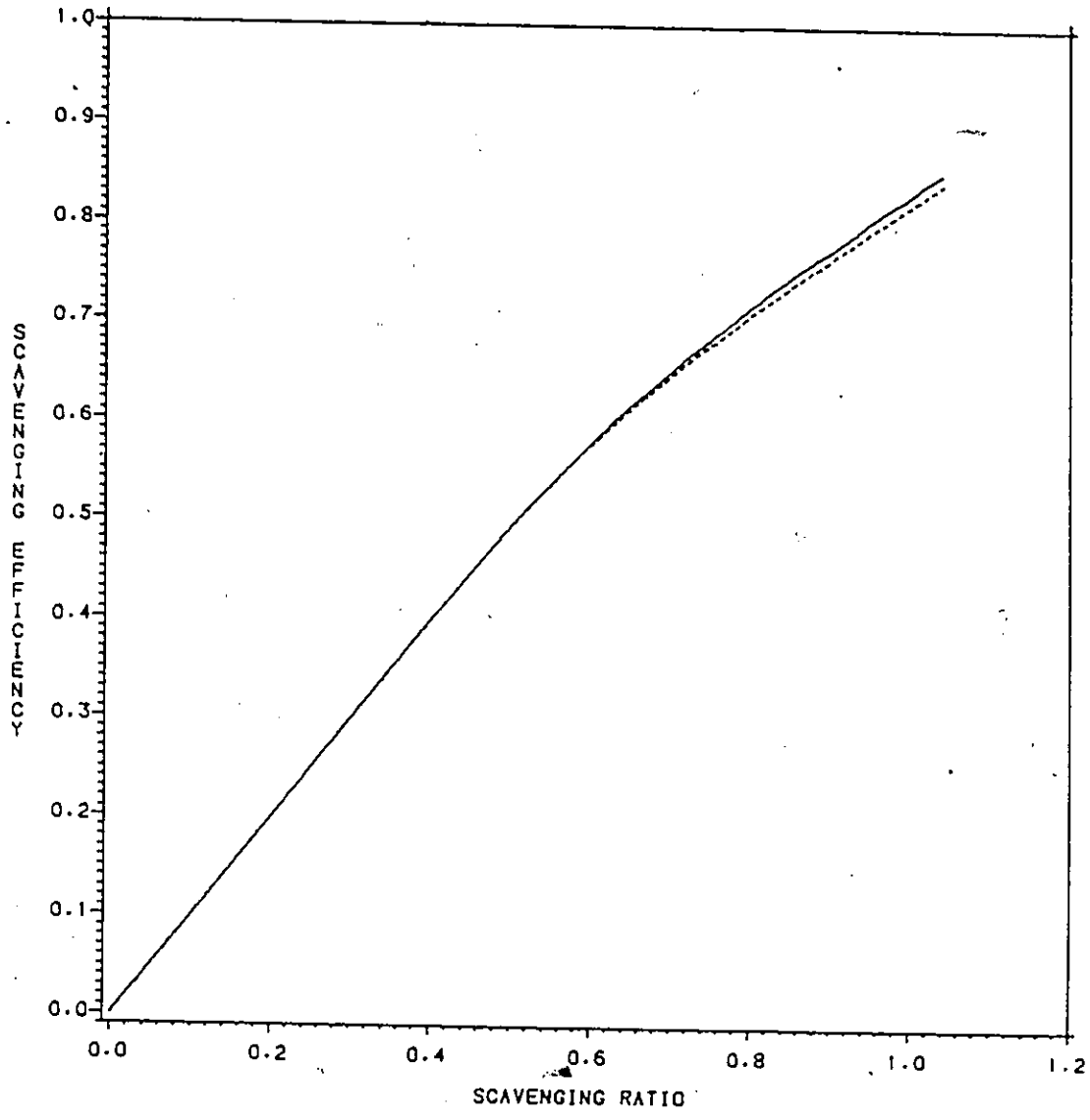

: — 2D MODEL -- : 3D MODEL

Figure 6.33 Comparison of the scavenging efficiency computed using the two and three dimensional models.

CHAPTER 7

HEAT TRANSFER CALCULATIONS

The heat transfer processes in internal combustion engines are complex and only empirical correlations based on experimental measurements are available. From the simulation point of view, the heat transfer from the cylinder gas to the cylinder walls is more important than the heat transfer from the cylinder wall to the coolant.

One of the early heat transfer models that has been proposed is by Nusselt [1] derived from experiments in a spherical bomb calorimeter. The proposed formula for the heat transfer coefficient is written as:

$$h = 0.0278(1.0 - 0.38C_m)(P^2T)^{0.33} + 1.27510^{-10}\frac{T^4 - T_w{}^4}{T - T_w} \qquad (7-1)$$

where:

C_m - is the mean piston speed in ft/s,

T_w - is the cylinder wall temperature in R,

P - is the cylinder pressure in psi, and

T - is the cylinder temperature in R.

In equation 7-1 the first term on the right hand side represents the heat transferred by convection and the second one by radiation.

Annand [2] in 1963, after reviewing several heat transfer correlations and performing dimensional analysis, proposed the following relation for the instantaneous heat flux:

$$q = 0.76\frac{k}{B}Re^{0.64}(T - T_w) + 1.610^{-12}(T^4 - T_w{}^4) \qquad (7-2)$$

where:

k - is fluid thermal conductivity in $\frac{Btu}{hr\,ft^2\,deg\,R}$,

B - is the cylinder bore in ft, and

Re - in the Reynolds number.

The radiation term in equation 7-2 was assumed zero during compression and scavenging.

The Woschni model [3] is probably one of the best known models for heat transfer computations. It was introduced in 1967 after experiments on a spherical combustion chamber and later on turbocharged engines [4]. Woschni concluded that the heat transfer in internal combustion engines is similar to heat transfer in pipe flow under turbulent conditions. Therefore, the Nusselt number is given as:

$$Nu = aRe^b \qquad (7-3)$$

Where:

Nu - is the Nusselt number ($Nu = \frac{hB}{k}$),

B - is the cylinder bore,

Re - is the Reynolds number ($Re = \frac{wB}{\nu}$), and

a, b - are constants.

In this correlation the cylinder bore is the characteristic length (B), and the gas velocity (w) is calculated using the following formulae depending on the cycle period:

During scavenging

$$w = C_1 C_m \qquad (7-4)$$

During compression

$$w = C_2 C_m \qquad (7-5)$$

During combustion - expansion

$$w = C_3 C_m + C_4 \frac{V_s T_r}{P_r V_r}(P - P_o) \qquad (7-6)$$

Where:

C_m - is the mean piston velocity ($C_m = \frac{S_d RPM}{30}$),

S_d - is the cylinder stroke,

V_s - is the swept volume,

P_o - is the cylinder motored pressure,

P_r,V_r,T_r - are the cylinder pressure,volume, and temperature in a reference state, and

C_1 to C_4 - are constants.

The reference state is usually taken as the point where the compression starts or where the combustion starts. The recommended numerical values of the constants are:

$a = 0.035$

$b = 0.80$

$C_1 = 6.18$

$C_2 = 2.28$

$C_3 = 2.28$

$C_4 = 0.00324$

Expressing the kinematic viscosity and thermal conductivity as functions of temperature and pressure [3], the heat transfer coefficient (h) from equation (7-3)

is written as:

$$h = 110.0B^{-0.2}P^{0.8}T^{-0.53}w^{0.8} \qquad (7-7)$$

Where:

P , T - are the cylinder pressure and temperature

In this equation, if B, P, T and w are in meters, atm, K, and m/s respectively, then the heat transfer coefficient is calculated in $Kcal/m^2Khr$.

Woschni [3], calculating the amount of heat transferred to the engine coolant fluid using proposed correlations, found the predictions different by as much as 200 percent. Therefore, the decision of using any particular model is difficult in the absence of experimental measurements for verification. In this study there are no data available for the total amount of heat rejected to the engine coolant. However, the heat transfer is significant in predicting the experimental cylinder pressures during the cycle. The Woschni model gives the ability of changing the heat transfer coefficient during compression, combustion-expansion and scavenging because of the different velocities used during the processes. Because of that the Woschni model was chosen for the heat transfer computations.

The heat transfer from the cylinder gas to the cylinder walls during the time interval Δt is calculated using Newton's formula:

$$\Delta Q = \Delta t h \sum_{i=1}^{n} A(i)(T - T_w(i)) \qquad (7-8)$$

Where:

$A(i)$ - is the area of surface i

$T_w(i)$ - is the wall temperature of surface i

n - is the number of surfaces in the cylinder enclosure

In the above formula (eqn. 7-8) the cylinder gas temperature is assumed to be uniform and the wall temperatures constant and uniform with respect to time. For the heat transfer computations the cylinder chamber is divided into four surfaces: a) piston head b) cylinder head (excluding the valves) c) the four valves and d) the cylinder sleeve. Each of these surfaces is assumed to have the same heat transfer coefficient but a different temperature. The estimation of the surface temperatures is discussed below:

a) Estimation of Piston Surface Temperature

The pistons in internal combustion engines are generally not working under ideal conditions because of lack of cooling. The piston materials are usually light aluminum alloys for low inertial forces. In these alloys the strength decreases rapidly for temperatures above 200 to 300 C. In the GM6V53t engine the piston is oil cooled by spraying it from the bottom. Woschni [5] carried out experiments on single and multi-cylinder, turbocharged and naturally aspirated engines, measuring the piston surface temperatures. Figures 7.1 and 7.2 show the measured temperatures and heat transfer coefficients on the piston surface in an oil cooled and a non-cooled piston. In these figures, the numerical values for the temperature contours are in degrees C and the heat transfer coefficient is in W/m^2K. In the $GM6V53T$ engine, it is expected that the oil cooling is less efficient than the one with the oil cooled channel but better than with the non-cooled. Therefore, the surface temperature is selected as 220 C.

b) Estimation of Valve Temperature

The highest temperatures in the combustion chamber occur at the exhaust valves due to lack of any type of cooling in small engines. The valve temperature depends on load, combustion chamber design, and type of scavenging. As reported by Sitkei [9] the temperature range in medium size diesel engines is in the order

of 600 to 700 C. Typical temperature distributions in exhaust valves are shown in figures 7.3 and 7.4. For the computations in the simulation model, the valve temperature was selected as 650 C.

c) Estimation of Sleeve and Head Temperatures

The cylinder sleeve temperature is designed to exceed 100 C because with lower temperatures the various acids produced during combustion will condense on the surface leading to corrosion. Particularly in diesel engines, sulfur trioxide may be produced even with temperatures higher than 100 C [6]. In figure 7.5 a typical temperature distribution for the cylinder wall is shown. In the simulation program a temperature of 120 C was selected for the sleeve.

The cylinder head contributes significantly to the heat transfer from the cylinder gas to the coolant. In two-valve engines the amount of heat transferred can be up to 50 per cent of the total heat transferred [9]. In the GM6V53T engine, with four valves overhead, it is expected to be less. The temperature of the cylinder head does not usually exceed 200 C. For the computations the selected temperature is 200 C.

REFERENCES

1 Nusselt, W. "Die Waermeuebergang in den Verbrennungs kraftmaschinen", Z. Ver. dtsch. Ing. 1923 67,692 and 708.

2 Annand, W. J. D. " Heat Transfer in the Cylinder of Reciprocating Internal Combustion Engines", Proc. Instn. Mech. Engs., Vol. 177, No 36, 1963.

3 Woschni, G. "A Universally Applicable Equation for the Instantaneous Heat Transfer Coefficient in the Internal Combustion Engines", SAE Paper 670931, 1967.

4 Woschni, G. "Prediction of Thermal Loading in Supercharged Diesel Engines", SAE Paper 790821, 1979.

5 Woschni, G. "Prediction of Thermal Loading of Supercharged Diesel Engines", SAE Paper 790821, 1979.

6 Sitkei, G. "Heat Transfer and Thermal Loading in Internal Combustion Engines", Akademiai Kiado, Budapest, 1974.

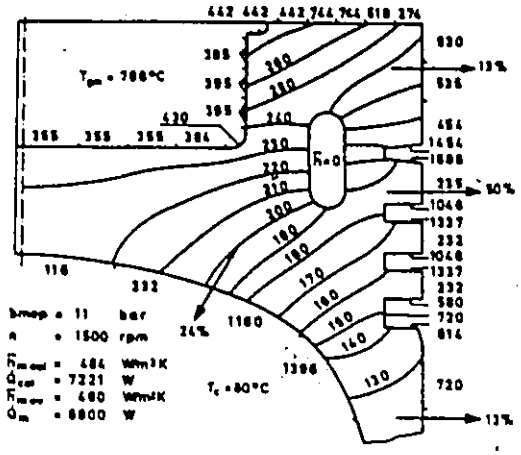

Figure 7.1 Temperatures and heat transfer coefficients on a piston with no oil supply.

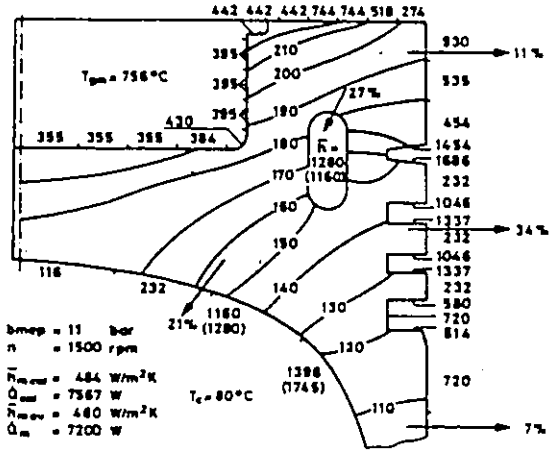

Figure 7.2 Temperatures and heat transfer coefficients on a piston with oil supply.

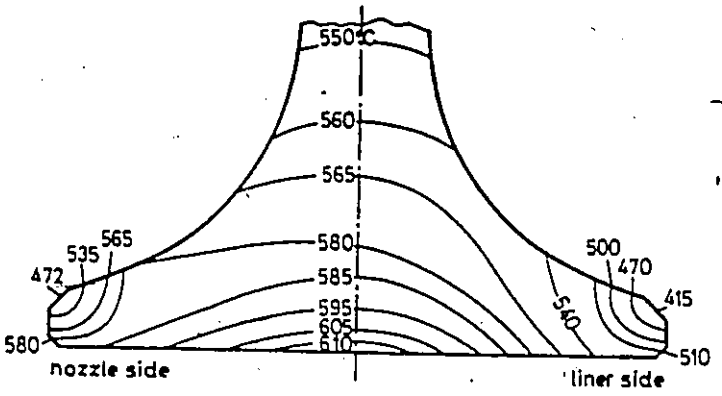

Figure 7.3 Exhaust valve temperature isotherms for a large size engine.

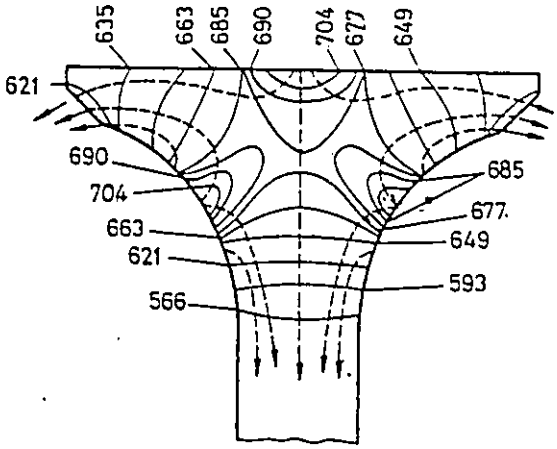

Figure 7.4 Exhaust valve isotherms for a small size engine.

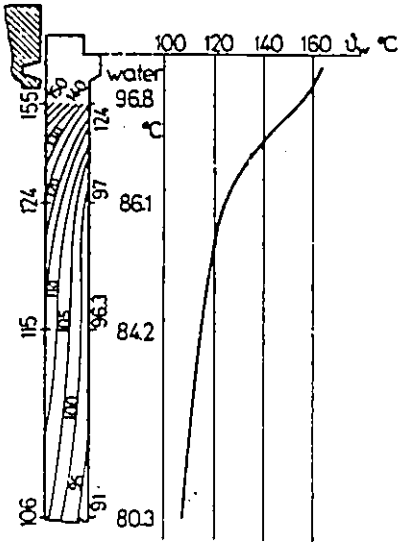

Figure 7.5 Temperature distribution over the cylinder wall.

CHAPTER 8

COMPUTATION OF THE FUEL BURNING RATE USING EXPERIMENTAL PRESSURE DATA

As discussed earlier, the combustion process is very important in the simulation model. It is not possible to measure the fuel mass burning rate ($FMBR$) experimentally but it can be calculated using experimentally measured cylinder pressures during combustion. The model for computing the experimental FMBR must include all the significant processes taking place in the engine. In two stroke engines, because the cylinder mass and the mass composition are not known prior to the combustion process, computed values from a simulation model must be used. In this chapter a method is proposed for computing the FMBR using the same technique as in the simulation program for calculating the pressure and temperature during the cycle. The parameters used in the combustion model presented in chapter 3 are evaluated using the FMBR. Direct comparison between the FMBR's obtained from the thermodynamic model and computed from experimental pressure data is also made in chapter 9.

The computations of the FMBR are performed at the end of the thermodynamic simulation cycle. Therefore, the cylinder mass and the cylinder gas composition are known. Initially, the onset of combustion is determined from the experimentally measured pressures. The onset of combustion is determined by searching the experimental pressure values in steps of 0.2 degrees until the pressure rise is over 1.16 kPa during each of the next three consecutive steps. The value of 1.16 kPa is arbitrary and was obtained from observations of the experimental pressure raise during compression, ignition delay and combustion [1]. The computational procedure is explained below:

a) The computations begin at the onset of combustion in time steps of Δt. Using the experimental pressures, the temperature at the beginning and the end of the time step are calculated using the ideal gas equation (T_1 and T_2 respectively).

b) Using the temperatures T_1 and T_2 the change of internal energy and the mean heat capacity during the step is calculated.

c) Using the following simplified energy equation the fuel mass burned during the step is calculated.

$$m_b = \frac{MC_v}{q_{lhv}}(T_2 - T_1(\frac{V_1}{V_2})^{\frac{R_{mol}}{C_v}}) \qquad (8-1)$$

Where:

C_v - is the average heat capacity during the step

d) The heat released by the fuel during the time step is calculated using mean values for the temperature and pressure. For the computations the fuel/air ratio based on the total unburned fuel in the cylinder is calculated.

e) The cylinder mass composition is updated

f) The internal energy E_2 using the new gas composition is calculated

g) The heat transferred to the cylinder walls (chapter 7) and the work (section 2.4) are calculated.

h) Check if the energy equation is satisfied. It is assumed satisfied if :

$$\Delta m = \frac{E_2 - E_1 + Q_w - W + m_b Q_{comb}}{Q_{comb}} < 10^{-15} \qquad (8-2)$$

Where:

Q_{comb} - is the amount of heat released during the time step

If the energy equation is satisfied, the computations are continued for the next time step (starting from step a).

If the energy equation (eqn. (8-2)) is not satisfied the cylinder gas composition is corrected together with the mass of fuel burned during the step as:

$$(m_b)_n = (m_b)_{n-1} + \Delta m \qquad (8-3)$$

The computations are repeated starting at step (d).

The experimental pressure traces provided by Flanagan and Menard [1] are in steps of 0.2 degrees crank angle. The computations of the FMBR can be performed in any crank angle step multiplier of 0.2 degrees using an experimental average pressure trace (mean pressure trace of thirty two consecutive engine cycles). During the computations of the FMBR close to the end of the combustion process, negative fuel burning rates are observed. The reason for that is the use of the mean pressure trace for computation of the FMBR. Similar observations have been reported in the past [2]. However, if negative rates are observed, the mass burning rate is assumed zero and the computations are continued. In figure 8.1 typical fuel burning rates for four different crank angle steps (0.2, 0.4. 0.6 and 0.8) are shown at 2200 RPM full rack. Comparison of the four FMBR show the same trends with high levels of small fluctuations in the computed FMBR using 0.2 and 0.4 crank angle steps. Comparison with values obtained from the thermodynamic model will be presented in chapter 9.

REFERENCE

1. Flanagan R. C. and Menard L. ' A Study of Wide Boiling Range Fuel-Engine Interaction: Engine Performance and Combustion Monitor Tests' Technical Report No UOME-EP-8403-1 Department of National Defense DREO, Ottawa Canada.

2. Krieger R. B. and Borman G. 'The Computation of Apparent Heat Release for Internal Combustion Engines' ASME paper 66-Wa/DGP-4 1966.

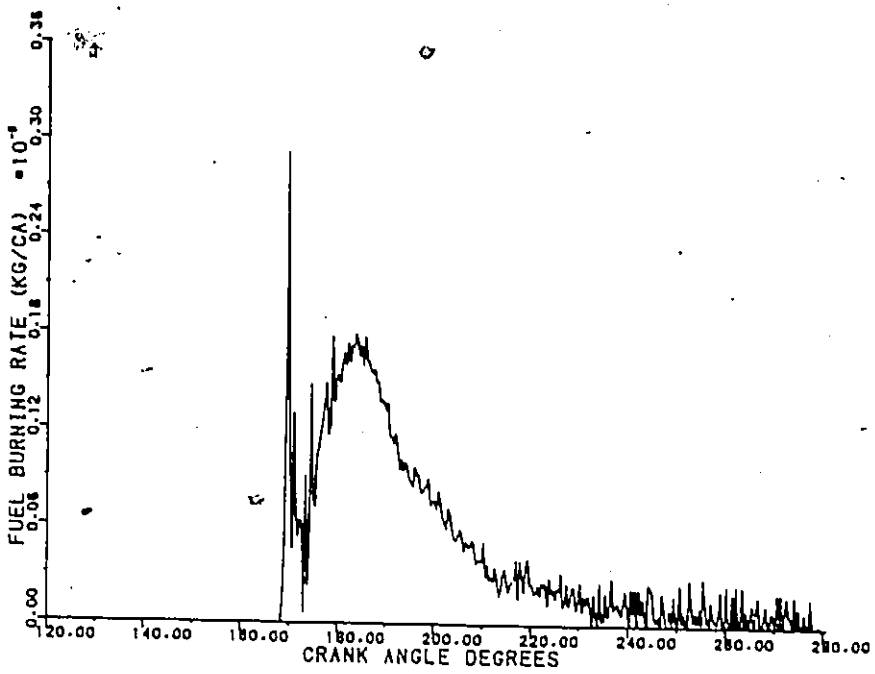

b) Crank angle step 0.4

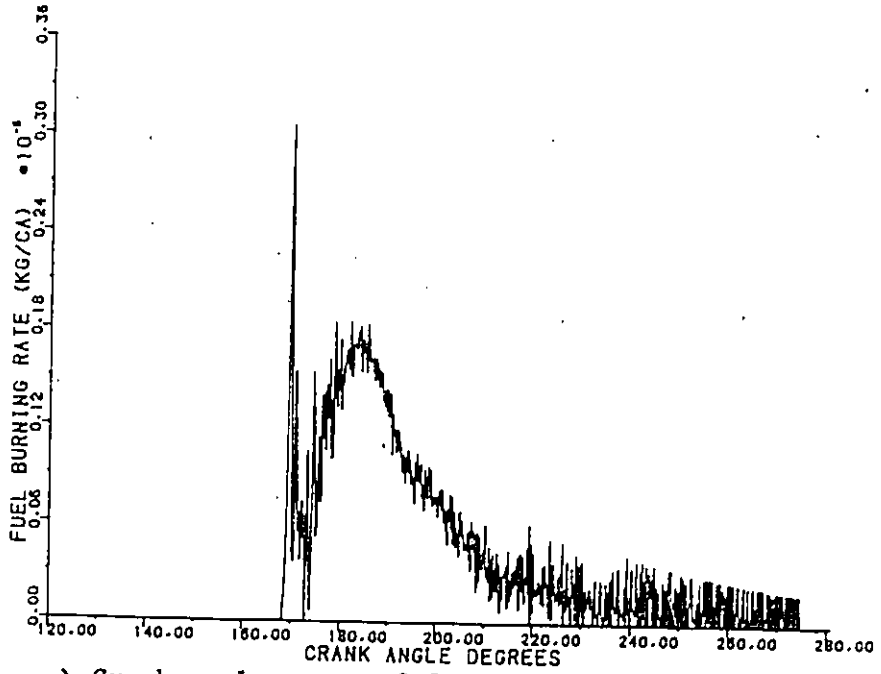

a) Crank angle step 0.2

Figure 8.1 Computed fuel mass burning rate using experimental pressure data for different crank angle steps (RPM 2200).

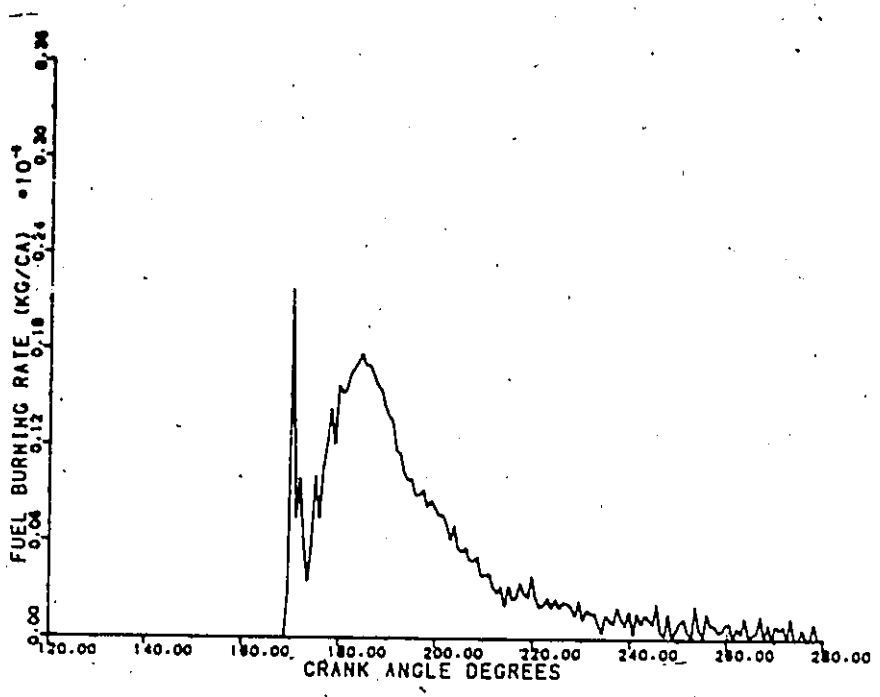

d) Crank angle step 0.8

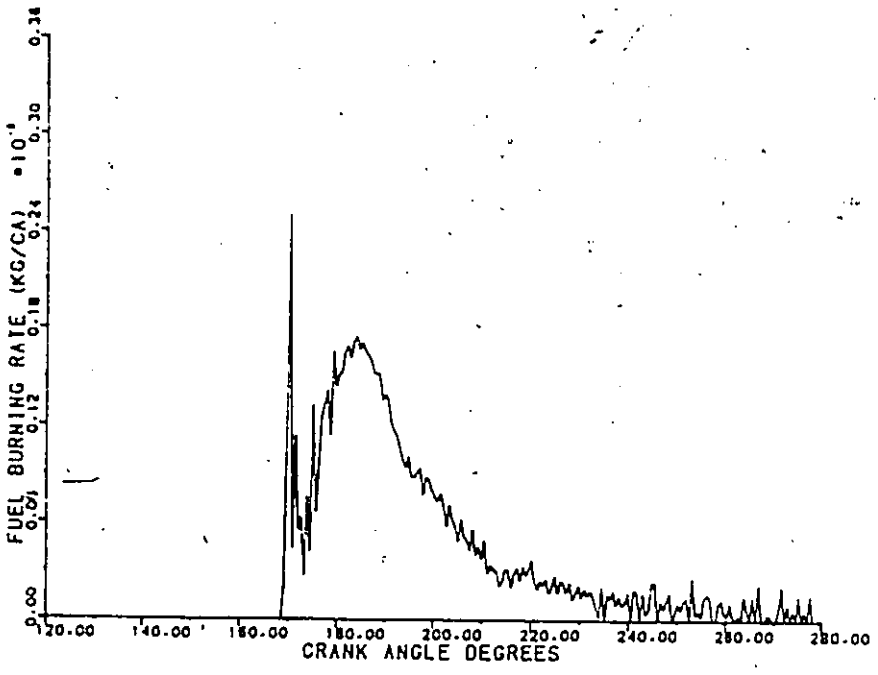

c) Crank angle step 0.6

Figure 8.1 Continued

CHAPTER 9

COMPARISON OF THE THERMODYNAMIC MODEL PREDICTIONS WITH EXPERIMENTAL DATA

9.1 INTRODUCTION

In this chapter, the numerical values of the parameters of the thermodynamic model and comparison of the model predictions with experimental data are presented. During scavenging the pressure in the exhaust manifold is not computed and the mean exhaust pressure measured is used. The equation derived from the multi-dimensional analysis is used for scavenging efficiency. Detailed comparison of the model predicted values with the experimentally obtained values are presented for full rack conditions at 2200 RPM engine speed. The computed indicated parameters for the engine speed operating range (1500 to 2800 RPM) at full torque are compared with the experimentally computed values from the mean pressure trace. All experimental data used were obtained from Flanagan and Menard [1].

9.2 MODEL CONSTANTS EVALUATION

The model parameters that must be established are the ignition delay, combustion and heat transfer model constants. After testing the model for different constants, the following were established:

IGNITION DELAY PARAMETERS

$$a = 2.2$$

$$b = 0.009 RPM^{0.5}$$

COMBUSTION MODEL CONSTANTS

Premixed Reaction Equation

$$a = 9.10^4$$

$$b = 1.2$$

$$c = 1.1$$

$$d = 20000$$

Fuel droplet diameter

$$d_o = 18 \text{ micron}$$

Mixing controlled Reaction Equation

$$a = 0.020$$

WOSCHNI HEAT TRANSFER MODEL

$$C_4 = 0.0025$$

The other constants for the models are as recommended. The model parameter evaluation is rather easy because the parameters are not directly related. Initially the ignition delay model parameters were evaluated. The ignition delay depends only on the cylinder pressure at the beginning of the fuel injection (equation 3-1). Therefore, the constants of the model can be evaluated by direct comparison of the computed ignition delay with the experimental values. The amount of fuel burned at early combustion is controlled by the amount of fuel evaporated during the ignition delay period. The amount of fuel vapour is highly affected by the fuel droplet size. Comparison of the amount of fuel burned at early combustion computed from experimental pressures and the model predicted values specify the fuel droplet diameter and the constants of the premixed reaction rate equation (PRRE). The PRRE affects only the early combustion (approximately three to five crank angle degrees after ignition). After that the combustion is controlled

by the mixing equation. It was found that the Whitehouse model underpredicts the amount of fuel burned during combustion and, therefore, the constant a in the mixing controlled reaction equation was modified. The pressure in the cylinder during combustion was underpredicted, therefore the constant C_4 in the heat transfer model was decreased. The constants C_4 in the heat transfer model and a in the MCRE were modified simultaneously because the fuel burning rate is affected by the cylinder pressure.

The air box pressure and temperature are used as initial conditions for the cycle computations. This pressure is essential only for the first iteration, after which it is established during scavenging (mainly from the air box and the exhaust pressure). Therefore, accurate experimental pressures for the air box and exhaust manifold are needed to establish correct initial conditions.

9.3 MODEL PREDICTIONS AND COMPARISON WITH EXPERIMENTAL DATA

The developed thermodynamic model discussed in the previous sections is tested against available experimental data for verification. The comparison of the model predictions with the experimental data is performed for the engine speed range of 1500 to 2800 RPM at full load conditions. The comparison with experimental data is performed for the GP30 reference diesel fuel. As discussed earlier, every cycle iteration starts at the point where the valves and ports are just closed and these conditions are assumed as initial. The final conditions for an iteration are the values just before the valve and ports close. For convergence of the program, a 1.35 kPa difference in pressure and 10 K difference in temperature between the initial and final values are allowed.

In the model predictions the correct ignition delay period is very important. Figure 9.1 shows the comparison of the computed ignition delay using Henein and

Bolt model with the experimental values for the engine operating speed range. The experimental ignition delay period was obtained using the mean pressure trace (mean value of 32 single pressure traces). The ignition delay period is the period from the point where the fuel start to be injected in the cylinder until the cylinder pressure increases by more than 70 kPa during each of three consecutive increments of 0.2 degrees crank angle [1]. The ignition delay is in crank angle degrees. As can be seen from figure 9.1 the model predictions are in good agreement with the experimentally obtained values.

Figure 9.2 shows the comparison between the experimentally measured cylinder pressure with the theoretical predicted at 2200 RPM. The TDC is at 180 degrees and the BDC at 360 or zero degrees. The experimental pressures are plotted at 1.0 degree intervals. In the model the interval used in the computations is 1 degree during the cycle, except at a window of 40 degrees around TDC where a 0.1 degree interval is used. The interval used for plotting is 1 degree. The agreement between the experimental and the predicted values of the cylinder pressure is good. The predicted ignition delay at 2200 RPM is 6.4 degree and the one obtained experimentally from the mean pressure trace in 6.5 degree. Fuel injection starts at 161.4 degrees crank angle and therefore combustion starts at 167.8 degrees. This can be seen in figure 9.2 where high pressure rates are observed after 168 degrees. The experimentally obtained peak pressure is 12.02 MPa, located at 7.0 degrees ATDC. This is in good agreement with the predicted values of 11.96 MPa and 6.3 degrees respectively.

Figure 9.3 shows the cylinder temperature variation during the cycle. At the beginning of the compression the temperature is 397 K. In the figure a smooth line can be seen around 55 degrees (point where compression starts) indicating a good matching between the temperature at the beginning of compression and the temperature at the end of scavenging. At the beginning of the combustion

process, because of high burning rates, high temperature gradients are observed. The temperature peaks at approximately 15 degrees ATDC. After that point the temperature decreases because of high heat transfer rates, the expansion process and the low fuel burning rates. After 280 degrees the blow down starts, decreasing the cylinder mass and, therefore, the cylinder temperature. After 305 degrees the scavenging process starts, reducing the temperature further by replacing the hot residual gases with air.

Figure 9.4 shows the model predicted fuel mass burning rate and one obtained experimentally from the pressure trace (crank angle step equal to 0.8 degrees). The experimental fuel burning rate is computed using the thermodynamic model but during combustion the experimental pressure trace is input and the fuel burning rate is computed (see chapter 8). The good agreement between the theoretical and experimental fuel burning rates is evident upon comparison of the two figures. Combustion starts with a high burning rate due to premixed conditions, which is typical in direct injection diesel engines. The amount of fuel burned under premixed conditions is the amount of fuel evaporated during the ignition delay. The amount of fuel evaporated depends on the engine speed. More fuel is evaporated at low RPM than at high RPM because more time is available. The amount of fuel evaporated during the ignition delay is about 3 to 8 percent of the total injected fuel. After this fuel has been consumed the combustion is controlled by mixing. The fuel burning rate peaks just after the TDC in both theoretical and experimental cases.

Figure 9.5 shows the mass variation of the major chemical species (O_2, CO_2 and H_2O) during the cycle in the cylinder. The mass of the species is constant during compression (from 55 to 168 degrees) because the cylinder is a closed system undergoing only a change in volume. During combustion (168 to 257) the cylinder oxygen is consumed with the production of carbon dioxide and water.

From 257 to 280 the mass in the cylinder remains constant because of the expansion process. During blow-down and early scavenging (280 to 310) the mass of all species decreases because the exhaust valves open and residual gases escape from the cylinder. During scavenging the mass of oxygen increases because air is supplied to the cylinder with the reduction of the mass of CO_2 and H_2O. In the oxygen curve a small jump can be seen at 55 degrees. The difference in value is between the initial assumed mass of oxygen and the final computed oxygen mass at the end of the cycle. A similar jump is not visible in the other two species.

Table 9.1 shows the comparison of the indicated horse power, indicated mean effective pressure, indicated thermal efficiency, peak pressure, peak pressure location and ignition delay with the experimentally measured values and with the ones computed from experimental data. The results show a good agreement for the entire engine operating range.

REFERENCES

1 Flanagan, R. C., and Menard, L. " A Study of Wide Boiling Range Fuel-Engine Interaction: Engine Performance and Combustion Monitor Tests", Technical Report No. UOME-EP-8403-1, Department of National Defense DREO, Ottawa Canada, 1984.

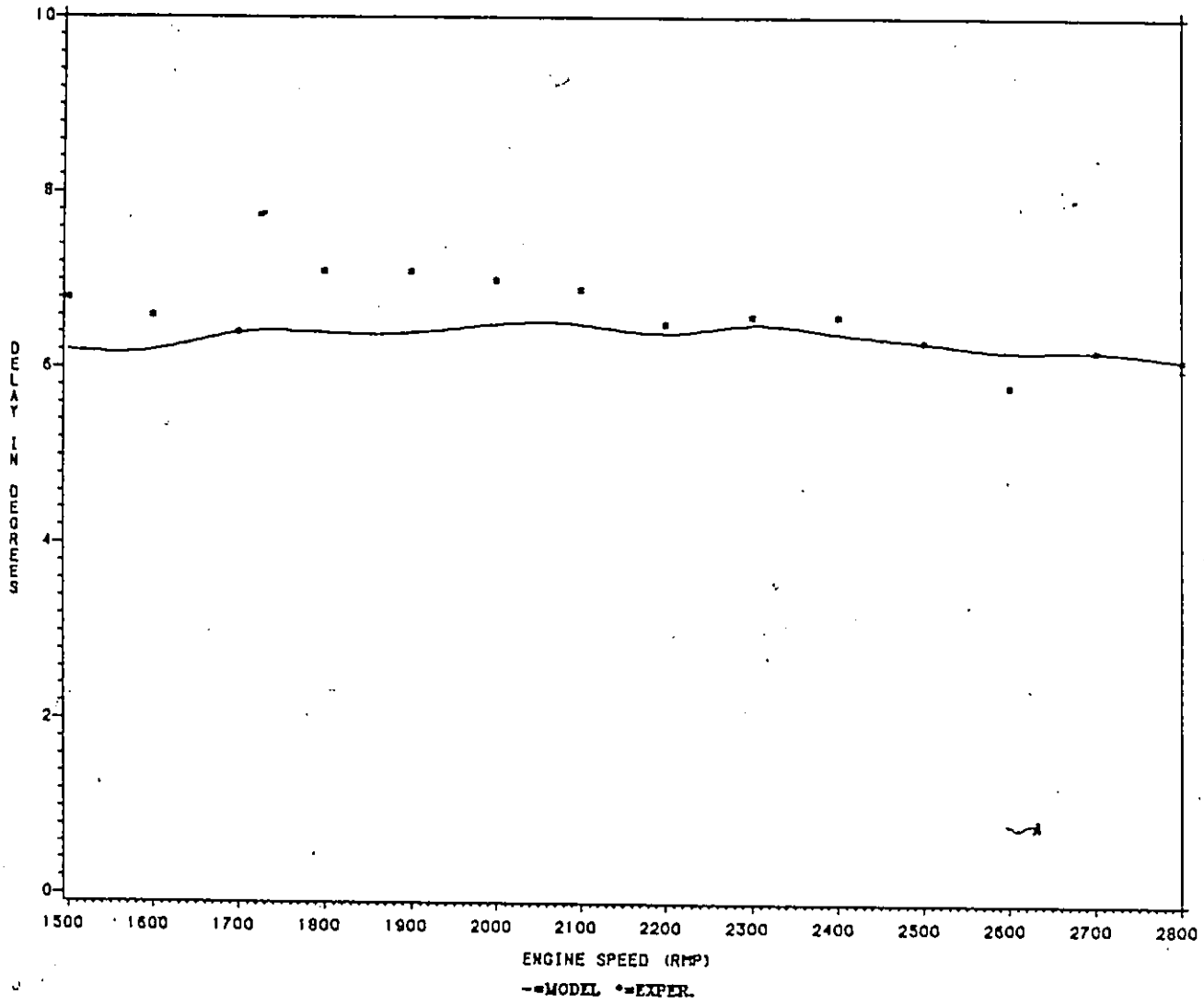

Figure 9.1 Ignition delay versus engine speed.

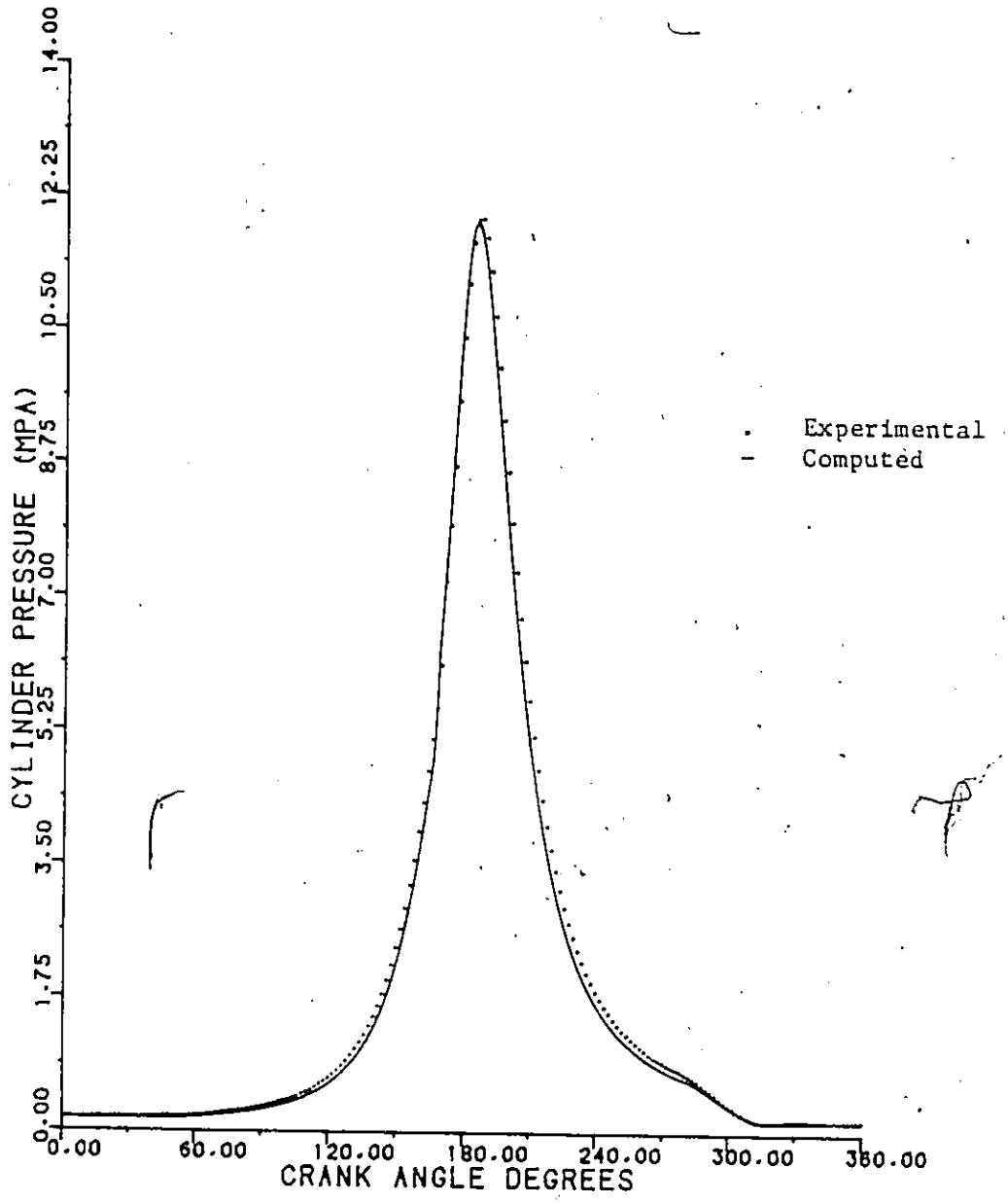

Figure 9.2 Comparison between experimental and computed pressure traces at 2200 RPM.

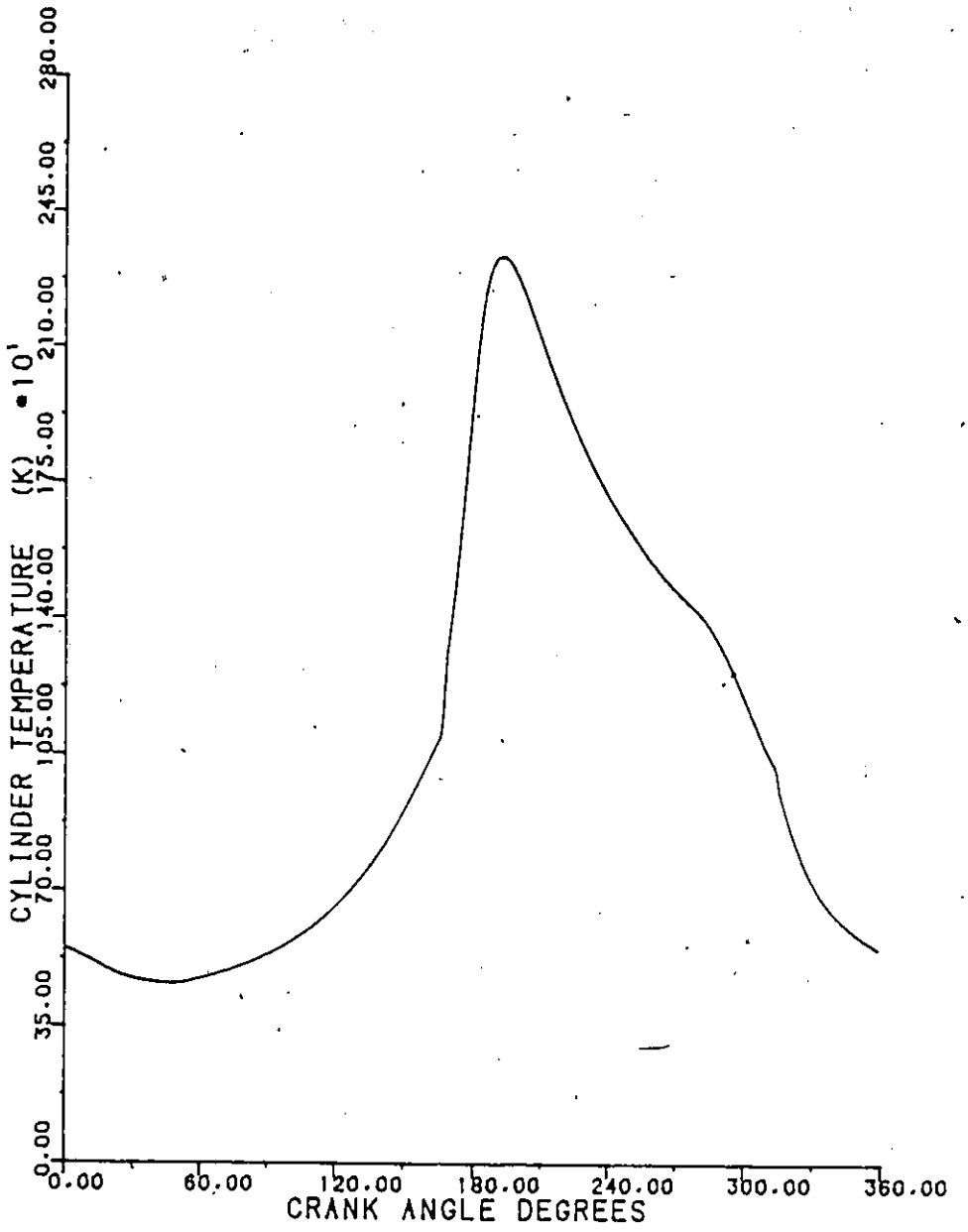

Figure 9.3 Computed cylinder temperature at 2200 RPM.

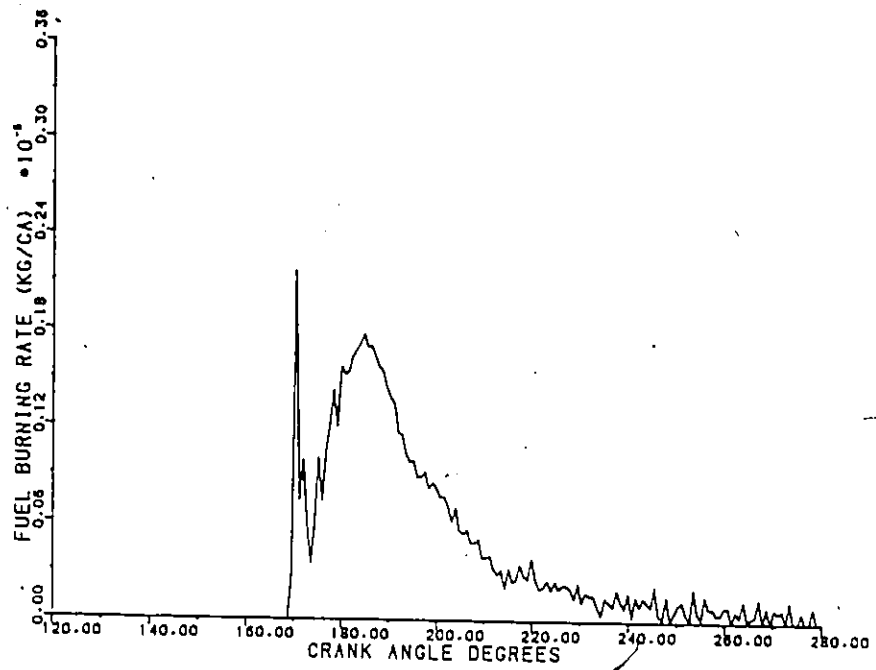

a) Experimental

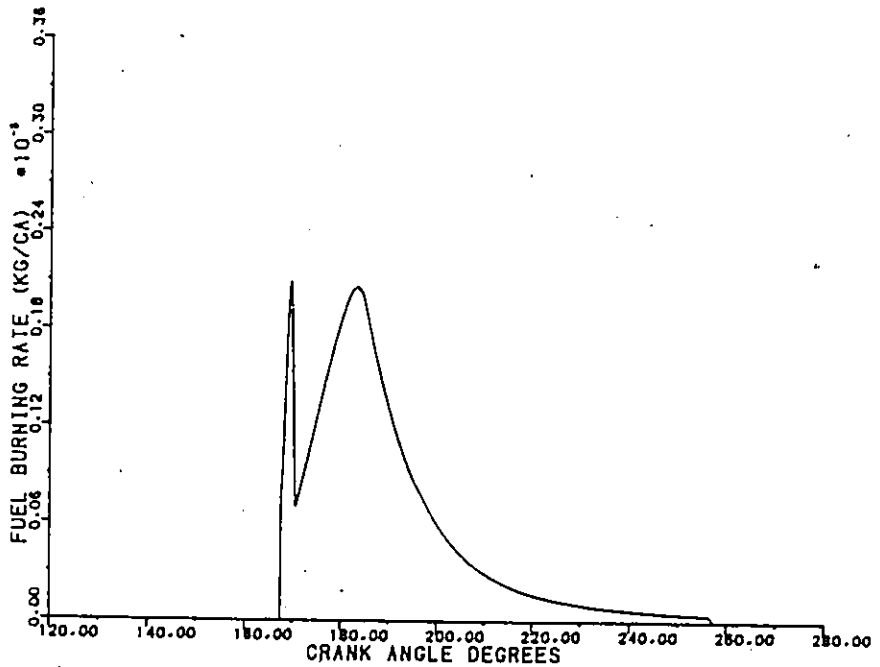

b) Computed

Figure 9.4 Comparison of mass fuel burning rates computed from experimental pressures to those predicted from the thermodynamic model at 2200 RPM.

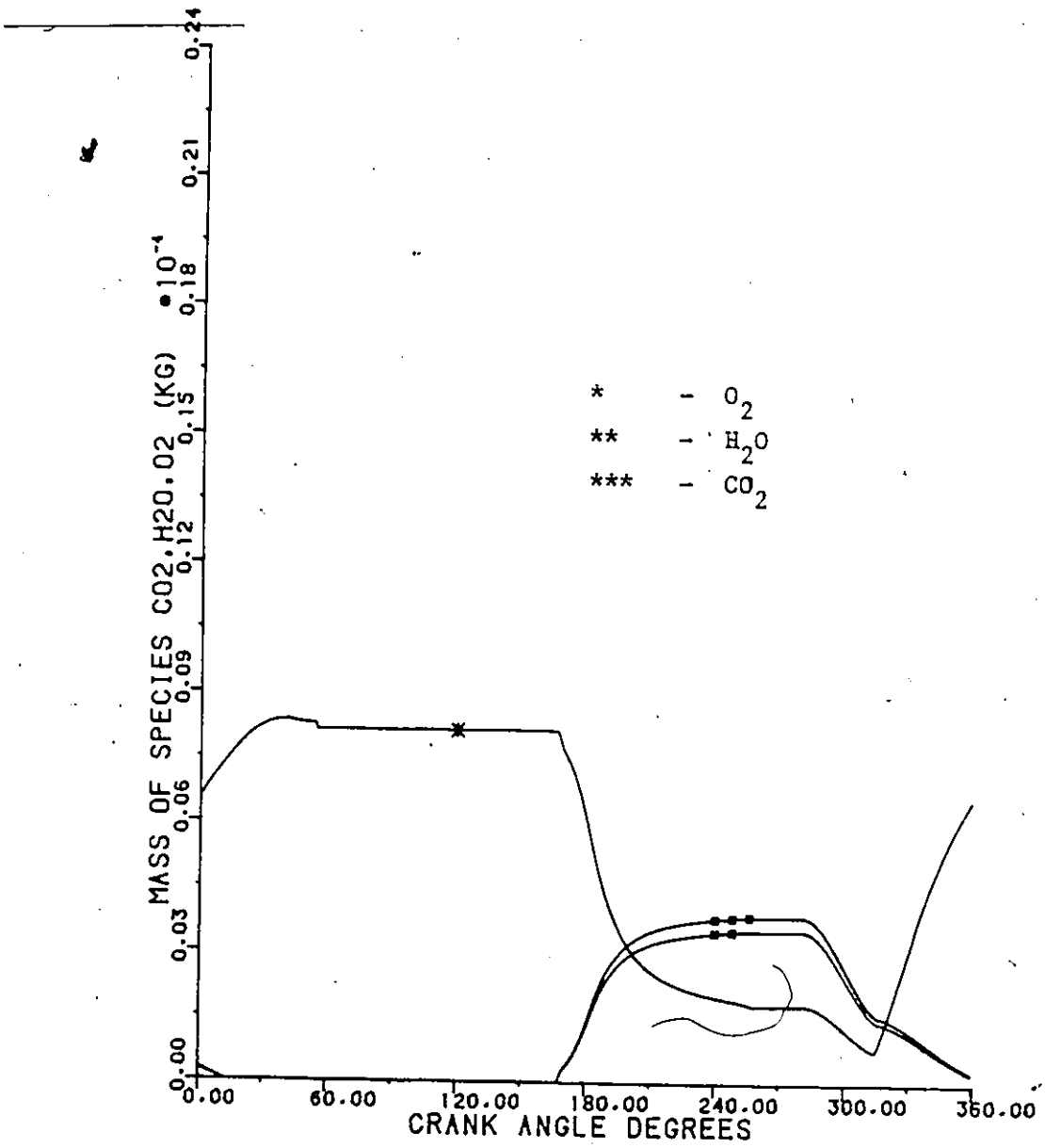

Figure 9.5 Mass variation of O_2, CO_2 and H_2O during the cycle at 2200 RPM.

TABLE 9.1

COMPARISON BETWEEN MODEL PREDICTIONS AND EXPERIMENTAL DATA

RPM	MAXIMUM PRESSURE (MPa) VALUE		LOCATION		IHP (HP)		ITE		IMEP (MPa)	
	EXP	THEOR	EXP	THEOR	EXP	THEOR	EXP	THEOR	EXP	THEOR
1500	11.44	11.37	6.0	5.5	178	182	32.8	33.5	1.02	1.04
1600	11.56	11.48	5.4	5.6	192	196	33.8	34.5	1.03	1.05
1700	11.79	11.38	6.4	5.6	206	205	34.8	34.6	1.04	1.04
1800	11.59	11.47	6.0	6.0	220	222	35.7	36.1	1.05	1.06
1900	11.62	11.59	6.6	6.3	234	241	35.6	36.7	1.06	1.09
2000	11.67	11.55	7.2	6.0	245	244	36.8	36.6	1.05	1.05
2100	11.90	11.70	7.0	6.2	260	259	37.6	37.3	1.06	1.06
2200	12.03	11.96	7.0	6.3	273	274	37.9	38.0	1.06	1.07
2300	12.07	12.14	7.8	6.4	282	287	38.0	38.7	1.05	1.07
2400	12.00	12.12	7.0	6.4	291	294	38.3	38.6	1.04	1.05
2500	12.11	12.31	7.4	6.2	299	303	38.6	39.1	1.03	1.04
2600	12.17	12.36	7.8	6.2	306	311	38.6	39.1	1.02	1.03
2700	11.90	12.50	6.6	6.2	311	320	38.3	39.4	1.00	1.02
2800	11.99	12.65	7.0	6.3	322	330	38.8	39.7	0.99	1.01

CHAPTER 10

SUMMARY AND CONCLUSIONS

A Thermodynamic model has been developed for predicting the indicated parameters of a two-stroke, direct injection, uniflow- scavenged diesel engine. During the thermodynamic cycle the pressure and temperature in the cylinder are computed using state and energy equations. The energy equation is approximated using finite differences and is solved simultaneously with the state equation using an iterative technique. The combustion model that is used is a two equation model. The fuel mass burning rate is calculated using premixed and mixing controlled reaction rate equations. The computed fuel burning rate is compared with a burning rate computed using experimental pressure data. During blow-down and scavenging the flow through the valves and ports is computed using the quasi-steady approach for isentropic compressible flow through an orifice. During scavenging the air concentration in the cylinder is computed using the scavenging efficiency - scavenging ratio relationship which is derived from multi-dimensional analysis.

For the scavenging studies both two and three dimensional models were developed. The flow is considered turbulent and the conservation equations are solved explicitly in time using finite differences. For the scavenging efficiency computation the concentration equation is solved simultaneously with the momentum equations. The density in the field is computed using the state equation and the temperature is obtained by solving the energy conservation equation. From the results and the discussion presented in the previous chapters the following are concluded:

a) MULTI-DIMENSIONAL MODELING

- The predictions of the multi-dimensional model developed for cavity flow are in good agreement with experimental data.

- Comparison of predictions of the developed multi-dimensional code with the TEACH code show good agreement.

- The flow in the cylinder is three-dimensional (3D) because of the exhaust valve geometry.

- At the early stages of the scavenging process (crank angle less than 140 degrees) there are two recirculation zones in the cylinder. The first one appears close to the cylinder wall (flow reattachment) and the second one in the piston bowl (very weak).

- As the scavenging process progresses the two recirculation zones grow in size and a third recirculation zone appears close to the cylinder axis.

- The recirculation zone close to the cylinder axis computed using the two-dimensional (2D) model is much stronger than the one computed using the 3D model. This is because the swirl velocities computed in the 3D model are smaller than the velocities computed in the 2D model. In the 3D computations the swirl velocities are smaller than the velocities computed in the 2D model because close to the exhaust valves circumferential velocities exist opposite to the swirl velocities imposed in the inlet ports.

- From the 2D computations it appears that both recirculation zones close to the cylinder wall and to the cylinder axis affect the scavenging efficiency. From the 3D computations it becomes clear, however, that only the recirculation zone close to the cylinder wall affects the scavenging efficiency.

- In the early scavenging stages no air escapes from the exhaust valves and the process can be considered as pure displacement.

b) THERMODYNAMIC MODELING

- The ignition delay predicted by the Henein and Bolt model is in good agreement with the experimental values.

- The computed fuel mass burning rate is in good agreement with the values computed from experimental data.

- The computed cylinder pressures during the cycle are in good agreement with the experimentally measured values.
- The fitting of the model to experimental data was possible with few modifications to model constants, suggesting that the model developed here is general enough to be used for other engines with minor modifications.

- The computed indicated parameters (indicated horse power, indicated thermal efficiency and indicated mean effective pressure) are in good agreement with the values obtained experimentally.